Calcium handling in rabbit ventricular myocytes – regional differences and changes after myocardial infarction

A thesis presented by

Dr Francis Russell Quinn

BA BM BCh MRCP

for the degree of Doctor of Philosophy at the University of Glasgow

Institute of Biological & Life Sciences

University of Glasgow

Glasgow

G12 8QQ

Sept 2004

For my father and mother, Murray & Rosamund Quinn.

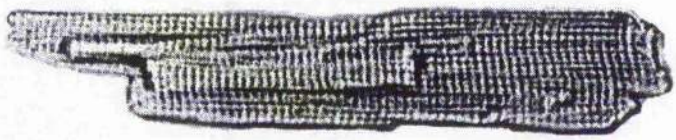

ABSTRACT OF THESIS

BACKGROUND: Calcium (Ca) has a central role in the mechanical and electrical properties of cardiac myocytes. This thesis examines cellular Ca handling in a rabbit infarct model of heart failure (8 weeks after coronary artery ligation), which exhibits left ventricular dysfunction (LVD), pulmonary and hepatic congestion and a propensity to arrhythmias.

AIMS: The main aims of this thesis were (i) to determine the properties of Ca handling in single cells from different transmural regions in sham-operated (Sham) and post-infarction animals, and (ii) to identify the underlying mechanisms behind any differences seen.

METHODS: Voltage clamp studies were performed at 37 °C on enzymatically-isolated single cells from the sub-endocardium (Endo) and sub-epicardium (Epi), loaded with the Ca indicator Fura-2. Baseline Ca transient characteristics were determined at different stimulation frequencies. Sodium-calcium exchanger (NCX) activity was estimated from the rate constant (RC) of Ca decay during 10 mmol/L caffeine application. Sarco(endo)plasmic reticulum Ca ATPase (SERCA) function was estimated from the RC of Ca decay after brief caffeine application in the presence of 10 mmol/L Ni. SR Ca content was calculated from the integral of the NCX current induced by caffeine application, and further analysis was used to quantify Ca buffering. These measures were each performed at steady state and were corrected for non-NCX Ca removal mechanisms. NCX current density was measured as the Ni-sensitive current in response to a ramp protocol, with major interfering currents blocked and intracellular [Ca] buffered to ~250 nmol/L. Allosteric regulation of NCX was studied

by examining the outward NCX current through a range of [Ca], using a voltage step protocol. Finally, integrative analysis was used to determine Ca fluxes during systole and diastole, and separate protocols were used to perturb excitation-contraction (E-C) coupling to give further insights into cellular Ca handling.

RESULTS: For both Sham and LVD animals, transmural differences in NCX were found, with higher current densities in Endo cells. In Sham animals, SERCA activity showed the converse, with greater Ca uptake in Epi cells, and this was associated with a higher SR Ca content in this region. In LVD cells, Ca transients were, in general, smaller compared to Sham, and exhibited a slower Ca decay. For both Endo and Epi regions, these findings were associated with reduced SR Ca content in LVD, and lower NCX current density and activity. For Epi cells, SERCA activity was also reduced in LVD. Studies of allosteric regulation of NCX by Ca showed that in LVD cells the exchanger was more sensitive to [Ca]. When Ca fluxes were studied, no difference in Ca entry *via* L-type Ca channels was found in LVD, but the gain of E-C coupling was reduced. This was likely to be due to the changes in SR Ca content. By studying E-C coupling in the presence of low concentrations of caffeine, there was some evidence of regional differences in SR Ca release.

CONCLUSIONS: Ca handling in the rabbit heart shows a number of differences between sub-endocardial and sub-epicardial cells. Following myocardial infarction, significant changes occur which may contribute to the impaired contraction and relaxation observed in this model of LVD.

TABLE OF CONTENTS

LIST OF FIGURES & TABLES

ABBREVIATIONS

AM	acetoxymethyl ester
ANOVA	analysis of variance
AP	action potential
APD	action potential duration
ATP	adenosine triphosphate
BAPTA	bis-(*o*-aminophenoxy)-ethane-N,N,N′,N′-tetra-acetic acid
BK	base Kreb's
B_{Max}	saturating capacity of the buffer
BSA	bovine serum albumin
$[Ca]_i$	intracellular calcium concentration
CaMKII	calcium / calmodulin-dependent protein kinase II
cAMP	cyclic adenosine monophosphate
CCD	charged coupled device
CICR	calcium-induced calcium release
C_m	membrane capacitance
DAD	delayed afterdepolarisation
DHPR	dihydropyridine receptor
DMSO	dimethylsulphoxide
EAD	early afterdepolarisation
E-C coupling	excitation-contraction coupling
EF	ejection fraction
EGTA	ethylene glycol-bis(β-aminoethyl ether)-N,N,N',N'-tetraacetic acid
E_m	membrane potential
E_{Rev}	reversal potential
Endo	sub-endocardial
Epi	sub-epicardial
FKBP	FK-506 binding protein
HEPES	N-(2-hydroxyethyl)piperazine-N'-(2-ethanesulphonic acid)

HF	heart failure
I	current
K_d	equilibrium constant for dissociation
K_m	Michaelis constant
K_{mCaAct}	Michaelis constant for calcium activation
LAD	left atrial dimension
LP	long-pass
LSD	least significant differences
LV	left ventricle
LVAD	left ventricular assist device
LVEDD	left ventricular end-diastolic dimension
LVH	left ventricular hypertrophy
LVD	left ventricular dysfunction
MI	myocardial infarction
MOI	multiplicity of infection
mRNA	messenger ribonucleic acid
NADH	nicotinamide adenine dinucleotide
NCX	sodium-calcium exchanger
n_{Hill}	Hill coefficient
ns	non-specific
n.s.	not significant
NT	normal Tyrode's
PDE	phosphodiesterase
PKA	protein kinase A
PKC	protein kinase C
PLB	phospholamban
PMT	photomultiplier tube
Q	charge
R	ratio of Fura-2 340 nm signal to 380 nm signal
RC	rate constant
RCC	rapid-cooling contracture

RV	right ventricle
RyR	ryanodine receptor
SEM	standard error of the mean
SERCA	sarco(endo)plasmic reticulum calcium adenosine triphosphatase
Sham	sham-operated
SM	sub-membrane
SR	sarcoplasmic reticulum
τ	time constant of decay
TEA	tetraethylammonium chloride
ti	transient inward
to	transient outward
T-tubule	transverse tubule
V	voltage
V_{Max}	maximal velocity
VT	ventricular tachycardia
4-AP	4-aminopyridine

ACKNOWLEDGEMENTS

The greatest of thanks to Godfrey Smith for supervising this thesis. His endless enthusiasm, intellectual stimulation, friendship and advice made it a very enjoyable and rewarding experience. Thanks also to my co-supervisor Stuart Cobbe for his valuable input throughout the project.

I am very grateful for the expert technical assistance of Anne Ward, Aileen Rankin and Margaret-Anne Craig. Thanks also to Dr Martin Hicks and the staff at Glasgow Royal Infirmary for the preparation of the animal model. I am indebted to Marie McIntosh for her patience and expertise in teaching me to patch-clamp.

Thanks to all in the lab for their friendship, chat and banter during my time there, and to Mark & Lard for helping while away the long afternoons in the dark.

This project was supported by a BHF clinical PhD studentship, for which I am very grateful.

I owe a huge debt of thanks to my parents, family, and friends for their support and encouragement.

Finally all my love and thanks to my wife, Karen, whose help, support, advice and understanding throughout this thesis made it all possible. Thanks also to my son, Connor, whose impending arrival set a biological deadline for completion – his gestation was certainly shorter than that of the thesis, and his arrival more eagerly anticipated.

DECLARATION

Adenoviral transfection and culturing of cardiac myocytes, as described in Chapters 2 and 3, was performed by Dr D Reynolds. The animal model was prepared and characterised using echocardiography by the staff at Glasgow Royal Infirmary, under Dr Martin Hicks. All other work within this thesis was the author's own.

PUBLICATIONS ARISING FROM THESIS

Papers

Quinn FR, Currie S, Duncan A, Miller S, Sayeed R, Cobbe SM, Smith GL. Myocardial infarction causes increased expression but decreased activity of the myocardial Na^+-Ca^{2+} exchanger in the rabbit. *J Physiol* 2003; 553: 229-242.

Prestle J, Quinn FR, Smith GL. Ca^{2+}-handling proteins and heart failure:- novel molecular targets? (Review) *Curr Medicinal Chem* 2003; 10: 967-981.

Abstracts

Quinn FR, Cobbe SM, Smith GL. Altered calcium handling in a rabbit model of heart failure: a cellular mechanism for diastolic dysfunction? (Abstract) *Heart* 2003; 89 (Suppl).

Quinn FR, Cobbe SM, Smith GL. Altered calcium handling in a rabbit model of left ventricular dysfunction – implications for contractile function and arrhythmogenesis. (Abstract) *Eur Heart J* 2002; 23 (Suppl): 404.

Quinn FR, Cobbe SM, Smith GL. Reduced sodium-calcium exchanger (NCX) function in a rabbit model of left ventricular dysfunction (LVD). (Abstract) *Biophys J.* 2002; 82: 2925

Quinn FR, McIntosh, MA, Cobbe, SM, Smith GL. Sodium-calcium exchange current density in normal and failing rabbit hearts. (Abstract) *Eur Heart J.* 2001; 22(Suppl): 55.

Quinn FR, McIntosh, MA, Cobbe, SM, Smith GL. Sodium-calcium exchange current density is higher in endocardial than epicardial cells. (Abstract) *Biophys J.* 2001; 80(1): 641a-642a.

CHAPTER 1

GENERAL INTRODUCTION

1.1 Chronic heart failure in the human

1.1.1 Definition and clinical consequences of heart failure

Heart failure (HF) is a syndrome which, at the most basic level, is caused by the inability of the heart to provide sufficient cardiac output to meet the metabolic demands of the tissues. Under these conditions, changes occur at a cell, tissue and organ level leading to the clinical "phenotype" of heart failure. The altered haemodynamic state has a number of consequences, including pulmonary and systemic congestion, causing amongst other things, breathlessness, fatigue and dependent oedema. A diagnosis of HF carries a poor prognosis – figures based on the Scottish population in 1991 gave a 5-year survival rate of 25% after a first admission with the condition (Stewart *et al.*, 2001), and a later study showed that for those over the age of 65, two thirds would die within 3 years (Cleland *et al.*, 1999).

To make the diagnosis of heart failure, clinical symptoms and signs should be accompanied by objective evidence of cardiac dysfunction (e.g. on echocardiography or radionuclide studies; Task force for the diagnosis and treatment of chronic heart failure, 2001). In cases where diagnostic doubt exists, then response to appropriate treatment can be taken into consideration. The typical finding on imaging studies is of impaired left ventricular (LV) function, although it is recognised that the clinical syndrome of heart failure can exist in the presence of preserved LV function. In the latter case, symptoms may be secondary to impaired LV relaxation / filling during diastole, and the condition has been termed "diastolic dysfunction". Some controversy still exists regarding the diagnosis and the treatment of patients who are felt to have this condition (reviewed in Zile & Brutsaert, 2002).

1.1.2 Aetiology of heart failure

It is important to realise that "heart failure" should not be regarded as a final diagnosis – the underlying cause of the condition should also be sought. This is critical for tailoring appropriate treatment and can have a bearing on estimating prognosis. In the Western world, heart failure is most commonly due to coronary artery disease, where LV dysfunction (LVD) is a consequence of myocardial ischaemia and/or infarction (McMurray & Stewart, 2000). This may be accompanied by changes secondary to hypertension. Other aetiological factors include valvular heart disease, cardiomyopathies and arrhythmias. Of course, a number of these factors may coexist, and can be additive in producing heart failure. The importance of coronary disease in the aetiology of HF is relevant when considering appropriate animal models to study the condition (reviewed further in Chapter 2).

1.1.3 Burden of heart failure

Numerous studies have examined the epidemiology of heart failure and the results are reviewed by McMurray & Stewart (2000). The reported overall prevalence of HF in the community is around 3-20/1000 population, with an annual incidence rate of around 1-4/1000. Such figures increase markedly with age, and the prevalence rate of symptomatic HF may exceed 10% in those aged over 65 years. With an ageing population and more patients surviving after myocardial infarction (MI), the burden of heart failure is increasing with time. This has significant implications for resource utilisation and healthcare expenditure, with over 5% of medical admissions being due to HF, and 1-2% of the overall healthcare budget being spent on the condition (McMurray & Stewart, 2000). These facts emphasise the ongoing need for studies into

the pathophysiology and treatment of HF, to reduce the individual and population impact of the condition.

1.2 Excitation-contraction coupling in cardiac myocytes

Before considering the cellular changes which occur in heart failure, it is worth briefly reviewing relevant aspects of cardiac myocyte physiology. The discussion below will emphasise the central role that calcium (Ca) plays in the cellular processes occurring during the cardiac cycle and it will be seen that altered Ca handling affects both contractile function and the propensity for arrhythmias.

1.2.1 Calcium entry & calcium-induced calcium release

Figure 1.1 summarises the events occurring during systole in the cardiac myocyte. During the cardiac action potential (AP), depolarisation of the cell membrane (sarcolemma) is rapidly carried deep into the cell via the transverse tubule (T-tubule) network, resulting in a coordinated opening of Ca channels (mainly L-type Ca channels, also known as dihydropyridine receptors, DHPRs). This allows Ca to enter the cell down its concentration gradient (around 2 mmol/L in the extracellular space compared to 80-250 nmol/L in the cytoplasm at rest; see Bers, 2001). This initial entry of Ca in turn leads to Ca release from its intracellular store, the sarcoplasmic reticulum (SR), *via* intracellular Ca release channels termed ryanodine receptors (RyRs, principally RyR isoform 2 in cardiac cells; see Fill & Copello, 2002). This process is known as Ca-induced Ca release (CICR) and leads to amplification of the initial Ca signal, such that a peak intracellular Ca concentration ($[Ca]_i$) of around 0.5-2 μmol/L is achieved. At this concentration, cytoplasmic Ca activates the myofilaments, causing contraction.

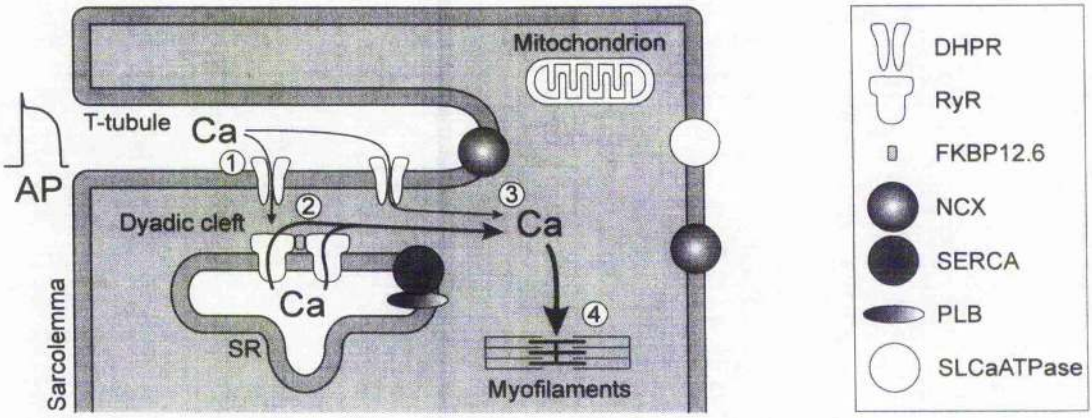

Figure 1.1 Ca entry and release in the cardiac myocyte. **1:** Depolarisation of the sarcolemma during the action potential (AP) causes opening of L-type Ca channels (DHPR) and entry of Ca down its concentration gradient. **2:** This activates clusters of ryanodine receptors (RyR), which are coupled by FKBP12.6 (see text), leading to release of Ca from the sarcoplasmic reticulum (SR). **3:** This amplifies the Ca signal and cytosolic Ca acts on the myofilaments to cause contraction (**4**). For other abbreviations see Figure 1.3.

1.2.2 Functional architecture of the dyadic cleft

The above brief outline mentions some of the critical players in the process of excitation-contraction (E-C) coupling, and the relationship between them is central to determining the characteristics of the systolic rise in $[Ca]_i$. The stage on which these events take place is the junctional, or dyadic, cleft – the space of around 10-15 nm between the sarcolemmal membrane (mainly at T-tubule sites) and the specialised junctional membrane of the SR (reviewed by Brette & Orchard, 2003; Weir & Balke, 1999; Fill & Copello, 2002). Evidence from recent studies suggests that the spatial arrangement of Ca channels and RyRs in this microdomain facilitates amplification of the Ca signal and allows a graded response to varying concentrations of trigger Ca. In

rabbit ventricular myocytes, each L-type Ca channel in the T-tubule membrane is associated with a cluster of around 4 RyRs (Milnes & MacLeod, 2001; Bers & Stiffel, 1993). The latter are large molecular complexes consisting of a tetramer of 564 kDa proteins, which display cooperative gating. In skeletal muscle there is evidence of a regular lattice-like array of RyR tetrads in the SR membrane, and in cardiac muscle a similar, although perhaps less strict, arrangement may be present (reviewed in Fill & Copello, 2002; Guatimosim *et al.*, 2002). This also has functional consequences – as discussed in section 1.2.3.2, there is evidence that coupling exists between adjacent tetrads (Marx *et al.*, 2001).

1.2.3 Regulation of RyR function

1.2.3.1 Luminal regulation by Ca

Ca is the principal activating ligand for the RyR on the cytoplasmic side of the SR membrane, but there is also evidence that the concentration of Ca *within* the SR affects the function of the channel. Early studies using RyR channels reconstituted into lipid bilayers showed that the channel open probability was dependent on luminal [Ca] in a voltage-dependent manner (Sitsapesan & Williams, 1994; Tripathy & Meissner, 1996). In similar studies, Györke & Györke confirmed the activating effects of Ca on the cytoplasmic side of the channel, demonstrating a bell-shaped dependence on [Ca], with inhibition of channel conductance at higher [Ca] (>~100 μmol/L; Györke & Györke, 1998). They then altered [Ca] on the luminal side of the channel, between 0.2-20 mmol/L, and showed that the open probability of the channel increased as [Ca] increased within this range. This appears to involve an allosteric site on the luminal side of the channel, rather than being due to an action on the cytoplasmic Ca binding site, since exposure to trypsin on the luminal side of the bilayers abolishes the effect

(Ching *et al.*, 2001). Other work has shown that luminal [Ca] has a similar effect on RyR function in intact ventricular myocytes (Lukyanenko *et al.*, 1996). Thus, altered SR Ca content, for example in heart failure, can have a direct effect on the functional properties of the RyR.

1.2.3.2 Phosphorylation of RyR and binding of FKBP

Several molecules associated with the RyR have been described, whose functions include stabilisation of the RyR structure and regulation of its activity. Marks' group have produced several papers documenting the association of various proteins with the RyR (see Marx *et al.*, 2000; reviewed in Marks *et al.*, 2002). These include protein kinase A (PKA) and protein phosphatases 1 & 2, which can alter the phosphorylation state of the RyR channel. Increased phosphorylation (e.g. through sympathetic stimulation) has been shown to activate the channel, increasing its sensitivity to [Ca]. Another molecule, one of the FK-506 binding proteins (FKBP12.6, in cardiac muscle), also associates with the RyR, with one molecule of FKBP12.6 able to bind to each subunit of the tetramer. FKBP12.6 appears to stabilise RyR gating and couple the gating of individual RyR tetramers with their neighbours, such that channel opening and closing can occur in a coordinated fashion during CICR (see Marx *et al.*, 2001; discussed below).

Marx *et al.* recorded single RyR channel activity under baseline conditions and with phosphorylation by PKA (Marx *et al.*, 2000). They demonstrated that phosphorylation of RyR markedly increased the open probability of the channel and also lead to the appearance of subconductance states, including long-lasting partially open states. The latter resembled previous findings when FKBP12.6 was dissociated from the RyR, and

Marx *et al.* concluded that hyperphosphorylation of the channel lead to loss of FKBP12.6, causing destabilised channel gating (Marx *et al.*, 2000). Under such conditions of increased Ca sensitivity, the channels would become "leaky", resulting in loss of Ca from the SR during diastole, depleting the pool of Ca available for contraction, and potentially being arrhythmogenic. Work by Prestle *et al.* is in support of this contention (Prestle *et al.*, 2001). They specifically overexpressed FKBP12.6 in rabbit ventricular myocytes using an adenoviral vector and demonstrated reduced RyR2-dependent Ca leak and increased SR Ca content. These changes were associated with increased fractional shortening. There remains some controversy as to the importance of altered FKBP12.6 binding *in vivo* and the role that it might play in heart failure (discussed in section 1.4.1.4).

1.2.3.3 Other proteins associated with RyR

Other proteins have been shown to co-localise and interact with RyR molecules, on each side of the SR membrane (see Fill & Copello, 2002; Bers, 2001 for reviews). Calmodulin binds on the cytoplasmic side and appears to have inhibitory effects on RyR2, although whether this is relevant at physiological [Ca] is unclear (Maier & Bers, 2002). Sorcin also appears to act on the cytoplasmic side of the SR membrane, and there is some evidence that it prolongs the RyR closed time and reduces burst frequency (discussed in Seidler *et al.*, 2003). On the luminal side of the membrane, calsequestrin, a high-capacity Ca-binding protein, can also affect RyR activity, although again its physiological role is yet to be clarified. Finally, the two luminal proteins junctin and triadin are also associated with the RyR, and there is some evidence that there is a Ca-sensitive interaction between these proteins, and also calsequestrin (discussed in Bers, 2001, Chapter 7).

1.2.3.4 Pharmacological manipulation of RyR function

A large number of pharmacological agents can be used to alter SR Ca release, as summarised by Bers (2001, Table 23) and reviewed by Eisner *et al.* (2000). One such compound used extensively in this thesis is the methylxanthine caffeine, whose effects are outlined in Chapter 5 (section 5.1.1).

1.2.4 "Local control" theory of CICR

The physical arrangement of channels and receptors in the dyadic cleft means that RyRs are placed to respond to changes in [Ca] within the small space between the T-tubule membrane and that of the SR (termed "fuzzy space" by Lederer *et al.*, 1990). There is increasing evidence that this is of critical importance in the normal process of CICR. This "local control" theory, where RyR senses [Ca] in the immediate environment of its subcellular compartment rather than the bulk cytoplasm, was first outlined by Stern (1992), and work since then has examined in detail the events involved in this process (reviewed by Weir & Balke, 1999; Bers, 2002; Guatimosim *et al.*, 2002). Current evidence suggests that Ca entry through one or two DHPR produces a sufficient local [Ca] to activate an adjacent cluster of RyRs. The resulting localised release of Ca has been termed a "spark" and was first visualised and described by Cheng *et al.* (1993). It was initially felt that a spark was due to release through a single RyR, but, as discussed in section 1.2.3.2, it now seems more likely that it is the result of the opening of a cluster of RyRs (perhaps 4-20). At resting diastolic [Ca], spontaneous sparks can be seen at a low rate within the cell, but this rate increases dramatically when Ca entry through DHPRs occurs. It has also been known for some time that under conditions of elevated SR Ca content, Ca sparks can activate neighbouring

clusters, causing a "wave" of Ca release to spread through the cell (Cheng *et al.*, 1996). Under these conditions, RyR [Ca] sensitivity may be increased so much (e.g. through activation by SR luminal [Ca]) that even resting diastolic [Ca] is sufficient to trigger a release. Similar events can also occur at normal levels of SR Ca content if RyR [Ca] sensitivity is abruptly increased by other means – e.g. through the application of caffeine (see section 5.1.1). Such spontaneous release events can generate arrhythmogenic inward currents and are discussed further in section 1.3.3.

Elegant, and technically demanding, experiments by Wang *et al.* demonstrated influx of Ca through single DHPRs, correlating local changes in [Ca] at the patch pipette with single I_{Ca} channel events (Wang *et al.*, 2001a). These events were termed "sparklets", and they further examined the relationship between these sparklets and RyR activity / sparks. Using a "loose-seal" configuration (where there is less deformation of the sarcolemma, and therefore a more preserved spatial relationship between DHPRs and RyRs than with a GΩ-seal) they showed that if I_{Ca} was blocked with nifedipine, or if Ca was substituted with Ba, then triggered sparks could not be activated. This provides evidence against the possibility of voltage-dependent Ca release (rather than CICR) in cardiac cells, which has been the subject of some debate (see Weir & Balke, 1999; Bers, 2001, Chapter 8; Piacentino III *et al.*, 2000 for discussion). In the absence of blockers, the latency between a sparklet and a spark was described well by a single exponential function with a time constant of 6.7 ms, and the coupling fidelity between a sparklet and a spark was around 0.71 – i.e. not all sparklets lead to activation of a RyR cluster. These properties suggest that the coupling relationship between DHPR and RyR is stochastic, or probabilistic, rather than deterministic. This fits well with the diffusion properties of the local microdomain and with coupled gating of RyRs.

Calculations by Bers based on the buffering and diffusion properties of the dyadic cleft suggest that within a 15 nm radius of the mouth of an open Ca channel there may be as little as one free Ca ion (and ~100 bound; Bers, 2001, Figure 118). Again, this fits with a stochastic DHPR-RyR relationship, and indeed, previous work has shown that a single Ca ion can be sufficient to activate the RyR complex (Fan & Palade, 1999).

1.2.4.1 Grading of CICR and "gain" of E-C coupling

There is an increasing acceptance that Ca sparks are the elementary events of SR Ca release, and that the cardiac action potential leads to a synchronised summation of several thousand such sparks through CICR, to produce the global Ca transient (see Guatimosim *et al.*, 2002). The properties of the system must be able to explain the graded nature of CICR, where changes in trigger [Ca] (amplitude or temporal properties), or pharmacological manipulation of the system, is reflected by altered SR Ca release. The details of how this comes about remain under some debate, as does the question of how a system with inherent positive feedback properties is limited from emptying the SR of Ca through a regenerative process. One factor contributing to both these issues may be the physical separation of RyR clusters, such that if trigger [Ca] is low then a sufficient concentration to activate RyR opening may only occur at the adjacent cluster. The rapid fall in [Ca] away from the mouth of the DHPR would prevent activation of neighbouring clusters, and would similarly limit Ca release from one RyR cluster from spreading to activate the next. Higher trigger [Ca] could recruit more clusters, leading to a larger overall Ca release. This is depicted in Figure 1.2, along with some other possible methods for producing a graded response. These different theoretical ways of altering SR Ca release are by no means mutually exclusive, and several may act in concert under physiological conditions. These factors

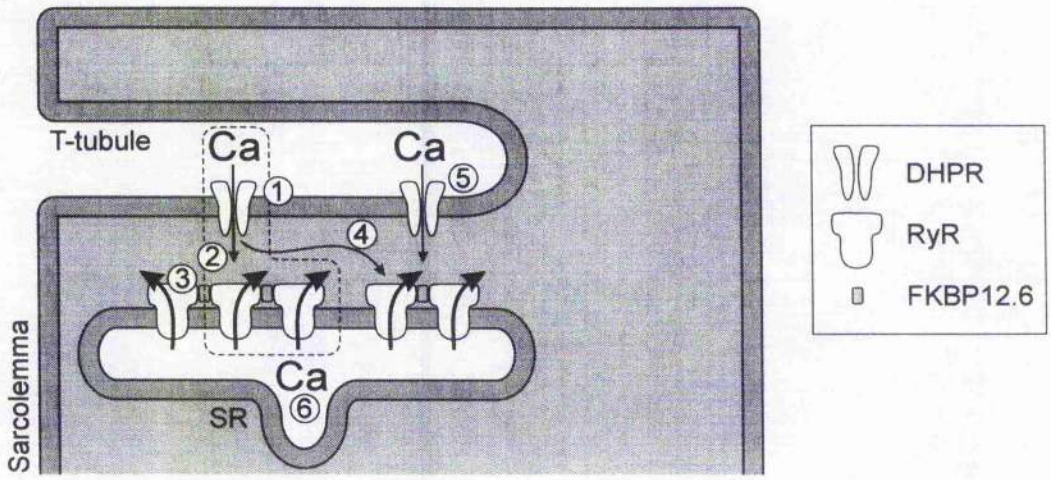

Figure 1.2 Potential mechanisms for grading of CICR. **1:** Baseline situation (outlined) where, for the purposes of illustration, a single DHPR causes opening of a coupled cluster of 2 RyRs. To achieve a graded response of CICR to increasing trigger Ca, a number of possibilities can be considered. **2:** Increased coupling fidelity, or increased RyR sensitivity to [Ca]. **3:** Recruitment of RyRs within a cluster. **4:** Recruitment of adjacent clusters. **5:** Recruitment of additional DHPRs or altered DHPR properties, e.g. reduced Ca-dependent inactivation. **6:** Increased SR Ca content (causing increased SR-cytoplasm Ca gradient and also activation of RyR by raised luminal [Ca]). Several mechanisms may act in concert to bring about the observed effect (discussed further in text). For abbreviations see Figure 1.1.

are also relevant when considering the situation in heart failure, where E-C coupling efficiency is often reduced (see sections 1.4.1.5 & 4.4.5).

The efficiency of E-C coupling is often expressed as the "gain" of the system. This compares the size of the "response" (SR Ca release) with that of the trigger (I_{Ca} flux) to give an amplification factor. Technical aspects of this calculation are outlined in section 4.3.6. Given the importance of SR Ca content in determining the magnitude of

Ca release, it is not surprising that E-C coupling gain is heavily dependent on this factor (e.g. Bassani *et al.*, 1995; Janczewski *et al.*, 1995). Shannon *et al.* studied this relationship in rabbit ventricular myocytes, along with the related measure of SR fractional release (Shannon *et al.*, 2000). They demonstrated that E-C coupling gain showed a non-linear dependence on SR content, with an increasingly steep relationship at higher SR loads. This implies some effect on the release process itself, rather than simply being due to increased Ca available for release (and increased SR-cytoplasm [Ca] gradient). This is in keeping with studies demonstrating regulation of RyR function by luminal [Ca] (see section 1.2.3.1).

1.2.4.2 Termination of SR Ca release

The local environment around a cluster of RyRs, and the properties of the receptors themselves, seem important in terminating the potentially regenerative process of CICR. A number of different mechanisms have been proposed, including local depletion of SR Ca, inactivation or adaptation of RyR, and "stochastic attrition" (Stern, 1992), the chance simultaneous closure of both DHPR and RyR interrupting the process of release. It seems unlikely that depletion of SR Ca is the only mechanism involved, since significant Ca stores still remain after SR release (Varro *et al.*, 1993; Negretti *et al.*, 1995; Bassani *et al.*, 1995), and long-lasting sparks can be demonstrated (Cheng *et al.*, 1993). Stochastic attrition may occur to some extent, but does not appear to be a robust enough method alone to terminate SR Ca release when a cluster of several RyRs is present (discussed by Sobie *et al.*, 2002).

The work of Wang *et al.* contributed some information to the debate (Wang *et al.*, 2001a). They examined the coupling latency between consecutive sparklets (DHPR Ca

fluxes) and resulting triggered sparks. They showed that if the first sparklet did *not* trigger a spark then the coupling latency for the subsequent sparklet was unchanged, however if the first sparklet *did* trigger a spark then the coupling latency was reduced for the second sparklet. This suggests some form of use-dependent inactivation or adaptation of the RyR cluster. This is also supported by experiments examining the collision characteristics of intracellular Ca waves. These studies have shown that when two waves meet they annihilate each other, suggesting a refractory period in the wake of each wave (e.g. Ishide *et al.*, 1990). Such mechanisms are discussed in detail by Fill & Copello (2002) and Bers (2001, 2002).

Sobie *et al.* devised a mathematical model of spark generation and termination, which included recent findings regarding RyR function and accounts for a number of experimental observations (Sobie *et al.*, 2002). They used the term "sticky cluster" to describe the behaviour of a number of coupled RyRs, with a cooperativity factor incorporated into the equations. When this was combined with the stochastic properties of individual RyR tetramers and modelling of [Ca] in the microdomain of both the dyadic cleft and the local junctional SR, the simulation matched experimentally observed spark behaviour well. It was also possible to mimic the effects of altered RyR coupling, as might be seen with changes in FKBP12.6.

1.3 Calcium removal mechanisms

During the diastolic period, the calcium released into the cytoplasm to cause contraction must be removed from the cell or re-sequestered into the SR. This enables relaxation of the cell and filling of the cardiac chambers. Several mechanisms allow this to take place (see Figure 1.3), the two main ones being the sodium-calcium

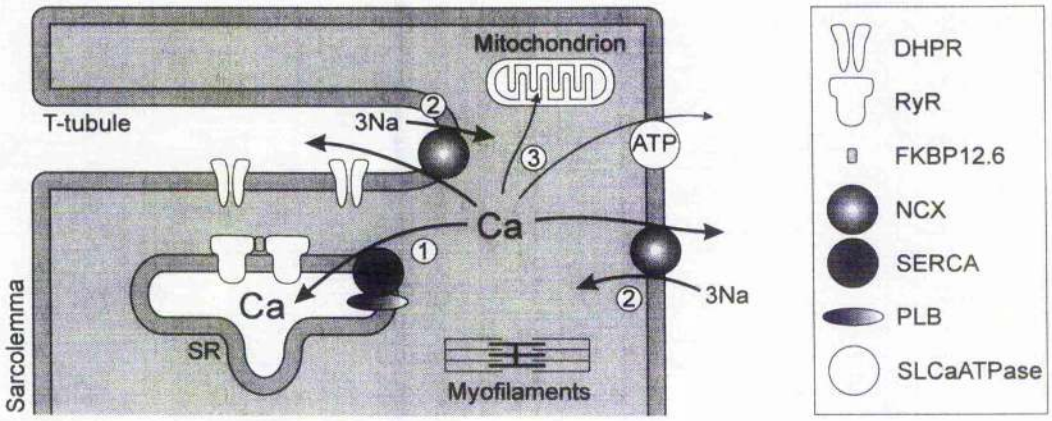

Figure 1.3 Removal of cytoplasmic Ca. **1:** Ca is actively resequestered into the SR by the sarco(endo)plasmic reticulum Ca-ATPase (SERCA), which is modulated by phospholamban (PLB). **2:** The sodium-calcium exchanger (NCX) leads to Ca efflux from the cell, utilising the transsarcolemmal [Na] gradient. NCX appears to be present on the cell surface as well as in the T-tubules (discussed in text). **3:** "Slow pathways" also operate, including the sarcolemmal Ca ATPase (SLCaATPase) and uptake *via* the mitochondrial uniporter. For other abbreviations see Figure 1.1.

exchanger (NCX), which utilises the Na gradient to remove Ca from the cell, and the sarco(endo)plasmic reticulum Ca-ATPase (SERCA), which actively pumps Ca back into the SR. Given their importance to normal Ca handling, and the role they play in heart failure, these two mechanisms will be discussed in more detail.

1.3.1 Sodium-calcium exchanger

1.3.1.1 Discovery

It has been known for over 50 years that the relationship between the concentrations of external Ca and Na has significant effects on the function of cardiac tissue (Wilbrandt & Koller, 1948), and it was demonstrated in 1958 that depletion of extracellular Na could bring about contraction of frogs' hearts (Lüttgau & Niedergerke, 1958). Further

work on cardiac, skeletal and smooth muscle demonstrated that changes in intracellular [Ca] could be brought about by manipulating external [Na] (Niedergerke, 1963; Cosmos & Harris, 1961; Briggs & Melvin, 1961; Goodford, 1967). Reuter and Seitz, in 1968, were the first to demonstrate that the efflux of Ca from mammalian cardiac muscle was dependent on the external concentrations of Na and Ca (Reuter & Seitz, 1968). They measured the rate of loss of ^{45}Ca from guinea-pig, sheep and calf cardiac tissue in the presence of external solutions with varying ionic composition and postulated the presence of a transport mechanism "very effective in reducing the intracellular Ca concentration ... without metabolic energy consumption". Subsequent experiments showed that intracellular [Na] also influenced Ca fluxes (Glitsch *et al.*, 1970), providing further evidence for a Na-Ca exchanger mechanism. Around the same time, such mechanisms were also reported in invertebrate neurones (Baker *et al.*, 1967; Baker & Blaustein, 1968; Blaustein & Hodgkin, 1969) and rat small intestine (Martin & DeLuca, 1969). Since then there has been considerable research on the structure, mechanism of action, distribution and physiological role of the sodium-calcium exchanger.

1.3.1.2 Structure, molecular aspects and tissue distribution

NCX was first cloned in 1990 from the cardiac sarcolemma (NCX1, Nicoll *et al.*, 1990) and since then two other mammalian isoforms have been found (NCX2 & NCX3). Recent modelling of NCX1 suggests that the final protein consists of 938 amino acids, with 9 transmembrane domains and a large intracellular loop with important regulatory functions and a site where alternative splicing can occur (Nicoll *et al.*, 1999; reviewed in Philipson & Nicoll, 2000). Mammalian NCX shows marked sequence homology across several species and cDNA probes derived from the human exchanger have been

used to study the tissue distribution of NCX1 in humans and rats (Kofuji *et al.*, 1992). Such studies, and others, have determined that NCX1 is present at high levels in heart and brain, with reduced expression in all other tissues tested. NCX2 and NCX3, however, have a more limited distribution, e.g. found in brain but not heart (reviewed by Shigekawa & Iwamoto, 2001; Blaustein & Lederer, 1999).

1.3.1.3 Distribution of NCX in cardiac cells

Immunofluorescence studies in cardiac myocytes have shown that NCX is located throughout the external surface of the cell, including within the T-tubules, but there is some debate regarding its relative distribution. Kieval *et al.* showed a relatively uniform distribution (Kieval *et al.*, 1992). Frank *et al.* reported only patchy labelling of the peripheral membrane in guinea-pig and rat, with staining concentrated in the T-tubules (Frank *et al.*, 1992), however a later study in rabbits showed a more even distribution (Chen *et al.*, 1995). A quantitative analysis suggested that in guinea-pig ventricular myocytes 52-55% of NCX has an intracellular (presumed T-tubule) location (McDonald *et al.*, 2000).

A recent paper by Yang *et al.* made a functional assessment of NCX activity in rat ventricular cells which were detubulated by osmotic shock with formamide (Yang *et al.*, 2002). The results showed that detubulation reduced cell capacitance by around one third, consistent with loss of T-tubule area, and this was accompanied by an almost complete loss of NCX current. These effects were not seen in atrial cells, which lack T-tubule structure, and suggest that in ventricular cells NCX function is localised almost entirely to the T-tubules.

1.3.1.4 Kinetics of NCX: stoichiometry

In early studies on squid giant axon, Blaustein & Hodgkin suggested that to maintain the gradient of $[Ca]_i$:$[Ca]_o$, the exchange of two Na ions for each Ca ion would be insufficient, but an exchange of 3Na:1Ca would theoretically suffice, and this was supported by their experiments (Blaustein & Hodgkin, 1969; Baker *et al.*, 1967). Early studies by Pitts on cardiac sarcolemmal vesicles examining the influx or efflux of Ca and Na radioisotopes suggested that 3 Na were exchanged for every one Ca (Pitts, 1979). Reeves & Hale confirmed this finding in a series of elegant experiments (Reeves & Hale, 1984). Studies on ventricular tissue and Purkinje fibres reported a stoichiometry in the range 2.4-≥3 Na:1Ca (Bers & Ellis, 1982; Sheu & Fozzard, 1985). Axelsen & Bridge re-interpreted the data of Sheu & Fozzard and, using thermodynamic considerations taking account of Ca leak across the membrane, suggested that the stoichiometry was close to 3Na:1Ca (Axelsen & Bridge, 1985). Using whole perfused rabbit hearts Axelsen & Bassingthwaighte concluded that the stoichiometry was 3:1, and could not be ≥ 4:1 (Axelsen & Bassingthwaighte, 1988). In a comprehensive set of experiments on single guinea-pig ventricular cells, Noma and co-workers also found a 3Na:1Ca exchange (Kimura *et al.*, 1986; Kimura *et al.*, 1987; Ehara *et al.*, 1989), as have other investigators (Wakabayashi & Goshima, 1981; Crespo *et al.*, 1990).

In an interesting recent paper, Fujioka *et al.* have reported a stoichiometry of around 4Na:1Ca, with some variation in the relationship when intracellular [Na] and [Ca] were altered (Fujioka *et al.*, 2000). Their experiments were performed on large "inside-out" excised patches from guinea-pig ventricular cells, allowing tight control of ionic conditions on either side of the patch – an important consideration, since relatively small changes in [Na] or [Ca] close to the membrane can have large effects on the

apparent kinetics of the exchanger. It should be noted that many of their conclusions are based on membrane patches pre-treated with trypsin to prevent Na_i-dependent inactivation of the current. They did not feel that trypsin treatment significantly altered their results, but examination of their data shows that the stoichiometry obtained from non-treated patches was generally less than that obtained from treated ones, and in particular at physiological levels for resting $[Na]_i$ it was closer to 3:1. In non-cardiac forms of NCX, stoichiometries of 4:1 have been established and in some cases K is co-transported with Ca (reviewed in Blaustein & Lederer, 1999). However, the weight of evidence on cardiac NCX, gathered under many different experimental conditions, supports an exchange of around 3 Na for each Ca. Potassium does not appear to be co-transported in cardiac NCX (Crespo *et al.*, 1990; Yasui & Kimura, 1990).

1.3.1.5 Kinetics of NCX: electrogenicity & reversal potential

With a stoichiometry for the exchanger of 3Na:1Ca, if Na and Ca are the only ions transported then the pump will be electrogenic, with a net gain of one positive charge for each Ca ion extruded. Early voltage clamp experiments in intact cells did show hyperpolarisation induced by removal of external Na (Coraboeuf *et al.*, 1981), a transient inward current on repolarisation (I_{ti}; Kass *et al.*, 1978) and a current on application of caffeine (Clusin *et al.*, 1983b; Clusin, 1983). However it was difficult to conclude that these currents were unequivocally due to NCX due to the possibility of contaminating currents and the lack of specific blockers (reviewed in Eisner & Lederer, 1985).

Two reports in the same issue of *Nature* in 1986 gave more definitive evidence of NCX currents. Kimura *et al.* used voltage ramp protocols with other significant currents

blocked, and altered internal and external [Na] and [Ca] (Kimura *et al.*, 1986; see also Kimura *et al.*, 1987). They showed that the currents obtained depended on the ion gradients and also the membrane potential in a manner predicted for NCX. Mechmann & Pott showed that Ca release from the SR (either spontaneous or induced by caffeine) generates an inward current which is consistent with NCX (Mechmann & Pott, 1986), see section 1.3.3.1. Since then, with refinements in experimental technique and acceptance that the stoichiometry of the exchanger is around 3:1, it has been established that the exchanger is electrogenic.

Studies have determined that operation of the sodium-calcium exchanger is bi-directional – depending on conditions it can either extrude calcium from the cell ("forward mode") or bring calcium in ("reverse mode"). Thermodynamic considerations dictate that the direction in which the exchanger operates will depend on the gradients of [Na] and [Ca] and also on the membrane potential. Assuming a stoichiometry of 3Na:1Ca, the equilibrium potential of NCX, $E_{Na,Ca}$, can be derived from the equation:

$$E_{Na,Ca} = 3\,E_{Na} - 2\,E_{Ca} \qquad \textbf{Equation 1.1}$$

where E_{Na} and E_{Ca} are the equilibrium potentials for Na and Ca calculated using the Nernst equation. At 37 °C, with physiological concentrations of ions ($[Na]_i$ = 10 mmol/L, $[Na]_o$ = 140 mmol/L, $[Ca]_i$ = 100 nmol/L, $[Ca]_o$ = 1.8 mmol/L), $E_{Na,Ca}$ will be around -49 mV.

1.3.2 Physiological role of NCX in the heart

1.3.2.1 Calcium extrusion & inward NCX current

In resting cardiac cells, the membrane potential (E_m, around -80 mV), is negative to $E_{Na.Ca}$ and extrusion of Ca will be favoured. Studies have shown that under physiological conditions, NCX plays a crucial role in the extrusion of Ca from the cell (e.g. Bers & Bridge, 1989; Crespo *et al.*, 1990). Under steady-state conditions, the amount of Ca entering the cell, principally via L-type calcium channels, must be removed during the diastolic period. This is mainly brought about by NCX, with a small contribution from the sarcolemmal Ca ATPase (Bridge *et al.*, 1990). The relative contribution of different systems in the removal of Ca from the cytoplasm is discussed in more detail in sections 1.3.6 & 4.4.6.

The inward current generated by Ca extrusion may have a significant effect on the shape of the cardiac AP. In conditions where I_{NCX} is blocked, or $[Ca]_i$ is buffered, the AP plateau and duration are much reduced (Janvier *et al.*, 1997a; reviewed in Janvier & Boyett, 1996). Computer modelling also supports a role for inward I_{NCX} in maintaining the AP plateau (Noble *et al.*, 1991). Recovery of inward I_{NCX} may also contribute to the time course of electrical restitution (Janvier *et al.*, 1997b).

1.3.2.2 Reverse-mode I_{NCX} during the action potential

Determining NCX function during the cardiac AP is complicated, given the simultaneous changes in membrane potential, $[Na]_i$ and $[Ca]_i$. In theory, during the early part of the AP where the membrane potential is positive, subsarcolemmal $[Na]_i$ is elevated and $[Ca]_i$ has yet to peak, conditions favour Ca entry via reverse-mode NCX.

There has been considerable debate in the literature as to whether reverse-mode NCX can trigger significant Ca release from the SR. In a study of rabbit ventricular myocytes, Litwin *et al.* provided evidence of putative reverse-mode I_{NCX} (sensitive to voltage, $[Na]_i$, $[Ca]_o$ and nickel) with other significant currents blocked (Litwin *et al.*, 1998). Separate experiments showed that the gain of SR Ca release was also dependent on voltage and $[Na]_i$, as predicted if reverse-mode NCX was contributing to CICR. A previous paper from Bridge's group also suggested that significant Ca entry could occur on reverse-mode NCX and that this could trigger SR release (Levi *et al.*, 1994), and similar findings have been reported elsewhere (Wasserstrom & Vites, 1996; Lipp & Niggli, 1994; Leblanc & Hume, 1990). Experiments such as these have supported the presence of a restricted ("fuzzy") space beneath the sarcolemma where ion concentrations much higher than those in the bulk cytoplasm can be achieved (Lederer *et al.*, 1990).

Using an action potential clamp, Grantham & Cannell suggested that Ca influx via NCX was less than 30% of that via I_{Ca}, but may be enough to contribute to CICR (Grantham & Cannell, 1996). Subsequent experiments by the same group failed to show significant Ca influx or release due to reverse-mode NCX when I_{Ca} was blocked (Evans & Cannell, 1997). Furthermore, they suggested that in other published work supporting a contribution of reverse-mode NCX to E-C coupling, failure of adequate voltage control over the cell (due to large I_{Na} currents), particularly within the dyadic clefts, might have allowed activation of I_{Ca}. Sham et al. reported similar results and conclusions (Sham *et al.*, 1992).

Sipido *et al.* showed that Ca entry via NCX could trigger SR Ca release, but with low trigger efficiency and only after a significant delay (Sipido *et al.*, 1997). In the presence of I_{Ca} they could not detect a contribution of reverse-mode NCX to CICR at potentials below +60 mV. Thermodynamic constraints and modelling of the dyadic cleft also suggest that reverse-mode NCX is unlikely to be a significant trigger under physiological conditions (Cannell *et al.*, 1996).

Weber *et al.* recently presented an elegant approach to the problem (Weber *et al.*, 2002). Since I_{NCX} will depend on submembrane (SM) [Ca], rather than bulk cytoplasmic [Ca], they derived a method for inferring $[Ca]_{SM}$ from I_{NCX} under controlled conditions. They then used this relationship to calculate $[Ca]_{SM}$ at different times in the AP, using an interrupted AP clamp. This demonstrated that $[Ca]_{SM}$ is significantly higher than bulk [Ca] (peak of 3-4 μmol/L in their Figure 4) until repolarisation has occurred and bulk [Ca] is decaying. I_{NCX} during the AP could then be modelled, based on $[Ca]_{SM}$, and this suggested that very little reverse mode NCX occurred during the AP (perhaps only for the initial 19 ms of their 250 ms AP). Similar findings were obtained in non-failing human cardiac myocytes, however a greater contribution from reverse-mode NCX was found in failing human myocytes (Weber *et al.*, 2003).

1.3.3 Role of NCX *in arrhythmogenesis*

Two aspects of NCX function have raised interest in the fact that it could contribute to arrhythmic events: 1) the current it carries can potentially depolarise the membrane and if this depolarisation is sufficiently large it could trigger an action potential; 2) NCX activity can influence the amount of calcium in the SR and calcium overload is known

to predispose to arrhythmias (Clusin *et al.*, 1983a). There is increasing evidence that NCX does indeed play a role in arrhythmogenesis, in particular it has been implicated in the phenomenon of "afterdepolarisations". These are abnormal depolarisations occurring during or after the AP. Those occurring after the cell has fully repolarised are termed delayed afterdepolarisations (DADs), while those occurring during the plateau or repolarisation phases of the AP are known as early afterdepolarisations (EADs; Cranefield, 1975).

1.3.3.1 Delayed afterdepolarisations

It has been known for some time that manoeuvres which increase cellular Ca loading (e.g. cardiac glycosides or β-adrenergic stimulation) can lead to the appearance of DADs (see January & Fozzard, 1988 for review of early studies). Under voltage clamp conditions it was shown that these events were due to a transient inward current (I_{ti}), and three potential charge-carriers were suggested: I_{NCX}, a Ca-activated chloride current ($I_{Cl(Ca)}$), and a Ca-activated non-specific cation current ($I_{ns(Ca)}$). It was also realised that DADs were correlated with the intracellular release of Ca from the SR (either spontaneous or induced by caffeine application), and that if SR function was disabled (e.g. with ryanodine) or if $[Ca]_i$ was heavily buffered, then they did not occur (Marbán *et al.*, 1986). Early studies with imaging cameras (Miura *et al.*, 1993) or by analysis of sarcomere length (Capogrossi *et al.*, 1987) showed that these release events tended to spread as waves through the cell. With the advent of modern fluorescence imaging techniques, such as confocal microscopy, it has been possible to examine in detail the subcellular events which occur during spontaneous Ca release (e.g. Cordeiro *et al.*, 2001). Such studies have shown spatially heterogeneous Ca release events at the

periphery of the cell, which could propagate as waves and were accompanied by I_{ti} and, at times, triggered action potentials.

The current responsible for I_{ti} has been extensively investigated (reviewed by January & Fozzard, 1988; Schlotthauer & Bers, 2000; Bers, 2001). $I_{ns(Ca)}$ appears to have an insignificant role in most preparations studied, and the relative importance of I_{NCX} and $I_{Cl(Ca)}$ seems to vary depending on the species and origin of the myocytes used (atrial, ventricular or Purkinje cells). Both I_{NCX} and $I_{Cl(Ca)}$ were shown to contribute to I_{ti} in canine (Zygmunt *et al.*, 1998) and sheep (Verkerk *et al.*, 2000) myocytes. In rat cells I_{NCX} accounted for the majority of the current in control cells, but there was a greater contribution from $I_{Cl(Ca)}$ in hypertrophied myocytes (Mészáros *et al.*, 2001). In rabbit ventricular myocytes, Schlotthauer & Bers found that I_{ti} was almost eliminated by removal of external Na, or in the presence of Ni (to block NCX), but was changed little by blocking $I_{Cl(Ca)}$ with niflumic acid (Schlotthauer & Bers, 2000). They estimated that I_{NCX} accounted for >90% of I_{ti}.

Thus, NCX plays a central role in the genesis of DADs and has therefore been implicated in triggered arrhythmias, such as the non-reentrant initiation of ventricular tachycardia (VT; January & Fozzard, 1988; Pogwizd *et al.*, 1999; Pogwizd *et al.*, 2001; Schillinger *et al.*, 2002). Additional factors which have been shown to be relevant in arrhythmogenesis include the SR Ca content, other currents which tend to stabilise E_m (e.g. the inward rectifier potassium current, I_{K1}), the profile of I_{ti} (rapid or slow change in current; Pogwizd *et al.*, 2001), and diastolic [Ca] (Baartscheer *et al.*, 2003; Edgell *et al.*, 2000) and [Na] (Díaz *et al.*, 1996; reviewed by Bers, 2001). Arrhythmogenesis in heart failure is discussed further in section 3.4.

When considering the causes of arrhythmias *in* vivo, it should also be remembered that changes at the single cell level must be related to the situation in the 3-dimensional syncytium of cells that exists in the heart. Neighbouring cells can act as current "sinks", reducing the effect, for example, of spontaneous Ca release in one cell. Thus, it may require simultaneous events in several cells for an arrhythmogenic afterdepolarisation to lead to a triggered arrhythmia (see Schlotthauer & Bers, 2000; Bers, 2001, Chapter 10).

1.3.3.2 Early afterdepolarisations

EADs tend to occur in situations where the AP is prolonged, and in a clinical context this would correspond to a prolongation of the QT interval, as seen in congenital or acquired long-QT syndromes. Patients with such conditions are prone to episodes of polymorphic VT ("torsade de pointes"), and EADs are implicated in this phenomenon. Volders *et al.* recently reviewed the literature on EADs, and the theories regarding which ionic currents are involved (Volders *et al.*, 2000). During the appropriate voltage "window" of the AP plateau and initial repolarising phase, sodium currents (I_{Na}) and L-type Ca currents (I_{CaL}) may be reactivated when a long AP has allowed sufficient recovery from channel inactivation (see Marbán *et al.*, 1986; Volders *et al.*, 2000). This can cause significant depolarisation of the membrane and triggering of a further arrhythmogenic AP. Beyond this phase, late EADs appear to be caused by a similar mechanism to DADs, i.e. through spontaneous release of Ca from the SR, with resulting inward currents (see Szabo *et al.*, 1995; Ming *et al.*, 1994). Thus, I_{NCX} has also been implicated in EADs. Volders *et al.* postulated a further role for I_{NCX}, in that it

provides inward current during the normal AP, which can prolong the plateau phase, making the reactivation of "window currents" more likely (Volders *et al.*, 2000).

1.3.4 Regulation of NCX

Calcium, as well as being one of the ions transported by NCX, also has an important role in the regulation of NCX function. In the presence of low internal [Ca], I_{NCX} will inactivate, even when conditions otherwise favour ion transport (Miura & Kimura, 1989). Thus, Ca appears to contribute to allosteric regulation of I_{NCX}, and molecular studies have identified a site on the large cytoplasmic loop of the molecule where this may take place (Levitsky *et al.*, 1994; Matsuoka *et al.*, 1995). This site binds Ca cooperatively with a Hill coefficient of between 1.6 (Fang *et al.*, 1998) and ~2 (Levitsky *et al.*, 1994). Early studies suggested that the exchanger may be fully activated at relatively low $[Ca]_i$ (e.g. Miura & Kimura, 1989), however later experiments using giant excised patches have suggested that the K_m for Ca activation (K_{mCaAct}) may lie within a physiologically-relevant range e.g. 300-600 nmol/L (Hilgemann *et al.*, 1992), ~400 nmol/L (Matsuoka *et al.*, 1995). Reeves & Condrescu expressed NCX1 in Chinese hamster ovary cells and obtained a K_{mCaAct} of ~300 nmol/L (Reeves & Condrescu, 2003). Interestingly, the activated state of the exchanger induced by Ca persisted for tens of seconds after subsequent removal of Ca and it was proposed that this was due to a lasting conformational change and/or a persisting local elevation in Ca. It is likely that the local environment and regulation of NCX is substantially different in intact ventricular myocytes and this phenomenon has not been reported.

Recently, Weber *et al.* demonstrated allosteric regulation of I_{NCX} in intact cardiac myocytes, by showing $[Ca]_i$-dependent increases in outward I_{NCX} (Weber *et al.*, 2001). They used a simple voltage protocol to produce alternating inward and outward I_{NCX}, whilst allowing control of $[Ca]_i$. For each voltage step, mean I_{NCX} was plotted against mean $[Ca]_i$ and the resulting data-points were fitted using a model of NCX function to derive a value for K_{mCaAct}. In ferret ventricular myocytes, they obtained a K_{mCaAct} of 125 ± 16 nmol/L. This implies that allosteric regulation of NCX by Ca could occur within the range of [Ca] seen on a beat-to-beat basis. In wild-type mouse ventricular myocytes, however, no appreciable allosteric regulation was observed. They were able to restore Ca activation by overexpressing canine NCX in mouse myocytes, and showed that if there was a mutation in the Ca regulatory domain (Δ680-685) then allosteric regulation was no longer conferred.

In a later paper, Weber *et al.* examined allosteric regulation in failing and non-failing human myocytes and found a similar K_{mCaAct} for both (150 ± 31 nmol/L; Weber *et al.*, 2003). In this thesis, allosteric regulation of I_{NCX} was examined in ventricular myocytes from control rabbits and those exhibiting LV dysfunction. The voltage protocol employed was similar to that used by Weber *et al.* and further details are given in Chapter 3.

1.3.5 Uptake of Ca into the SR

1.3.5.1 SERCA structure, distribution & kinetics

SERCA proteins are members of the Mg-dependent P-type ATPase family, and are encoded by three different genes, displaying significant sequence homology (MacLennan *et al.*, 1997). Overall, SERCA has a widespread distribution in excitable

and non-excitable cells, functioning to remove Ca actively from the cytoplasm against its concentration gradient. Particular SERCA isoforms are tissue specific, with SERCA1a found in adult fast-twitch skeletal muscle (replacing SERCA1b from foetal/neonatal tissues), SERCA2a found in the heart, and SERCA2b & 3 expressed more ubiquitously in non-muscle tissues (reviewed by Periasamy & Huke, 2001; MacLennan *et al.*, 1997).

SERCA2a is a 105 kDa protein consisting of a large cytoplasmic "head" (containing the nucleotide binding domain and phosphorylation site) connected by a "stalk" to the transmembrane and luminal domains. Hydrolysis of ATP appears to bring about a conformational change in the structure of SERCA, such that two Ca ions bound to the transmembrane domain are discharged into the SR lumen for each molecule of ATP consumed (MacLennan *et al.*, 1997). There is some variation in the reported K_m of the SERCA pump for [Ca], which in part may be due to differences in the techniques used for its estimation. A reasonable estimate would be in the range of around 300 – 650 nmol/L, with a Hill coefficient of 1.6 – 1.7 (see Movsesian & Schwinger, 1998; Bers, 2001, Chapter 7). Thus, the K_m appears to be within the physiological range of cytoplasmic [Ca], and any shift in K_m through regulation of the pump can have significant effects on Ca uptake. The turnover rate for each SERCA2a pump has been estimated to be around 10-15 Ca ions/s, and the SERCA pumps are present in the cell at a concentration of around 14 – 100 μmol/L cytosol (see Levitsky *et al.*, 1981; Bers, 2001, Chapter 7). The expression level of SERCA appears to be critical for normal contractile function in the heart, since it contributes significantly to diastolic relaxation and replenishes the SR Ca stores for the next systole (Periasamy & Huke, 2001). The

relationship between SERCA function and SR Ca content is discussed further in Chapter 4, sections 4.4.2 & 4.4.3.

1.3.5.2 Regulation of SERCA2a

In the heart, SERCA2a is tightly regulated by the homopentameric phosphoprotein phospholamban (PLB), which has a total molecular weight of around 22 kDa (Frank *et al.*, 2003; Movsesian & Schwinger, 1998). PLB is present at a concentration of around 2 – 2.5 PLB monomers per SERCA molecule (Colyer & Wang, 1991) and acts as an inhibitor of SERCA function, increasing the K_d for [Ca], with little change in the V_{Max} (reviewed by Frank *et al.*, 2003). The regulatory action of PLB can have important implications for contractile function. Sato *et al.* demonstrated that knockout of PLB could reverse some of the abnormalities of CICR and Ca handling which occur when calsequestrin is overexpressed in mice (Sato *et al.*, 2001).

Phospholamban itself can be phosphorylated at three sites – by PKA, Ca-activated phospholipid-dependent protein kinase C (PKC), and Ca / calmodulin-dependent protein kinase II (CaMKII). PKA phosphorylation blocks the interaction of PLB with SERCA, shifting the K_d for [Ca] to the left and restoring function (see Colyer & Wang, 1991; Frank *et al.*, 2003; Rapundalo, 1998). CaMKII phosphorylation also lowers the K_d for [Ca] of SERCA, and may also increase the V_{Max} (see Frank *et al.*, 2003). CaMKII may also be able to directly phosphorylate SERCA and RyR, altering their activity (Wehrens *et al.*, 2004; reviewed by Bers, 2001). The functional significance of PLB phosphorylation by PKC *in vivo* is unclear.

1.3.6 Other mechanisms for removal of cytosolic Ca

NCX and SERCA are the main mechanisms by which Ca is removed from the cytoplasm during systole. A lesser role is played by the sarcolemmal Ca-ATPase (another P-type ATPase) and uptake of Ca into other organelles, for example *via* the mitochondrial uniporter. These other removal mechanisms are often referred to as the "slow systems". The relative contribution of the different removal systems to the decline in Ca during a twitch or caffeine application has been extensively investigated by Bassani and co-workers (e.g. Bassani *et al.*, 1992; Puglisi *et al.*, 1996; Bassani *et al.*, 1994). They used selective block of each system and determined the change in the time-course of Ca decline or myocyte relaxation. From such experiments they concluded that the slow systems were responsible for 1-3% of Ca removal during a twitch, depending on the species studied (rabbit or rat) and the experimental conditions. Negretti *et al.* found a similar contribution from the slow systems in the rat, with 1.7% of removal attributed to mitochondrial uptake and 2.6% to the sarcolemmal Ca-ATPase (Negretti *et al.*, 1993). Choi & Eisner also examined the role of the sarcolemmal Ca-ATPase in rat cells (Choi & Eisner, 1999a; Choi & Eisner, 1999b). By comparing Ca entry *via* I_{Ca} and Ca efflux in diastole (which must balance at steady state), and using the blocker carboxyeosin, they concluded that the sarcolemmal Ca-ATPase contributed around 24% of the total Ca efflux from the cell (Choi & Eisner, 1999a). This also equates to around 3% of total removal, if it is assumed that the SR removes 87% (Negretti *et al.*, 1993).

The relative contribution of different systems to Ca removal in the rabbit differs to values determined for the rat (see Bassani *et al.*, 1994). This is discussed further in

Chapter 4, section 4.4.6, along with the findings in the model of HF studied in this thesis.

1.4 Calcium handling in heart failure

There is an extensive literature on the changes in Ca handling in heart failure, with many different animal models of the condition, and a full review is beyond the scope of this thesis. Some relevant points will be discussed here and, in addition, pertinent findings are included in each results chapter.

1.4.1 Contractile abnormalities in heart failure

At a basic mechanistic level, the reduced strength of myocyte contraction in heart failure could be due to smaller Ca transients or altered myofilament function (for example reduced sensitivity to [Ca]). Of course, a combination of both may be involved. Changes in myofilament function have been investigated by a number of workers and altered levels of contractile proteins, cross-bridge cycling and phosphorylation state have been reported. Intrinsic [Ca]-sensitivity of the myofilaments does not appear to be greatly altered in HF (reviewed by Mittmann *et al.*, 1998).

There has been much interest in documenting the abnormalities in Ca handling in failing or hypertrophied myocytes. In general, Ca transients are smaller in amplitude and have a slower upstroke and decline (reviewed by Balke & Shorofsky, 1998; Wickenden *et al.*, 1998; Houser & Margulies, 2003). Such findings in animal models of HF are discussed in section 4.4.1. In studies of human HF, a similar situation has been demonstrated (see Piacentino III *et al.*, 2003; Pieske *et al.*, 1999; Davies *et al.*,

1995; Sipido & Callewaert, 1995; reviewed in Hasenfuss & Pieske, 2002; Balke & Shorofsky, 1998), and is particularly evident at higher stimulation rates. This negative force-frequency relationship (i.e. as stimulation frequency increases, force [or cell shortening] decreases) is a common finding in HF. Given the previous discussion on E-C coupling and Ca removal, it will be apparent that defects at many different levels could result in impaired Ca handling and hence contractile dysfunction.

1.4.1.1 L-type calcium current

Rather heterogeneous results have been obtained when $I_{Ca,L}$ has been studied in animal models of hypertrophy and HF (reviewed by Richard *et al.*, 1998; Hasenfuss, 1998). In general, in animals with HF it appears to be unchanged or downregulated (see Table 1 in both review papers), and there may be differences depending on the stage of HF that is studied (Hasenfuss, 1998). Recently, He *et al.* studied $I_{Ca,L}$ in dogs with pacing-induced HF and demonstrated that the overall current density and *I-V* characteristics were unchanged, but the number of channels (estimated from the intramembrane charge movement due to I_{Ca} gating) was reduced by >50% in HF (He *et al.*, 2001). This implies some upregulation of the function of individual channels. The findings were also associated with abnormalities of T-tubule structure (see section 3.4.4).

Studies in human myocytes also suggest little change in I_{Ca} under baseline conditions (see Piacentino III *et al.*, 2003; Hasenfuss & Pieske, 2002; Hasenfuss, 1998; Richard *et al.*, 1998), although one study showed a significant decrease in I_{Ca} current density and Ca entry (Terracciano *et al.*, 2003). Regulation of I_{Ca} may be altered in failing myocytes and Piot *et al.* reported that the response to increased frequency of

stimulation was different, with failure of the current to augment in cells from patients with an ejection fraction (EF) <40% (Piot *et al.*, 1996).

1.4.1.2 SR Ca content

Given the almost exponential relationship between SR Ca content and SR Ca release (see section 1.2.4.1), there has been much interest in determining whether this is the primary defect in HF. In 1998, Lindner *et al.* demonstrated that caffeine-induced Ca transients were reduced by around one half in ischaemic and dilated cardiomyopathy in humans (Lindner *et al.*, 1998). They also showed that there was a significant positive correlation between the size of the caffeine-induced Ca transient and the EF for each patient (r=0.76). They suggested that the altered SR content was sufficient to explain the defective Ca transients in HF. In a later study, Pieske *et al.* used rapid cooling contractures (RCCs) to estimate SR Ca content in 26 failing and 4 non-failing human hearts (Pieske *et al.*, 1999). Although they do not report absolute values for developed tension during RCCs under baseline conditions, they showed that SR content fell during long rest intervals and augmented little as stimulation frequency increased in failing muscle strips, compared to non-failing muscle. In a recent paper, Piacentino III *et al.* showed that SR content was reduced by around 42% in failing cells, mainly as a result of diminished uptake by SERCA, and contended that this abnormal SR function accounted for the smaller Ca transients and slower [Ca] decline in HF (Piacentino III *et al.*, 2003). However, not all studies demonstrate reduced SR Ca content in human HF (Terracciano *et al.*, 2003).

Reduced SR Ca content has been found in canine (Hobai & O'Rourke, 2001; Pu *et al.*, 2000), rabbit (Pogwizd *et al.*, 2001; Baartscheer *et al.*, 2003) and ferret (Díaz *et al.*,

2004) models of HF or hypertrophy. Some studies of HF in the rat have revealed unchanged SR Ca content (McCall *et al.*, 1998; Gómez *et al.*, 2001), although Zhang *et al.* did find smaller caffeine-induced contractures after MI (Zhang *et al.*, 1999). Studies in this thesis included an estimation of the Ca content of rabbit ventricular cells 8 weeks after MI (see Chapter 4).

Given the general finding of reduced SR Ca content in HF, the documentation of triggered arrhythmias which rely on SR Ca overload seems paradoxical. Pogwizd *et al.* attempted to explain this paradox in their combined pressure and volume overload model of HF in the rabbit (Pogwizd *et al.*, 2001). They showed that although the SR content was reduced in HF, the cells retained β-adrenergic responsiveness and in the presence of isoproterenol the SR content would rise (through stimulation of SERCA) to the point where spontaneous release would occur. The threshold level of SR [Ca] for spontaneous release was no different to control cells (around 100 μmol/L cytosol) but they postulated that the increased NCX and lower inward rectifier current (I_{K1}) in HF meant that a given SR release was more likely to trigger an AP.

1.4.1.3 SERCA function and regulation by PLB

One critical determinant of SR Ca content is the level of activity of SERCA. Numerous studies have examined SERCA2a expression and function in heart failure. Hasenfuss & Pieske summarise the results of 11 studies of SERCA protein levels in HF, and the majority showed a significant reduction (Hasenfuss & Pieske, 2002). This also appears to be the case for mRNA levels and functional studies (summarised by Bers, 2001, Table 26; Houser *et al.*, 2000). Similar findings have been reported for animal models of HF (e.g. O'Rourke *et al.*, 1999; Yao *et al.*, 1998; reviewed by Phillips

et al., 1998; Hasenfuss & Pieske, 2002). Studies on the rabbit infarct model of HF are discussed in Chapter 4, section 4.4.2.3.

Several groups have also studied the expression of PLB in HF, and most report that it is unchanged or reduced. However, given that in general there is a greater reduction in SERCA expression in HF, the ratio of PLB to SERCA may rise, indicating higher basal levels of inhibition (reviewed by Hasenfuss & Pieske, 2002). There may also be changes in the phosphorylation state of PLB (Currie & Smith, 1999; reviewed by Sjaastad *et al.*, 2003; Bers, 2001, Chapter 10).

1.4.1.4 RyR function & SR Ca leak

A number of groups have reported reduced RyR expression in animal models of HF (e.g. reduced [^{3}H] ryanodine binding in a rabbit pressure-overload model; Milnes & MacLeod, 2001), although the situation in humans appears to be more heterogeneous (reviewed by Hasenfuss & Pieske, 2002; Bers, 2001, Table 26). One recent theory is that the abnormalities seen in HF may be due to defective regulation of RyR. As outlined in section 1.2.3.2, Marks' group have suggested that alterations in RyR-FKBP12.6 interactions could have profound effects on channel function, with phosphorylation of RyR leading to dissociation of FKBP12.6, causing abnormal gating, "leaky" channels and reduced SR Ca content. There has been considerable debate as to the importance of this mechanism in HF (Eisner & Trafford, 2002; Bers *et al.*, 2003). Marx *et al.* reported that PKA phosphorylation of RyR was around four times higher in tissue from failing human hearts and from dogs with pacing-induced HF (Marx *et al.*, 2000). They proposed that this could account for the contractile abnormalities that were observed. However, Jiang *et al.* also examined RyR levels, function and

phosphorylation state in human tissue and canine pacing-induced HF (Jiang *et al.*, 2002). They found no difference in RyR protein density, [^{3}H] ryanodine binding, channel open probability or presence of subconductance states in failing tissue. Similarly, phosphorylation levels of RyR were no different, and when PKA was incubated with RyRs there was no evidence of dissociation of FKBP12.6. There are also theoretical reasons why alterations in RyR function alone may not alter steady-state Ca transients, even in the face of reduced SR Ca content (discussed in detail in section 5.1.1.1). Thus, the debate regarding RyR function in HF has yet to be resolved.

1.4.1.5 Gain of E-C coupling

Given that I_{Ca} flux may be changed little in HF (see section 1.4.1.1), if Ca transients are smaller then the amount of Ca released from the SR must be reduced, and the overall "gain" of E-C coupling will be lower. As discussed previously, E-C coupling gain is dependent on SR Ca content and in many cases this may be the underlying defect which causes the reduced gain in HF (e.g. Hobai & O'Rourke, 2001; Pogwizd *et al.*, 2001). However, some groups have reported reduced gain even in the presence of maintained SR content. Gómez *et al.* studied Ca handling in rat cells following MI, and showed that under conditions where caffeine-induced Ca transients were similar, $\Delta[Ca]_i/I_{Ca}$ was reduced compared to control cells (Gómez *et al.*, 2001). They suggested that this could be due to altered organisation of DHPR and RyR in HF, with "mismatch" of proteins, increased size of the dyadic cleft or "orphan" RyRs due to T-tubule remodelling (see He *et al.*, 2001). Some other means by which SR Ca release could be smaller for a given I_{Ca} flux can be postulated by considering the reverse of the mechanisms outlined in Figure 1.2.

Milnes & MacLeod found that the ratio of RyR to DHPR was reduced in a pressure-overload model of left ventricular hypertrophy (LVH) in the rabbit, and suggested that this could account for slowed contraction in this model (Milnes & MacLeod, 2001). Litwin *et al.* suggested that a similar situation could exist in the rabbit infarct model of HF (Litwin *et al.*, 2000). They documented that Ca sparks in this model were dyssynchronous, and correlated this with the slowed upstroke of Ca transients.

Again, there are theoretical grounds to suggest that cells may compensate for some of the above abnormalities, with changes in SR content. This is discussed in more detail in sections 5.1.1.1 and 5.4.1.2.

1.4.1.6 NCX

There has been considerable interest in the expression, activity and regulation of NCX in heart failure, given its central role in Ca removal (section 1.3.2.1) and arrhythmogenesis (section 1.3.3). In addition, the balance between NCX and SERCA in the removal of cytoplasmic Ca may influence SR Ca content and therefore could affect systolic Ca release. The findings in a large number of studies of animal and human HF / hypertrophy were recently reviewed by Sipido *et al.* (2002). They show that there is considerable heterogeneity in the results reported in the literature – for example in 29 animal studies, 14 reported an increase in NCX expression and/or function, whilst 10 showed a decrease, and 5 no change. Variables such as the means of producing HF / hypertrophy, the time when cells or tissues were studied and the investigative techniques used (biochemical / functional) can all have a bearing on the results achieved. Chapter 3 addresses NCX function in the rabbit infarct model of HF,

and the relevant literature regarding NCX in human and animal HF is reviewed in detail in that chapter (sections 3.4.2 & 3.4.5).

1.5 Regional differences in ion channels and Ca handling

Given the functional, structural and electrical specialisation of different regions of the heart, it is not surprising that ion channels and Ca handling proteins vary at a cellular level. Differences can be considered in a number of planes, for example: atrium-ventricle, apex-base, LV-RV and transmurally (endocardium-epicardium). In some models of heart failure, other considerations can be made – for example cells differ in the peri-infarct zone from those at more remote sites – variation in the expression of NCX and SERCA between these areas have been reported (Yoshiyama *et al.*, 1997; Wasserstrom *et al.*, 2000).

Schram *et al.* recently reviewed the expression of ion channels in different regions of the heart and documented the marked differences in action potential shape and underlying cellular currents (Schram *et al.*, 2002). Previously, Antzelevitch had reviewed such differences in the ventricle (Antzelevitch *et al.*, 1991). Cells from the epicardium demonstrate a prominent "spike and dome" in the AP shape, compared to endocardial cells, which have a flatter plateau and longer action potential duration (APD), features which are important in producing the T-wave on the surface electrocardiogram. Epicardial cells have a larger transient outward current (I_{to}) which may be a consequence of differing expression of certain K-channel isoforms (see Schram *et al.*, 2002). The longer APD in endocardial cells has been shown previously for the animals used in this thesis (McIntosh *et al.*, 1998; McIntosh *et al.*, 2000). These AP differences and variation in properties of I_{to} have also been demonstrated for human

cells, and changes have been shown in failing hearts, with a selective fall in I_{to} in epicardial cells (Näbauer *et al.*, 1996).

In addition to mediating repolarisation of the cardiac AP, potassium currents have important membrane-stabilising effects, and downregulation of some such currents has been linked to an increased likelihood of arrhythmias (Pogwizd *et al.*, 2001). Endocardial-epicardial gradients in the inward rectifier K-current (I_{K1}) and delayed rectifier current (I_{Kr} & I_{Ks}) may exist in some species (reviewed by Schram *et al.*, 2002), although no significant difference in I_{K1} was found in the rabbit (McIntosh *et al.*, 1998).

The distribution of other ion channels and transporters has also been investigated, although few studies have examined NCX. Bryant *et al.* reported no significant difference between endocardial and epicardial cells in Ca-activated tail currents induced by interrupted AP clamp protocols (Bryant *et al.*, 1997). However the amplitude of this current will also depend on the cytoplasmic [Ca] at the point where the AP is interrupted, and this was not measured in the study. Zygmunt *et al.* used two methods to estimate I_{NCX} in cells from different transmural regions in the dog (Zygmunt *et al.*, 2000). The most valid measure was made by rapidly removing external Na and examining the resulting current, and this showed no significant difference between endocardial and epicardial cells. However, this only measures I_{NCX} in one direction (outward) and at a fixed membrane potential. Experiments in this thesis examined transmural differences in I_{NCX} in more detail (Chapter 3).

Transmural Ca handling characteristics have also been reported in the literature. McIntosh *et al.* showed longer Ca transients in endocardial cells compared to epicardial cells in the rabbit, without significant differences in diastolic or peak systolic [Ca] (McIntosh *et al.*, 2000). Similar results for the Ca transient amplitude have been found in the rat (Chamunorwa & O'Neill, 1995), although diastolic and systolic [Ca] appear to be higher in endocardial cells (Figuerdo *et al.*, 1993). The decay of Ca transients has been shown to be longer in endocardial sites (Laurita *et al.*, 2003). The expression of certain Ca handling proteins has also been examined and the findings for SERCA and RyR are discussed in sections 4.4.2.1 and 5.4.1.1, respectively.

This thesis examines in detail several aspects of Ca handling in endocardial and epicardial cells from rabbits under control conditions and 8 weeks following myocardial infarction.

CHAPTER 2

GENERAL METHODS AND CHARACTERISTICS OF ANIMAL MODEL

2.1 Animal models of heart failure

As discussed in the previous chapter, heart failure due to left ventricular dysfunction is an increasing problem in the Western world, causing significant morbidity, mortality and cost to the healthcare system. Significant advances have been made in the management of condition, but there is still much to be learned about the underlying cellular processes involved. Animal models of LVD have played an important role in advancing the understanding of the pathophysiology of heart failure.

There are many animal models of heart failure in the literature, using a number of different species. Methods of induction of LVD include myocardial infarction (Litwin & Bridge, 1997; Zhang *et al.*, 1996), pressure overload (Wang *et al.*, 2001b), combined pressure and volume overload (Pogwizd *et al.*, 1999), rapid pacing (Yao *et al.*, 1998; Hobai & O'Rourke, 2000), complete atrioventricular block (Sipido *et al.*, 2000), and infusion of catecholamines (Muders *et al.*, 1999) or cardiotoxic substances (Arnolda *et al.*, 1985; Shah *et al.*, 1997). There will always be concern over extrapolating results from animal models to the situation in humans. In order to minimise these concerns it is desirable to choose a model which mimics human pathophysiology as closely as possible. This study used a rabbit model of LVD, eight weeks after myocardial infarction, a model which has several advantages.

Firstly, coronary artery disease, and in particular myocardial infarction, is the commonest cause of heart failure in humans (reviewed by McMurray & Stewart, 2000) so it is an advantage to use a model where similar haemodynamic alterations may occur. The coronary structure of the rabbit is similar to that of the human, with little collateral circulation, unlike that of other animals such as the guinea pig (Maxwell *et*

al., 1987). After infarction there is a similar process of thinning / scarring of the infarcted zone and hypertrophy of the remaining LV tissue (Pye *et al.*, 1996; Burton & Cobbe, 2000).

Secondly, this model has been well characterised in terms of haemodynamic function and arrhythmias. Pye *et al.* found a good correlation between echocardiographic measurements of ejection fraction and invasive measures of cardiac output (r=0.78 for *in vivo* cardiac index, r=0.84 for *in vitro* cardiac index; Pye *et al.*, 1996). They observed a 35% reduction in EF and significant reductions in cardiac output following infarction. The animals often exhibited signs of congestive cardiac failure, with pleural effusions, ascites or scrotal oedema (Pye & Cobbe, 1996). Using an extrastimulus protocol, it was found that ventricular arrhythmias were more easily induced in failing hearts (Pye & Cobbe, 1996). Indeed, in animals which survive the initial postoperative period, there is an increased mortality rate amongst those which have undergone coronary ligation. Kaplan-Meier survival curves for sham-operated (Sham) and LVD animals are shown in Figure 2.1 (Dr M. Hicks, unpublished observations). Although unconfirmed, it is likely that these deaths are due to ventricular arrhythmias. Similarly, in human heart failure ventricular arrhythmias are the commonest cause of sudden death following myocardial infarction (Underwood *et al.*, 1997).

Thirdly, the size of the rabbit heart allows reliable isolation of cells from different regions, both along the apex-base axis and transmurally. As discussed in Chapter 1, regional differences in single cell electrophysiology have been demonstrated in a number of species. Reproducible isolation of cells from different regions allows further

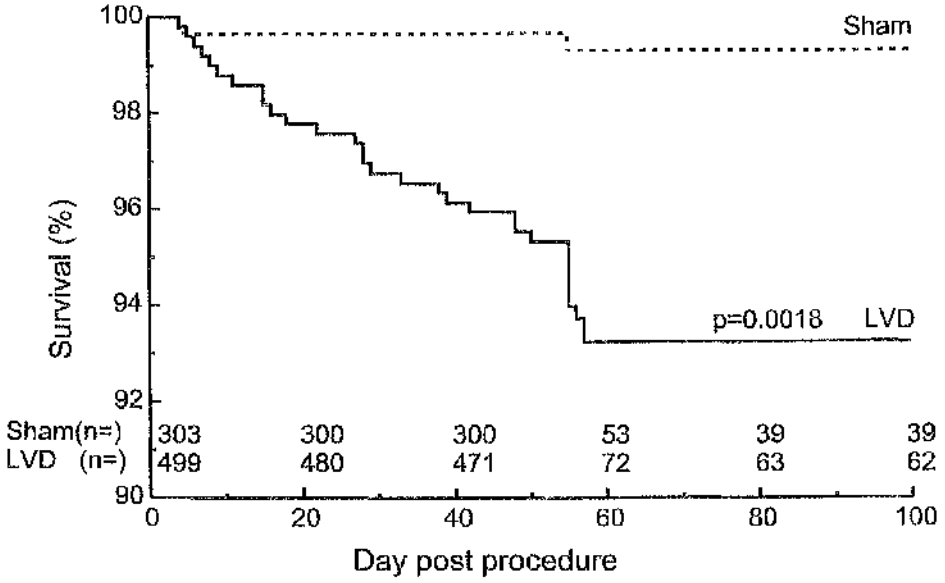

Figure 2.1 Kaplan-Meier survival curves for sham-operated and LVD animals.

study of this phenomenon and also ensures that cells from like regions are used when comparing control animals to those with LVD.

Fourthly, as discussed in Chapter 1, aspects of cellular calcium handling differ between species. The rabbit, like non-failing human tissue, exhibits increased twitch force as the stimulation frequency increases (positive force-frequency relationship; Maier *et al.*, 2000; Pieske *et al.*, 1999). In contrast, in the rat there is a negative force-frequency relationship (Maier *et al.*, 2000). The relative contribution of different calcium removal systems (NCX, SERCA, "slow" systems) to the decay in $[Ca]_i$ during diastole appears to be similar in rabbit and non-failing human cells (Bers, 2000). The situation in failing human tissue is more complex and the adaptive (and maladaptive) responses may differ according to the pathophysiology of the ventricular dysfunction and the time-course of remodelling.

2.2 Coronary artery ligation procedure

All procedures were carried out in accordance with the United Kingdom Animals (Scientific Procedures) Act 1986. The coronary artery ligation technique was performed as previously described (Pye & Cobbe, 1996; Pye *et al.*, 1996; Ng *et al.*, 1998; McIntosh *et al.*, 2000). The operative procedures and echocardiographic characterisation of the animals was performed by technical staff in a separate laboratory.

Male New Zealand White rabbits (12 weeks old, 2.5 – 3 kg) were pre-medicated with 0.4 mL/kg intramuscular Hypnorm (0.315 mg/mL fentanyl citrate: 10 mg/mL fluanisone; Janssen Pharmaceutica, Beerse, Belgium) and given antibiotic prophylaxis with 100 mg intramuscular Amfipen (Mycofarm UK Ltd, Cambridge, UK). The marginal ear vein was cannulated and anaesthesia was induced with 0.25-0.5 mg/kg midazolam (Hypnovel; Roche, Basel, Switzerland). The animal was intubated and anaesthesia was maintained with 1% halothane in a 1:1 mixture of oxygen and nitrous oxide, delivered by a Harvard small animal ventilator (Harvard Apparatus Ltd, Edenbridge, Kent, UK). Access to the heart was obtained by a left thoracotomy through the fourth intercostal space. The marginal branch of the circumflex coronary artery, which supplies most of the left ventricular free wall, was identified and ligated mid-way between the atrioventricular groove and the apex. This produces a homogeneous infarcted area comprising 30-40% of the left ventricle. 10 mg/kg quinidine hydrochloride (Sigma-Aldrich Company Ltd, Poole, Dorset, UK) was administered prophylactically as an antiarrhythmic agent, but in approximately 30% of cases ventricular fibrillation occurred, requiring a 5-10 J epicardial direct current shock to restore sinus rhythm. After ensuring the animal was stable, the thoracotomy was

closed and animals were given 20 mL intravenous saline to replace operative losses. Analgesia was administered (0.04 mg/kg intramuscular buprenorphine hydrochloride; Reckitt Benckiser Pharmaceuticals Inc., Richmond, VA, USA) immediately after operation and again the next morning. During recovery animals were monitored for signs of distress. Sham-operated animals underwent the same surgical procedure, with the exception of the coronary tie.

2.2.1 Characterisation of model

One week before animals were sacrificed they were assessed by echocardiography (Sonolayer 100, Toshiba Medical Systems Europe Ltd, Zoetermeer, Netherlands) using a 5 MHz paediatric probe, under sedation with 0.3 mg/kg Hypnorm. Measurements of left ventricular end-diastolic dimension (LVEDD) and left atrial dimension (LAD) were taken from a parasternal long-axis view. Ejection fraction was assessed from the parasternal short axis view.

The haemodynamic changes induced by cardiac failure (e.g. increased pre-load) can lead to altered hydrostatic pressures in the tissues, causing venous distension and tissue oedema. Once animals had been sacrificed and their hearts removed for myocyte isolation, the liver and lungs were dissected out and weighed (wet, after blotting) to look for signs of congestion.

A summary of echocardiographic and pathological findings is presented in Table 2.1. It is apparent that the animals in the LVD group had a much-reduced EF (47.1 ± 0.9 % *vs* 71.7 ± 0.8 %; $p<0.0001$) and this was accompanied by cardiac enlargement and greater liver and lung weights (see table).

	Sham (n)	LVD (n)	p-value
Animal weight (kg)	3.6 ± 0.05 (39)	3.5 ± 0.04 (49)	0.11
Liver weight (% bodyweight)	2.52 ± 0.06 (32)	2.73 ± 0.07 (41)	0.04
Lung weight (% bodyweight)	0.29 ± 0.03 (3)	0.44 ± 0.02 (33)	0.04
LV ejection fraction	71.7 ± 0.8 (38)	47.1 ± 0.9 (47)	<0.0001
LV end-diastolic dimension (mm)	17.7 ± 0.2 (37)	20.9 ± 0.2 (47)	<0.0001
LA dimension (mm)	12.8 ± 0.2 (38)	15.6 ± 0.2 (47)	<0.0001

Table 2.1 Baseline characteristics of rabbit infarct model of LVD.

2.3 Cardiac myocyte isolation

Eight weeks after the coronary ligation procedure, animals were killed with 0.5 mL/kg of intravenous Euthatal (200 mg/mL sodium pentobarbitone, Rhône Mérieux Inc, Athens, GA, USA), mixed with 500 IU of heparin (CP Pharmaceutical Ltd, Wrexham, UK). The heart was rapidly excised, including ~1 cm of the ascending aorta, and placed in ice-cold BK solution (all solution compositions described in section 2.5.1). It was then perfused retrogradely via a cannula in the aorta (Langendorff technique) with 150 mL nominally Ca-free BK solution at 37 °C at a rate of 25 mL/min. Next, the heart was perfused with enzyme solution, which was re-circulated, and after 2-3 minutes, 100 mmol/L $CaCl_2$ solution was added to give a concentration of 0.05 mmol/L. Digestion was continued for 6-9 min, until the heart began to soften to the touch. At this point the

heart was perfused with 100 mL of bovine serum albumin (BSA) solution containing 0.075 mmol/L Ca. Towards the end of the perfusion, the atria and right ventricle were removed and discarded. The apical area of infarction, with a 3-5 mm rim of non-infarcted tissue, was removed. Histological studies have shown that this will remove myocytes from the peri-infarct border zone (Burton & Cobbe, 2000). In the case of sham-operated animals, an equivalent-sized area was removed from the apex. The remaining basal LV tissue was cut down and placed into a Petri dish containing 0.075 mmol/L Ca BSA solution. Using fine forceps and scissors, small pieces of tissue around 1 mm deep were dissected from the subendocardial (Endo) and subepicardial (Epi) surfaces in turn, and placed into 10 mL of BSA solution in 25 cm^2 tissue culture flasks (Bibby Sterilin Ltd, Stone, Staffordshire, UK). The remaining mid-myocardial layer of tissue was also cut into small pieces and placed into a flask. The three flasks were placed in a shaking water bath at 37 °C for 1 hr (first digest) or 2 hr (second digest), whereupon the cell suspension from each flask was removed into 15 mL centrifuge tubes (Elkay Laboratory Products Ltd, Basingstoke, Hampshire, UK) and gently spun down. The supernatant was removed and replaced with 0.125 mmol/L Ca BSA solution, the cells were then spun down again and the supernatant replaced with 0.25 mmol/L Ca BSA solution. The cells were then allowed to settle under gravity and the [Ca] was increased in stages to 0.5 mmol/L and then 1 mmol/L.

The cell yield did not differ significantly between Sham and LVD animals. Cells were stored in 1 mmol/L Ca BSA solution at room temperature for up to 8 hr until used. Experiments were only performed on rod-shaped cells with clearly visible striations and no evidence of spontaneous activity.

2.4 Virus transfection and cell culture

When cells were required for culture, myocytes from the septum were used and the above process was carried out using sterile techniques and sterile-filtered solutions. Once cells were in 1 mmol/L Ca BSA solution they were allowed to settle and then re-suspended in 15 mL cell culture medium (see section 2.5.2) at a density of 1×10^5 rods/mL. The resulting cell suspension was added to a 75 cm^2 culture flask (Iwaki brand, Bibby Sterilin Ltd, Stone, Staffordshire, UK) and the appropriate virus was added at a multiplicity-of-infection (MOI) of 100. Adenoviruses were kindly supplied by Dr J. Prestle (University of Göttingen, Germany). Cells were transfected with NCX adenovirus, and compared with two control groups. For a non-transfected control group, cells were treated as above, with the exception of the addition of the virus solution. A transfected control group was achieved by incubating with an adenovirus encoding β-galactosidase (Lac-Z gene). Cells were cultured for up to 2 days at 37 °C in a 5% CO_2 incubator (Napco, Winchester, VA, USA).

2.5 Solutions

The following solutions were used (concentrations in mmol/L, except where stated otherwise). In each case, solutions were brought to the correct pH at the appropriate temperature. Chemicals were purchased from Sigma (Sigma-Aldrich Company Ltd, Poole, Dorset, UK) or BDH (marked with asterices; BDH Laboratory Supplies, Poole, Dorset, UK) unless otherwise indicated.

2.5.1 Solutions for cell isolation procedure

2.5.1.1 Base Krebs' (BK) solution

NaCl (120), KCl* (5.4), N-(2-hydroxyethyl)piperazine-N'-(2-ethanesulphonic acid) (HEPES, 20), NaH_2PO_4* (0.56), $MgCl_2$ (3.5), 2-aminoethanesulfonic acid (taurine, 20), N-amidinosarcosine(α-methylguanido)acetic acid (creatine, 10), glucose (11.1); pH adjusted to 7.4 with NaOH. Nominally Ca-free, and 0.075 mmol/L Ca solutions were made up.

2.5.1.2 Enzyme solution

0.67 mg/mL collagenase (Worthington Biochemical Corporation, Lakewood, NJ, USA) and 0.04 mg/mL protease were added to the BK solution.

2.5.1.3 BSA solution

1 mg/mL BSA (fraction V) solution was made up using BK solution, with the following Ca concentrations: 0.075, 0.125, 0.25, 0.5, and 1.

2.5.2 Cell culture medium

The following compounds were added to Medium 199 (M-199, HEPES modification): taurine (5), β-hydroxy-γ-(trimethylammonio)butyrate (DL-carnitine, 5), creatine (5), 5 mL 100x penicillin-streptomycin solution (final concentration: 100 units/mL penicillin, 0.1 mg/mL streptomycin). The solution was passed through a sterile filter (0.2 μmol/L, Sartorius Ltd, Epsom, Surrey, UK).

2.5.3 Normal Tyrode's (NT) solution

NaCl (140), KCl* (4), HEPES (5), $MgCl_2$ (1), $CaCl_2$* (1.8), glucose (11.1); pH adjusted to 7.4 with NaOH. Phosphate was omitted from this solution since it caused precipitation in nickel-containing solutions.

2.5.4 Solutions for NCX & SERCA activity studies (Chapters 3, 4 & 5)

2.5.4.1 Superfusate

As for NT, with added 4-aminopyridine (5 mmol/L, to block K currents) and niflumic acid (0.1 mmol/L, to block Ca-activated Cl currents); pH adjusted to 7.4 with HCl.

2.5.4.2 Pipette solution

KCl* (20), K aspartate (100), tetraethylammonium chloride (TEACl, 20), HEPES (10), $MgCl_2$ (4.5, calculated free [Mg] ≈ 0.9 mmol/L, using the computer program "React II", G.L.Smith & L.S.Duncan, University of Glasgow), disodium ATP (4), disodium creatine phosphate (1), EGTA (0.01); pH adjusted to 7.25 with KOH.

2.5.5 Solutions for NCX current density studies (Chapter 3)

2.5.5.1 Superfusate

NaCl (140), CsCl (4), HEPES (5), $MgCl_2$ (1), $CaCl_2$* (1.8), glucose (11.1), *N*-acetylstrophanthidin (0.01, to block Na-K pump) and nifedipine (0.01, to block $I_{Ca,L}$); pH adjusted to 7.4 with NaOH.

2.5.5.2 Pipette solution

CsCl (45), EGTA/CaEGTA (Cs 100, EGTA 50, Ca 25, calculated free [Ca] = 258 nmol/L), HEPES (20), $MgCl_2$ (11, calculated free [Mg] ≈ 1.2 mmol/L), disodium ATP (10); pH adjusted to 7.25 with CsOH.

2.5.6 Solutions for studies of Allosteric regulation of NCX (Chapter 3)

2.5.6.1 Superfusate

NaCl (140), CsCl (4), HEPES (5), $MgCl_2$ (1), $CaCl_2$ (1.8), glucose (11.1), *N*-acetylstrophanthidin (0.01), nifedipine (0.01) and niflumic acid (0.1) pH adjusted to 7.4 with NaOH.

2.5.6.2 Pipette solution

CsCl (20), Cs aspartate (100), tetraethylammonium chloride (TEACl, 20), HEPES (10), $MgCl_2$ (4.5, calculated free [Mg] ≈ 0.9 mmol/L), disodium ATP (4), disodium creatine phosphate (1), EGTA (0.01); pH adjusted to 7.25 with CsOH.

2.6 Rapid solution switcher

A heated rapid solution switcher was custom-built as outlined in Figure 2.2. The solution heater consisted of a drilled aluminium block (35 mm × 18 mm × 3 mm), heated by two 15 mm × 15 mm Peltier devices (RS components Ltd, Corby, Northamptonshire, UK) controlled by a power supply with variable voltage (Farnell, Leeds, West Yorkshire, UK). Solution flow under gravity was regulated by solenoid valves (The Lee Company, Essex, CT, USA) controlled by a manual selector. After heating, the solutions passed to a manifold, with a perfusion tip made from a short

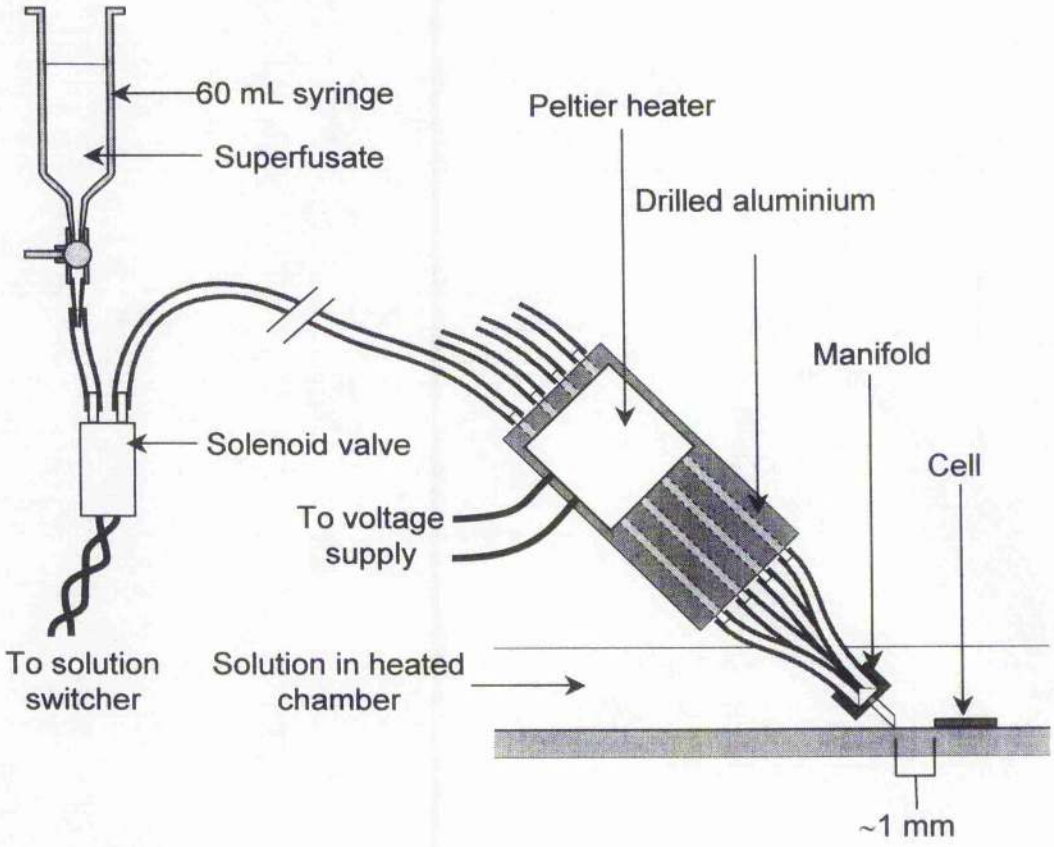

Figure 2.2 Perfusion apparatus for delivery of heated solutions to the cell. Flow from four reservoir syringes was controlled by solenoid valves with a manual switching device. The solutions were heated by passing them through a drilled aluminium block to which two Peltier devices were attached. These were controlled by a variable voltage supply, adjusted so that the temperature of flowing solution 1 mm from the perfusion tip was 36.5 ± 0.5 °C. The four solutions came together at a manifold with a ~2 μL dead-space, the tip of which was placed ~1 mm from the cell.

piece of plastic tubing, 0.8 mm outside diameter, 0.5 mm inside diameter. The dead-space of the manifold and perfusion tip was ~2 μL. The heating assembly and manifold inflow tubing were insulated with high-density foam to minimise heat loss.

At the beginning of each experiment, it was ensured that the flow of each solution was equal (~2 mL/min) and the solution temperature was measured at the tip of the manifold and adjusted to give 36.5 ± 0.5 °C. The change in temperature when switching between solutions was <1 °C. During experiments, the tip of the manifold was placed ~1 mm from the cell, once voltage clamp had been achieved. This placed it opposite the outflow region of the chamber, and observations made using coloured solutions demonstrated that this would reliably place the cell in a jet of the heated solution, without interference from re-circulation of solution in the rest of the bath. Under voltage clamp, switching solutions was not found to disrupt the micropipette seal.

2.6.1 Speed of solution change

The low dead-space of the manifold allowed for rapid switching of solutions perfusing the cell, which was essential for several of the techniques outlined in this thesis. In a number of experiments, rapid application of caffeine was used to release SR Ca, and analysis of simultaneous membrane current recordings could be used to determine certain parameters for the perfusion device. Time-to-onset of caffeine was measured from the artefact spike due to solution switching to the start of the inward current. Time-to-peak was measured from the same artefact spike to the peak of the inward current. An onset-to-peak time could then be determined, giving an estimate of the time taken from the arrival of caffeine at the cell / SR to its full effect at the SR (with the assumption that the time from SR Ca release to efflux on NCX producing the inward current is negligible). Time-to-onset, time-to-peak and onset-to-peak were measured at 293 ± 18 ms, 404 ± 21 ms and 111 ± 5 ms, respectively (n=22).

A further assessment of the speed of solution change at the cell was made using solutions containing low or high Ca concentrations in the presence of the fluorescent Ca indicator Fluo-3. Fluorescence was measured, as outlined below, from an area of the image field masked off to the size of a typical cell, whilst the perfusing solution was repeatedly switched between a nominally Ca-free solution and one containing 10 mmol/L Ca. The fluorescence signal was then analysed and the transition between the two solutions was fitted with a single exponential function using the graphical analysis program OriginPro 6.1 (OriginLab Corporation, Northampton, MA, USA; see Chapter 4, Figure 4.4). The time constant for the switch was found to be 90 ± 8 ms (n=10).

2.7 Experimental apparatus

Cells were studied in a thermostatically-controlled heated chamber (Warner Instrument Corp., Hamden, CT, USA), with a circular coverslip (uncoated) forming the base (thickness no. 0; BDH Laboratory Supplies, Poole, Dorset, UK). Generally, other cells in the bath which were not sealed on to the micropipette were washed away by the flow from the solution switcher, so fresh cells were introduced after each experiment. The solution level was kept constant by suction from a roller pump (Watson-Marlow Ltd, Falmouth, Cornwall, UK) with outflow from the bath downstream from the perfusion apparatus.

The chamber was mounted on the stage of an inverted microscope (Nikon Diaphot, Nikon UK Limited, Kingston upon Thames, Surrey, UK), which supported a coarse micromanipulator for the solution manifold and both coarse and fine micromanipulators for the micropipette (Narishige International Ltd, London, UK).

Cells were viewed at ×40 magnification using an oil immersion lens with ultra-low autofluorescence immersion oil (Nikon UK Limited, Kingston upon Thames, Surrey, UK) under illumination from above. During fluorescence experiments a 780 nm long-pass filter (Chroma Technology Corp., Brattleboro, VT, USA) was introduced into the light-path. Cells could be viewed throughout the experiment on a black-and-white monitor via a CCD camera (Watec Corp., Las Vegas, NV, USA, see Figure 2.3).

2.7.1 Electrophysiological recording

Micropipettes were pulled from borosilicate glass (GC120F-10; Harvard Apparatus Ltd, Edenbridge, Kent, UK; 1.2 mm outside diameter, 0.69 mm internal diameter, with internal filament) using multi-stage protocols on a Flaming/Brown micropipette puller (model P-97; Sutter Instrument Company, Novato, CA, USA). For current clamp (action potential) experiments, pipettes were fine-tipped, with a resistance of 15-25 MΩ, and filled with 2 mol/L KCl. For voltage clamp work, pipettes were lightly heat-polished (Narishige microforge model MF-9, Narishige International Ltd, London, UK) giving a final resistance of 2-5 MΩ (tip diameter ≈1 μm), except in the case of the NCX current density studies, where the resistance was 1-2.5 MΩ (tip diameter ≈1.5 μm) to enhance dialysis of pipette contents. Pipettes were back-filled with filtered pipette solution immediately before use.

The micropipette electrode was fashioned from a length of silver wire, electrolytically coated with silver chloride using a custom-built chloriding unit. Electrodes were freshly coated at the start of each day's experiments. The bath electrode consisted of an $Ag/AgCl_2$ pellet, which was positioned near the bath outflow.

The microscope and associated apparatus was positioned on a Micro-g air table (Technical Manufacturing Corporation, Peabody, MA, USA) to minimise vibration, and was contained within a Faraday cage. Electrophysiology recordings were made using Axon Instruments equipment (Axon Instruments Inc., Union City, CA, USA) on an Axoclamp 2B amplifier, with a headstage gain of 0.1 (model HS-2A). Signals were digitised using a 16-bit data acquisition system (Digidata 1320A) and P-Clamp 8.0.2 software was used for recording of signals on an 866 MHz desktop computer (Dell Computer Corporation, Round Rock, TX, USA). Current, voltage and fluorescence signals were also displayed on a chart recorder (Gould Nicolet Technologies, Ilford, Essex, UK).

2.7.2 Electrophysiology protocols

Current- and voltage-clamp protocols were generated using P-Clamp 8.0.2 software (Axon Instruments Inc., Union City, CA, USA). Specific protocols are described in the relevant chapters, but some procedures were common to all experiments.

2.7.2.1 Whole-cell current- and voltage-clamp procedures

Micropipettes were introduced into the bath with positive pressure applied to prevent superfusate from contaminating the pipette solution. Voltage offset and pipette resistance were then balanced in "bridge" mode, and the pipette resistance could be read off a dial on the Axoclamp amplifier. For current-clamp work, cells were impaled using a short, but abrupt, downward movement of the pipette. It was occasionally necessary to apply a small amount of positive or negative pressure or a brief oscillating voltage ("buzz") to gain adequate access to the cell interior. For voltage-clamp

experiments the micropipette was brought down onto the cell membrane and a seal was formed using gentle negative pressure. The seal was monitored using small voltage steps (10 mV, 4 Hz) from a holding potential of 0 mV. Once a gigaohm seal was formed, the holding potential was set to -80 mV and whole-cell access was obtained by brief, sharp suction to rupture the underlying membrane. Once stable access was obtained, the mode was switched to discontinuous single-electrode voltage clamp, which allows more accurate measurement of actual membrane voltages. To minimise potential difficulties in obtaining adequate voltage control of large cells ("space clamp"), the microelectrode was always placed towards the middle of the cell, and suspected double cells were excluded. The liquid junction potential was measured at ≤1 mV and was not corrected.

For each cell, optimal settings for capacitance neutralisation and gain were set and the sampling rate of the clamp was adjusted to around 8 kHz. Cells where adequate levels of gain could not be achieved were rejected. Depending on the type of protocol used, the output bandwidth was set to between 0.3 kHz and 1 kHz, to give a good compromise between filtering of noise and resolution of rapid voltage or current changes. The output from the Axoclamp amplifier was sampled at ≥2 kHz to avoid aliasing. In general, further filtering of the signals was not employed, but, where appropriate, traces were averaged.

2.7.2.2 Cell capacitance measurement and cell volume calculation

Cell capacitance was usually measured using the built-in protocol in P-Clamp 8, which uses the following method. Small depolarising and hyperpolarising voltage pulses (5 mV) are applied around the holding potential to produce capacitance transients in the

current trace. The small size of the voltage steps allows the ohmic properties of the cell membrane to be measured, without activation of significant ionic currents. The pulse rate is chosen to allow adequate time for each capacitance transient to decay (generally 1.3 Hz). The time constant (τ) of the decay of the capacitance transients is obtained from a single exponential fit of a running average trace. The total charge (Q_t) passed for a given change in voltage (ΔV) can be calculated from the area under the transient above the steady-state current (Q_1), plus a correction factor ($Q_2=\Delta I^* \tau$). Membrane capacitance (C_m) is then calculated using the following formula:

$$C_m = \frac{Q_t}{\Delta V} \qquad \textbf{Equation 2.1}$$

In addition to using the built-in algorithm, for each cell a similar voltage-clamp protocol was applied and the resulting currents were recorded for later analysis. If there was any doubt over the accuracy of the automated analysis, then these currents were analysed manually by the same method.

Cell volume was calculated from the capacitance measurements using a conversion factor obtained by Satoh *et al.* (1996). They used confocal microscopy to measure the cell volume of calcein-loaded myocytes and related the results to cell capacitance, assuming a "specific capacitance" for cell membranes of 1 $\mu F/cm^2$. For adult rabbit ventricular myocytes, a value of 4.58 ± 0.45 F/L was obtained. This gives an estimate of the total cell volume, including organelles. In cases where accessible (non-mitochondrial) cell volume was required, a value of 6.44 ± 0.63 F/L was used, which corrects for the proportion of the cell volume taken up by mitochondria (38.9% for rabbit cardiac myocytes; Barth *et al.*, 1992).

2.7.3 Calcium measurement using fluorescent dyes

The development of new [Ca]-sensitive fluorescent dyes based on bis-(*o*-aminophenoxy)-ethane-N,N,N′,N′-tetra-acetic acid (BAPTA) in the 1980s greatly facilitated the measurement of intracellular Ca signals (Grynkiewicz *et al.*, 1985; Sipido & Callewaert, 1995). When excited at appropriate wavelengths, the emission intensity of these indicators varies as a function of [Ca] and, with appropriate measurement and calibration, an accurate estimation of $[Ca]_i$ can be made, with excellent temporal resolution.

In this thesis, the indicator Fura-2 was used, in its acetoxymethyl ester (AM) form. This dye alters its excitation spectrum when Ca binds, and this is detected by exciting the dye at two wavelengths (340 nm & 380 nm) and recording emitted light at a single wavelength (Grynkiewicz *et al.*, 1985). This ratiometric technique eliminates problems due to motion artefact experienced with previous indicators, and is also independent of the absolute dye concentration within the cell. The AM form of the dye is membrane-permeant, and once inside the cell is hydrolysed by intracellular esterases to release the [Ca]-sensitive indicator.

2.7.3.1 Dye-loading procedure

A stock solution of Fura-2 AM (Molecular Probes Europe, Leiden, The Netherlands) was produced by dissolving 1 mg in 1 mL of anhydrous dimethylsulphoxide (DMSO), and this was stored in aliquots at -20 °C. When required, 5 µL of this stock solution was added to 1 mL of the cell suspension (see section 2.3), giving a final Fura-2 concentration of ~5 µmol/L. This was incubated for 10-15 min at room temperature to

allow entry of the dye into the cells and de-esterification. A further 2 mL of NT solution was then added to dilute the Fura-2, slowing further loading, and the first 0.5 mL aliquot of cell suspension was used immediately. Further aliquots of cells could be used for up to 45 min, before a fresh batch of cells was loaded. Removal of extracellular Fura-2 was achieved by the perfusion of superfusate once the cells were added to the bath chamber. Preliminary experiments varying the loading conditions (Fura-2 concentration, temperature and loading time) showed that the above protocol would reliably produce a good signal-to-noise ratio on the Ca signal, without evidence of excessive Ca buffering by Fura (as determined by the rate of decline of the Ca transient).

2.7.3.2 Fluorescence measurement apparatus

Figure 2.3 outlines the optical setup to allow fluorescence measurements. Light from a 150 W xenon arc lamp is focused by a reflector, then collimated by a lens and diffracted by a computer-controlled monochromator (Cairn Research Ltd, Faversham, Kent, UK) to give the appropriate wavelengths for stimulation of Fura-2 (see below). The light is then conveyed to the microscope by a flexible liquid light guide, passes through a further focusing lens which is adjusted to give even illumination, and is reflected by a 45° 400 nm long-pass (LP) dichroic mirror. A ×40 oil immersion lens focuses the excitation light onto the cell and collects the emission light. Appropriate emitted wavelengths pass through the dichroic mirror and are reflected out the sideport of the microscope. Here they pass through a rectangular diaphragm which is adjusted to match the outline of the cell under study, masking off light from any other cells or debris in the optical field. A further LP dichroic mirror reflects the light through a 510 nm LP filter (Chroma Technology Corp., Brattleboro, VT, USA) for collection by a

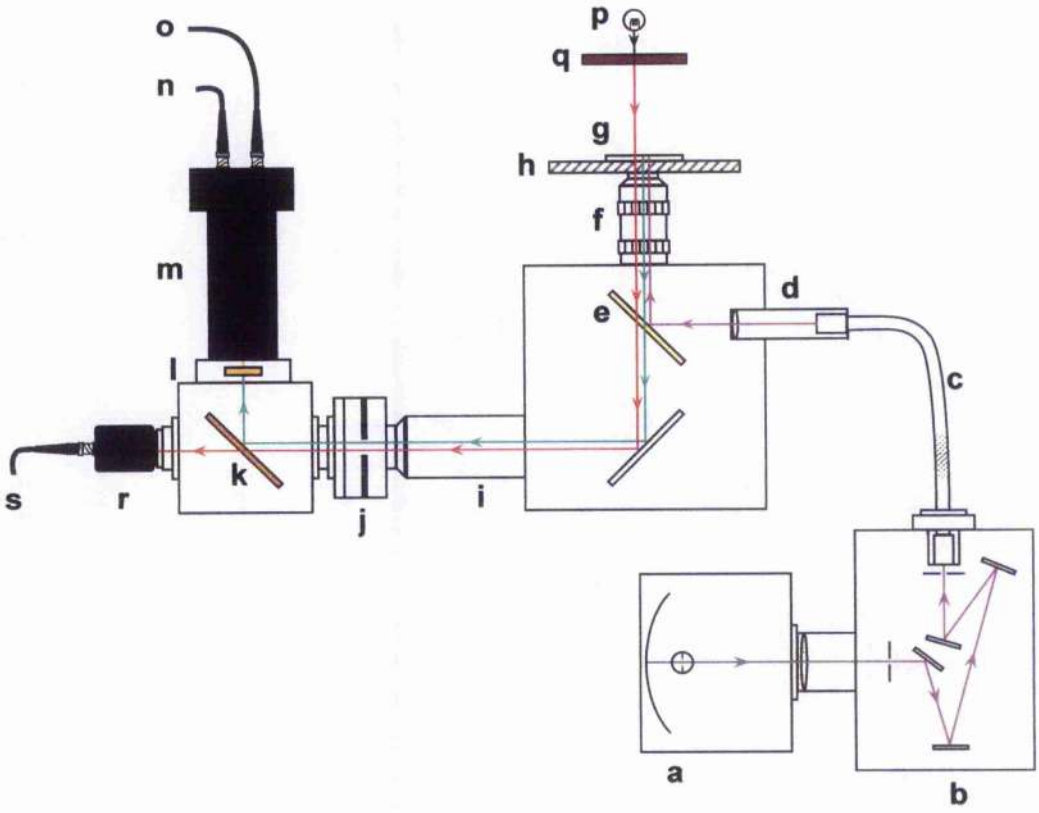

Figure 2.3 Optical apparatus for fluorescence measurement. **a** = xenon arc lamp; **b** = monochromator, controlled by Cairn Optoscan device; **c** = flexible liquid light guide; **d** = focusing lens; **e** = 400 nm LP dichroic mirror; **f** = ×40 oil immersion objective; **g** = cell loaded with Fura-2; **h** = coverslip forming bottom of solution chamber; **i** = microscope sideport; **j** = rectangular diaphragm to limit collected light to cell dimensions; **k** = LP dichroic mirror; **l** = 510 nm LP emission filter; **m** = photomultiplier tube (PMT); **n** = from high-tension voltage supply; **o** = PMT output to Optoscan; **p** = microscope light-source; **q** = 780 nm LP filter; **r** = CCD camera; **s** = to monitor. Full details in text.

photomultiplier tube (PMT). The voltage output of the PMT is measured by an Optoscan device (Cairn Research Ltd, Faversham, Kent, UK), which also controls the monochromator. The output from the Optoscan (raw wavelength signals and a 340/380 ratio signal) was passed through the analogue-to-digital converter (Digidata 1320A,

Axon Instruments Inc., Union City, CA, USA) for display on the chart recorder and recording by P-Clamp 8.0.2 software.

As outlined in section 2.7, cells could be observed during fluorescence experiments using a CCD camera and monitor.

2.7.3.3 Optoscan parameters for fluorescence recording

Published data for Fura-2 suggest that the maximal changes in emission in response to [Ca] occur at around 340 nm and 380 nm, with an isosbestic point (wavelength where output is insensitive to changes in [Ca]) at 360 nm (Grynkiewicz *et al.*, 1985; Sipido & Callewaert, 1995). The Optoscan equipment allows an assessment to be made of the wavelength profile of the intracellular dye, under the optical conditions used during an experiment. With a constant voltage setting for the PMT input, a cell loaded with Fura-2 was centred on the field, and the diaphragm was stopped down to the boundaries of the cell. A wavelength scan was then performed, with readings of the PMT output taken at 2 nm intervals from 300 nm to 500 nm. This was performed with a quiescent cell (low $[Ca]_i$) and then with the cell punctured in 1.8 mmol/L NT solution (high $[Ca]_i$), to observe the Ca-dependent wavelength shift (absolute values of $[Ca]_i$ are unimportant for this, as long as there is a sufficient difference between them). An example is shown in Figure 2.4. For 4 cells, the mean isosbestic point (arrowed on figure) was 361.3 ± 1.5 nm, with peak differences between low and high $[Ca]_i$ at 346.8 ± 1.4 nm and 383.0 ± 0.9 nm. Thus the ratio of the 340 nm to 380 nm signals gives an almost maximal dynamic range, and these wavelengths were used throughout.

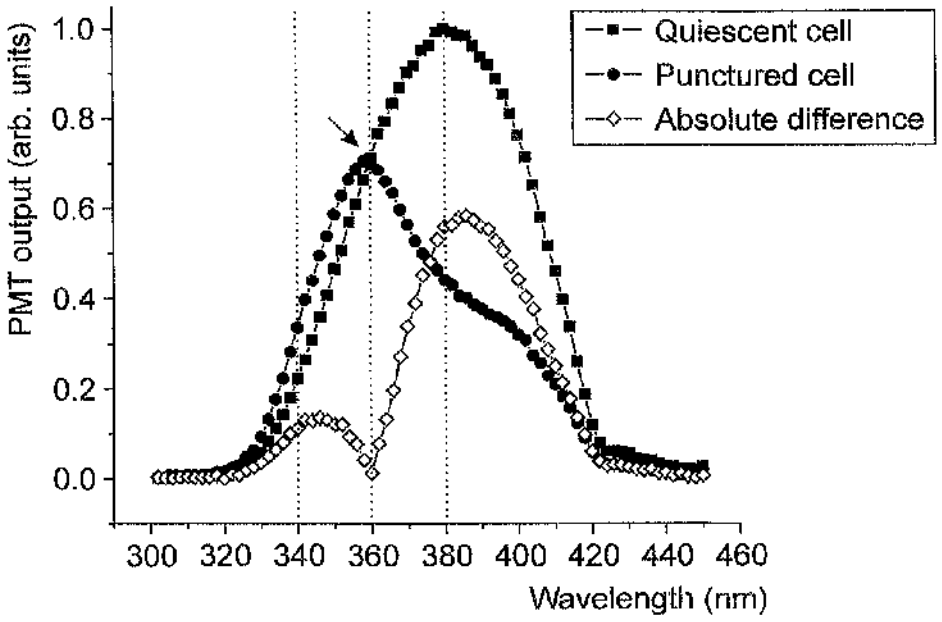

Figure 2.4 Wavelength scans to determine intracellular properties of Fura-2. Scans were performed in 2 nm steps for a quiescent cell (low $[Ca]_i$) and a ruptured cell (high $[Ca]_i$). Absolute difference between scans is also plotted, and isosbestic point, where output is independent of [Ca] is arrowed. 340 nm, 360 nm and 380 nm wavelengths are indicated.

The Optoscan also allows tight control over the wavelengths delivered and the time spent at each wavelength. Preliminary experiments showed that a bandwidth of 5 nm centred on each wavelength, with 8 ms at 340 nm and 4 ms at 380 ms, gave a good signal-to-noise ratio. Shorter times at each wavelength were possible, but since high temporal resolution on the Ca signal was not required (e.g. the upstroke of the Ca transient was not under study), the timings chosen were considered acceptable.

2.7.3.4 Background subtraction

To optimise the quality of the signals at each wavelength, background fluorescence must be subtracted. Ideally this would be achieved by measuring the autofluorescence of the particular cell under study, prior to loading with Fura-2. However, given that

loading was achieved with Fura-2 AM, this was not possible. Instead, non-cellular background fluorescence was subtracted from each wavelength signal. This was achieved by setting the diaphragm mask to the size of the cell and then moving it to an adjacent area of the field, free from cells or debris (and in the presence of perfusion to remove Fura-2 from the bath solution). In this position, the output of each wavelength signal was zeroed on the Optoscan. It was assumed that additional cellular autofluorescence would be minimal, especially since much of the autofluorescence is due to mitochondrial nicotinamide adenine dinucleotide (NADH), whose peak emission is at 447 nm (Eng *et al.*, 1989), which would be filtered out by the 510 LP emission filter.

2.7.3.5 Calibration of fluorescence signals and conversion to [Ca]

After background subtraction for each wavelength, ratio signals (R) were converted to [Ca] by the method of Grynkiewicz *et al.* (1985), using the following formula:

$$[Ca] = K_d * \beta * (R-R_{min}) / (R_{max}-R) \qquad \textbf{Equation 2.2}$$

where K_d is the dissociation constant of Fura-2; β is the ratio of the 380 nm signal with no Ca binding to that with saturating Ca binding; and R_{min} and R_{max} are the ratio signals at minimum and maximum [Ca], respectively. The latter two terms were determined for each cell studied. R_{min} was taken as the fluorescence ratio of the quiescent cell at the start of each experiment, prior to any stimulation. Separate experiments demonstrated that this ratio was indistinguishable from that obtained when cells were dialysed with a 10 mmol/L EGTA solution. R_{max} was determined at the end of each experiment by impaling the cell in NT solution (1.8 mmol/L Ca) and measuring the

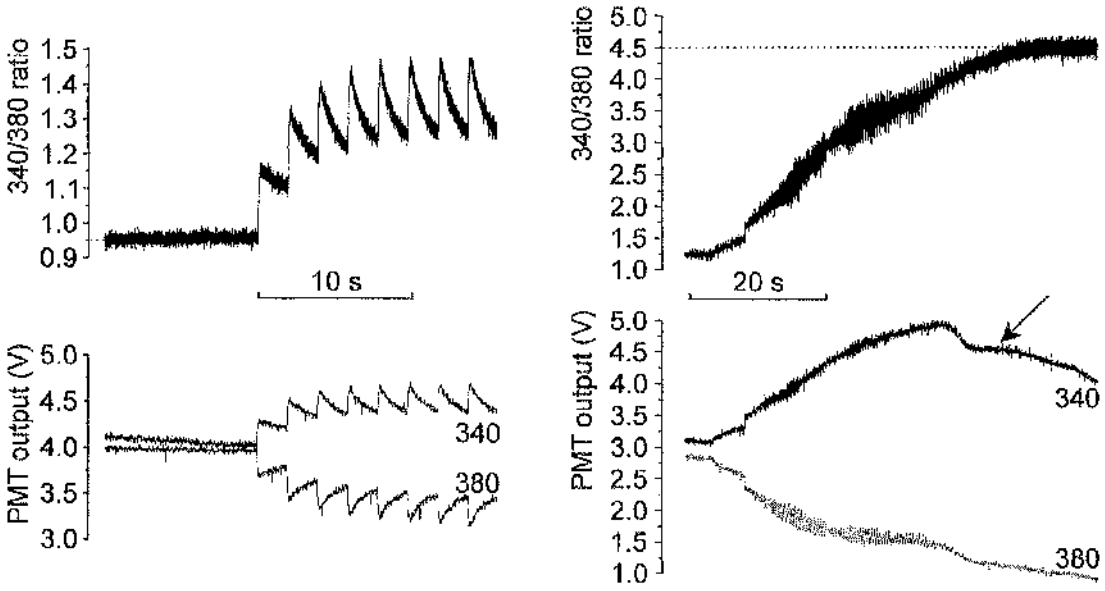

Figure 2.5 Determination of R_{min} and R_{max}. Left panel shows stimulated Ca transients from quiescent state, with ratio signal above and 340 nm & 380 nm signals below, as indicated. R_{min} is taken as the minimum ratio at the start of the experiment (0.95 in this example). Right panel shows determination of R_{max} (note different axes). Just after the beginning of the sweep, the cell is punctured and [Ca] rises (rapid oscillations of Ca can be seen). R_{max} is taken at the ratio peak, prior to significant loss of dye from the cell. This is judged from the 340 nm signal - after the peak there is an initial small drop as the cell balls up in the field, then a short plateau before loss of dye from the cell. R_{max} is taken at the arrowed point (4.5 in this example).

peak ratio before significant loss of intracellular dye (judged from the individual wavelength signals). Figure 2.5 shows an example of the estimation of R_{min} and R_{max}, along with the ratio signal during stimulation of the cell at 0.5 Hz.

In order to determine K_d and β, it is necessary to calibrate the Fura-2 340/380 ratio signal against known concentrations of Ca. *In vitro* calibration of the Fura-2 salt with solutions of known [Ca] is straightforward, however the intracellular properties of

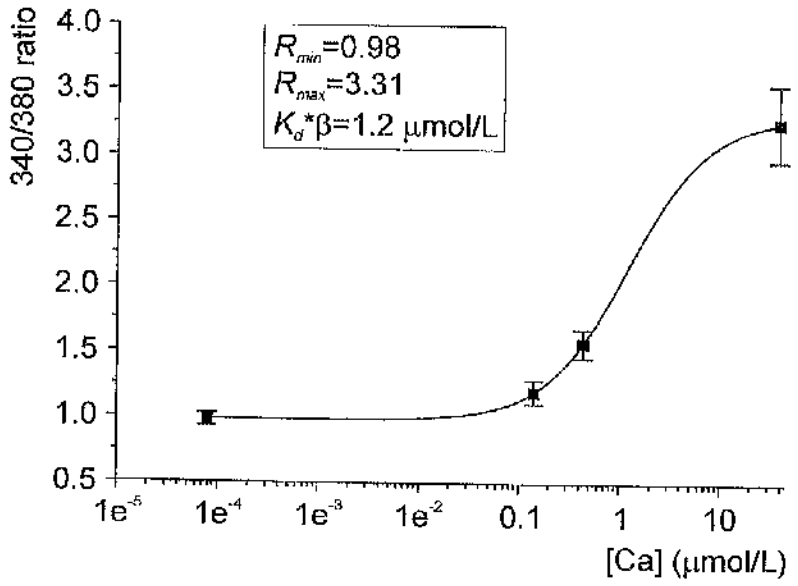

Figure 2.6 Intracellular calibration curve for Fura-2. Permeabilised cells were exposed to 4 different concentrations of Ca. A logistic regression curve was fitted to the data, with resulting parameters as shown. n = 9 cells for the lowest point, n = 6 cells for all other points.

Fura-2 have been shown to differ (see Sipido & Callewaert, 1995), so an *in vivo* calibration is preferred. This was performed by permeabilising cells with 0.1 mg/mL β-escin (Sigma-Aldrich Company Ltd), then perfusing with a mock intracellular solution, with [Ca] buffered to different levels using EGTA. Four solutions were used, with each cell exposed to only one solution. The concentrations of Ca (μmol/L), estimated using the computer program "React" were: 8e^{-5} (for R_{min}), 0.14, 0.44 and 39 (for R_{max}). The results are shown in Figure 2.6, with the fitting parameters for a logistic regression. This gave an estimate of $K_d * \beta$ of 1.2 μmol/L, which was used throughout the thesis. β itself is more difficult to determine since it must be measured in individual cells and is very sensitive to loss of dye from the cell. From the experiment shown in Figure 2.6, β was estimated at 3.03 ± 0.23 (n=6), giving a K_d for Fura-2 of around 400 nmol/L. This compares well with data provided by the manufacturer, where a K_d of 371 nmol/L was obtained in astrocytoma cells (see www.probes.com/handbook/sections/2001).

2.8 Statistical analysis

Data are presented in the text and on figures as mean ± standard error of the mean (SEM). Error bars are excluded on figures when they are smaller than symbols. Descriptive statistics were calculated within spreadsheets on Microsoft Excel 2000. Statistical comparisons were made using InStat software (v2.05, GraphPad software, AD Cunningham, University of Glasgow). Single comparisons were made using two-tailed Student's t-tests, with paired or unpaired data, as appropriate, and statistical significance was taken at the $p=0.05$ level. For multiple comparisons, Fisher's protected Least Significant Differences (LSD) method was used. This was chosen over standard analysis of variance (ANOVA) methods (e.g. Tukey's) since the number of *planned* comparisons to be made was less than the total *possible* number of comparisons. For example, for the four groups under study in the majority of experiments (Sham Endo, Sham Epi, LVD Endo, LVD Epi), there were four predetermined comparisons to be made: 1) between regions for each animal type (i.e. Sham Endo *vs* Sham Epi and LVD Endo *vs* LVD Epi), and 2) between animal types for each region (Sham Endo *vs* LVD Endo and Sham Epi *vs* LVD Epi). For Fisher's protected LSD method, a one-way ANOVA is first performed and if the F-value does *not* reach significance then no significant difference between the groups is reported. If the F-value *is* significant then the predetermined comparisons can be made using Student's t-tests. This method holds the chance of reporting a significant difference when there is none to 5%.

CHAPTER 3

SODIUM-CALCIUM EXCHANGER FUNCTION UNDER CONDITIONS OF FIXED AND VARYING $[Ca]_i$

3.1 Introduction

3.1.1 Quantification of NCX function

A variety of methods have been used to measure the function of NCX, making use of the electrochemical properties of the exchanger. Changes in either the voltage or the ionic conditions will affect NCX function, and to quantify activity of the exchanger usually one of these factors is kept constant and the other is altered, while measuring a variable which is proportional to NCX function (e.g. current or [Ca]).

Early experiments commonly used radiolabelled ions (e.g. ^{22}Na and ^{45}Ca) to demonstrate flux across the membrane, and these experiments gave some limited information on the rate of exchanger function for a given weight of tissue (e.g. Baker *et al.*, 1969; Glitsch *et al.*, 1970).

The first detailed measurements of NCX function in single myocytes were performed by Kimura *et al.* (Kimura *et al.*, 1986; Kimura *et al.*, 1987). They carefully controlled the internal and external ionic conditions in whole-cell voltage-clamped guinea pig ventricular myocytes, in the presence of blockers of K and Ca currents and the Na-K ATPase. I_{NCX} was determined using triangular voltage ramps to +60 mV and back to -120 mV. More recently, Convery & Hancox analysed the effects of different ramp and step protocols, and different Ca buffers, on the characteristics of I_{NCX} (Convery & Hancox, 1999). They demonstrated that the direction of the ramp (ascending compared to descending) had a significant impact on the reversal potential and the shape of the current. They provided evidence that subsarcolemmal [Ca] was perturbed more by a descending ramp than an ascending one, with local accumulation of Ca under the membrane. This altered the shape of the I_{NCX}/V curve and shifted the reversal potential

further away from the predicted value. The I_{NCX}/V relationships obtained by ascending ramps were very similar to those obtained by voltage steps and the authors suggested that ascending ramps allowed better control of ionic conditions. Further experiments did not show any significant effect of using BAPTA rather than EGTA as the Ca buffer. For these reasons, ascending ramps were used in this study, and ionic conditions and control of $[Ca]_i$ were verified as outlined in the methods section (3.2.1.1).

The voltage-clamp methods discussed above refer to measurement of I_{NCX} under conditions where the ionic composition on either side of the membrane is tightly controlled. NCX function can also be measured where voltage is kept constant and $[Ca]_i$ is allowed to vary. Since NCX is responsible for the majority of calcium extrusion from the cell, measuring the rate of extrusion can give information on NCX function. Commonly, a train of stimuli is used to produce steady-state loading of the SR, followed by a prolonged caffeine application to produce a maximal release of Ca, at the same time preventing its re-accumulation into the SR. Some measure of the rate of Ca decay can then be used as a measure of NCX function (e.g. Varro *et al.*, 1993; Negretti *et al.*, 1995). This measure can be corrected for non-NCX removal mechanisms (e.g. sarcolemmal Ca-ATPase) by repeating the caffeine application in the presence of nickel (Varro *et al.*, 1993; Negretti *et al.*, 1995) or in the absence of Ca and Na (Bassani *et al.*, 1992; Puglisi *et al.*, 1996).

One further method of quantifying NCX function is to keep the membrane potential constant and produce a sudden change in the external ionic conditions (e.g. to [Na]=0) using a rapid solution switcher. An inward or outward current will be produced, the

amplitude of which will vary according to exchanger function. This approach has been widely used by Barry, Bridge and co-workers (e.g. Su *et al.*, 1999).

In this chapter, in addition to the voltage ramp protocols, NCX function was also estimated based on the rate of Ca decay during prolonged caffeine application, corrected for non-NCX removal using nickel.

3.2 Methods

3.2.1 NCX current density

3.2.1.1 Solution compositions

The solutions used tightly controlled the intracellular and extracellular ionic conditions, and eliminated, as far as possible, currents other than I_{NCX}. Hence, the solutions were potassium-free to abolish K-currents (K replaced by Cs); *N*-acetylstrophanthidin was added to block the Na-K pump; and nifedipine was present to block $I_{Ca,L}$. It was also essential to constrain [Na] and [Ca] tightly, such that a current-voltage relationship could be determined for a given set of internal and external ionic conditions. The pipette solution was designed to buffer $[Ca]_i$ heavily, to ~258 nmol/L (calculated using the computer program "React II", G.L.Smith & L.S.Duncan, University of Glasgow). To confirm the [Ca] conditions, two approaches were used. Firstly, Fura-2 acid (10 µL of 1 mg/mL Fura-2 per mL of solution) was added to the pipette solution. This gave an estimated [Ca] of around 200 nmol/L. Secondly, experiments with Fura-2 AM loaded cells dialysed with the pipette solution suggested a $[Ca]_i$ of 353 ± 52 nmol/L (n=11). The calculated value was felt to reflect a reasonable estimate of the calcium concentration since it fell between these two values. In the absence of EGTA there was a significant rise in $[Ca]_i$ during the ramp protocol, which was eliminated by 50 mmol/L EGTA (see Figure 3.1). Preliminary experiments with 10 mmol/L EGTA in the pipette showed some escape of $[Ca]_i$ during the ramp protocol, so the higher concentration of EGTA was used throughout.

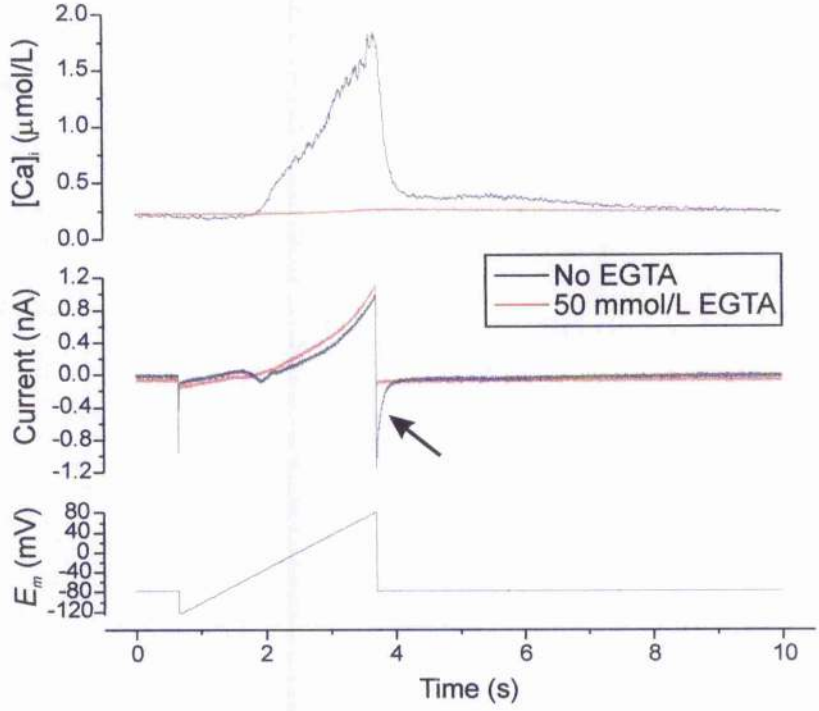

Figure 3.1 Effects of internal Ca buffering during ramp protocol. **Bottom panel:** voltage ramp protocol. **Middle panel:** resulting currents in the absence (black trace) and presence (red trace) of 50 mmol/L EGTA in the pipette solution. Note the distortion of the current profile during the ascending ramp and the significant tail current on repolarisation (arrow). **Upper panel:** $[Ca]_i$ during the ramp protocol. Note that in the presence of 50 mmol/L EGTA the rise in Ca is almost completely abolished.

3.2.1.2 Voltage-clamp protocol

After achieving the whole-cell configuration, a period of 5-10 min was allowed for dialysis of the pipette solution into the cell. Currents were then measured in response to a ramp from -120 mV to +80 mV from a holding potential of -80 mV. The ramp protocol was performed at 0.1 Hz until steady-state currents were achieved, whereupon data from up to 12 ramps were averaged. The protocol was repeated in the presence of 5 mmol/L $NiCl_2$ to obtain the background (non-NCX) current. Initial experiments were performed varying the duration of the ramp from 1 s to 4 s. Voltage ramps of 1 and 2 s

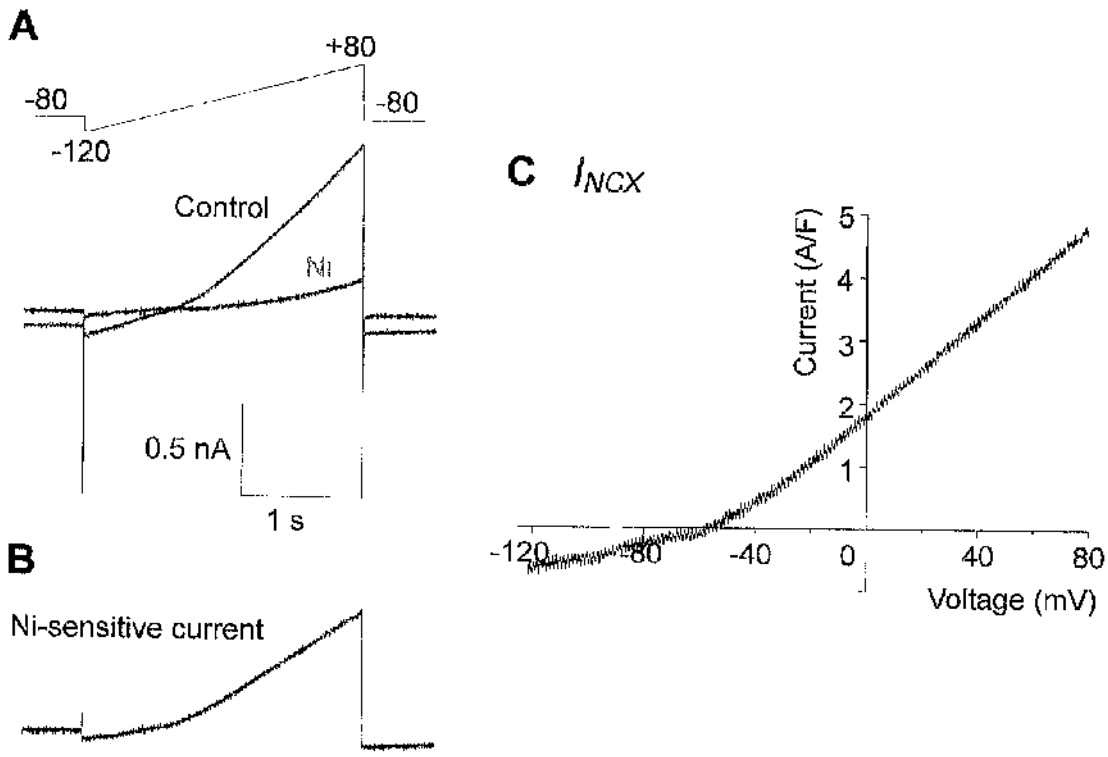

Figure 3.2 Voltage clamp protocol and initial data analysis. **A:** Voltage ramp protocol and resulting currents in the absence and presence of 5 mmol/L Ni. **B:** Current in Ni subtracted from control current to give current due to NCX. **C:** *I-V* curve, corrected for cell capacitance.

showed some activation of the sodium current, contaminating I_{NCX}, and a 3 s ramp was found to give the best balance between speed of the protocol and adequate voltage control.

3.2.1.3 Data analysis

For each cell, continuous sweeps of current against time in the absence and presence of nickel were separately averaged and the data in the presence of nickel were then subtracted to give the current attributable to NCX. This was converted to current versus voltage (*I-V*) data, which was then corrected for cell capacitance (Figure 3.2).

$$I_{NCX} = Allo_{NCX} \cdot \frac{V_{Max}\left\{[Na]_i^3[Ca]_o \exp\left(\frac{\eta VF}{RT}\right) - [Na]_o^3[Ca]_i \exp\left(\frac{(\eta-1)VF}{RT}\right)\right\}}{\kappa_{NCX}\left\{1 + k_{Sat}\exp\left(\frac{(\eta-1)VF}{RT}\right)\right\}}$$

$$Allo_{NCX} = \frac{1}{1+\left(\frac{K_{mCaAct}}{[Ca]_i}\right)^{n_{Hill}}}$$

$$\kappa_{NCX} = K_{mCa_o}[Na]_i^3 + K_{mNa_o}{}^3[Ca]_i + K_{mNa_i}{}^3[Ca]_o\left(1+\frac{[Ca]_i}{K_{mCa_i}}\right) + K_{mCa_i}[Na]_o^3\left(1+\frac{[Na]_i^3}{K_{mNa_i}{}^3}\right) + [Na]_i^3[Ca]_o + [Na]_o^3[Ca]_i$$

Equation 3.1 Mathematical model of I_{NCX}. See text for details.

Data points were generated at 10 mV intervals between -120 mV and +80 mV. These data were averaged for each cell type (Sham Endo / Epi, LVD Endo / Epi) to allow for statistical comparison at given voltages (-110 mV and +70 mV).

The data points for each cell were also fitted using the model of NCX function of Weber *et al.* (Equation 3.1; Weber *et al.*, 2001), which is modified from the work of Segel (1993), Mullins (1979) and Luo & Rudy (1994). Briefly, I_{NCX} is expressed as the product of an electrochemical factor and an allosteric factor. The electrochemical factor is based on a V_{Max} (which is assumed to be equal for forward and reverse flux), the internal and external concentrations of Ca and Na, and dissociation constants (K_m) for each ion on either side of the membrane. The allosteric factor represents regulation of NCX as an instantaneous Hill equation for Ca binding to the regulatory site and the Hill coefficient (n_{Hill}) was taken as 2, based on previous studies (Levitsky *et al.*, 1994). For

Term	$[Na]_o$	$[Ca]_o$	$[Ca]_i$	K_{mNao}	K_{mNai}	K_{mCao}	K_{mCai}	K_{sat}	K_{mCaAct}	η	n_{Hill}
Units	mmol/L	mmol/L	nmol/L	mmol/L	mmol/L	mmol/L	µmol/L		nmol/L		
Value	143	1.8	258	87.5	12.3	1.3	3.6	0.27	125	0.35	2
Ref.				*1*	*2*	*3*	*2*	*3*	*4*	*3*	*3*

Table 3.1 Values for terms in I_{NCX} model. References: *1* – Kimura *et al.*, 1987; *2* – Hilgemann *et al.*, 1991; *3* – Pogwizd *et al.*, 1999; *4* – Weber *et al.*, 2001.

$$[Na]_i = \frac{[Na]_o}{\sqrt[3]{\frac{[Ca]_o}{[Ca]_i}}\exp\frac{FE_{Rev}}{RT}}$$

Equation 3.2 Calculation of $[Na]_i$. F = 96500 $Cmol^{-1}$, E_{Rev} = reversal potential, R = 8.3143 $Jmol^{-1}K^{-1}$ and T = 310 K.

simplicity, when fitting the I_{NCX} data it was assumed that no differences in allosteric regulation existed between cell types, and the K_m for calcium activation (K_{mCaAct}) was taken to be 125 nmol/L, based on data from the literature (ferret; Weber *et al.*, 2001). Later experiments designed to study in detail allosteric regulation in Sham and LVD cells are described below and the implications of the findings are examined in the discussion, section 3.4.3.2.

Values for the dissociation constants and other terms were derived from the literature, and are summarised, with references, in Table 3.1. Since subsarcolemmal [Na] is difficult to buffer adequately, and small discrepancies in $[Na]_i$ have a large effect on the quality of the model fit, $[Na]_i$ was calculated for each cell. This was based on the reversal potential of each I_{NCX} *I-V* curve, using Equation 3.2. This equation is derived

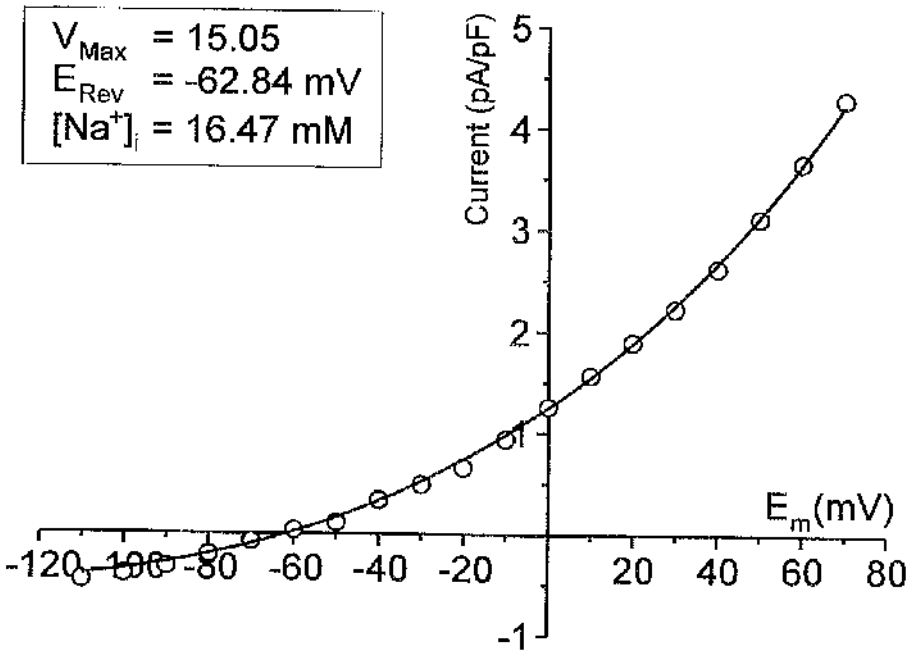

Figure 3.3 Example of I_{NCX} model fit to raw data from a Sham endocardial cell. Reversal potential (E_{Rev}) and calculated $[Na]_i$ are indicated.

from the Nernst equation for NCX, assuming a stoichiometry of 3Na: 1Ca. The calculated $[Na]_i$ was used in the fitting function for each cell, along with the values outlined in Table 3.1, to derive a V_{Max} for each cell. Fitting of the I_{NCX} function was performed using the graphical program OriginPro 6.1 or 7.0 (OriginLab Corporation, Northampton, MA, USA). An example of a typical curve fit is shown in Figure 3.3.

3.2.1.4 Viral transfection of cultured cells

In order to confirm the sensitivity of the above protocol for assessing NCX current density, the technique was also performed on cultured cells overexpressing NCX. As described in section 2.4, myocytes derived from the interventricular septum were cultured for 2 days in the presence of adenoviruses encoding NCX or Lac-Z, at an MOI of 100. NCX current density in these cells was compared with that in non-transfected

control cells. The data points for each cell were fitted using the model of NCX function, as outlined in the previous section.

3.2.2 NCX-mediated Ca efflux

3.2.2.1 Solution compositions

In these experiments, intracellular $[Ca]_i$ was allowed to vary, and the rate of Ca removal attributable to NCX could be estimated. The solutions were designed to block some ionic currents which could indirectly affect $[Ca]_i$ or influence voltage control (see 2.5.4). Thus, 4-aminopyridine was present in the superfusate, and tetraethylammonium chloride in the pipette solution, to block K-currents; and Ca-activated chloride currents were minimised using niflumic acid. The Na-K ATPase was not blocked, to allow for cellular regulation of $[Na]_i$.

3.2.2.2 Experiment protocol

Myocytes were held at -80 mV and stimulated for 30 s by a 1 Hz depolarising train to 0 mV for 150 ms, to achieve steady-state contractions. NCX activity was then estimated by rapidly switching to 10 mmol/L caffeine for a period of 10 s at a holding potential of -80 mV (see Figure 3.4). This produced a sudden rise in intracellular calcium due to SR release, followed by a decay phase as calcium was removed from the cell. The decay phase is accompanied by an inward current due to Ca extrusion by NCX. The protocol was repeated with 10 mmol/L $NiCl_2$ applied just prior to, and during, the caffeine application to provide an estimate of non-NCX Ca removal mechanisms. Under these conditions NCX is inhibited, the rate of Ca decay is markedly slowed, and the inward current is virtually abolished.

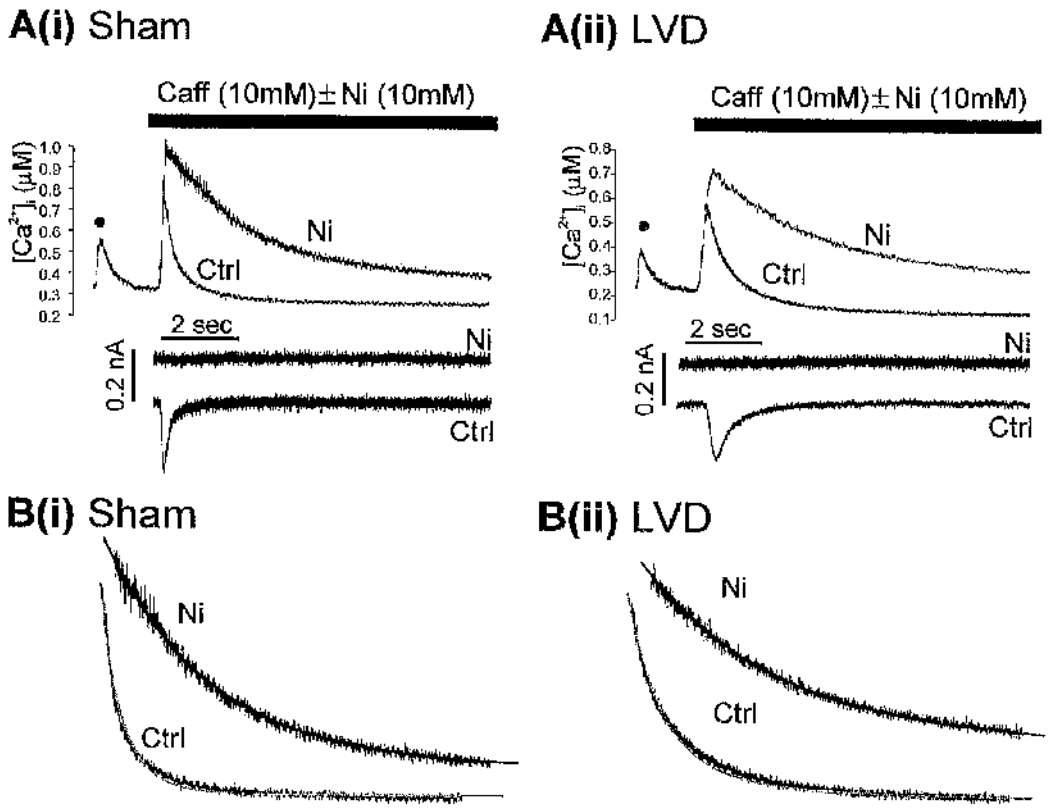

Figure 3.4 Protocol for estimating NCX activity. Panel **A** shows the final steady-state calcium transient at the end of a 1 Hz train of stimuli (•), followed by the rapid application of 10 mmol/L caffeine (Caff, black bar) in the absence (Ctrl) and presence (Ni) of 10 mmol/L $NiCl_2$. The corresponding current traces are illustrated below, vertically separated for clarity. Note that on caffeine application there is an inward current, which is virtually abolished in the presence of Ni. **B:** Expanded Ca decay phases, with superimposed single exponential fit functions, to estimate the rate constant of decay. In each panel, typical traces are illustrated for **(i)** Sham and **(ii)** LVD cells.

In most cases, the protocol could be applied more than once in a given cell, and for each cell the results were averaged. Since parts of the experiments described in Chapter 4 were carried out with the same solution compositions and identical voltage-clamp protocol, analysis of the Ca decays and characteristics of the inward current in

the presence of caffeine from these experiments could be included in the analysis. These protocols did not include the application of caffeine in the presence of nickel, so the analysis of the rate of Ca decay under these conditions relates only to the cells studied in this chapter.

3.2.2.3 Data analysis

Fura-2 fluorescence ratio data were converted to [Ca] as outlined in section 2.7.3.5 and the Ca decay phase after caffeine application was fitted with a single exponential decay function using OriginPro 6.1 (OriginLab Corporation, Northampton, MA, USA). The amplitude of the caffeine-induced inward current was measured and the decay phase of the current was also fitted with a single exponential function, to provide a further estimate of NCX activity.

3.2.3 Allosteric regulation of NCX

3.2.3.1 Solution compositions

Solutions were designed to isolate I_{NCX} from contaminating currents and to prevent Ca uptake into the SR, to allow the relationship between I_{NCX} and $[Ca]_i$ to be studied. Thus, after voltage-clamp was achieved in NT solution, the cell was treated with 1 μmol/L of the SERCA inhibitor thapsigargin (Calbiochem, La Jolla, CA, USA) for ~1 min to disable the SR, then 10 mmol/L caffeine was applied to ensure that the SR had emptied of Ca. The superfusing solution was then changed to a K-free solution containing 10 μmol/L nifedipine (to block I_{CaL}), 10 μmol/L *N*-acetylstrophanthidin (to block Na-K ATPase), and 100 μmol/L niflumic acid (to block the Ca-activated Cl current). The pipette solution used throughout was K-free (K replaced with equimolar Cs) and contained 20 mmol/L TEA to block any remaining potassium currents.

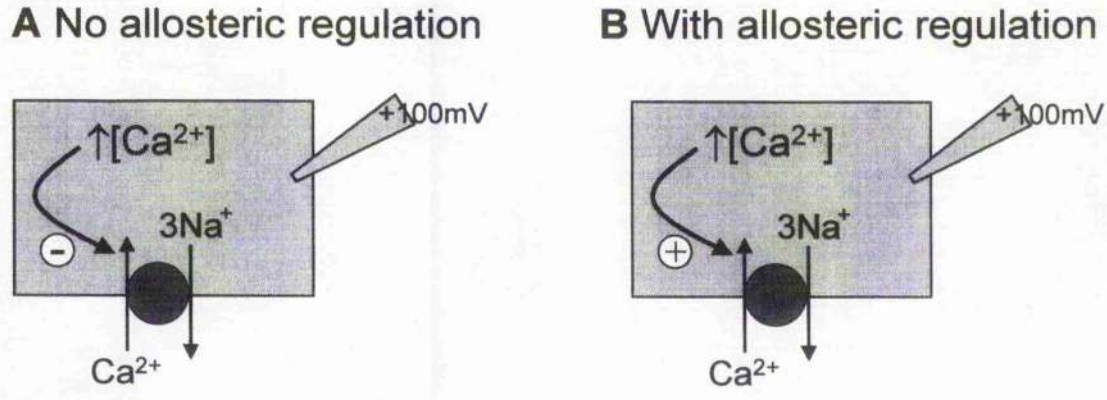

Figure 3.5 Theory behind voltage protocol for investigating allosteric regulation of NCX. The cell is shown held at +100 mV, thus favouring outward (reverse-mode) NCX current. In the case where no allosteric regulation exists (**A**), as $[Ca]_i$ rises, the Ca gradient is reduced and the outward current will diminish. In the presence of allosteric regulation (**B**), in spite of the reduced Ca gradient, the exchanger is activated by the rise in $[Ca]_i$ and the outward current increases.

3.2.3.2 Voltage-clamp protocol

To determine whether allosteric regulation of NCX was occurring in rabbit cardiomyocytes, a protocol was devised based on that of Weber *et al.* (2001) which entails examining the outward (reverse-mode) current as $[Ca]_i$ rises. The theory behind the protocol is illustrated in Figure 3.5. Briefly, in the absence of allosteric regulation of NCX by $[Ca]_i$, outward (reverse-mode) NCX current will fall as $[Ca]_i$ rises, since the gradient for Ca across the membrane will be reduced. However, if allosteric regulation is present then increasing $[Ca]_i$ will at first *increase* the outward current.

Myocytes were initially held at -100 mV to initialise them to conditions of low $[Ca]_i$, whereupon they were stepped to +100 mV 20 times, with 100 ms intervals between

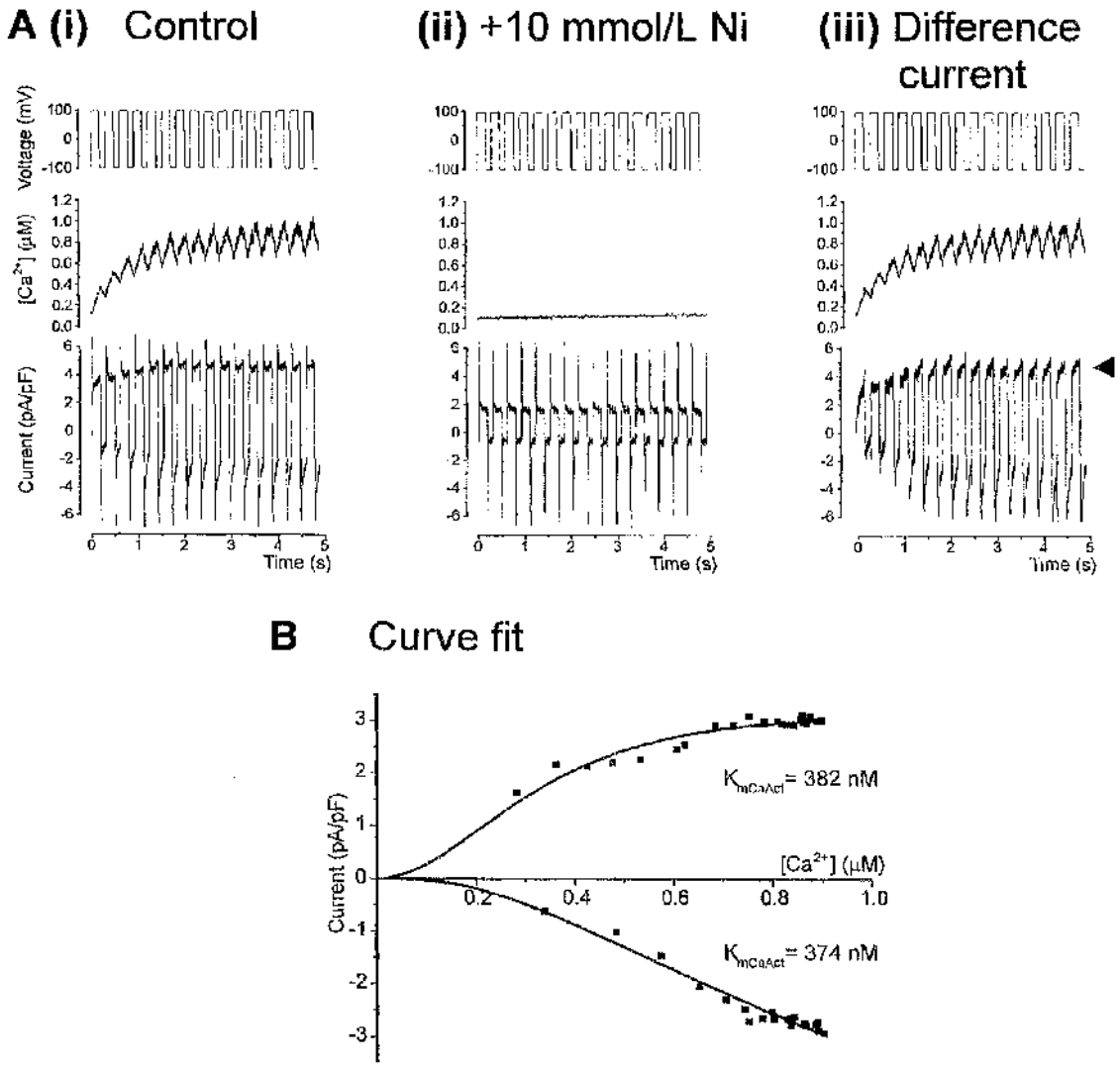

Figure 3.6 **A:** Voltage clamp protocol used to investigate the allosteric regulation of NCX by intracellular Ca. Cardiomyocytes were alternately clamped at -100 mV and +100 mV as described in section 3.2.3.2 in the **(i)** absence and **(ii)** presence of 10 mmol/L Ni. Resulting Ca and current traces are illustrated in each panel. **A(iii):** Difference current generated by subtracting current in **(ii)** from that in **(i)**. Outward current is indicated with arrowhead (◀). **B:** For each voltage step, mean current was plotted against mean $[Ca]_i$ and the resulting data points were fitted using Equation 3.1 to generate a K_m for calcium activation (K_{mCaAct}).

each step (see Figure 3.6). The duration of the voltage pulse (100 or 200 ms) was

chosen for each cell to produce a rise in $[Ca]_i$ within a physiological range. The protocol was repeated in the presence of 10 mmol/L $NiCl_2$ and the background current generated was subtracted.

3.2.3.3 Data analysis

The difference current (obtained by subtracting the current in the presence of Ni) and $[Ca]_i$ were averaged for each voltage step to yield a plot of current (corrected for cell capacitance) against $[Ca]_i$ (Figure 3.6 B). The data points were then fitted using Equation 3.1, with V_{Max} and K_{mCaAct} allowed to vary, and ion concentrations appropriate for the solutions used. The values for other terms in the equation are given in Table 3.1. The fitting function was performed separately for inward (V=-100 mV) and outward (V=+100 mV) currents. The latter generally gave a better fit to the data, perhaps because of the more pronounced sigmoid shape of the curve, and in some cases it was not possible to find a satisfactory fit to the inward current. Cells were rejected if the range of $[Ca]_i$ was too narrow to produce a reliable fit to the data.

3.3 Results

3.3.1 I_{NCX} *current density*

3.3.1.1 Regional differences and altered NCX current density in LVD

I_{NCX} current density was estimated for each cell type using a voltage ramp protocol in the absence and presence of 5 mmol/L Ni. Mean I_{NCX} current-voltage relationships, corrected for cell capacitance, are illustrated in Figure 3.7 A, with results for Sham cells (Fig. 3.7 A(i)) and LVD cells (Fig. 3.7 A(ii)) plotted on the same scale. The number of cells in each group is stated on the figure; the cells were obtained from 5 sham-operated animals and 4 LVD animals. On average, results were obtained from 4-5 cells from each region in each animal.

Figure 3.7 A demonstrates that I_{NCX} current is larger in endocardial cells than epicardial cells in both Sham and LVD animals, with the differences apparent at both positive and negative voltages. However, the currents in LVD cells were significantly smaller than those in Sham cells. This is illustrated further in the summary data in the lower panel (Fig. 3.7 B) at two sample voltages (-110 mV and +70 mV). Statistical analysis confirms the endocardial-epicardial differences in both Sham and LVD animals, although the difference for LVD animals at –110 mV does not quite reach significance ($p=0.07$). Comparing like regions from Sham to LVD animals gives highly significant results (generally, $p<0.001$). For example, at +70 mV, the current in LVD is around 68% of that in Sham animals (e.g. for endocardial cells, 3.15 A/F versus 4.62 A/F; $p<0.001$).

The raw data for each cell were also fitted with the model of NCX function of Weber *et al.* (2001). This generated a V_{Max} value for each cell, and also enabled a comparison

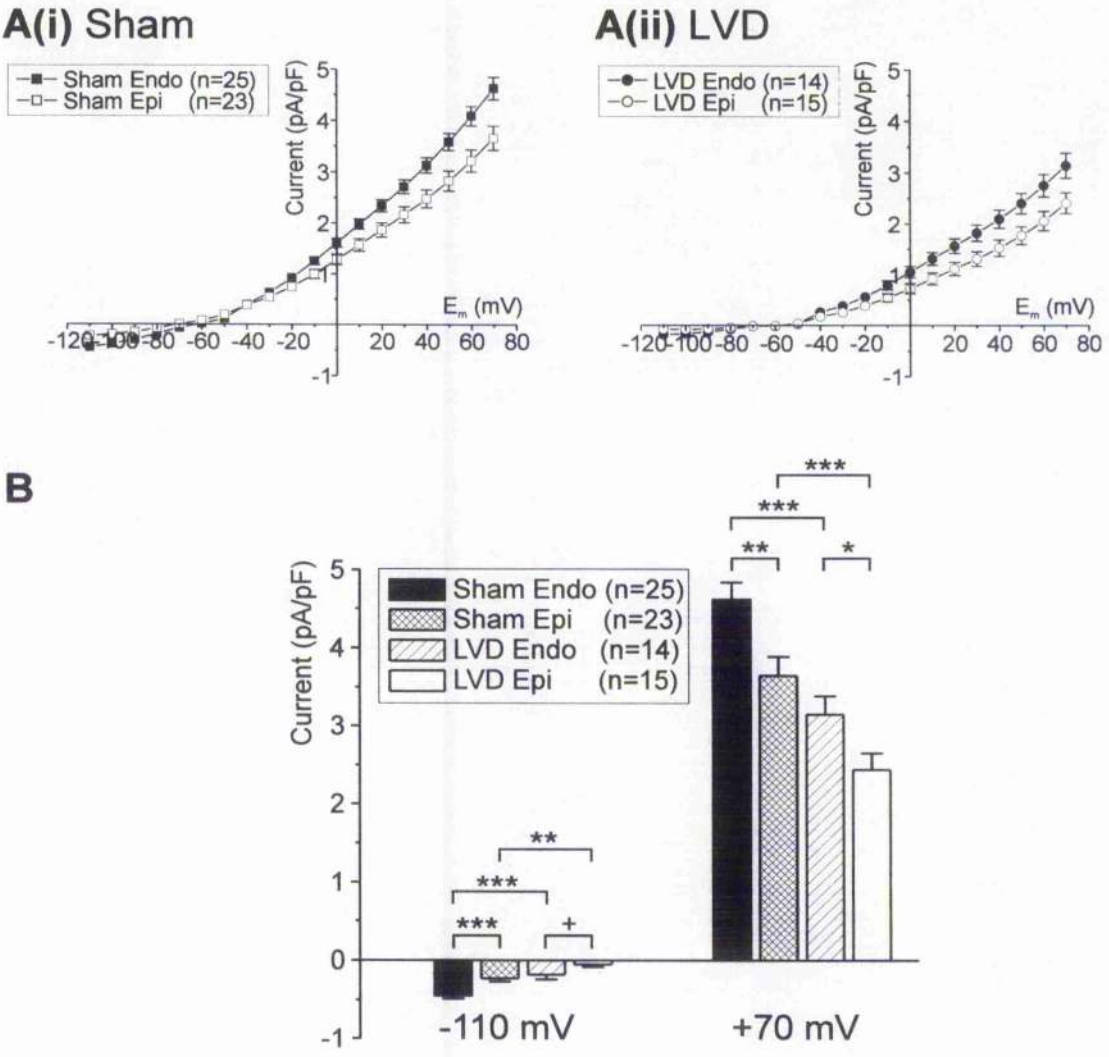

Figure 3.7 Results – **A:** Current-voltage relationships for Sham and LVD cells. In both cases the current density is higher in Endo than Epi cells. **B:** Summary bar graphs showing current density at -110 mV and +70 mV for Sham and LVD cells. *p<0.05, ** p<0.01, ***p<0.001, + p=0.07.

between the shape of the *I-V* curves obtained in these experiments and the shape of an *I-V* curve from a published model. As shown in Figure 3.3, good fits to the raw data could be obtained, using dissociation constants derived from the literature, and ionic concentrations based on the solutions used or calculated using the reversal potential, as described in the methods section, 3.2.1.3. Summary data for the same set of cells

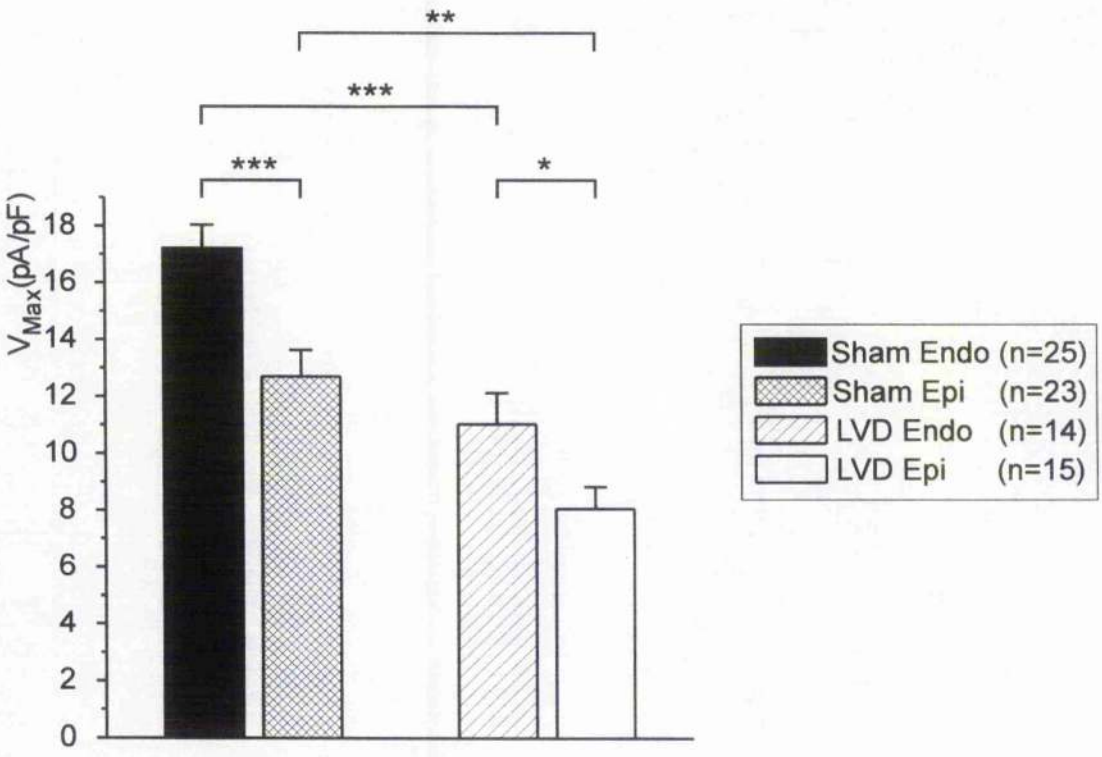

Figure 3.8 Bar graph summarising mean V_{Max} data from I_{NCX} curve fits, for each cell type. * $p<0.05$, ** $p<0.01$, *** $p<0.001$.

shown in Figure 3.7 are shown in Figure 3.8. These data again demonstrate the significant endocardial-epicardial differences, with the V_{Max} in epicardial cells being around 74% of that in endocardial cells in both Sham and LVD animals (e.g. for Sham cells, 12.70 A/F *vs* 17.21 A/F; $p<0.001$). The Sham-LVD differences are also apparent – the V_{Max} in LVD is around 64% of that in Sham animals (e.g. for endocardial cells, 11.04 A/F versus 17.21 A/F; $p<0.001$).

3.3.1.2 Viral transfection of NCX

Figure 3.9 shows the results of analysing I_{NCX} current density in day-2 cultured myocytes. No significant difference was found between non-transfected cells and the

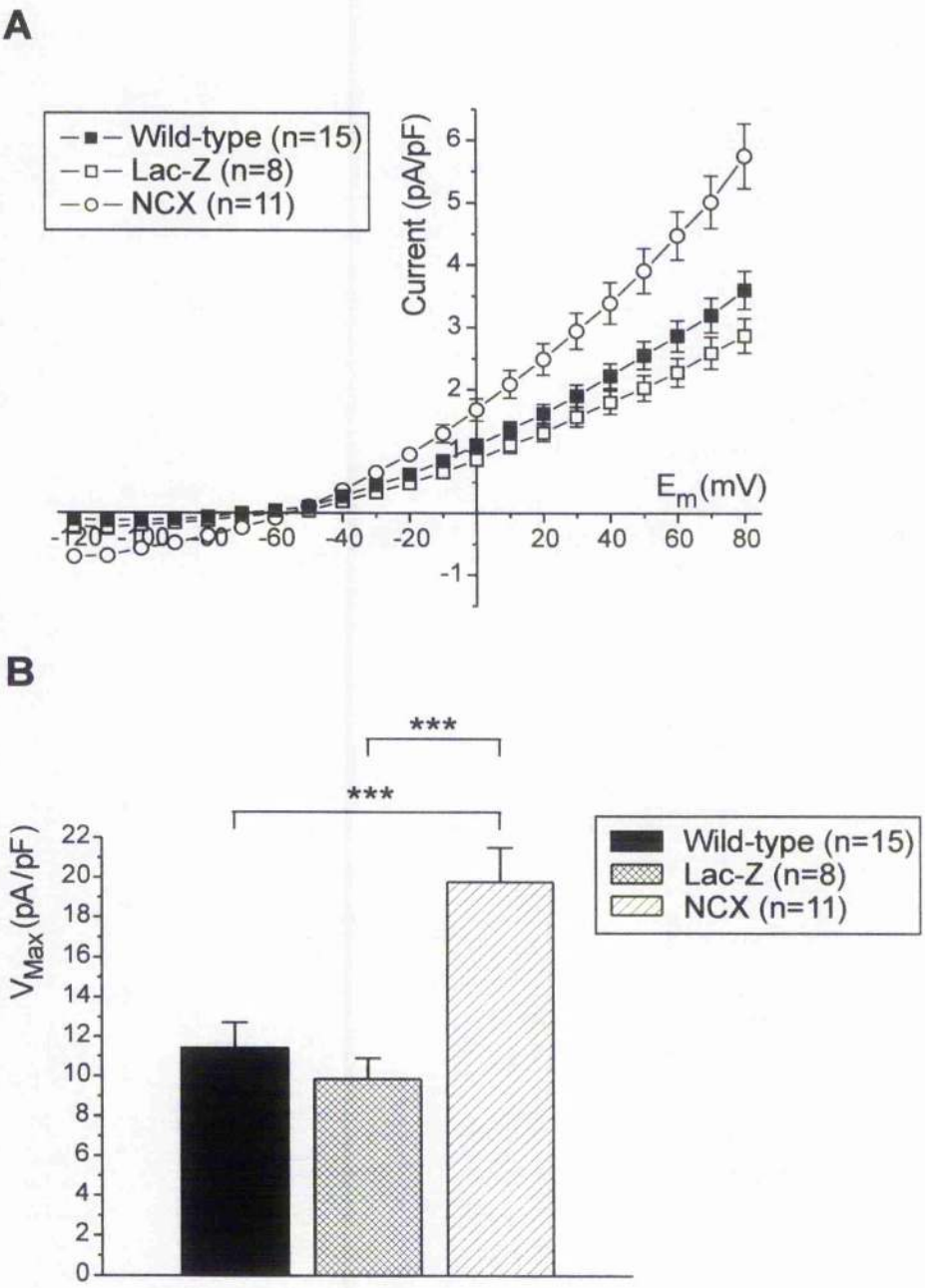

Figure 3.9 NCX current density in day-2 cultured cardiomyocytes. **A:** comparison of I_{NCX} in non-transfected (wild-type) cells with those transfected with Lac-Z or NCX adenoviruses. **B:** Bar graph summarising mean V_{Max} data from I_{NCX} curve fits, for each cell type. *** $p<0.001$.

transfected control cells expressing Lac-Z. However, adenoviral transfection of NCX resulted in a significantly higher NCX current density, with an increase in V_{Max} of 73%

Cell type	n	Capacitance (pF)	I_{NCX} reversal potential (mV)	$[Na]_i$ (mmol/L)
Sham Endo	25	176.8 ± 10.9	-62.5 ± 1.4	16.5 ± 0.3
Sham Epi	23	188.0 ± 10.2	-70.3 ± 2.2 *	18.2 ± 0.5 *
LVD Endo	14	256.2 ± 14.4 ***	-68.1 ± 2.4	17.7 ± 0.5
LVD Epi	15	216.9 ± 16.4	-68.4 ± 2.2	17.7 ± 0.5

Table 3.2 Cell characteristics – measured capacitance and I_{NCX} reversal potential, with calculated $[Na]_i$. * $p<0.05$ versus Sham Endo, *** $p<0.001$ versus Sham Endo, other statistical comparisons not significant.

compared to non-transfected cells, and 100% compared to Lac-Z transfected cells ($p<0.001$ in both cases).

3.3.2 Cell characteristics

3.3.2.1 Cell capacitance

Table 3.2 summarises the baseline characteristics of the cells studied. It is apparent that the capacitance of the LVD endocardial cells studied is significantly higher than the capacitance of the Sham endocardial cells, but other comparisons were not significant. Whilst this may reflect a true difference in cell size, the comparison is not valid since it is heavily biased by operator selection – in an attempt to standardise voltage clamp conditions, cells of a roughly similar size are chosen irrespective of the cell group under study. However, previous studies of this animal model specifically aimed at determining cell size have indeed shown evidence of significant hypertrophy in the LVD cells (McIntosh *et al.*, 2000; Quinn *et al.*, 2003).

3.3.2.2 Reversal potential and $[Na]_i$

Analysis of the reversal potential (E_{Rev}) data shows that E_{Rev} in Sham endocardial cells is significantly more positive than that in Sham epicardial cells (-62.5 ± 1.4 mV *vs* -70.3 ± 2.2 mV; $p<0.05$), but other comparisons are non-significant. Since $[Na]_i$ is calculated from the reversal potential, this similarly shows a small difference between Sham endocardial and epicardial cells (16.5 ± 0.3 mmol/L *vs* 18.2 ± 0.5 mmol/L; $p<0.05$).

Close examination of the curves in Figure 3.7 shows that the portion of the curve crossing the abscissa is relatively flat, meaning that small variations in the curve can have large effects on the estimated E_{Rev}. It is also apparent that there is a small negative indentation in the curve around this point, which may be due to slight contamination of the current by I_{Na} – it is much more marked when a faster ramp depolarisation is used (e.g. 1 s, data not shown). Both these factors must be kept in mind before attributing the apparent difference in E_{Rev} between Sham endocardial and epicardial cells to a property of the exchanger itself.

3.3.2.3 Stoichiometry of NCX

Altered stoichiometry of the exchanger in LVD would result in a shift in the reversal potential of I_{NCX} and the curve fitting function can be used to investigate this. If it is assumed that full equilibration of pipette contents with the cytoplasm takes place and that good control of $[Na]_i$ is achieved, then $[Na]_i$ can be set to 20 mmol/L, rather than being allowed to vary, as in the analysis above. With these parameters set, the stoichiometry of the exchanger (n) can be allowed to vary, to produce the best fit to the

data, including E_{Rev}. Using this approach, no significant difference is found in the stoichiometry between Sham cells (n=3.21 ± 0.05) and LVD cells (n=3.16 ± 0.05).

3.3.3 NCX-mediated Ca efflux

These experiments were designed to estimate NCX activity in each cell type by measuring the rate of calcium removal from the cytoplasm under conditions where re-sequestration into the SR is prevented. A train of stimuli was used to achieve steady-state SR loading whereupon 10 mmol/L caffeine was applied, resulting in Ca release from the SR and removal of Ca mainly via NCX. Both the calcium signal and the inward current on application of caffeine were analysed.

Figure 3.10 summarises the results for each cell type. The "Caffeine" data were obtained from 14 animals for Sham Endo, Sham Epi and LVD Endo; and 13 animals for LVD Epi. The "Caffeine+Ni" data were obtained from 4 animals for each group. As shown in Figure 3.10 A, no significant differences were found in the rate of Ca removal with caffeine application in the presence of nickel. Under these conditions, SR re-sequestration and Ca removal on NCX are both inhibited and the decay observed is due to Ca removal by the sarcolemmal Ca-ATPase, and uptake into non-SR organelles (e.g. mitochondria; Bassani *et al.*, 1992). These results suggest that there are no differences across the cell types in the rate of Ca removal by these "slow" pathways.

In the presence of caffeine alone, calcium removal is achieved mainly by NCX, but there will also be a contribution from the "slow" pathways. Since the latter appear unchanged when the different cell types are compared, any differences in the rate constant of Ca decay with caffeine can be ascribed to differences in NCX activity. If it

is assumed that the Ca removal mechanisms act independently, and thus additively, then the rate constant of decay attributable to NCX can be calculated by subtracting the rate constant for caffeine+Ni from the rate constant for caffeine alone. This analysis is pursued further in Chapter 4.

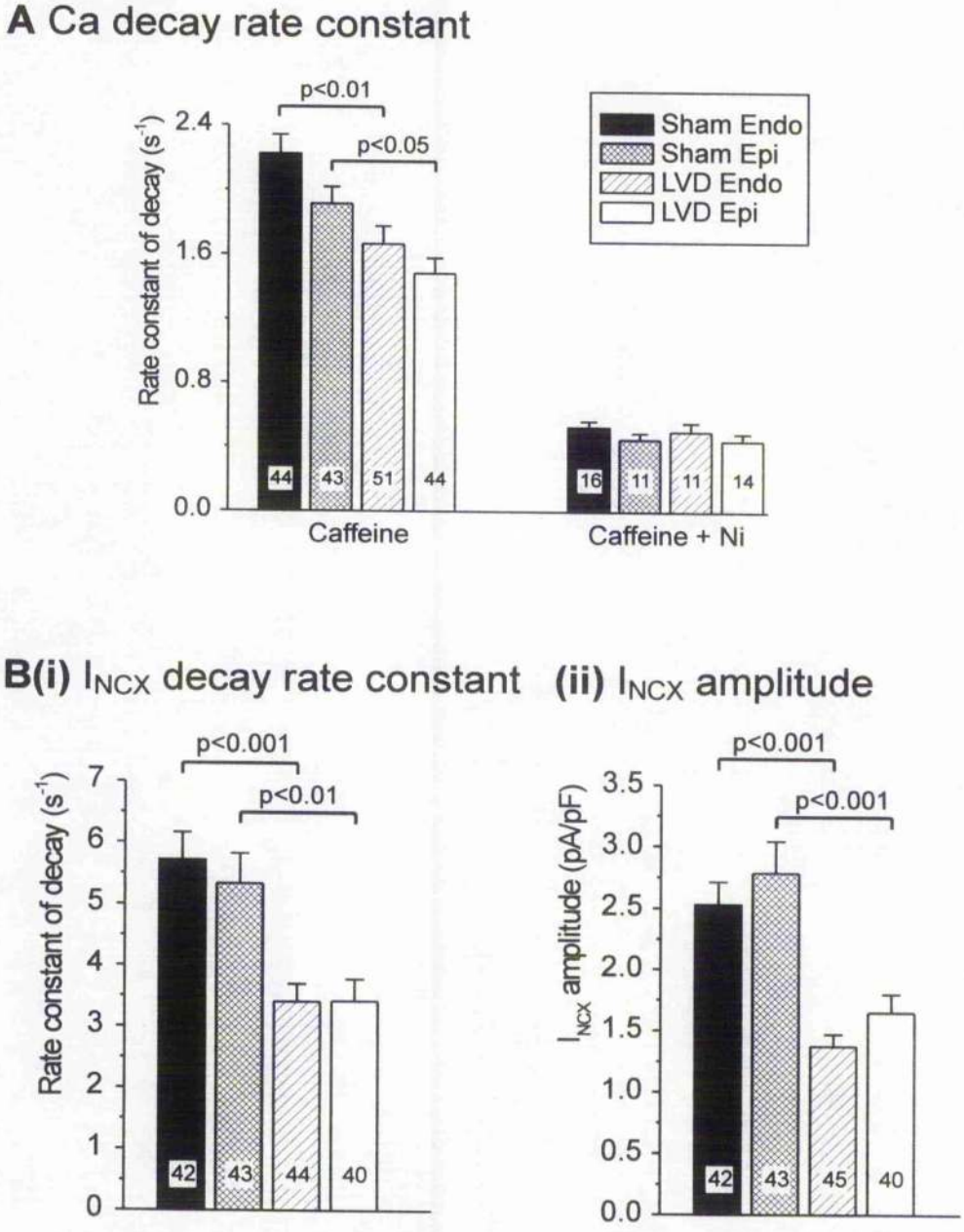

Figure 3.10 NCX activity – summary data. **A:** rate constant of Ca decay on application of 10 mmol/L caffeine, in the absence and presence of 10 mmol/L Ni, for each cell type, as indicated. **B:** Characteristics of the resulting inward current due to NCX on caffeine application – **(i):** rate constant of decay; **(ii):** amplitude, corrected for cell capacitance. The figure legend in panel **A** refers to all three bar charts; number of cells is indicated on each column; statistically significant differences are indicated.

Figure 3.10 A illustrates that Ca removal in the presence of caffeine is significantly slower in LVD when cells from like regions are compared (e.g. for endocardial cells, $1.67 \pm 0.11\ s^{-1}$ *vs* $2.22 \pm 0.12\ s^{-1}$; $p<0.01$), indicating reduced NCX activity in LVD. The endocardial-epicardial differences, which were apparent with the voltage ramp protocols, do not reach statistical significance in these experiments.

Figure 3.10 B summarises the findings on analysis of the inward current generated by NCX when caffeine is applied. Again, the rate constant of decay is significantly slower in LVD (e.g. for endocardial cells, $3.41 \pm 0.29\ s^{-1}$ *vs* $5.72 \pm 0.44\ s^{-1}$; $p<0.001$). This is accompanied by a smaller amplitude current in LVD (e.g. for endocardial cells, 1.38 ± 0.10 A/F *vs* 2.53 ± 0.19 A/F; $p<0.001$). These results support the data in panel A, confirming reduced NCX function in the LVD cells.

One unusual observation is that the rate constant of decay for the caffeine-induced inward current is around 2-2.5 times higher than the rate constant of Ca decay during the same caffeine application. This effect is consistently seen when the traces from individual cells are examined. The reason for this is unclear, but two factors could contribute. Firstly, the relationship between $[Ca]_i$ and I_{NCX} is non-linear, as is apparent from examining Equation 3.1, and simulating the ionic conditions shows that this is especially marked at lower levels of $[Na]_i$ (<~10 mmol/L). Figure 3.11 models the relationship, with a typical exponential Ca decay being converted to a current decay using the NCX model. The predicted I_{NCX} decay is close to exponential, but the rate constant is around 25% higher. The second possible factor is that Ca may be released into a restricted subsarcolemmal space where it could be rapidly extruded on NCX before it has much effect on the bulk [Ca] sensed by Fura-2. The discrepancies

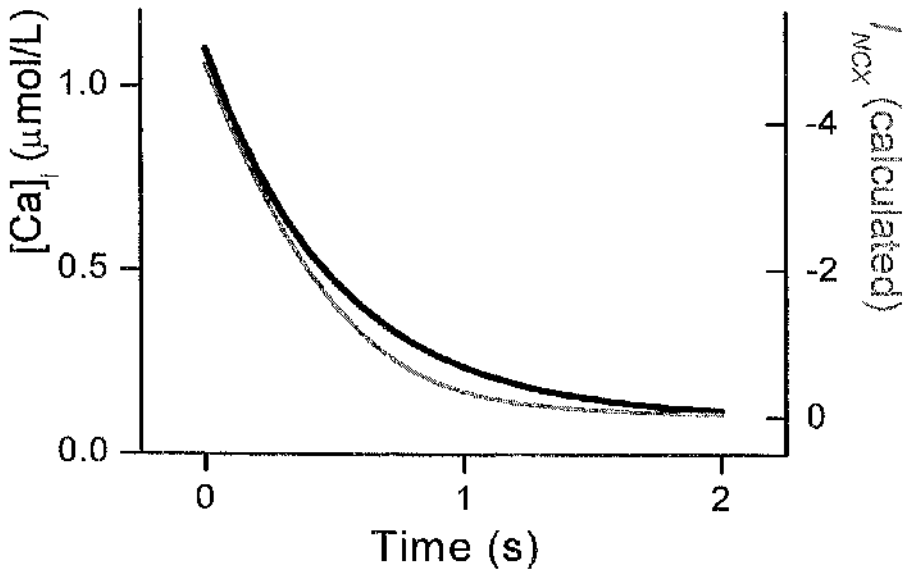

Figure 3.11 Conversion of a simulated exponential Ca decay (black line) to a current decay (grey line) using Equation 3.1. See text for discussion.

between subsarcolemmal [Ca] and bulk [Ca] are being increasingly recognised, particularly at times when Ca is changing rapidly, for example at the peak of the Ca transient (Weber *et al.*, 2002), and this is likely to be the case on caffeine application. Other workers have noted that the measured tail current on repolarisation (due to NCX) decays faster than that predicted from the changes in bulk [Ca] (Trafford *et al.*, 1995).

3.3.4 Allosteric regulation of NCX

These experiments were designed to establish whether there was evidence of allosteric regulation of NCX in rabbit cardiomyocytes, and, if present, to characterise this regulation in terms of the calcium sensitivity of the exchanger. By examining the outward NCX current as $[Ca]_i$ increases, it is possible to determine whether allosteric regulation is present, based on the theory outlined in Figure 3.5. Figure 3.6 illustrates the results from a typical cell. It is apparent from examining the difference current

(Fig. 3.6 A(iii)) that outward I_{NCX} initially increases as $[Ca]_i$ increases, implying that allosteric regulation does indeed occur – the exchanger is being activated by calcium.

For each cell, the protocol generated a number of values of I_{NCX} over a range of $[Ca]_i$ and these data were fitted with a mathematical model of NCX function, to generate a V_{Max} and K_m for calcium activation (K_{mCaAct}). The function could also be applied without the "Allosteric" factor and under these circumstances the fit to the data was generally poor, again suggesting that allosteric regulation was occurring.

3.3.4.1 K_m *for calcium activation in Sham and LVD animals*

Data were obtained from 22 cells from 8 Sham animals and 18 cells from 8 LVD animals. For both Sham and LVD animals, no significant difference was found between the K_{mCaAct} for the fit to the inward current data, compared to that for the outward current data (e.g. for Sham, 415.7 ± 98.8 nmol/L *vs* 375.4 ± 62.4 nmol/L; p=0.73). Since the fit to the outward current data was generally more reliable, these values were used when comparing Sham to LVD. Similarly, in both Sham and LVD animals, no difference was found between the K_{mCaAct} for endocardial and epicardial cells, so data from both regions were pooled. Analysing these data showed that the K_{mCaAct} was significantly lower in LVD myocytes (206.2 ± 42.4 nmol/L *vs* 375.4 ± 62.4 nmol/L; p=0.03), indicating that the exchanger was significantly more sensitive to calcium. For both Sham and LVD cells, the K_{mCaAct} falls within the physiological range of Ca for each cell type (see Chapter 4), suggesting that allosteric regulation by Ca could modulate the exchanger during the cardiac cycle. The values obtained are higher than those reported by Weber *et al* for ferret ventricular myocytes (125 nmol/L; Weber

et al., 2001), but compare well with those of Reeves & Condrescu for NCX1 expressed in Chinese hamster ovary cells (~300 nmol/L; Reeves & Condrescu, 2003).

3.3.4.2 V_{Max} *in Sham and LVD animals*

As well as deriving a K_{mCaAct} for each cell, applying the model of NCX function to the data in these experiments also gave a V_{Max} value. As in the experiments examining NCX current density, the V_{Max} was significantly lower in LVD cells (24.8 ± 3.2 A/F *vs* 40.8 ± 6.9 A/F; p=0.045).

3.4 Discussion

The experiments in this chapter examined the activity and regulation of the sodium calcium exchanger in cells from the endocardial and epicardial regions of the left ventricular free wall of sham-operated rabbits and those with infarct-induced left ventricular dysfunction. The results show transmural differences in NCX current density and reduced NCX activity in animals with LVD. These findings will now be discussed in more detail.

3.4.1 Endocardial – epicardial differences in NCX function

As discussed in Chapter 1, regional differences have been demonstrated in a number of ion channels in the heart and these differences have functional consequences in terms of action potential shape, contractile function and arrhythmogenesis (Antzelevitch *et al.*, 1991; Schram *et al.*, 2002). Few data are available on the transmural distribution of NCX, and only limited functional assessments have been reported (Bryant *et al.*, 1997; Zygmunt *et al.*, 2000; see Chapter 1, section 1.5). The experiments in this chapter address this issue in detail, by examining NCX activity in endocardial and epicardial cells from the base of the LV free wall.

In the experiments examining I_{NCX} current density, ionic conditions were tightly controlled and regional differences in I_{NCX} were observed. Higher current density was demonstrated in endocardial cells compared to epicardial cells, and this difference was preserved in LVD animals (Fig. 3.7 & 3.8). This parallels regional differences in NCX protein expression measured in membrane fractions of tissue homogenates from this model (Quinn *et al.*, 2003). When NCX-mediated Ca efflux was examined in separate experiments, the mean rate constant for Ca efflux was higher in endocardial cells than

epicardial cells for both Sham and LVD animals (Fig. 3.10), but neither difference reached statistical significance, even with relatively high numbers of cells in the analysis. The internal conditions are controlled less rigidly in these experiments and this may contribute to the greater variability in the data. In particular, small differences in intracellular [Na] between cells could affect NCX activity, and regional differences in $[Na]_i$ have been observed in the rabbit (Cook *et al.*, 1997).

3.4.1.1 Functional significance of regional differences in NCX

Previous studies investigating regional electrophysiological properties in normal rabbits have demonstrated significant prolongation of the action potential duration in sub-endocardial cells compared to sub-epicardial cells (McIntosh *et al.*, 1998; McIntosh *et al.*, 2000). In the later study by McIntosh *et al.*, the APD was around 30% longer in sub-endocardial than sub-epicardial cells from Sham animals, and this was accompanied by a significantly longer Ca transient (by around 20%) but no difference in peak systolic [Ca]. The prolonged APD may allow a greater flux of Ca into endocardial cells during systole (*via* $I_{Ca,L}$) and increased NCX current density could facilitate the removal of a larger quantity of cytoplasmic Ca during diastole. The inward current generated by the removal of this Ca may even contribute to the prolongation of the APD in endocardial cells (see discussion in Chapter 1), since there do not appear to be significant regional differences in I_{K1} or I_{to} in Sham cells (McIntosh *et al.*, 1998). Computer modelling of increased I_{NCX}, for example using the program LabHEART (D. Bers & J. Puglisi, Dept of Physiology, Loyola University, Chicago), does indeed generate slightly longer APDs.

Higher NCX current density in endocardial cells could also make this region more prone to arrhythmogenic afterdepolarisations, since for a given Ca release from the SR, one would expect a larger inward current to be generated. Observations in a non-ischaemic model of heart failure in the rabbit have demonstrated that premature ventricular complexes arise in the sub-endocardial region (Pogwizd, 1995) and this could be the focus for triggered arrhythmias. Similarly, in a dog model of ischaemic cardiomyopathy, ventricular arrhythmias tended to arise from focal sub-endocardial sites (Pogwizd, 1994). There is also some evidence from human studies that the sub-endocardial region may be important in arrhythmogenesis. Using 3-dimensional intraoperative cardiac mapping, Chung *et al.* showed that of 36 beats of non-sustained VT, 42% initiated in the sub-endocardium by focal mechanisms, whilst the remainder were the result of macroreentry (Chung *et al.*, 1997). Pogwizd *et al.* showed that 9 of 11 beats of spontaneous ventricular arrhythmias arose focally in the sub-endocardium (Pogwizd *et al.*, 1998). Further work is required in the rabbit infarct model of LVD to establish whether arrhythmias also tend to arise in this region.

3.4.2 NCX function in LVD

As mentioned in Chapter 1, a large number of studies have investigated changes in the sodium-calcium exchanger in various models of heart failure. Variables examined have included mRNA levels, protein expression and functional assessments such as current density and Ca removal (reviewed by Sipido *et al.*, 2002; Pogwizd, 2000; Hasenfuss & Pieske, 2002). The results in this chapter have demonstrated that NCX activity is significantly lower (by around 30%) in this model of LVD, whether assessed by current density (Fig. 3.7 & 3.8) or by examining NCX-mediated Ca decay or current decay during caffeine application (Fig. 3.10). These results apply to both endocardial

and epicardial regions and both forward and reverse modes of the exchanger (Fig. 3.7). There is no evidence that the stoichiometry of the exchanger is significantly altered in LVD (Section 3.3.2.3). It is also unlikely that altered intracellular conditions in LVD (e.g. raised $[Na]_i$ or lowered pH_i) play a major role in this animal model since comparable results were obtained in myocytes with minimal intracellular dialysis (Fig. 3.10) and those dialysed with EGTA and 20 mmol/L Na (Fig. 3.7 & 3.8).

3.4.3 Potential mechanisms for reduced NCX activity

Modelling I_{NCX} can give insights into possible mechanisms to explain the reduced NCX activity in LVD. Examination of Equation 1 reveals three principal factors which could be involved:

(i) reduced V_{Max}, representing a reduced number of exchangers available in the sarcolemma and/or reduced turnover of individual units;

(ii) reduced affinity of the exchanger for Ca and/or Na;

(iii) reduced sensitivity of the exchanger to allosteric regulation by Ca.

Simulating changes in any one of these factors, whilst keeping the other two constant can result in an equally good fit to the data in LVD, as illustrated in Figure 3.12, demonstrating that the *I-V* curve alone cannot distinguish between them.

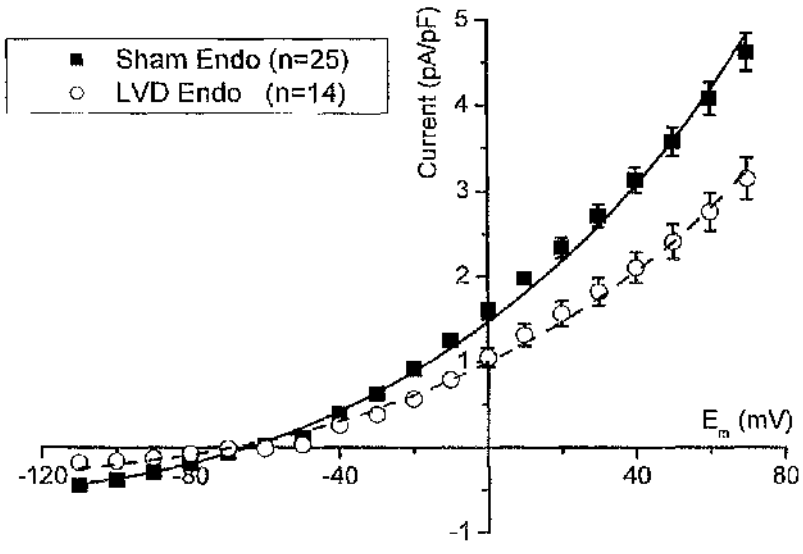

Parameter	Units	Sham	LVD(i)	LVD(ii)	LVD(iii)
V_{Max}	A/F	**42.1**	**27.3**	42.1	42.1
K_{NCX}	mmol/L	47.2	47.2	**78.6**	47.2
K_{mCaAct}	nmol/L	375.4	375.4	375.4	**502.6**

Figure 3.12 Modelling of NCX function. Parameters allowed to vary are shown in bold. First, data points for Sham endocardial cells were fit using Equation 1, with K_{NCX} derived from the literature (see Table 3.1), K_{mCaAct} experimentally-derived for Sham cells and V_{Max} allowed to vary. The resulting parameters were then used in the equation to fit the LVD endocardial data, with one of the three parameters allowed to vary, as indicated in the table. The resulting curve-fits are superimposable (dashed line).

3.4.3.1 Affinity of NCX for Ca & Na

The term k_{NCX} in Equation 1 incorporates the affinity constants for Ca and Na on each side of the sarcolemma. Experiments to determine these affinity constants in this model are beyond the scope of this thesis. Modelling the k_{NCX} term shows that it is most sensitive to changes in the K_m for Ca, particularly to changes in K_{mCai}. Even so, the K_{mCai} would need to increase by around 180% to account for the reduced I_{NCX} in LVD.

Previous studies have shown that cardiac NCX (NCX1) activity can be modulated by protein kinase-A (Perchenet *et al.*, 2000; Ruknudin *et al.*, 2000) and -C (Iwamoto *et al.*, 1996). Phosphorylation of NCX1 results in up-regulation of exchanger activity with increased currents (Perchenet *et al.*, 2000; Ruknudin *et al.*, 2000) or uptake of ^{45}Ca (Iwamoto *et al.*, 1996). Therefore, decreased phosphorylation of NCX in LVD could result in reduced exchanger activity. The phosphorylation status of the exchanger has not been measured in this model, however evidence to date suggests *increased* phosphorylation of proteins in heart failure (Rapundalo, 1998) and activation of protein kinase A can result in a phenotype of dilated cardiomyopathy with reduced contractility and increased mortality (Antos *et al.*, 2001; Carr *et al.*, 2002).

3.4.3.2 Allosteric regulation of NCX in LVD

Experiments in this chapter have addressed the third possibility above: that changes in allosteric regulation of NCX by Ca could account for the differences seen in LVD. If this were the sole factor to account for the observed differences in I_{NCX} then examination of Figure 3.12 shows that the K_{mCaAct} in LVD would need to increase by

around 34% (from 375.4 nmol/L to 502.6 nmol/L). In fact, the measured K_{mCaAct} in LVD is around 45% *lower* than that in Sham animals (206.2 + 42.4 nmol/L *vs* 375.4 ± 62.4 nmol/L; p=0.03), showing that the exchanger is significantly *more* sensitive to regulation by Ca. If the measured values for K_{mCaAct} in Sham and LVD animals are used in Equation 1 to fit the data, then even larger differences in V_{Max} result (43.4 ± 2.1 *vs* 14.7 ± 1.4 A/F for Sham Endo & LVD Endo, respectively, p<0.001; 32.0 ± 2.3 *vs* 10.7 ± 1.0 A/F for Sham Epi & LVD Epi, respectively, p<0.001). This analysis suggests that the V_{Max} in LVD is around one third of that in Sham animals. Considering this from another viewpoint, the reduced K_{mCaAct} in LVD could be seen as an adaptive mechanism, upregulating NCX function for a given $[Ca]_i$ in an attempt to compensate for reduced exchanger numbers.

3.4.3.3 NCX protein expression & mRNA levels

Perhaps the simplest explanation for regional differences in NCX function and the changes seen in LVD would be altered expression of NCX protein in the cell, resulting in changes in V_{Max}. Other workers in the group have studied NCX protein levels in tissue homogenates and membrane fractions from Sham and LVD animals (Quinn *et al.*, 2003). These experiments have demonstrated higher expression of NCX protein in membrane fractions from endocardial regions compared to epicardial regions in both Sham and LVD animals, in keeping with the results in this chapter. However, NCX protein levels in LVD were found to be significantly *higher* than those in Sham animals, by around 20-40%. NCX mRNA levels were similarly raised. This discrepancy between protein / mRNA levels and function merits some consideration, and highlights the potential danger of drawing conclusions from biochemical data alone, without confirmatory functional studies.

3.4.4 Relationship between NCX protein levels and NCX function

Several possibilities could explain increased protein expression but reduced NCX function in this model:

(i) presence of defective NCX protein,

(ii) presence of isoforms of NCX with reduced function,

(iii) downregulation of functional NCX units (discussed above),

(iv) NCX units present in the cell with no access to the extracellular space (therefore non-functional).

The presence of defective NCX protein is difficult to assess. The primary antibody used to measure NCX protein levels in this model detected both a 120 kDa band, which reflects the mature NCX protein, and a 70 kDa band which is thought to be a proteolytic subfragment of the full length exchanger. Densitometry was performed on both bands and the results summed to give a total NCX level for each region. There was no evidence that greater relative amounts of the proteolytic fragment were present in LVD – the ratio of 70:120 kDa bands was the same (Quinn *et al.*, 2003).

The presence of different NCX isoforms in LVD would also require further study. There is evidence of isoforms shifts in a number of channels and transporters in heart failure, including the Na-channel (Muller-Ehmsen *et al.*, 2002; Schwinger *et al.*, 1999), Na-K ATPase (Pagancili *et al.*, 2001), and Na-H exchanger (Yokoyama *et al.*, 2000). A number of splice-variants of cardiac NCX have been identified (Quednau *et al.*, 1997; Kim *et al.*, 1998) and their relative proportions do not appear to change during

development in the rat (Koban *et al.*, 1998) or mouse (Kim *et al.*, 1998). To date, no study of the relative expression of different isoforms of NCX in heart failure has been published.

Another mechanism whereby increased protein expression could be accompanied by reduced function would be for NCX units to be present in the myocyte with no access to the extracellular space – either not inserted into the plasma membrane or present in membrane which is not continuous with the sarcolemma. As discussed in Chapter 1, there is ongoing debate in the literature about the distribution of NCX in the cell, in particular the proportion which is present in T-tubules compared to surface portions of the membrane. Disruption of the T-tubule system could result in blind ending, "nipped-off" tubules within the cell, where NCX could not contribute significantly to Ca removal or produce a measurable current, but would still be detected on Western blotting.

There is recent evidence that the T-tubule system may indeed be disrupted in heart failure. He *et al.* assessed T-tubule density in canine tachycardia-induced heart failure using the membrane dye di-8-ANNEPS and quantified I_{Ca} using voltage clamp protocols (He *et al.*, 2001). They report that T-tubule density was reduced by around 24% in failing cells and this was accompanied by a reduction in charge movement on I_{Ca} of around one half. Interestingly, overall I_{Ca} density appeared unchanged and they postulate that this is due to functional upregulation of a smaller number of Ca channels. Using confocal and electron microscopy, Kostin *et al.* showed altered T-tubule structure in human myocytes from patients with cardiomyopathy (Kostin *et al.*, 1998).

Studies of the T-tubule structure in our model of LVD have been performed by other workers in the laboratory, also using di-8-ANNEPS and image processing to quantify T-tubule density (Quinn *et al.*, 2003). These experiments have shown that T-tubule staining within the cell is reduced by 41%, and this is accompanied by a reduction in the surface area:volume ratio. Further studies are underway to determine whether "nipped-off" tubules are present within LVD myocytes. Such ultrastructural changes could help explain the apparent disparity between NCX protein / mRNA levels and NCX function in this model.

3.4.5 Comparison with other models of LVD

Sipido *et al.* have recently reviewed the literature on NCX in heart failure and hypertrophy and it is apparent that a full range of responses can be seen – from upregulation to downregulation or no change in exchanger activity (Sipido *et al.*, 2002). In part, these differences may depend on the type of animal studied (for example fewer rat models showed upregulation) and also the means by which hypertrophy / failure was achieved.

Some other studies have also found discrepant results between NCX abundance and function. Boateng *et al.* studied rats with cardiac hypertrophy induced by aortic constriction (Boateng *et al.*, 2001). They showed that in tissue from hypertrophied hearts, NCX mRNA levels more than doubled and protein levels increased by more than four-fold. In spite of these marked changes, decline of Ca in the presence of caffeine following rapid cooling contractures (which is mainly dependent on NCX) was no different.

3.4.5.1 Comparison with other infarct models of LVD

A number of groups have used ligation of the left coronary artery in the rat as a model of infarct-induced LVD. Dixon *et al.* (1992), Sethi *et al.* (1999) and Makino *et al.* (1996) found slowed Na-dependent Ca uptake into sarcolemmal vesicles in this model, implying reduced NCX function. This effect could be diminished or abolished by *in vivo* treatment with propionyl L-carnitine (Sethi *et al.*, 1999) or Angiotensin Type 1 receptor blockade (Makino *et al.*, 1996). Contractile abnormalities post-MI in the rat could also be reversed by transgenic overexpression of NCX, including an increase in SR Ca content (Min *et al.*, 2002).

Zhang *et al.* also demonstrated reduced NCX function, with diminished NCX currents (Zhang *et al.*, 1996) and slower Ca decay in the presence of caffeine (Zhang *et al.*, 1999) and these changes were associated with reduced SR Ca content and contractile abnormalities. Interestingly, immunoblotting showed no difference in NCX protein levels between post-MI and sham-operated animals (Zhang *et al.*, 1998). In contrast, Wasserstrom *et al.* found increased NCX protein levels, mRNA, and NCX current in a similar animal model (Wasserstrom *et al.*, 2000). Similarly, Yoshiyama *et al.* found significantly increased NCX mRNA levels in hypertrophied post-MI rat cells remote from the infarct site, although no functional assessment was performed (Yoshiyama *et al.*, 1997). The reasons for the differences between the latter two studies and the remaining rat MI studies are unclear, but Yoshiyama *et al.* demonstrated two possible factors - both the timing post-MI and the site from which myocytes were harvested influenced the level of NCX mRNA seen (Yoshiyama *et al.*, 1997). For example, at 1 week and 3 weeks, NCX levels were *higher* in post-MI animals, but by 3 months the levels were *lower*.

NCX has also been studied following myocardial infarction in the dog. Pu *et al.* examined NCX activity in the epicardial border zone 5 days after infarction to determine whether early changes were present which could provide an arrhythmic substrate (Pu *et al.*, 2000). They found altered Ca handling in these cells, but no significant difference in NCX current or Ni-sensitive Ca efflux.

3.4.5.2 Comparison with other rabbit models of LVD

As discussed in section 2.1, there are theoretical advantages to using the rabbit heart to model the situation in human heart failure, and this has been done by a number of groups. Pogwizd *et al.* have recently characterised a rabbit model with combined pressure and volume overload due to aortic constriction and aortic valvular regurgitation (Pogwizd *et al.*, 1999; Pogwizd *et al.*, 2001). These animals exhibit severely depressed LV function, with reduced cardiomyocyte twitch amplitude, and spontaneous ventricular arrhythmias. Analysis showed that NCX protein levels were approximately doubled and there was a 2.7-fold increase in NCX mRNA levels. These changes were accompanied by a 2-fold increase in NCX current and a faster decline of $[Ca]_i$ during caffeine application. In the initial paper, no significant difference was found between the SR Ca content in control and heart failure (assessed by the amplitude of caffeine-induced contractures; Pogwizd *et al.*, 1999), however in the later paper, a 40% reduction in SR Ca content was reported (assessed by the amplitude of caffeine-induced Ca transients; Pogwizd *et al.*, 2001).

In a pressure-overload model of LVD in the rabbit, due to aortic constriction alone, Naqvi *et al.* found no change in NCX protein levels (nor the levels of SERCA2 or

phospholamban), SR Ca content (derived from the integral of the caffeine-induced inward current) or NCX-mediated relaxation in the presence of caffeine (Naqvi *et al.*, 2001). This animal model differed from that of Pogwizd *et al.* in that volume overload was not present (the aortic valve was not made incompetent) and the studies were carried out much earlier in the development of heart failure (at 6 weeks compared to a mean of 9.5 months post-operatively).

In a pure volume-overload model of heart failure induced by arteriovenous shunting, Takahashi *et al.* show a reduction in NCX mRNA levels at 4 and 12 weeks, but no data on NCX function are reported (Takahashi *et al.*, 2000).

Yao *et al.* produced LVD in the rabbit by rapid pacing and studied cells 3-5 weeks later, when clinical heart failure was apparent (Yao *et al.*, 1998). At this stage the Ca transients were markedly reduced in amplitude (to <30% of those in control animals). NCX mRNA levels were strikingly reduced and the outward NCX current elicited by abruptly switching to a 0 Na external solution was decreased by around 24%.

The model most closely resembling the one used in this thesis is that of Litwin *et al.* who induced MI in rabbits of the same age by tying off the same branch of the left circumflex artery (Litwin & Bridge, 1997; Litwin *et al.*, 2000). The animals were sacrificed for study at the same stage post-MI (8 weeks) and showed evidence of myocyte hypertrophy. With field stimulation, the amplitude of contraction appeared larger in MI cells (Litwin & Bridge, 1997), however in the later paper, the peak $[Ca]_i$ of voltage-clamped cells was significantly reduced (Litwin *et al.*, 2000). This discrepancy is not commented upon, but may partly be explained by prolongation of the action

potential in the non-voltage-clamped MI cells (Litwin & Bridge, 1997). In neither paper was a significant difference in SR Ca content seen, although there was a trend towards increased SR content in the MI cells.

Litwin *et al.* assessed NCX current density using the amplitude of the outward current induced by rapid switching to a 0 Na external solution, corrected for cell capacitance. In contrast to the results in this chapter, they found a significantly *increased* NCX current density (by 32%) in the infarcted hearts (Litwin & Bridge, 1997). They also showed that there was augmented SR loading by reverse-mode NCX in the MI cells after loading pulses to positive potentials.

One major difference between the studies of Litwin *et al.* and those reported here is in the origin of the cells examined. Litwin *et al.* selectively took cells from the 2-3 mm border zone around the infarct scar, whereas the cells in this thesis were taken from the basal region of the LV, remote from the scar, and cells from different transmural areas were studied separately. This important difference may help explain the discrepant results we have obtained. Overall, the peri-infarct border zone represents a small proportion of the remaining viable myocardium and whilst it may be important as an area where arrhythmias can arise, cells remote from this site will dictate the majority of the contractile performance post-MI. In addition, the border zone is likely to be a heterogeneous region, with areas of fibrosis and possible residual ischaemia. One cannot assume that results from border zone cells can be extrapolated to cells elsewhere in the surviving myocardium – indeed, Yoshiyama *et al.* and Wasserstrom *et al.* have demonstrated that NCX mRNA levels differ when peri-infarct and remote sites are compared in the rat (Yoshiyama *et al.*, 1997; Wasserstrom *et al.*, 2000). Litwin *et al.*

do mention in their earlier paper that in some animals, cells from the remote area of myocardium were studied, but they do not present any data for these cells (Litwin & Bridge, 1997).

3.4.5.3 Comparison with human studies

Studies of NCX expression and function in human heart failure have also given varying results (reviewed by Sipido *et al.*, 2002; Hasenfuss & Pieske, 2002; Houser *et al.*, 2000). The majority of studies have compared tissue from failing hearts explanted at the time of transplantation with tissue from donor hearts which were not suitable for transplanting. Most studies have only made biochemical measurements of NCX – i.e. mRNA or protein levels – since it is difficult to isolate sufficient cells for electrophysiological study.

In an early study by Komuro *et al.*, NCX mRNA levels were significantly lower in foetal hearts, but there was no significant difference in hearts from end-stage heart failure (Komuro *et al.*, 1992). Similarly, Schwinger *et al.* studied myocardial NCX protein levels in patients with dilated cardiomyopathy and NYHA functional class IV and found no significant difference compared to non-failing hearts (Schwinger *et al.*, 1999). Kubo *et al.* examined NCX protein abundance in hearts from patients with dilated and ischaemic cardiomyopathies and again found no difference compared to control hearts (Kubo *et al.*, 2001).

The groups of Studer, Reinecke, Drexler *et al.* have reported results on patients with end-stage heart failure and detected an increase in NCX mRNA (Studer *et al.*, 1994) and protein (Reinecke *et al.*, 1996). They also made a functional assessment of NCX

by measuring Na-dependant ^{45}Ca uptake into inside-out sarcolemmal vesicles prepared from a crude membrane fraction. This showed an 87% increase in transport activity in preparations from failing hearts (Reinecke *et al.*, 1996). Schwinger *et al.* (1999) have questioned the methodology of Studer *et al.* in assessing NCX protein abundance, since in the latter paper they included a 40 kDa band as well as the 120 and 70 kDa bands normally detected by anti-NCX antibodies. Schwinger *et al.* point out that the 40 kDa band is not detected by monoclonal antibodies to NCX, nor does it enrich when sarcolemmal membranes are purified. Flesch *et al.* detected increased NCX mRNA and protein levels in failing human hearts (Flesch *et al.*, 1996), however in a later study, this group reported no difference in NCX protein levels (Schwinger *et al.*, 1999). The reason for this discrepancy is not commented upon in the later paper, but may indicate significant phenotypic variability between patients – a suggestion supported by considerable scatter when results from individual patients are plotted (e.g. see Hasenfuss *et al.*, 1999; Heerdt *et al.*, 2000). Heerdt *et al.* reported a discrepancy between NCX mRNA levels and NCX protein abundance in patients treated with a left ventricular assist device (LVAD; Heerdt *et al.*, 2000) – whilst mRNA levels increased significantly with LVAD treatment, protein levels remained unchanged.

Hasenfuss *et al.* have attempted to clarify some of these inconsistencies by dividing patients into subgroups according to their contractile function. Specifically, they separated patients into groups based on the change in diastolic force with increasing stimulation rates (Hasenfuss *et al.*, 1999). They found that NCX protein levels were only significantly elevated in patients who exhibited no frequency-dependent rise in diastolic force (i.e. preserved diastolic function). In these patients there was no significant difference in SERCA levels compared to non-failing hearts. In contrast, in

patients with no change in NCX levels, SERCA function was significantly depressed. Thus, irrespective of the group, the ratio of NCX:SERCA was increased in heart failure, compared to controls. An additional factor in determining NCX expression may by the degree of sympathetic activation that patients display. Schillinger *et al.* have reported that NCX levels in human HF show a significant positive correlation with plasma noradrenaline levels (Schillinger *et al.*, 2002). They also found an increased incidence of ventricular arrhythmias in patients with higher noradrenaline and NCX levels.

In an interesting paper, Piper *et al.* used quantitative PCR to examine NCX mRNA levels in endomyocardial biopsies from 40 patients with myocardial dysfunction of different aetiologies and severity, and these results were compared with samples from 13 hearts explanted at the time of transplantation (Piper *et al.*, 2000). Samples from 7 controls were also obtained. They found no significant difference in NCX mRNA levels between controls and endomyocardial biopsies from patients in any group – whether divided up by disease aetiology, NYHA functional class, ejection fraction or wall stress. The only samples showing increased NCX transcription levels were those obtained from explanted hearts, suggesting two main possibilities – either it was a response to severe haemodynamic, biochemical and neurohumoral changes pre-transplantation, or it was due to peri- / intra-operative events. The fact that even patients with the most severely reduced ejection fraction, and worst functional class showed no significant change in NCX on biopsy tissue provides some evidence against the former possibility, since one might expect these patients to show some similarities with pre-transplant patients.

3.5 Conclusions

The experiments in this chapter have demonstrated transmural differences in NCX current density in cells from both Sham and LVD animals. In post-infarction myocytes, NCX current density and activity are reduced by around ⅓. Altered allosteric regulation of NCX by [Ca] is also apparent in these cells. Since others in the group have found slightly *increased* NCX expression in LVD animals, it is clear that functional measurements are essential when interpreting biochemical data. There is evidence that altered myocyte structure, in particular the arrangement of T-tubules, may account for some of the experimental findings.

CHAPTER 4

CALCIUM HANDLING IN SYSTOLE AND DIASTOLE – SR FUNCTION, E-C COUPLING AND RELATIVE CONTRIBUTIONS OF CALCIUM REMOVAL SYSTEMS

4.1 Introduction

4.1.1 Measurement of SR Ca content

In the literature, a variety of methods have been employed to estimate the Ca content of the SR in intact single cells. To make this measure, all the available Ca in the SR must be released, which can be achieved by exposure to an adequate concentration of caffeine, or by rapidly cooling the cell. The magnitude of Ca release can then be determined. One non-quantitative method to accomplish this is to compare the extent of cell contraction when SR Ca is released, as in "rapid cooling contractures" (RCCs; e.g. Bers & Bridge, 1989) or caffeine contractures (e.g. Bassani *et al.*, 1992). A further commonly used method is to load the cells with a Ca-indicator and use the amplitude of the caffeine-induced Ca transient as an indication of the SR Ca content (e.g. Lindner *et al.*, 1998). At best this method is semi-quantitative, since the peak of the caffeine-induced transient will depend on a number of factors including cellular buffering characteristics and sarcolemmal Ca-removal mechanisms.

A quantitative method for estimating the SR Ca content was developed by Varro *et al.* (Varro *et al.*, 1993). This method makes use of the electrogenic nature of NCX to calculate the amount of Ca removed from the cell during caffeine exposure, and from this the total amount released from the SR. If it is assumed that the stoichiometry of NCX is 3Na:1Ca, then for each Ca ion removed from the cell there is a net gain (inward current) of one positive charge. Using Faraday's constant, the total charge movement can be converted to give the number of moles of Ca removed on NCX. To estimate the total amount of Ca released from the SR, this figure must be corrected for non-NCX (electroneutral) Ca removal systems, such as the sarcolemmal Ca-ATPase and uptake into mitochondria and other organelles ("slow pathways"). It is also

important that potential contaminating currents (e.g. Ca-activated Cl currents) are blocked.

In this chapter, the latter method was used to determine the SR content. Corrections for non-NCX removal mechanisms were made based on the results in Chapter 3 where caffeine was applied in the presence of nickel (see Figures 3.4 and 3.10). Comparing the rate constant of Ca decay in the presence of Ni with that for caffeine alone can indicate the proportion of Ca removed by NCX during caffeine exposure. In view of the fact that there were significant differences in Ca removal rates with caffeine between sham-operated animals and those with LVD, separate correction factors were calculated for each group. Using this approach, for Sham animals it is estimated that 76 ± 1 % of the Ca is removed by NCX during caffeine exposure, whereas for LVD animals the figure is 70 ± 2 % ($p<0.001$). These values are lower than those found in the rabbit by Bassani, Bers and co-workers (Bassani *et al.*, 1992; Bassani *et al.*, 1994), as discussed in section 4.4.6.2.

Since cells were loaded with the Ca indicator Fura-2, the amplitude of the caffeine-induced Ca transient could also be measured. Results based on this approach could be compared with those obtained using the above method.

Finally, recent advances in the chemistry of fluorescent dyes have lead to novel methods for the measurement of the SR Ca content. Shannon *et al.* successfully used an intra-SR Ca-sensitive dye to report free [Ca] within the SR (Shannon *et al.*, 2003a). They used a long loading period to allow entry and de-esterification of the low-affinity Ca indicator Fluo-5N into the SR of rabbit ventricular myocytes. In an elegant study

they were able to measure the dynamic changes in $[Ca]_{SR}$ during voltage-stimulated Ca transients at different rates.

4.1.2 Measurement of SERCA activity

Several techniques have been described for estimating Ca uptake via SERCA in cardiac cells. Both direct and indirect methods have been reported. One approach is to permeabilise the cell and control conditions to allow a measure of SR Ca uptake. Neary *et al.* (Neary *et al.*, 2002) used β-Escin to permeabilise rabbit ventricular cells, and added ruthenium red to prevent SR Ca leak and dipotassium oxalate to precipitate Ca within the SR (thus preventing intra-SR [Ca] from rising and inhibiting further Ca uptake). Cells were suspended in cuvettes and Ca was measured in a mock intracellular solution with Fura-2. When Ca is added to the cuvette, it is taken up by the SR and the decay of bulk solution [Ca] can be attributed to SERCA. A similar approach can be used for isolated SR vesicles (Currie & Smith, 1999).

Yao *et al.* used a rapid solution-switcher to estimate SERCA function relative to NCX function in intact rabbit cardiomyocytes (Yao *et al.*, 1998). They compared the rate of Ca decline for normal electrically-stimulated twitches (where all extrusion systems are operating) with twitches induced by rapid switching to a 140 mmol/L K solution in the absence of Na and Ca (i.e. NCX inhibited). Differences in the time-course of Ca decline could be attributed to SERCA activity. Boateng *et al.* estimated SERCA function by releasing SR Ca by rapid cooling, then rewarming the cells in Na-free, Ca-free solution (Boateng *et al.*, 2001). Under these conditions, the decline in $[Ca]_i$ is mainly determined by SERCA, although the slow pathways will also contribute.

Finally, Bassani, Bers and co-workers have examined Ca decay under conditions where removal systems are selectively inhibited, to determine the contribution of each to Ca removal (e.g. see Bassani *et al.*, 1994; Puglisi *et al.*, 1996; reviewed in Bers, 2000; Bers, 2001). SERCA activity was determined from the decay of Ca in the absence of external Na (i.e. NCX disabled), which was then corrected for flux via slow pathways (measured separately in the presence of caffeine and Na-free, Ca-free external solution). Alternatively, SERCA activity could be inferred from the decay of a normal twitch if the characteristics of Ca flux in relation to $[Ca]_i$ were known for the other two systems (McCall *et al.*, 1998).

In this chapter, a novel, reversible, method was used to estimate SERCA function, as described in Section 4.2.3.1.

4.2 Methods

4.2.1 Solution compositions

To allow for assessment of SR Ca content using the techniques outlined below, the internal and external solutions were designed to allow accurate quantification of Ca flux on NCX. Thus, blockers were present to minimise major interfering currents as described in sections 2.5.4 and 3.2.2.1. Ca transients for each cell type were measured under the same conditions so that Ca flux during a train of stimuli could be determined in systole and diastole.

4.2.2 Ca transient characteristics & estimation of SR Ca content

4.2.2.1 Experiment protocol

Cells were stimulated for 30 s at 0.5 Hz from a resting potential of -80 mV, with a 150 ms depolarisation to 0 mV, to achieve steady-state contractions. To allow estimation of the SR Ca content and cellular buffering characteristics, at the end of this train, the superfusing solution was rapidly switched to 10 mmol/L caffeine, which was perfused for 10 s (Figure 4.1). Cells were held at the resting potential of -80 mV during caffeine exposure. In some cells, Ca transients were also measured at 1 Hz and 2 Hz.

4.2.2.2 Data analysis

After conversion of Fura-2 ratio data to [Ca], Ca transients were averaged from the point at which steady-state contractions were achieved to the end of the train. This allowed data for diastolic $[Ca]_i$, peak systolic $[Ca]_i$ and rate constant for Ca decay to be obtained. In most cells, the train of stimuli was repeated on a number of occasions and for each cell the diastolic and systolic $[Ca]_i$ for each train was averaged to give mean data for that cell.

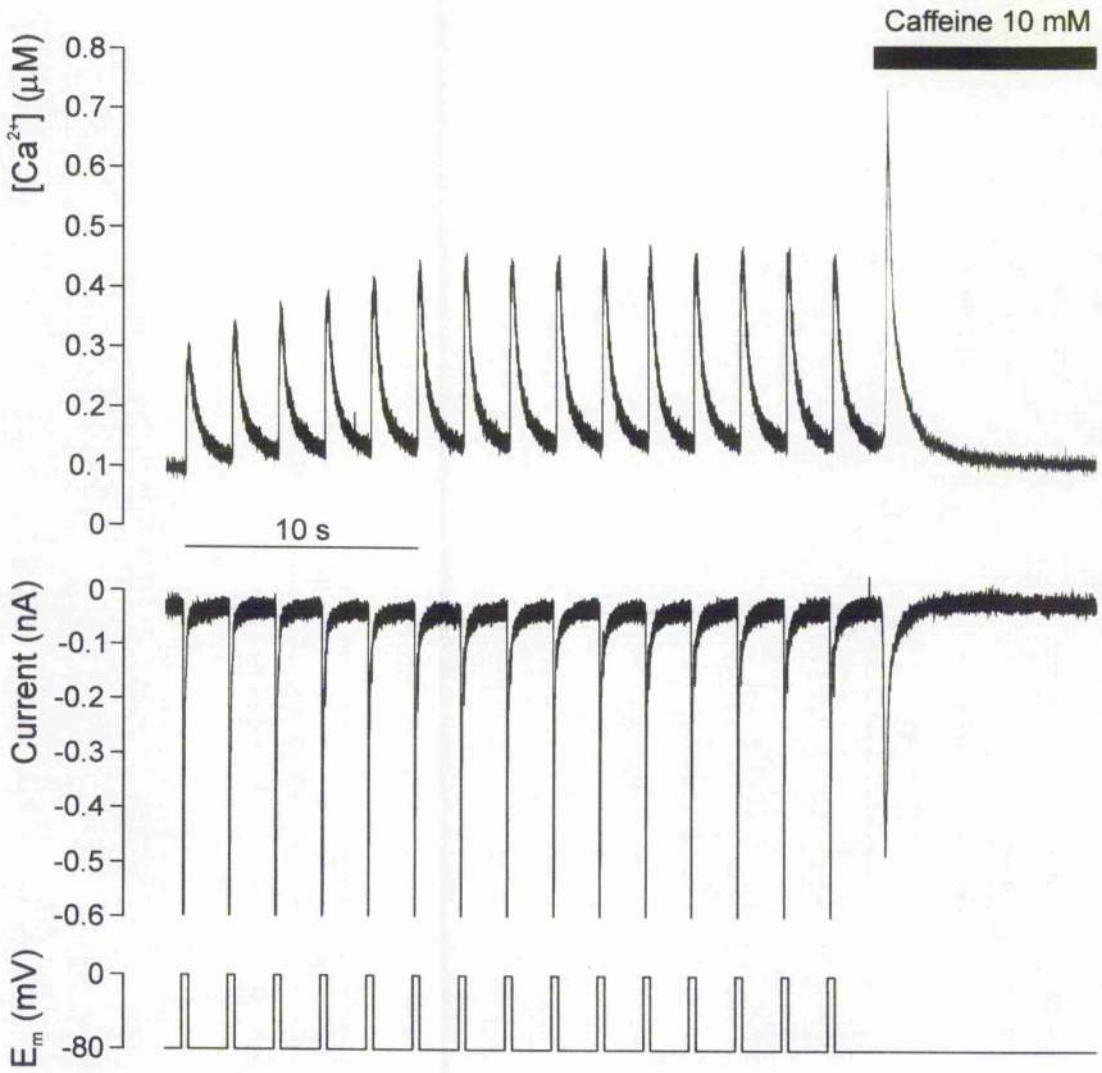

Figure 4.1 Protocol for determining Ca transient characteristics, SR Ca content, and cellular buffering parameters. **Bottom panel:** voltage protocol; **middle panel:** membrane current – for clarity, the capacitance spikes have been subtracted and the scale was chosen to demonstrate the inward current on application of caffeine (peak inward current on depolarisation is off-scale at this range – see Figure 4.6); **top panel:** $[Ca]_i$. The cell was stimulated at 0.5 Hz from a resting potential of -80 mV for 30 s, allowing steady-state transients to be achieved. 10 mmol/L caffeine was applied for 10 s at the end of the train.

$$SR\ Ca\ content\ (mol/L\ cytosol) = \frac{Int \times SL\ factor}{F \times Vol}$$

Equation 4.1 Estimation of SR Ca content. *Int* = cumulative integral at end of inward current during application of 10 mmol/L caffeine; *SL factor* = correction for non-NCX Ca removal (1.31 for Sham, 1.42 for LVD, see text for details); F = 96500 C/mol; *Vol* = accessible cell volume = cell capacitance / 6.44 (see section 2.7.2.2).

SR Ca content was determined using the technique of Varro *et al.* (1993), as outlined in the chapter introduction (section 4.1.1) and illustrated in Figure 4.2. The analysis was performed on the raw current trace obtained during caffeine exposure using a customized routine in the graphical analysis program OriginPro 6.1 or 7.0 (OriginLab Corporation, Northampton, MA, USA). Briefly, the current trace was integrated with respect to time between user-defined start- and end-points, and the amount of Ca released from the SR was back-calculated from the resulting cumulative integral (charge movement) using Equation 4.1. The integration was performed between the time at which caffeine was applied and the time when the current had fully returned to baseline, as shown in Figure 4.2. As discussed in section 4.1.1, a correction factor was applied to allow for Ca removed from the cell by non-NCX mechanisms. The correction factors for Sham and LVD cells were 1.31 and 1.42, respectively. The resulting SR Ca content was expressed relative to the accessible cell volume, as described in the Methods chapter, section 2.7.2.2.

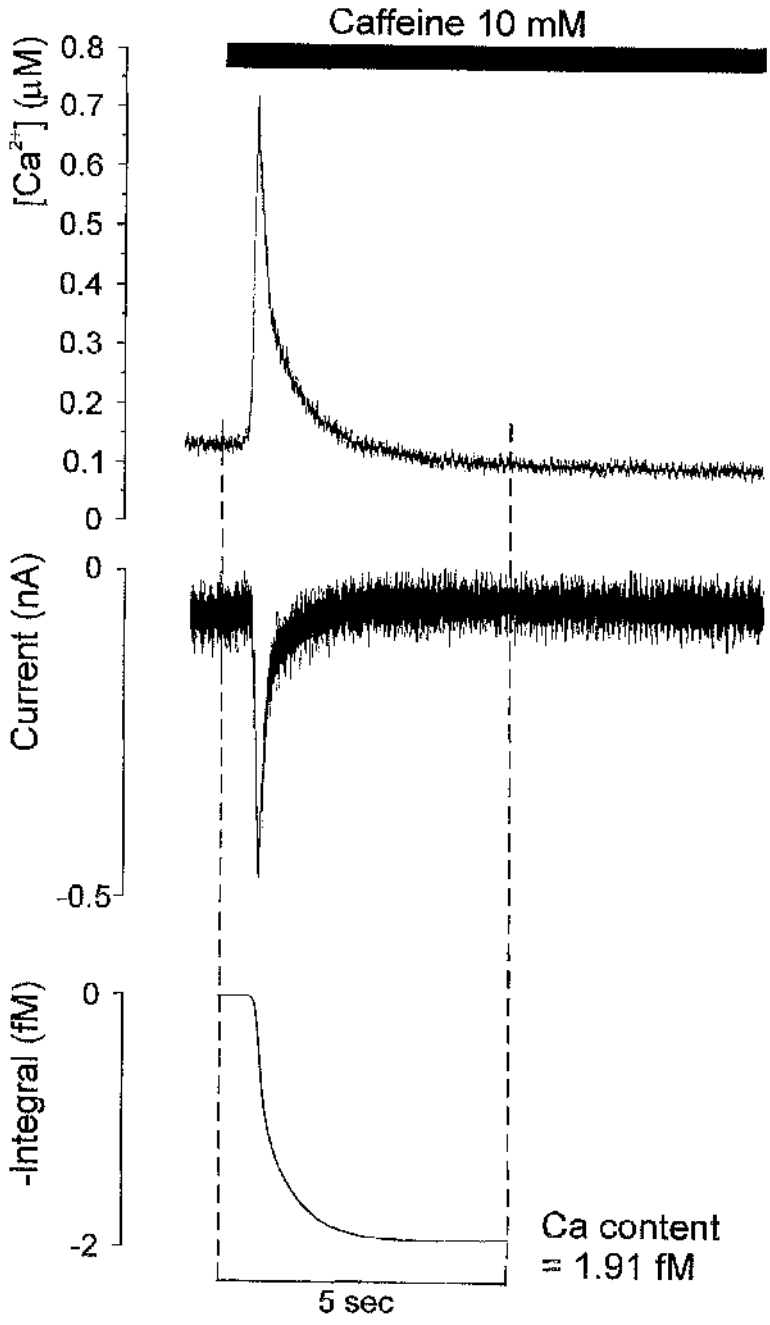

Figure 4.2 Estimation of SR Ca content by integration of the inward current on application of 10 mmol/L caffeine. **Top panel:** $[Ca]_i$ during application of 10 mmol/L caffeine (black bar). **Middle panel:** resulting inward I_{NCX} current. **Bottom panel:** cumulative integral of NCX current, corrected for non-NCX removal mechanisms to allow determination of SR Ca content.

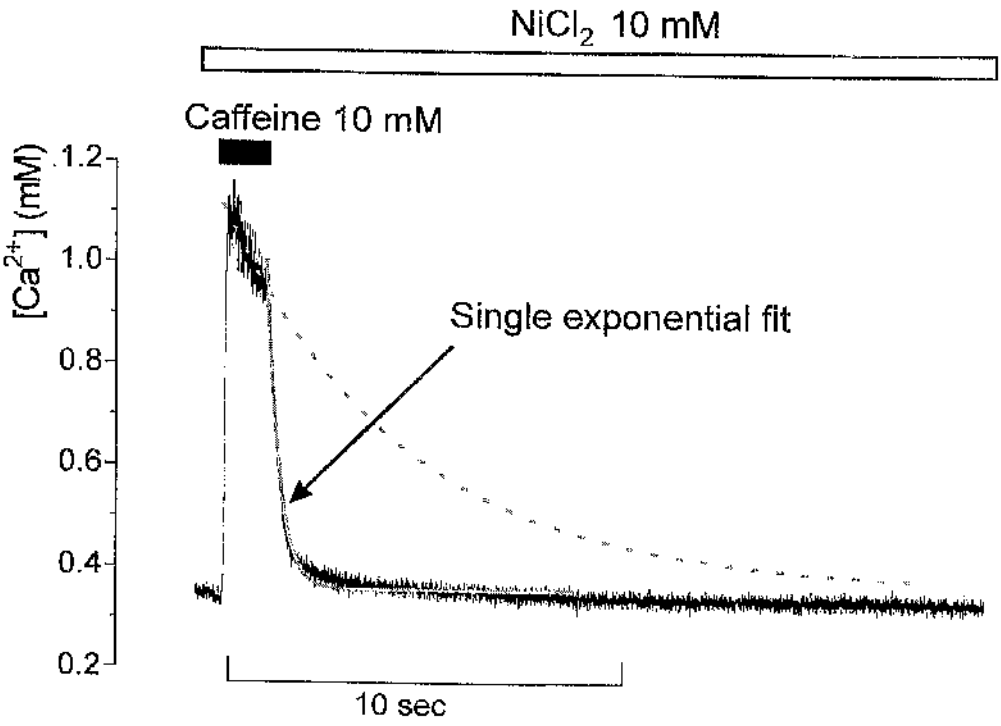

Figure 4.3 Estimation of SERCA activity. In the continued presence of 10 mmol/L $NiCl_2$ (open bar) to inhibit NCX, 10 mmol/L caffeine is briefly applied (black bar) to release SR Ca. On abrupt withdrawal of caffeine, Ca is removed from the cytoplasm, mainly *via* SERCA. The Ca decay during this phase can be fitted using a single exponential function (grey line). A correction can be made for Ca removal by "slow" pathways by determining the rate constant for Ca decay in the presence of 10 mmol/L caffeine + 10 mmol/L $NiCl_2$ in the same cell (dashed grey line, superimposed on the above trace). See text for details.

4.2.3 Estimation of SERCA function

4.2.3.1 Experiment protocol

A novel technique was employed to give an estimate of SERCA function in intact cells, making use of the rapid solution switcher. Once again, cells were stimulated for 30 s to achieve steady-state contractions, as described in section 4.2.2.1. At the end of the conditioning train, the superfusing solution was switched to one containing 10 mmol/L

$NiCl_2$ for 20 s, to eliminate Ca removal on NCX. Immediately after switching to this solution, and in the continued presence of Ni, 10 mmol/L caffeine was briefly perfused and abruptly withdrawn (see Figure 4.3). This resulted in release of SR Ca, followed by its re-uptake via SERCA. "Slow" removal pathways will also be operating during this phase, and to estimate their contribution to the decay, the protocol was repeated for each cell with application of 10 mmol/L caffeine + 10 mmol/L $NiCl_2$ after the conditioning train of stimuli.

4.2.3.2 Limitations of technique

Since uptake on SERCA has a rapid time course, this technique relies on the prompt removal of caffeine when the solution is switched. Examination of the Ca trace during the protocol (Figure 4.3) shows that there is an abrupt change in the rate of Ca decay, suggesting that caffeine removal is rapid and complete. Testing of the perfusion system as outlined in section 2.6.1, suggests that the solution at the cell is changed with a time constant of around 90 ms. Some additional time must be allowed for the full removal of the effects of caffeine on the RyR. This compares with the time constant for Ca decay when caffeine is withdrawn of around 300 ms or longer (see results section 4.3.3). A comparison of typical decays for the solution switcher and caffeine withdrawal is shown in Figure 4.4. In theory, the time course of the solution switch should remain constant, and any error it introduces to the estimation of SERCA function should be the same irrespective of the cell type being studied. Therefore, although there may be a small error in the absolute value for SERCA activity, comparisons across cell types will remain valid.

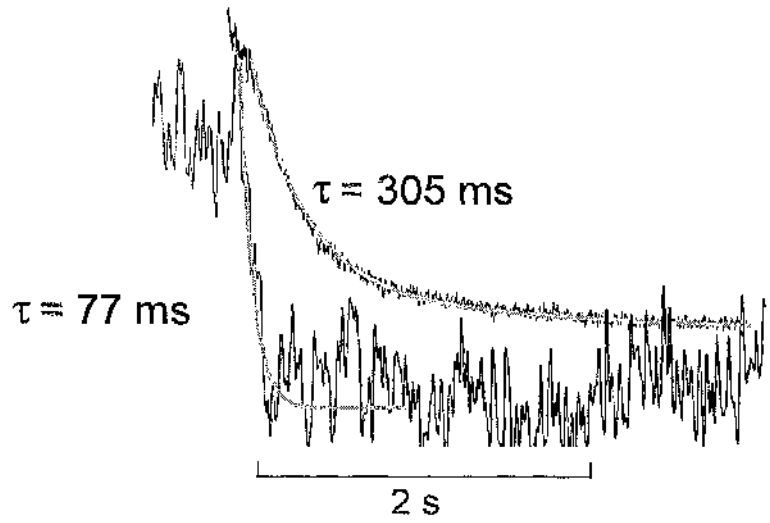

Figure 4.4 Comparison of timecourse of solution switching (noisy trace) with that of Ca decay on abrupt withdrawal of 10 mmol/L caffeine (upper trace). The decay for each is fitted with a single exponential function (grey lines).

It should also be noted that this technique estimates SERCA activity under relatively non-physiological conditions – i.e. taking up cytoplasmic Ca into an "empty" SR. Given the complex regulation of SERCA, including the effects of SR luminal [Ca], as the SR fills an interplay of factors will determine the rate of SERCA activity. For this reason, in analysing the data, the RC of Ca decay was mainly determined from the initial steep portion of the decay, after the abrupt change in the rate of Ca decline with removal of caffeine (see Fig. 4.3). Over this range, the cytoplasm-to-SR [Ca] gradient is high and luminal [Ca] is still relatively low, meaning that the measure of SERCA activity may be made under conditions where the pump is maximally activated.

4.2.3.3 Data analysis

For each cell, the rapid Ca decay on withdrawal of caffeine was plotted on an expanded timescale and the early part of the decay was fitted with a single exponential function to

obtain a rate constant, $RC_{Caff\ off}$. Similarly, the decay in the presence of caffeine + Ni was analysed to obtain a rate constant for the "slow pathways" – RC_{Slow}. The rate constant attributable to SERCA could then be determined by subtracting RC_{Slow} from $RC_{Caff\ off}$. This approach assumes that the Ca removal mechanisms act independently, such that the rate constants for each system will be additive.

4.2.4 Estimation of cellular buffering power

An estimation of intracellular buffering properties was made on a cell-by-cell basis, using the current and calcium traces during caffeine exposure to determine the relationship between free and total $[Ca]_i$. This method was described by Trafford *et al.* (1999). As outlined in section 4.2.2.2, the inward current on NCX during caffeine application can be integrated and corrected for non-NCX removal mechanisms and cell volume to give an indication of *total* $[Ca]_i$ (expressed as mol/L cytosol). If these data are plotted against the simultaneous *free* $[Ca]_i$ reported by Fura-2, then the buffering curve can be established (Figure 4.5). For an estimation of the buffering characteristics, this curve is fitted with an equation of the form:

$$Ca_{Total} = a + \frac{B_{Max}\left[Ca^{2+}\right]_i}{\left(K_d + \left[Ca^{2+}\right]_i\right)} \qquad \textbf{Equation 4.2}$$

where a is an arbitrary offset, B_{Max} is the saturating capacity of the buffer and K_d is the dissociation constant. The offset a is necessary because of the method used to calculate Ca_{Total} – the back-calculation of Ca_{Total} from the current integral means that Ca_{Total} is set to 0 at the end of the current decay, at a time when free $[Ca]_i$ is at the resting Ca level at the end of the caffeine application. Thus, the buffering curve will cross the abscissa at the value for resting free $[Ca]_i$, and the buffering relationship can only be

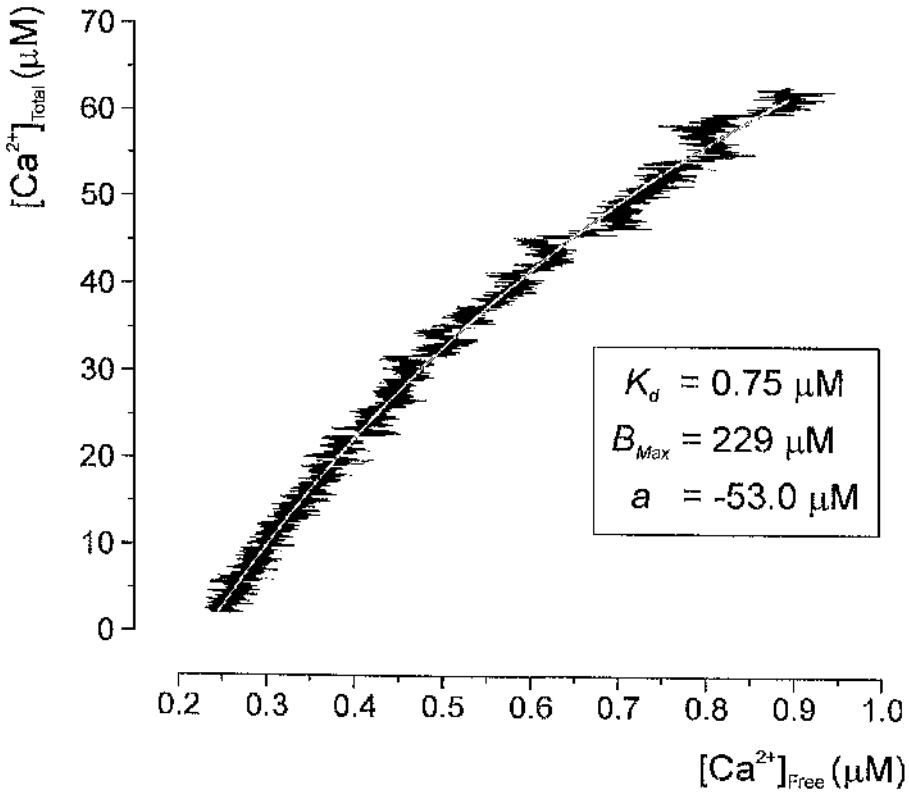

Figure 4.5 Estimation of cellular buffering characteristics. $[Ca]_{Total}$ calculated from the integral of the inward current on NCX is plotted against $[Ca]_{Free}$ measured by Fura-2. The resulting buffering curve is fitted (grey line) using Equation 4.1, to derive a dissociation constant (K_d), maximum buffering capacity (B_{Max}), and intersect (a).

determined for values of $[Ca]_i$ above this point. The overall buffering curve includes the intrinsic buffering properties of the cell and the buffering properties of the Fura-2 within the cell. Thus, since the buffering characteristics are determined for each cell, small differences in Fura-2 loading amongst different cells will be taken into account in the analysis.

4.2.5 Analysis of Ca flux on I_{Ca} and tail currents

4.2.5.1 Experiment protocol

Under the internal and external conditions outlined above (section 4.2.1), cells were stimulated at 0.5 Hz for 30 s to achieve steady-state contractions, using a protocol allowing determination of Ca fluxes across the sarcolemma during systole and diastole. The voltage protocol consisted of an initial 50 ms ramp from a resting potential of -80 mV to a potential of -40 mV, which was then held for 25 ms, before stepping to 0 mV for 150 ms. The initial ramp-and-hold allowed for activation and inactivation of the Na current, which would otherwise have contaminated the initial portion of I_{Ca} if a simple step to 0 mV had been used. Preliminary experiments showed that this voltage protocol was effective in minimising the effects of I_{Na} and that the addition of the Na channel blocker tetrodotoxin gave little additional benefit (data not shown). The voltage protocol is outlined in Figure 4.6, along with typical current and Ca traces. For the majority of cells, the protocol was repeated a number of times and for each cell the mean values of I_{Ca} and I_{Tail} were used for further analysis.

4.2.5.2 Data analysis

For each train of stimuli, the current and Ca signals were averaged from the point at which steady state was achieved, until the end of the train. Ca flux on I_{Ca} was determined by integrating the inward current from a point just after the capacitance spike until the end of the 150 ms depolarising step. The resulting charge movement was converted to give the total amount of Ca entering the cell during systole, by dividing by Faraday's constant and halving the result (since two positive charges are carried by each Ca ion).

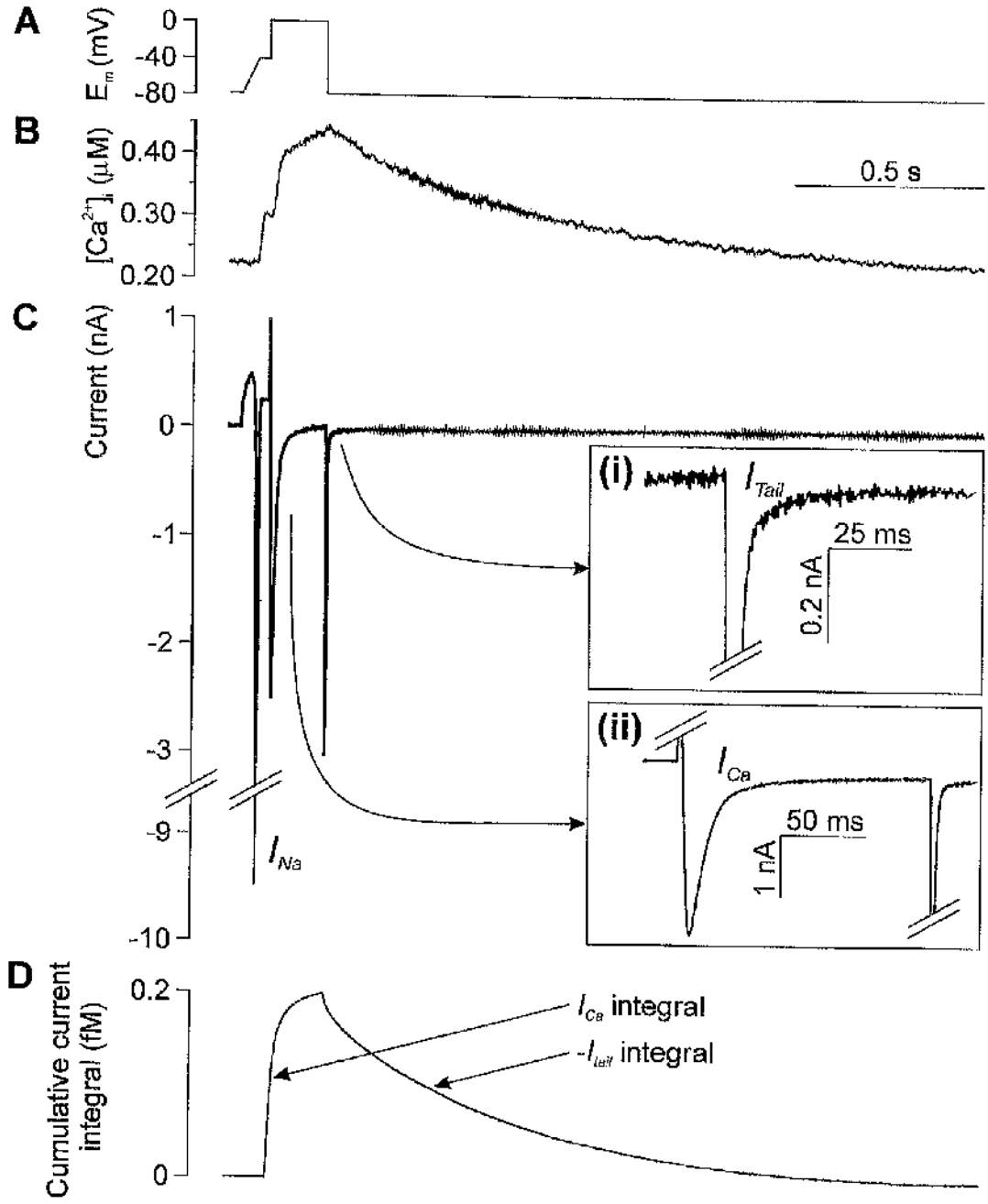

Figure 4.6 Measurement of Ca flux on L-type Ca current (I_{Ca}) and NCX tail current (I_{Tail}). **A:** voltage clamp protocol – initial ramp to -40 mV activates sodium current (I_{Na}), step to 0 mV results in Ca entry *via* I_{Ca}. **B:** intracellular [Ca]. **C:** resulting membrane current, with inserts showing expanded tail current **(i)** and I_{Ca} **(ii)**. **D:** cumulative integral of I_{Ca} followed by I_{Tail} (corrected for non-NCX Ca removal mechanisms).

The tail current on repolarisation represents Ca removal on NCX, and Ca flux during this phase was calculated using a similar approach to that outlined in section 4.2.2.2. The tail current was integrated following the capacitance spike, until the end of the diastolic period (which was also taken to be the zero current level). This integral was converted to give the total amount of Ca removed from the cell by dividing by Faraday's constant and correcting for non-NCX removal mechanisms as previously described.

For both I_{Ca} and I_{Tail}, the calculated Ca flux was corrected for cell volume as outlined in section 2.7.2.2, and expressed as mol/L cytosol. An example of the cumulative integral for I_{Ca} and I_{Tail} is shown in Figure 4.6 D.

4.3 Results

4.3.1 Ca transient characteristics

Ca transients were examined under the conditions described in section 4.2.1, during trains of stimuli and on application of 10 mmol/L caffeine. Figure 4.7 A shows the mean amplitude of Ca transients at 0.5 Hz for each of the cell types, along with the amplitude of corresponding caffeine-induced Ca transients. Data were obtained from 14 sham-operated animals and 14 LVD animals, and the number of cells for each group is indicated in the figure. There were no significant differences between the diastolic levels of Ca at 0.5 Hz in each group (275 ± 26 nmol/L, 262 ± 25 nmol/L, 240 ± 20 nmol/L and 223 ± 22 nmol/L, for Sham Endo, Sham Epi, LVD Endo and LVD Epi cells, respectively), nor were there significant differences between Ca levels before caffeine application (267 ± 25 nmol/L, 257 ± 28 nmol/L, 211 ± 21 nmol/L, 211 ± 23 nmol/L, for Sham Endo, Sham Epi, LVD Endo and LVD Epi cells, respectively).

For each animal type, at 0.5 Hz there was no significant difference between the amplitude of Ca transients in endocardial cells and the amplitude of Ca transients in epicardial cells. However, transients were of smaller amplitude in LVD cells compared to control cells (218 ± 11 nmol/L, n=76, *vs* 261 ± 13 nmol/L, n=74; p=0.01). Likewise, caffeine-induced transients were also significantly smaller (by around 25%) in LVD cells (576 ± 28 nmol/L, n=71, *vs* 767 ± 32 nmol/L, n=68; p<0.0001).

The rate constant of Ca decay during 0.5 Hz trains of stimuli was also determined, with results shown in Figure 4.7 B. In general, the rate of decay was faster in endocardial cells than epicardial cells, although this only reached statistical significance in LVD animals (for Sham animals: 3.31 ± 0.24 *vs* 2.71 ± 0.23 s^{-1}; p=0.07; for LVD animals:

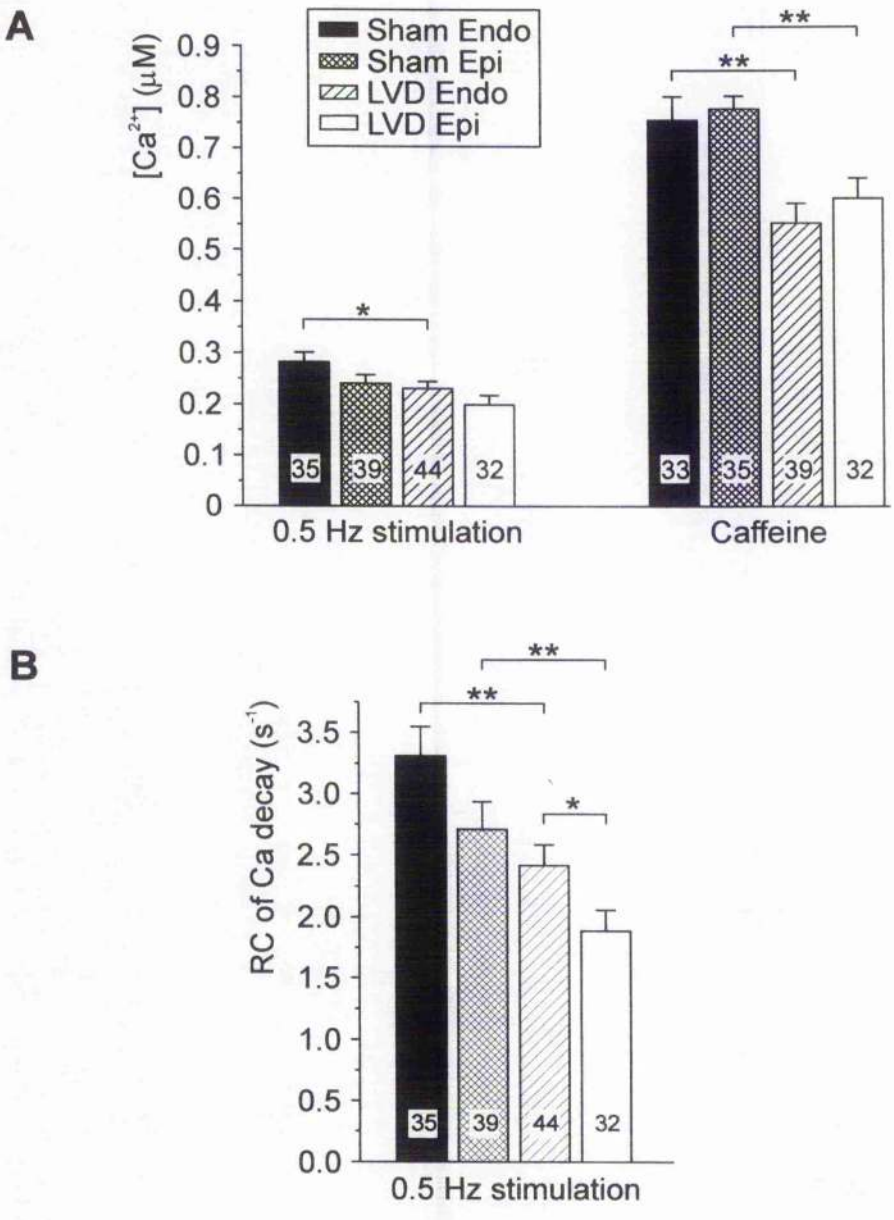

Figure 4.7 Characteristics of steady-state Ca transients and caffeine-evoked transients. **A:** Amplitude of Ca transients evoked by voltage-clamp protocol (**left panel**; 0.5 Hz stimulation train) and application of 10 mmol/L caffeine (**right panel**), for each cell type. **B:** Rate constant of Ca decay for voltage-clamped cells stimulated at 0.5 Hz. For each panel, number of cells is shown on each bar. Key refers to all panels. Statistically significant comparisons are indicated: * $p<0.05$, ** $p<0.01$.

A

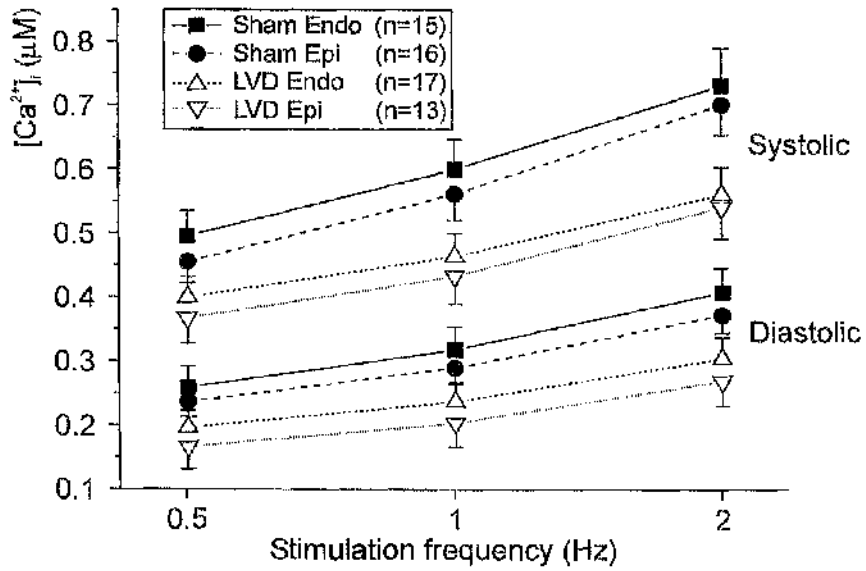

B

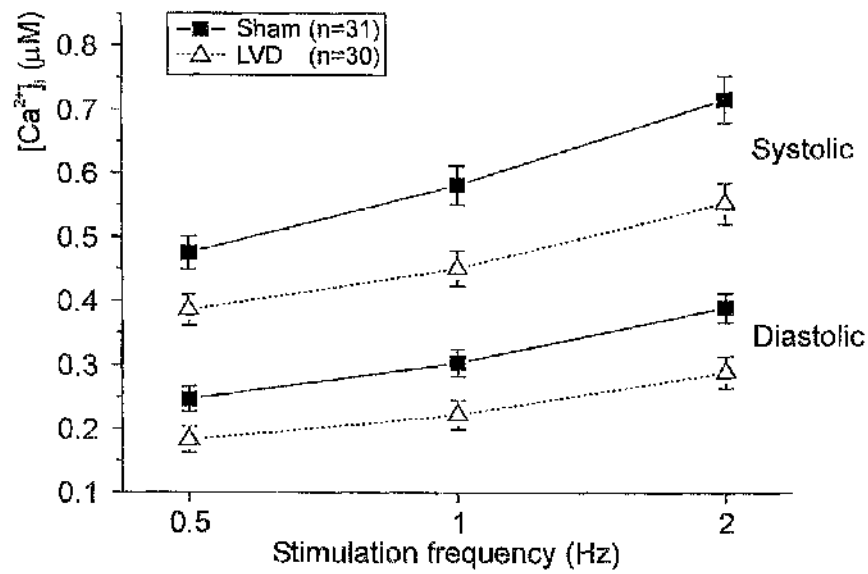

C

	0.5 Hz			1Hz			2Hz		
	Dias	Sys	Ampl	Dias	Sys	Ampl	Dias	Sys	Ampl
Sham v LVD p-value	**0.03**	**0.01**	0.3	**0.01**	**0.003**	**0.047**	**0.005**	**0.001**	**0.04**

Figure 4.8 Effect of stimulation rate on Ca transients. Lower data points in each panel indicate diastolic [Ca] and upper data points systolic [Ca]. **A:** Each cell type shown. **B:** Overall data (Endo + Epi) for Sham & LVD cells. **C:** Table summarising statistical comparisons from panel B. Dias = diastolic value, Sys = systolic value, Ampl = amplitude of Ca transient. Statistically significant results in bold.

2.42 ± 0.17 *vs* 1.89 ± 0.17 s^{-1}; p=0.04). For each area of myocardium, the Ca decay was slower in LVD cells than Sham cells (for endocardial cells p=0.002; for epicardial cells p=0.008).

In a subset of cells, the effect of stimulation rate on Ca transient characteristics was determined. The results are summarised in Figure 4.8. With each increase in rate, irrespective of cell type, diastolic [Ca], systolic [Ca] and the amplitude of the Ca transient increased (all p-values by paired t-test <0.0001). Again, there was no significant difference between endocardial and epicardial cells for each animal type. For clarity, Figure 4.8 B compares overall data (endocardial and epicardial cells combined) for Sham and LVD animals, with statistical comparisons in the accompanying table. It is apparent that at each rate both diastolic and systolic [Ca] are lower in LVD animals (e.g. at 1 Hz, diastolic [Ca]: 223 ± 23 nmol/L *vs* 304 ± 22 nmol/L; p=0.01; systolic [Ca]: 452 ± 28 nmol/L *vs* 581 ± 31 nmol/L; p=0.003). The amplitude of the Ca transients is also smaller at 1 and 2 Hz (1 Hz: 228 ± 17 nmol/L *vs* 277 ± 17 nmol/L; p=0.047; 2 Hz: 263 ± 20 nmol/L *vs* 326 ± 23 nmol/L; p=0.04). At 0.5 Hz, the difference does not meet statistical significance (203 ± 17 nmol/L *vs* 227 ±15 nmol/L; p=0.3).

4.3.2 SR Ca content – regional differences and changes in LVD

The SR Ca content for each cell was estimated from the integral of the inward NCX current on application of caffeine, as outlined in section 4.2.2. Results are summarised in Figure 4.9. In sham-operated animals, the SR Ca content in epicardial cells is greater than that in endocardial cells (77.9 ± 3.4 *vs* 66.6 ± 3.8 μmol/L cytosol; p=0.03), but in LVD animals this difference does not reach statistical significance. The figure

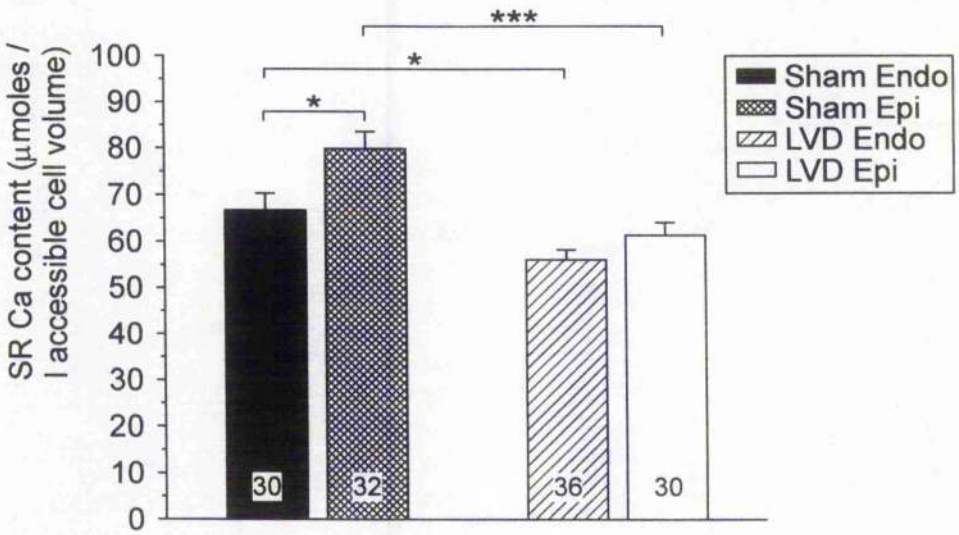

Figure 4.9 SR Ca content for each cell type. SR content was calculated from the integral of the inward NCX current on application of 10 mmol/L caffeine, as outlined in Figure 4.2 and in the text. Number of cells is shown on each bar. Statistically significant comparisons are indicated: * $p<0.05$, *** $p<0.001$.

also demonstrates that the SR Ca content in LVD animals is significantly smaller than that in sham-operated animals (for endocardial cells: 55.2 ± 2.1 *vs* 66.6 ± 3.8 µmol/L cytosol; $p=0.008$; for epicardial cells: 59.0 ± 2.4 *vs* 77.9 ± 3.4 µmol/L cytosol; $p<0.0001$). Overall, the SR content in LVD is around 22% smaller than that in control animals. One must ensure that this difference is not simply a consequence of the method used to estimate SR Ca content, in particular the correction for cell volume. If the cell capacitance/volume ratio was altered in LVD then this could confound the result. However, a further estimation of the SR Ca content was made by examining the amplitude of the Ca transients on application of caffeine, as shown in Figure 4.7, and this is independent of cell volume. This confirms the difference in SR Ca content between LVD animals and control animals (for endocardial cells: 554 ± 39 nmol/L *vs* 755 ± 47 nmol/L; $p=0.003$; for epicardial cells: 602 ± 40 nmol/L *vs* 778 ± 44 nmol/L;

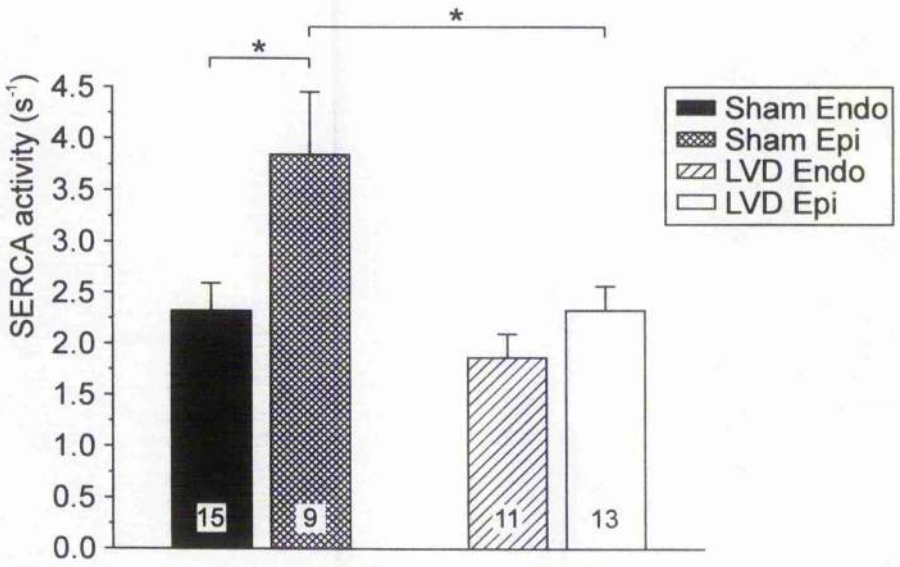

Figure 4.10 Measured SERCA activity for each cell type. SERCA activity was estimated by briefly applying 10 mmol/L caffeine in the continued presence of 10 mmol/L $NiCl_2$ and determining the rate constant of Ca decay on caffeine withdrawal, followed by correction for "slow" removal pathways, as shown in Figure 4.3. Number of cells is shown on each bar. Statistically significant comparisons are indicated: * $p<0.05$.

p=0.005). In this case, the difference between LVD and control animals is around 25%. This value compares well with that obtained from the integral of the NCX current on application of caffeine, suggesting that the differences in LVD are genuine. The caffeine-induced transients do not show significant differences between endocardial and epicardial cells for either animal type.

4.3.3 SERCA function

In this chapter a novel method was used to estimate SERCA function for each of the cell types. The technique measured the rate constant of Ca uptake on SERCA in the presence of Ni to block efflux on NCX. For each cell the rate constant was corrected for Ca removal *via* the "slow" removal mechanisms. Figure 4.10 summarises the

results. Cells were obtained from 4 sham-operated animals and 4 LVD animals. In general, SERCA activity was higher in epicardial cells than endocardial cells, although the difference was only statistically significant for Sham cells (3.84 ± 0.61 s^{-1} *vs* 2.32 ± 0.36 s^{-1}; p=0.03). SERCA activity was higher in Sham epicardial cells than LVD epicardial cells (3.84 ± 0.61 s^{-1} *vs* 2.33 ± 0.24 s^{-1}; p=0.02), but the difference for endocardial cells was not significant (2.32 ± 0.36 s^{-1} *vs* 1.87 ± 0.23 s^{-1}; p=0.33).

One reason for some comparisons failing to reach significance is the degree of variability of the raw data, resulting in a relatively high variance and standard error. Technical aspects of the experimental protocol may contribute to this variability, in that it is difficult to reproduce exactly the conditions of solution flow at each cell. This may result in variability in the efficiency of solution-switching, affecting the time-course of Ca decay when caffeine is abruptly withdrawn.

4.3.3.1 SR Ca content in relation to SERCA function

The relationship between SERCA activity and SR Ca content is examined in Figure 4.11. Panel 4.11 A plots the mean SR content data from Figure 4.9 against the mean SERCA activity from Figure 4.10 for each cell type. The plot suggests that there may be a relationship between the two variables – for example, cells with the highest measured SERCA activity (Sham epicardial cells) also have the highest SR Ca content.

This relationship was examined further by producing a similar plot for individual cells from the experiment shown in Figure 4.3. For those cells where data were available on SR content (n=21 for Sham animals, n=21 for LVD cells), these values were plotted against SERCA activity. Separate scatter plots were produced for Sham and LVD cells

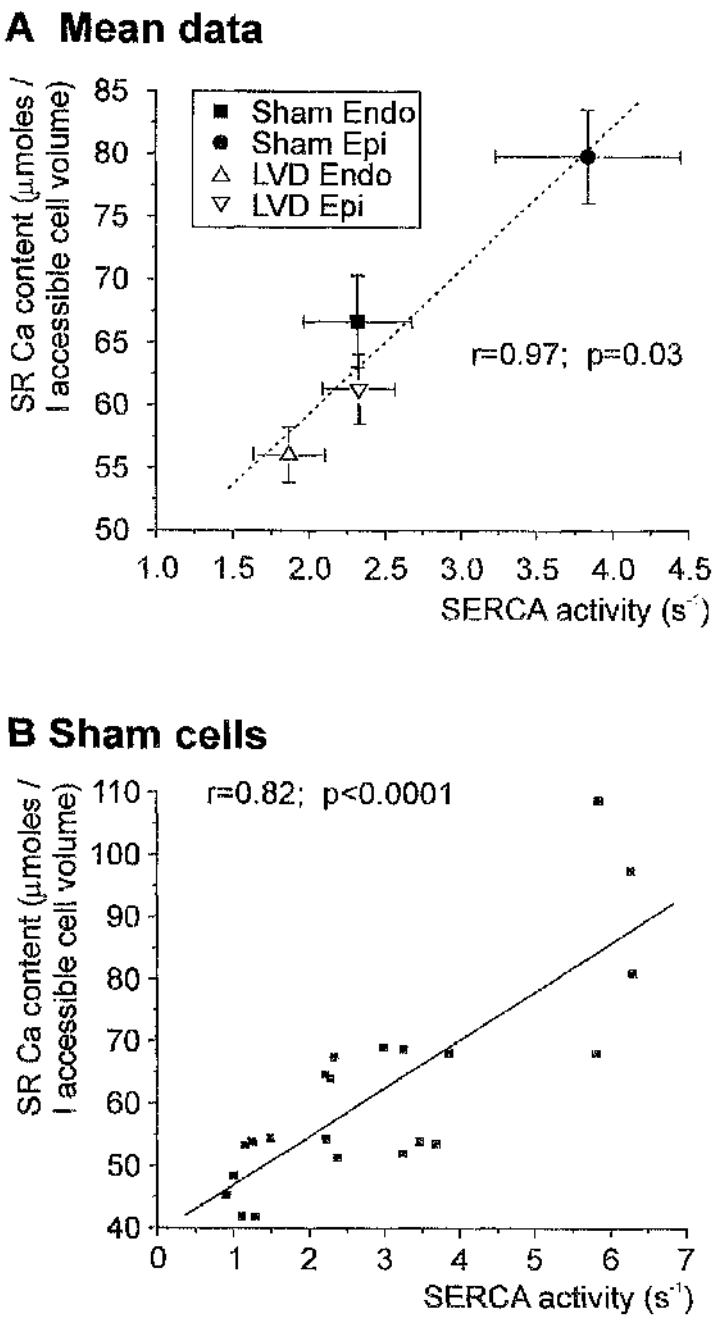

Figure 4.11 Relationship between SERCA activity and SR Ca content. **A:** Overall mean data for each cell type, derived from data in Figures 4.9 and 4.10. **B:** Example of relationship for individual cells. Sham cells from the experiment illustrated in Figure 4.3, where SR content data were available (n=22), were plotted as individual points. Linear regression was then performed, with a correlation coefficient, *r*, of 0.82 ($p<0.0001$).

Cell type	n	K_d (µmol/L)	B_{Max} (µmol/L)	a (µmol/L)
Sham Endo	28	0.80 ± 0.06	176 ± 15	-46.7 ± 9.3
Sham Epi	32	0.85 ± 0.07	246 ± 18	-54.7 ± 7.5
LVD Endo	35	0.89 ± 0.08	200 ± 16	-36.6 ± 4.3
LVD Epi	30	0.82 ± 0.08	222 ± 18	-48.9 ± 7.4

Table 4.1 Buffering characteristics for each of the cell types. For each cell, a plot of total $[Ca]_i$ against free $[Ca]_i$ was fitted using Equation 4.2 to generate the above values. B_{Max} and a are expressed relative to accessible cell volume. There were no statistical differences amongst the four cell types.

and linear regression analysis was performed. Figure 4.11 B illustrates the results for Sham cells. The results suggest a significant positive correlation, with a correlation coefficient of 0.82 ($p<0.0001$). The correlation was less strong, but still significant, for LVD cells ($r=0.69$; $p=0.001$).

4.3.4 Cellular buffering characteristics

The relationship between free and total $[Ca]_i$ was determined as outlined in Figure 4.5, and fitted using Equation 4.2 to determine the buffering characteristics for each cell. Mean values are reported in Table 4.1 and show that there were no significant differences in the buffering properties amongst the four cell types. The overall values for K_d and B_{Max} (0.84 ± 0.04 µmol/L and 212 ± 9 µmol/L cytosol, respectively) are comparable to those published in the literature - e.g. Trafford *et al.* using ferret ventricular myocytes and the indicator Fluo-3 reported a K_d of 0.6 µmol/L and a B_{Max} of 175 µmol/L cytosol (Trafford *et al.*, 1999), and Berlin *et al.* found a K_d of 0.96 µmol/L and a B_{Max} of 123 µmol/L cytosol in rat ventricular myocytes (Berlin *et al.*, 1994).

As mentioned in the methods section, because the final cytosolic concentration of Fura-2 is unknown (since loading is via the Fura-2 AM form of the dye, rather than from a known concentration of Fura-2 in the pipette solution), only the overall buffering characteristics of the cell can be determined. It is not possible to separate out the proportion of the buffering that is due to the dye from that due to the intrinsic buffers in the cell. However, this is unimportant for the purposes of converting values of free [Ca] to total [Ca], since this is determined by the overall buffering curve.

4.3.5 Analysis of Ca flux

4.3.5.1 Relationship between I_{Ca} *and tail currents*

In steady-state conditions, to maintain cellular Ca balance the amount of Ca entering the cell during systole must be matched by the amount leaving the cell in diastole. Therefore, in theory an accurate measure of steady-state I_{Tail}, appropriately corrected for non-NCX Ca removal mechanisms, must equate to the flux of Ca into the cell during systole. Conversely, if the amount of Ca entering the cell *via* I_{Ca} (and other lesser pathways) can be determined, then this will equate to the Ca flux out of the cell in diastole.

The protocol outlined in section 4.2.5 was designed to determine whether this relationship could be demonstrated under the chosen experimental conditions. The voltage protocol allowed for accurate measurement of Ca flux on I_{Ca} and I_{Tail}, with interfering currents blocked and contamination of I_{Ca} by I_{Na} eliminated as far as possible (see Figure 4.6). Paired measurements were made in each cell and results are summarised in Table 4.2. Overall systolic I_{Ca} flux of around 10 μmol/L cytosol is in excellent agreement with previously reported values for rabbit ventricular myocytes

Cell type	n	I_{Ca} amplitude (A/F)	I_{Ca} flux (μmol/L)	Diastolic Ca flux (μmol/L)	p-value (I_{Ca} *vs* diastolic flux)
Sham Endo	12	15.7 ± 1.4	9.5 ± 0.8	9.7 ± 0.5	0.77
Sham Epi	15	18.3 ± 1.1	10.0 ± 0.8	10.7 ± 0.6	0.38
LVD Endo	8	15.3 ± 1.4	12.1 ± 1.1	11.8 ± 0.5	0.76
LVD Epi	12	17.0 ± 1.4	10.3 ± 0.6	11.3 ± 0.4	0.14

Table 4.2 I_{Ca} amplitude and cumulative Ca flux on I_{Ca} and in diastole for each cell type. In each case flux is expressed relative to accessible cell volume. Diastolic Ca flux was calculated by correcting the integral of I_{Tail} for non-NCX Ca removal mechanisms, as described in the text. The final column indicates the statistical comparison between I_{Ca} and diastolic Ca flux for each cell type, made by paired *t*-test on the raw data. Separate comparisons *between* cell types showed no significant differences for I_{Ca} amplitude, I_{Ca} flux, or diastolic Ca movement.

under similar conditions (Delbridge *et al.* report a value of 9.7 ± 0.5 μmol/L cytosol; Delbridge *et al.*, 1996). For each cell type, there was no significant difference between Ca flux on I_{Ca} and Ca flux in the diastolic period, and indeed when all cells were considered, the difference remained non-significant (p=0.19). Overall, when all the data were combined, I_{Ca} flux was 96 ± 3% of the measured diastolic flux (n=47, p=n.s.). It is likely that any minor discrepancy is partly due to some failure of voltage control of the cell due to the large Na current, activating a little Ca entry on I_{Ca} which will not be included in the subsequent current integral. This is supported by the small initial Ca rise seen during the ramp phase of the protocol (see Figure 4.6). In addition, the I_{Ca} integral may be contaminated by Ca movement on I_{NCX} during the voltage pulse. However, without modelling subsarcolemmal [Na], [Ca] and E_M during the pulse, the

direction of this effect (i.e. the proportion of forward mode and reverse mode NCX) will be hard to determine. In similar experiments to measure I_{Ca} in rabbit ventricular myocytes, Delbridge *et al.* judged that the I_{Ca} integral was underestimated by around 10%. However, this estimate was not based on a full modelling of I_{NCX}, taking no account of possible reverse-mode NCX early in the voltage pulse (Delbridge *et al.*, 1996).

The above analysis shows that at steady state, the corrected I_{Tail} integral is an excellent surrogate measure for Ca entry into the cell on I_{Ca}. This enabled an expanded dataset to be included in the analysis of cellular Ca flux outlined in section 4.3.6 – a number of cells had been studied under the same conditions but with a voltage protocol not including a ramp-and-hold prepulse - for these cells the corrected I_{Tail} integral was used as a measure of Ca entry during systole.

4.3.5.2 Comparison of I_{Ca} *and* I_{Tail} *between cell types*

The protocol also allowed the total systolic and diastolic Ca flux to be compared between cell types. No significant differences were found, implying that total Ca entry during systole does not differ between endocardial and epicardial cells, nor does it differ in LVD. Peak I_{Ca} was also examined (see Table 4.2), and again there were no significant differences amongst cell types.

4.3.6 Analysis of systolic Ca flux and E-C coupling

The preceding data on Ca transient parameters, cellular buffering properties, SR Ca content, and I_{Ca} flux can be used to determine overall movements of Ca during systole and characteristics of E-C coupling. Firstly, for each individual cell, steady-state

diastolic and systolic free [Ca] was converted to total Ca using Equation 4.1 and the buffering properties determined for that cell. For a small number of cells where an adequate fit to the buffering curve was not possible, mean buffering data for either Sham cells or LVD cells were used. The change in cytosolic total Ca ($\Delta[Ca]_{Total}$) during systole was then calculated. The amount of Ca released from the SR was determined by subtracting Ca flux on I_{Ca} ($\int I_{Ca}$) from $\Delta[Ca]_{Total}$. This enabled the fractional release of SR Ca to be established, as well as the relative contribution of the SR to $\Delta[Ca]_{Total}$. Finally, the gain of E-C coupling was determined. By convention, gain is calculated as the magnitude of the response divided by the magnitude of the stimulus. In this case, the "response" was taken to be the amount of Ca released from the SR, and the "stimulus" was taken to be $\int I_{Ca}$. Thus, E-C coupling gain was defined as $(\Delta[Ca]_{Total} - \int I_{Ca}) / \int I_{Ca}$ – an approach also used by Bers and co-workers (see Bers, 2001; Shannon *et al.*, 2000). The results of this analysis are summarised in Figure 4.12.

4.3.6.1 Systolic Ca flux

Figure 4.12 A gives an overall summary of the approach described above, showing the mean SR Ca content for each cell type, along with the Ca flux on I_{Ca} and the amount of Ca released from the SR, summating to give $\Delta[Ca]_{Total}$. A statistical comparison of $\Delta[Ca]_{Total}$ amongst the cell types is shown. This shows $\Delta[Ca]_{Total}$ to be greater in Sham epicardial cells than Sham endocardial cells (32.0 ± 1.5 *vs* 27.8 ± 1.1 μmol/L cytosol, respectively; p=0.03), in parallel with the difference in SR Ca content between the two regions (see section 4.3.2). In LVD animals, there was no difference in $\Delta[Ca]_{Total}$ between the two regions (25.2 ± 1.5 μmol/L cytosol for epicardial cells *vs* 24.3 ± 1.1

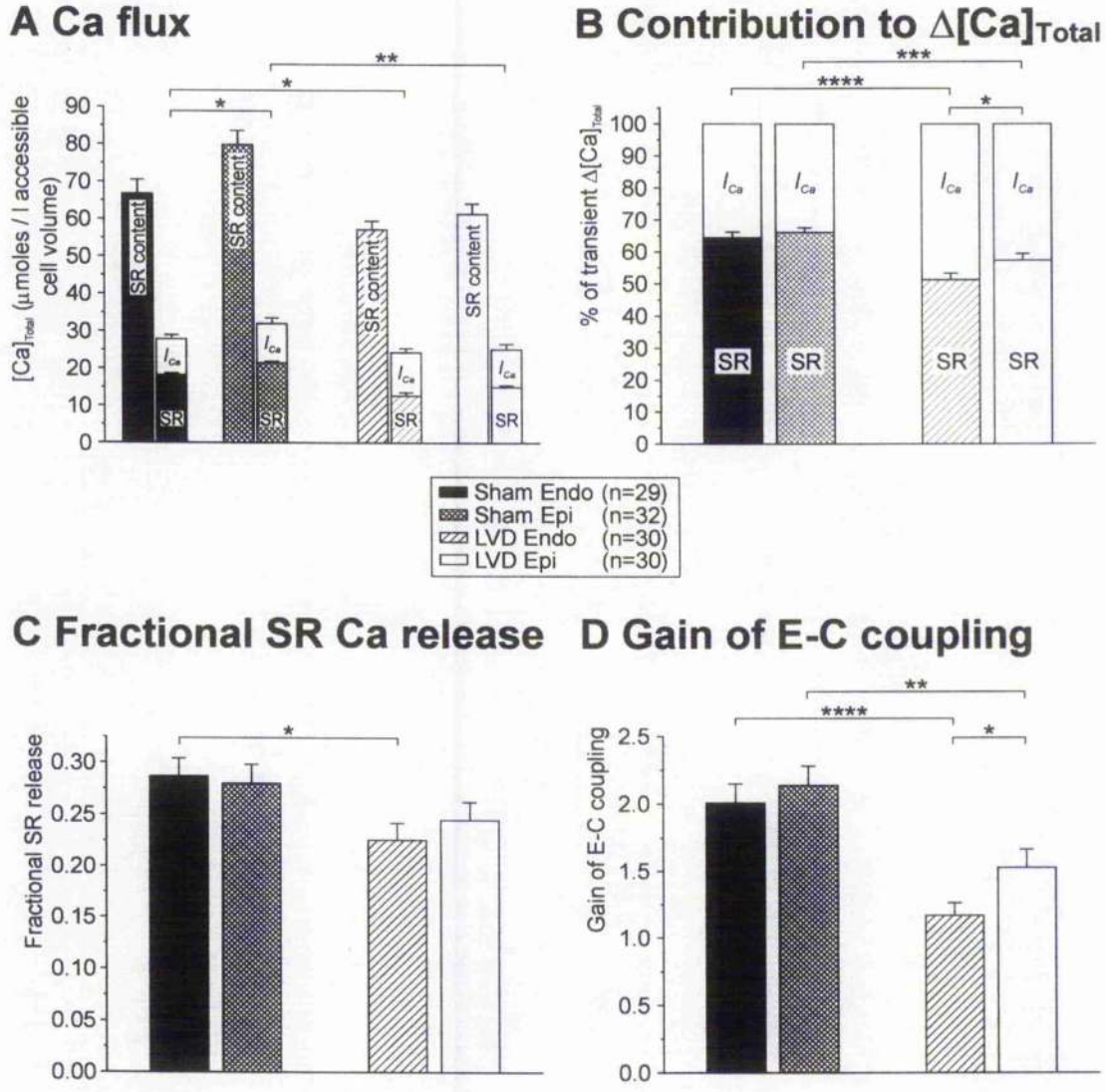

Figure 4.12 Systolic Ca flux. **A:** Summary of SR Ca content and systolic flux. For each cell type, the left column shows SR Ca content estimated from the integral of I_{NCX}, and the right column shows $\Delta[Ca]_{Total}$ during systole, split to show the absolute contribution of I_{Ca} and SR release, as indicated. Statistically-significant comparisons of $\Delta[Ca]_{Total}$ are shown (comparisons of SR Ca content are made in Figure 4.9). **B:** Relative contribution of I_{Ca} and SR release to $\Delta[Ca]_{Total}$. **C:** Fractional SR Ca release during systole. **D:** Gain of E-C coupling, defined as $(\Delta[Ca]_{Total} - \int I_{Ca}) / \int I_{Ca}$. Key refers to all panels. Statistically significant comparisons are indicated: * $p<0.05$, ** $p<0.01$, *** $p<0.001$, **** $p<0.0001$.

μmol/L cytosol for endocardial cells; p=0.63). Comparing Sham to LVD animals, $\Delta[Ca]_{Total}$ was significantly lower in LVD animals for each region (p=0.03 for endocardial cells, p=0.002 for epicardial cells). Given that Ca flux on I_{Ca} was similar amongst the regions (see Table 4.2), the difference in $\Delta[Ca]_{Total}$ in LVD must be due to less Ca release from the SR, and this was indeed the case (for endocardial cells: 12.7 ± 0.9 *vs* 18.2 ± 1.0 μmol/L cytosol; p=0.0001; for epicardial cells: 15.0 ± 1.3 *vs* 21.4 ± 1.3; p=0.001).

Figure 4.12 B shows the *relative* contribution of I_{Ca} and SR release to $\Delta[Ca]_{Total}$, illustrating that in LVD the SR makes a smaller contribution to the Ca transient than it does in Sham cells (for endocardial cells: 51.3 ± 2.1 % *vs* 64.5 ± 1.8 %; p<0.0001; for epicardial cells: 57.4 ± 2.4 % *vs* 66.1 ± 1.5 %; p=0.001). For Sham cells, the overall percentage contribution of I_{Ca} to $\Delta[Ca]_{Total}$ of 34.7 ± 1.1 % is higher than a previous published estimate for rabbit ventricular myocytes (23 ± 2 %), although the flux on I_{Ca} relative to SR Ca content, at 14.4 ± 0.5 %, is virtually identical (14 ± 2 %; Delbridge *et al.*, 1996).

4.3.6.2 Fractional SR Ca release and E-C coupling gain

Figure 4.12 C compares fractional Ca release from the SR across the cell types. Fractional release was calculated as ($\Delta[Ca]_{Total}$ - $\int I_{Ca}$) / SR Ca content (derived from $\int I_{NCX}$ on application of caffeine – see section 4.2.2.2). Overall fractional release in Sham cells was around 0.28, and in LVD cells, 0.23. In neither animal type was there a significant difference between fractional release in endocardial and epicardial cells. Fractional release in LVD endocardial cells was less than that in Sham cells from the

same region (0.22 ± 0.02 *vs* 0.29 ± 0.02; p=0.01) but for epicardial cells the difference was not significant (0.24 ± 0.02 for LVD cells *vs* 0.28 ± 0.02 for Sham cells; p=0.17).

The gain of E-C coupling was calculated as outlined above, and is summarised in Figure 4.12 D. In LVD, gain was found to be higher in epicardial cells than endocardial cells (1.53 ± 0.14 *vs* 1.17 ± 0.09; p=0.03), although this was not the case in Sham animals. However, gain was significantly lower in LVD animals in both regions (for endocardial cells: 1.17 ± 0.09 *vs* 2.01 ± 0.14; p<0.0001; for epicardial cells: 1.53 ± 0.14 *vs* 2.14 ± 0.14; p=0.003). This suggests defective E-C coupling in LVD cells, and is discussed further in sections 4.4.4 & 4.4.5.

4.3.7 Relative contribution of different systems to diastolic Ca decline

Experiments in this chapter and the last enable an estimation to be made of the relative contribution of different removal systems to the diastolic decline of Ca. The studies involving application of caffeine in the presence and absence of nickel, along with the studies described in section 4.2.3, allow a comparison to be made between the rate constants of Ca decline attributable to SERCA, NCX and the slow removal pathways. For each cell, these comparisons are made over similar ranges of $[Ca]_i$ (see Figure 3.4), although peak $[Ca]_i$ with caffeine application in the presence of Ni was generally slightly higher than that in the absence of Ni. This is because in the absence of Ni, NCX acts to lower the peak $[Ca]_i$ by beginning to remove Ca from the cell during the upstroke of the caffeine-induced transient. It should also be noted that the peak $[Ca]_i$ on application of caffeine exceeds that of normal voltage-stimulated Ca transients at 0.5 Hz (see Figures 4.1 and 4.7). However, at higher stimulation rates, the peak systolic

A

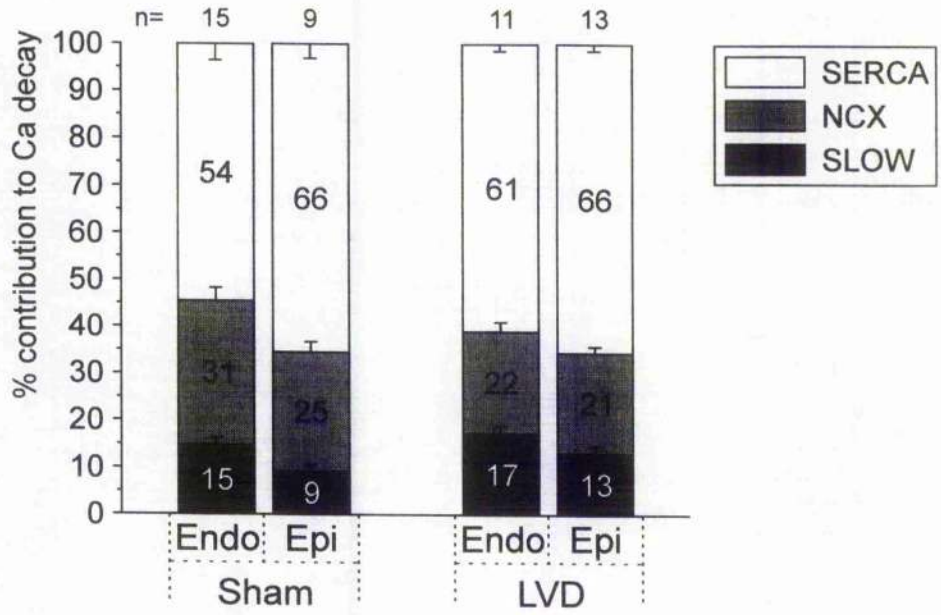

B

	Sham Endo *vs* Sham Epi	LVD Endo *vs* LVD Epi	Sham Endo *vs* LVD Endo	Sham Epi *vs* LVD Epi
SERCA	**0.04**	**0.04**	0.15	1.00
NCX	0.19	0.89	**0.02**	0.13
SLOW	**0.03**	0.08	0.27	0.11

Figure 4.13 Relative contribution of removal systems to Ca decay. **A:** Bar chart showing percentage contribution of SERCA, NCX and slow removal systems to Ca decay for each cell type. Numerical values are indicated on each bar, with number of cells noted above. **B:** Summary of statistical comparisons (p-values) between cell types, with significant results indicated in bold.

$[Ca]_i$ does approach these levels, therefore comparing Ca removal across this range of $[Ca]_i$ appears valid.

Results for each cell type are summarised in Figure 4.13, with data derived from 4 sham-operated animals and 4 LVD animals. Examining endocardial-epicardial

differences first, it is apparent that the relative contribution of SERCA to Ca removal is higher in epicardial cells, for both animal types (for Sham animals: 65.6 ± 3.1 % *vs* 54.5 ± 3.5 %; p=0.04; for LVD cells: 65.6 ± 1.4 % *vs* 61.0 ± 1.5 %; p=0.04). This appears to be in keeping with the previous results demonstrating lower NCX current density in epicardial cells (e.g. see Figure 3.7) and higher SERCA activity in this region (see Figure 4.10, difference only statistically significant for Sham cells). The proportion of Ca removed by NCX is not significantly different between endocardial and epicardial cells (although tending to be less in epicardial cells), so the greater removal *via* SERCA is mainly at the expense of less removal *via* slow pathways (for Sham animals: 9.1 ± 1.5 % *vs* 14.7 ± 1.6 %; p=0.03; for LVD cells: 13.1 ± 1.7 % *vs* 17.3 ± 1.6 %; p=0.08).

Comparing Sham animals to LVD animals, one would anticipate that the relative contribution of each system to Ca removal would depend on the relative change in each system between Sham and LVD animals – e.g. if all three removal pathways were reduced by around the same amount, then the overall contribution of each in LVD may not change compared to Sham. Figure 4.13 suggests that for endocardial cells, NCX function has been reduced by a greater amount than SERCA function in LVD, resulting in a smaller role for NCX in Ca removal in these animals (21.7 ± 2.0 % *vs* 30.8 ± 2.8 %; p=0.02). For epicardial cells, the reduction in activity of these two systems appears more proportional, such that although the percentage of Ca removed by NCX is a little lower in LVD, it is not significantly so (21.4 ± 1.4 % *vs* 25.3 ± 2.3 %; p=0.13). In LVD, with reduced NCX and SERCA function, there is a trend towards a greater role for the slow pathways in Ca removal (for endocardial cells: 17.3 ± 1.6 % *vs* 14.7 ± 1.6 %; p=0.27; for epicardial cells: 13.1 ± 1.7 % *vs* 9.1 ± 1.5 %; p=0.11).

4.4 Discussion

The experiments in this chapter have examined fundamental properties of Ca handling in sham-operated and LVD animals, with data from different regions of the myocardium being presented. The results have allowed a detailed analysis of systolic and diastolic Ca flux to be carried out, and a number of differences amongst the cell types have been shown.

4.4.1 Properties of Ca transients in the rabbit infarct model of LVD

As mentioned in Chapter 1, many changes in Ca handling have been described in human heart failure and animal models of the condition. The majority of studies presenting data on Ca transients have shown that these are significantly reduced in amplitude, often with an increased diastolic [Ca] and reduced systolic [Ca] (reviewed by Balke & Shorofsky, 1998; Wickenden *et al.*, 1998; Houser & Margulies, 2003). Commonly, these changes are accompanied by slower diastolic [Ca] decay (or twitch decay).

In this chapter, Ca transient characteristics were determined at different stimulation rates for endocardial and epicardial cells from Sham and LVD animals. The results are summarised in Figures 4.7 and 4.8. Systolic [Ca] was significantly lower in LVD animals at all stimulation rates and, in general, transients were of smaller amplitude, particularly at higher stimulation rates. In contrast to some previous studies, however, diastolic [Ca] was also significantly *lower* in LVD cells. These results are in keeping with studies by other workers in the laboratory, as outlined below.

4.4.1.1 Comparison with other studies of the rabbit infarct model of LVD

Neary *et al.* presented results on field-stimulated ventricular myocytes from a separate set of rabbits with infarct-induced LVD (Neary *et al.*, 2002). They found very similar levels for diastolic [Ca] to those reported here (see their Figure 1), although the difference between Sham and LVD cells was not statistically significant. They also found reduced systolic [Ca] and Ca transient amplitude at all stimulation rates. Their absolute values for systolic [Ca] were higher than those reported in this chapter – e.g. at 1 Hz, ~0.95 μmol/L *vs* 0.58 μmol/L. It is likely that this is due to differences in the experimental technique – in this chapter cells were voltage-clamped and dialysed with the same mock intracellular solution, compared with field-stimulated, intact cells in the study by Neary *et al.*

As shown in Figure 4.8 B, the rise in systolic [Ca] with increasing stimulation rate was less steep in LVD cells, a finding which was also apparent in the study by Neary *et al.* This may correlate with an impaired force-frequency relationship – a common finding in animal models of LVD (e.g. Neary *et al.*, 2002), and in cells from humans with end-stage heart failure (e.g. Davies *et al.*, 1995; Pieske *et al.*, 1999). However, the force-frequency relationship was not directly measured in this thesis.

Cells from the rabbit infarct model of LVD were studied under current-clamp conditions, with simultaneous measurement of $[Ca]_i$, by McIntosh *et al.* (2000). For epicardial cells, they found very similar results to those presented in this chapter – both systolic and (at higher stimulation frequencies) diastolic [Ca] were lower in LVD cells, particularly those from animals with more severe LVD (EF≤44%). However, for endocardial cells from animals with EF≤44%, peak systolic [Ca] was significantly

higher than that in Sham cells, and at a stimulation rate of 3 Hz, diastolic [Ca] was also higher. Again, there are differences in the experimental technique in this study compared to the approach used in this chapter, which may contribute to these discrepant findings. McIntosh *et al.* used high resistance microelectrodes filled with 2 mol/L KCl, and action potential durations were allowed to vary, whereas in this chapter all cells were dialysed with the same solution and the duration of the voltage pulse was the same for all cells studied.

In studies by a separate group, using cells from the infarct border zone, cell shortening during field stimulation was *greater* in MI cells than control cells at 0.5 Hz, although this was not the case at higher stimulation frequencies (Litwin & Bridge, 1997). In a later paper where intracellular Ca was measured using Fluo-3, the amplitude of the Ca transient in field-stimulated and voltage-clamped cells was significantly *smaller* in cells from the infarcted hearts (Litwin *et al.*, 2000). Since they used a pseudoratio method for calculating [Ca], absolute values for diastolic [Ca] could not be determined. In this paper, time-to-peak [Ca] and time-to-50%-decline were both prolonged and it was suggested that this was due to dyssynchronous Ca sparks. The addition of 0.1 μmol/L isoproterenol lead to improved spark synchronisation, higher peak [Ca] and a faster rise and decline in the Ca transient.

4.4.1.2 Comparison with other rabbit models of LVD

In the combined pressure- and volume-overload model of Pogwizd *et al.*, Ca transients were smaller, with no significant difference in diastolic [Ca] or in the time constant of Ca decay (Pogwizd *et al.*, 1999; Pogwizd *et al.*, 2001). Naqvi *et al.* studied a pressure-overload model of LVH in the rabbit and found slowed contraction and relaxation, but

no significant change in diastolic or peak systolic [Ca] (Naqvi *et al.*, 2001). Yao *et al.* induced heart failure by 3-5 weeks of rapid ventricular pacing (Yao *et al.*, 1998). Myocytes from these animals showed markedly reduced Ca transient amplitudes (0.09 μmol/L *vs* 0.33 μmol/L; $p<0.001$), with lower diastolic [Ca] and much reduced systolic [Ca]. The transients also showed slower decline of [Ca], mainly due to slowing of the late phase of decay.

4.4.2 SR Ca content and SERCA activity – regional differences and changes in LVD

4.4.2.1 Regional SR Ca handling in control (sham-operated) rabbit hearts

Experiments in this chapter have demonstrated increased SERCA activity and SR Ca content in epicardial myocytes compared to endocardial myocytes from sham-operated rabbit hearts (see Figures 4.9 & 4.10). These findings are accompanied by a higher $\Delta[Ca]_{Total}$ in epicardial cells (see Figure 4.12). To my knowledge, this is the first direct functional demonstration of endocardial-epicardial differences in SERCA function and SR Ca content in the heart.

These findings are in keeping with reports of SERCA expression across the myocardial wall. Igarashi-Saito *et al.* demonstrated greater SERCA mRNA levels in epicardial cells compared to endocardial cells in the dog, and this difference was maintained in dogs with pacing-induced heart failure (Igarashi-Saito *et al.*, 1999). Transmural SERCA2a protein levels were measured in the dog by Laurita *et al.* and they also showed higher levels in epicardial cells compared to endocardial or mid-myocardial cells (Laurita *et al.*, 2003). Ca transient characteristics were also measured, using optical mapping of transmural wedges, and it was found that decay of the Ca transient was significantly faster in epicardial cells. Prestle *et al.* measured both mRNA and

protein levels for SERCA2a in non-failing and failing human hearts (Prestle *et al.*, 1999). In failing hearts, both levels were significantly higher in epicardial cells than endocardial cells, but in non-failing hearts, although a similar trend was observed, this did not reach statistical significance.

4.4.2.2 Regional SR Ca handling in LVD

In contrast to the results for sham-operated animals presented above, transmural differences in LVD were not as marked. SERCA activity and SR Ca content were a little higher in epicardial cells, but not significantly so (Figures 4.9 & 4.10). Mean $\Delta[Ca]_{Total}$ was virtually the same in both areas (Figure 4.12). Few studies have examined regional differences in SERCA in failing hearts. As mentioned above, Prestle *et al.* found higher SERCA2a mRNA and protein levels in epicardial cells compared to endocardial cells, from human hearts with LVD due to dilated or ischaemic cardiomyopathy (Prestle *et al.*, 1999). This was accompanied by 23% less PLB protein in endocardial tissue compared to epicardial tissue. Spragg *et al.* studied dogs with pacing-induced heart failure and also found higher levels of SERCA2a protein in mid-wall/epicardial cells compared to endocardial cells, but only in dogs with dyssynchronous (right ventricular rather than right atrial) pacing (Spragg *et al.*, 2003).

4.4.2.3 Changes in SR Ca content and SERCA function in LVD

The value obtained for SR Ca content in Sham animals (estimate for endocardial and epicardial cells combined = 73.2 ± 2.7 μmol/L cytosol) was in keeping with previously published values for rabbit ventricular myocytes under similar conditions (e.g.Delbridge *et al.* estimated SR content at 87 ± 13 μmol/L cytosol, and 66 ± 7

μmol/L cytosol in a subset of cells; Delbridge *et al.*, 1996). Endocardial and epicardial cells from rabbits with infarct-induced LVD showed reduced SR Ca content when compared with similar areas in sham-operated animals (Figure 4.9). This has previously been demonstrated for non-voltage clamped cells in the same laboratory (Neary *et al.*, 2002), although in this study cells were taken from across the whole ventricular wall. The result is also in keeping with the majority of published data from animal models of heart failure (reviewed by Sjaastad *et al.*, 2003; Houser & Margulies, 2003). It is also a common finding in studies of human heart failure (see Piacentino III *et al.*, 2003; Hasenfuss & Pieske, 2002; Lindner *et al.*, 1998; Sjaastad *et al.*, 2003) although not universal (Terracciano *et al.*, 2003).

Taken together with the findings of Litwin *et al.* on the same animal model, the results in this chapter suggest that cells are phenotypically distinct in the area adjacent to the infarcted tissue. Cells taken from this border zone tended to have higher SR Ca contents (Litwin & Bridge, 1997; Litwin *et al.*, 2000, online supplement). With the addition of increased NCX function reported for these cells (Litwin & Bridge, 1997), one could hypothesise that this area would be particularly at risk of triggered arrhythmias secondary to spontaneous Ca release.

Further experiments in this chapter demonstrated reduced SERCA activity in LVD epicardial cells compared to Sham epicardial cells (Figure 4.10). For endocardial cells, SERCA function tended to be reduced in LVD, although not significantly so. Two other studies in this animal model have also shown slowed SR Ca uptake in LVD – in permeabilised cells (Neary *et al.*, 2002) and SR vesicles (Currie & Smith, 1999). In the latter study, SERCA2a protein levels were reduced in LVD, by 61% in tissue

homogenates and by 47% in SR vesicle preparations. These findings were accompanied by increased phosphorylation of phospholamban in LVD.

As discussed in the Chapter 1, reduced SERCA expression and function is almost universal in animal models of LVD and in human heart failure (also reviewed by Bers, 2001, pp 318 – 320; Hasenfuss & Pieske, 2002; Houser & Margulies, 2003). Altered regulation of SERCA (e.g. PLB levels, phosphorylation status or CaMKII activity) may contribute to the decreased activity (for review, see Frank *et al.*, 2003). Reduced SERCA function and SR Ca content critically affects Ca handling and may play a central role in producing the contractile abnormalities seen in LVD.

4.4.3 What determines SR Ca content?

In simple terms, steady-state SR Ca content will be determined by the balance between Ca uptake on SERCA and Ca efflux via the ryanodine receptor. The latter includes Ca release during systole and Ca "leak" during the diastolic period. Non-RyR leak pathways (e.g. SERCA "backflux") have also been described (see Bers, 2001, Chapter 7). Activity of NCX must also be considered, since it will compete with SERCA during diastole for the available cytoplasmic Ca. If NCX only acted to remove Ca from the cell (i.e. forward mode only), one would expect an inverse relationship between NCX activity and SR Ca content. However, as preceding discussions have alluded to, the relationship is more complex, and in certain circumstances reverse mode NCX may play a significant role in bringing Ca into the cell. For example, Litwin *et al.* suggested that NCX significantly contributed to SR Ca loading in their model of LVD (Litwin & Bridge, 1997). These considerations have also been reviewed by Sjaastad *et al.* (2003).

The analysis presented in this chapter allows some conclusions to be drawn regarding the importance of the above mechanisms in determining SR Ca content under the conditions studied. Figure 4.11 demonstrates a strong positive relationship between SERCA activity and SR Ca content with an *r*-value of 0.97 for the mean data (Figure 4.11 A). When data from individual cells are considered (see example Figure 4.11 B), an *r*-value of 0.82 was obtained for Sham cells (n=21; $p<0.0001$) and a value of 0.69 for LVD cells (n=21; $p<0.001$). A similar analysis was performed for SR content against NCX activity (as estimated from the Ca decay in the presence of 10 mmol/L caffeine) and is shown in Figure 4.14. In this case there was no significant relationship between the two variables for either the mean data or for individual cells (for Sham cells: $r=0.08$, n=62; $p=0.54$; for LVD cells: $r=0.24$, n=65; $p=0.06$). The weak positive trend for LVD cells implies that some reverse mode NCX could affect SR content.

The above considerations suggest that the main determinant of SR Ca content in this model is SERCA activity. The experiments in this chapter did not address the role of SR leak. Shannon *et al.* have examined this factor in intact rabbit cells in a different model of LVD (Shannon *et al.*, 2003b). They used tetracaine to block RyR-dependent SR leak and eliminated sarcolemmal Ca flux *via* NCX with 0 Na, 0 Ca solution. Under these conditions they used the rate of fall of cytoplasmic [Ca], and increase of SR [Ca], to infer the leak rate prior to application of tetracaine. They found that SR Ca leak was significantly increased in LVD for any given SR [Ca]. Further experiments would be required to determine whether this is also the case for intact cells from the model of LVD used in this thesis.

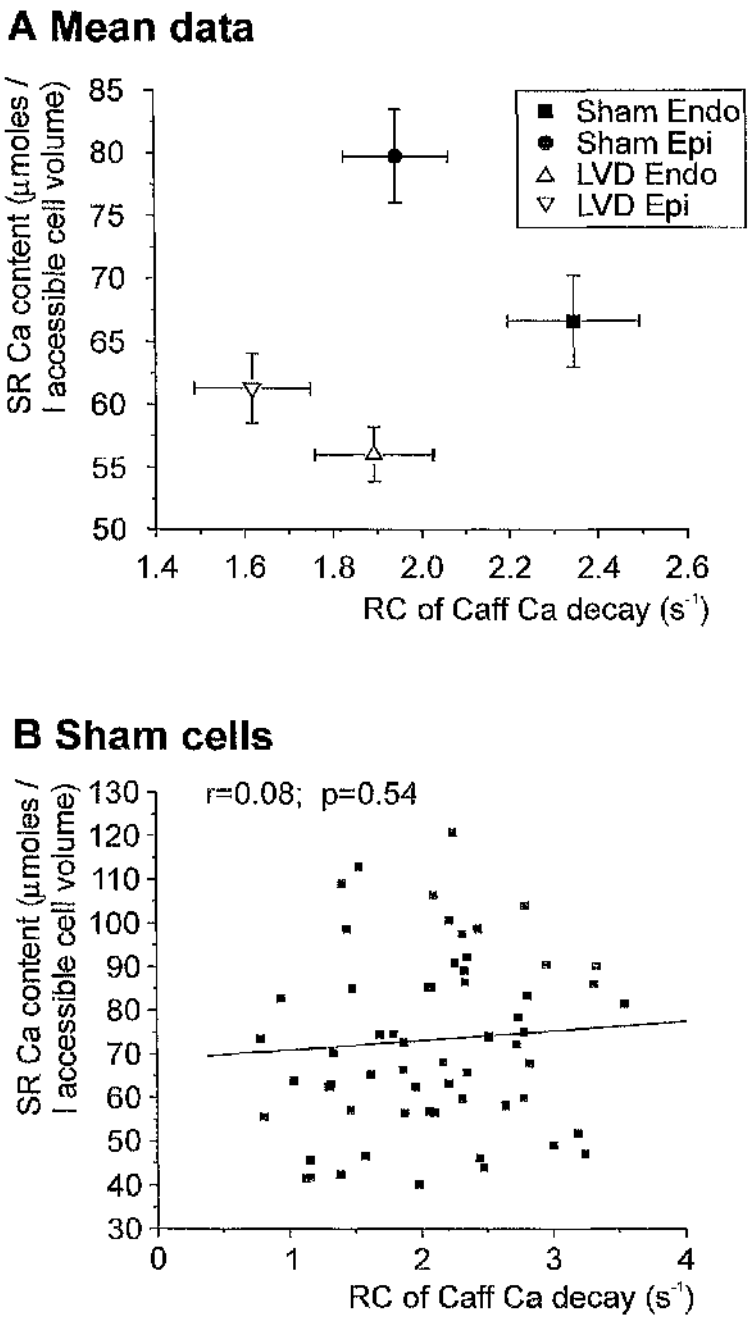

Figure 4.14 Relationship between NCX activity (estimated from the rate constant (RC) of Ca decay in 10 mmol/L caffeine) and SR Ca content. **A:** Overall mean data for each cell type. **B:** Example of relationship for individual Sham cells (endocardial and epicardial cells combined). Linear regression was performed, with a correlation coefficient, *r*, of 0.08 (p=0.54).

4.4.4 What determines steady-state $\Delta[Ca]_{Total}$?

4.4.4.1 Considering individual cells

For each cell, $\Delta[Ca]_{Total}$ will depend on the amount of Ca entering the cell and the amount released from the SR. The relative importance of these two factors could vary. At one extreme, if flux on I_{Ca} was constant from cell to cell, then differences in $\Delta[Ca]_{Total}$ would have to be due to differences in SR Ca release. Conversely, constant SR Ca release would mean that differences in $\Delta[Ca]_{Total}$ would have to be due to differences in Ca flux on I_{Ca}. In both of these cases, E-C coupling gain would need to vary from cell to cell. Figure 4.15 examines some of these relationships. It is apparent that the principal factor determining $\Delta[Ca]_{Total}$ is the amount of Ca released from the SR (Figure 4.15 B), with *r*-values of 0.94 for Sham cells and 0.91 for LVD cells. Variation in flux on I_{Ca} plays a smaller role (Figure 4.15 A), implying that there is less disparity in Ca entry on I_{Ca} amongst individual cells.

Figure 4.15 C illustrates that there is a significant correlation between SR Ca content and $\Delta[Ca]_{Total}$, with a correlation coefficient of 0.60 for Sham cells, and 0.52 for LVD cells. Following on from this, Figure 4.15 D shows that SR release is also dependent on SR Ca content. However, the correlation, although significant, is not especially strong (*r*-value of 0.44 for Sham and 0.50 for LVD). This implies that some other factor is also important in determining SR release. Differences in ryanodine receptor numbers or properties may account for the remaining variability in the amount of Ca released from the SR. If altered RyR function was the *only* change from cell to cell, then, in theory, compensatory changes in SR content would occur to normalise the amount of Ca released from the SR (discussed in detail by Eisner and co-workers;

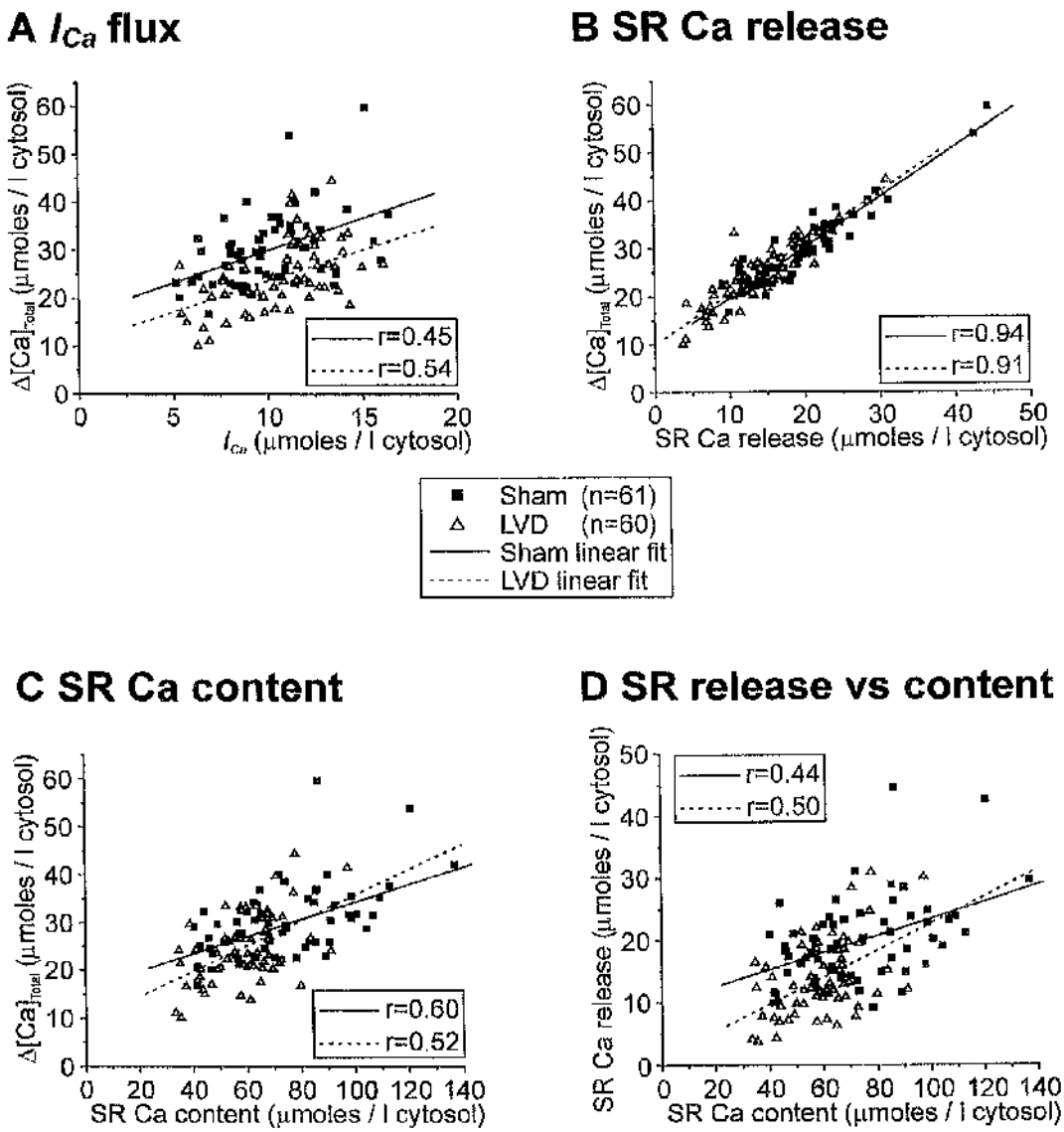

Figure 4.15 Determinants of $\Delta[Ca]_{Total}$ for individual cells. Data is from cells presented in Figure 4.12. For each animal type, data for endocardial and epicardial cells were combined. Linear regression was performed, with correlation coefficients as shown. In all cases the linear fit was highly significant, with $p<0.001$. Relationships are shown between $\Delta[Ca]_{Total}$ and: **A:** flux on I_{Ca} (either directly measured, or calculated from diastolic Ca flux), **B:** calculated SR Ca release and **C:** SR Ca content. Panel **D** relates SR Ca release to SR Ca content. Key refers to all panels.

Eisner *et al.*, 2000; Trafford *et al.*, 1998). However, altered RyR activity, along with concomitant changes in other Ca handling proteins (for example SERCA) could increase or decrease Ca cycling between the cytoplasm and the SR. These aspects of E-C coupling are discussed further in the next chapter.

4.4.4.2 Considering different cell types

Figure 4.12 illustrates that $\Delta[Ca]_{Total}$ is significantly reduced in LVD. In this study no significant difference was found between I_{Ca} flux in Sham and LVD cells, nor were endocardial-epicardial differences seen (see Table 4.2). Several other studies have also found similar levels of I_{Ca} flux in animals with heart failure compared to control animals, and this may also be the case in human heart failure (reviewed in Sjaastad *et al.*, 2003). With unchanged I_{Ca}, differences in $\Delta[Ca]_{Total}$ must be accounted for by reduced SR Ca release in LVD. Figure 4.12 indeed shows that the SR makes a smaller contribution (both absolute and relative) to the Ca transient. Figure 4.15 B suggests that for all cell types, the relationship between $\Delta[Ca]_{Total}$ and absolute SR Ca release can be described by a single linear fit. This line crosses the ordinate at the predicted point for mean Ca flux via I_{Ca} (around 10 μmol/L cytosol) – i.e. when SR release is 0, $\Delta[Ca]_{Total}$ will be entirely due to I_{Ca}.

The importance of SR Ca content in determining characteristics of the Ca transient has been widely recognised (reviewed in Sjaastad *et al.*, 2003; Bers, 2001, Chapter 8). Considering mean data for each cell type, the relationship between SR Ca content and aspects of Ca handling is explored further in Figure 4.16. In the figure, $\Delta[Ca]_{Total}$, SR Ca release, SR fractional release and E-C coupling gain are related to SR Ca content.

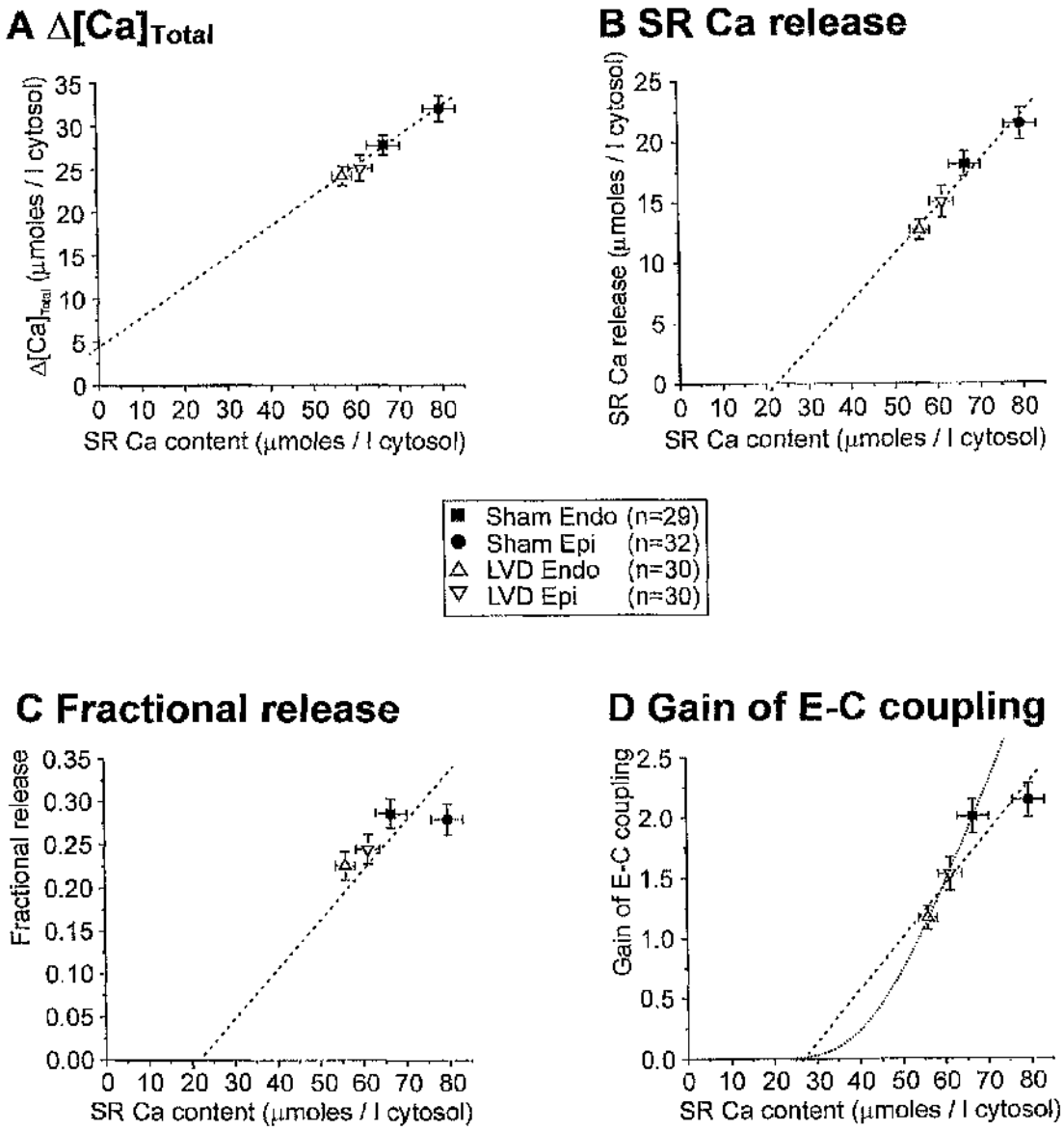

Figure 4.16 Characteristics of E-C coupling in relation to SR Ca content. Data is from cells presented in Figure 4.12. **A:** $\Delta[Ca]_{Total}$. **B:** Absolute SR Ca release, with linear fit. **C:** Fractional SR Ca release, with linear fit, assuming same intercept with abscissa as panel **B** (i.e. when SR release = 0, fractional release = 0). **D:** Gain of E-C coupling, with linear fit and possible alternative fit (dotted line, based on Bers, 2001). See text and Figure 4.12 legend for definition of terms. Key refers to all panels.

For illustrative purposes, linear fits to the data were performed. In each case, it is appreciated that a linear relationship may be an oversimplification, but since there are only four data points, and in several cases the data is over a limited range, more complex relationships are hard to discern. It is apparent that there is an excellent correlation between SR Ca content and both $\Delta[Ca]_{Total}$ (Figure 4.16 A) and SR Ca release (Figure 4.16 B), with linear relationships describing the data well. Again, the data points for LVD appear to follow a similar relationship to those for Sham cells. This perhaps implies that altered SR Ca release and $\Delta[Ca]_{Total}$ in LVD could be accounted for by the fall in SR Ca content.

Figure 4.16 C plots data for fractional SR release against SR Ca content. An arbitrary line was plotted through the data, crossing the abscissa at the same point as the linear fit in Figure 4.16 B (i.e. when SR release = 0, fractional release = 0). The data for Sham epicardial cells does not appear to follow the same relationship as the other three cell types – although SR content is higher in Sham epicardial cells than Sham endocardial cells, fractional SR Ca release is similar. The reason for this is unclear, but it could indicate lower than expected (for a given SR Ca content) efficiency of trigger Ca in causing SR release (i.e. altered gain characteristics).

The relationship between E-C coupling gain (as defined in section 4.3.6) and SR Ca content is explored in Figure 4.16 D. A simple linear fit does not appear adequate to describe all the data. One could speculate an alternative curve, based on data from Shannon *et al.* (2000), who found a non-linear relationship between gain and SR content, with an increasingly steep relationship at high SR contents. It should be noted, however, that their relationship was determined for individual cells under conditions of

progressive SR loading from "empty". Using this approach, again Sham epicardial cells appear not to follow the trend of the other data, with a lower gain than one would anticipate for a given SR Ca content.

Overall, the measured values for E-C coupling gain are somewhat lower than those previously reported for rabbit ventricular myocytes. Shannon *et al.* found a gain of around 3-8 in their experiments (Shannon *et al.*, 2000). Compared to the studies in this chapter, their conditions would tend to produce higher SR loads (longer voltage pulses, with Na-free solutions, higher resting membrane potential and slightly higher $[Ca]_o$). The lower gains in this chapter could be accounted for by the lower SR content, and a different stimulation protocol and/or solutions may result in more comparable values.

4.4.5 E-C coupling in LVD

The discussion above suggests that the fundamental difference in this model of LVD is the lower SR Ca content. This may be brought about by reduced SERCA activity, and leads to reduced E-C coupling gain, with less SR Ca release for a given I_{Ca} trigger. Figures 4.15 and 4.16 suggest that in LVD, $\Delta[Ca]_{Total}$, SR Ca release , SR fractional release and E-C coupling gain follow a similar relationship to SR Ca content that they do in Sham cells. This implies that the overall "effectiveness" of E-C coupling (gain for a given SR content) may be relatively unchanged in LVD.

Similar results were reported by Hobai & O'Rourke for canine tachycardia-induced heart failure (Hobai & O'Rourke, 2001). They found unchanged I_{Ca} amplitude, with reduced Ca transients that could be entirely explained by the fall in SR Ca content. E-C coupling gain was reduced in failing myocytes, but this was in proportion to the

lowered SR content, and defective E-C coupling could be reversed by restoring SR Ca to the level found in control cells. Similarly, in a combined pressure and volume overload model of heart failure in the rabbit, Pogwizd *et al.* demonstrated that Ca transients were ~40% lower, with unchanged I_{Ca} and a ~40% reduction in SR Ca content (Pogwizd *et al.*, 2001). As discussed in Chapetr 1, other workers have shown reduced E-C coupling gain in the presence of maintained SR content (e.g. Gómez *et al.*, 2001; reviewed by Sjaastad *et al.*, 2003) and some have proposed that this could be due to altered T-tubule structure (He *et al.*, 2001).

4.4.6 Diastolic Ca flux – regional differences and changes in LVD

4.4.6.1 Regional differences in diastolic Ca flux

This study is the first to demonstrate that regional differences exist in the relative proportion of Ca removed by NCX, SERCA and slow removal pathways (Figure 4.13). In control epicardial cells, with increased SERCA activity and reduced NCX function, SERCA plays a greater relative role in the removal of cytoplasmic Ca during the diastolic period. Slow pathways play a proportionally lesser role. These differences are reflected in the greater SR Ca content in epicardial cells (Figure 4.9). For LVD cells, these endocardial-epicardial differences are less marked, although there is a similar pattern in terms of increased relative removal via SERCA for epicardial cells ($p=0.04$), with less removal via slow pathways ($p=0.08$), and a slightly higher SR content (p=n.s.).

4.4.6.2 Diastolic Ca flux in Sham cells

Bassani, Bers and co-workers have extensively investigated relative Ca removal via different systems in cardiomyocytes (e.g. Bassani *et al.*, 1994; Puglisi *et al.*, 1996;

reviewed in Bers, 2000; Bers, 2001, Chapter 9). For non-failing rabbit ventricular myocytes, they found values for relative removal via SERCA, NCX and slow pathways of 70%, 28% and 2%, respectively. The principal difference in these figures compared to those obtained in this chapter is that their contribution of slow pathways is much smaller (2% *vs* 12.6 ± 1.3 %, for combined Sham cells, n=24). This may be because when estimating removal via the slow pathways it is difficult to achieve complete inhibition of NCX and SERCA function using 10 mmol/L Ni and 10 mmol/L caffeine. If either system is still operating, even at a much-reduced level, then the amount of Ca removed by the slow pathways will be overestimated. In the studies quoted above, slow pathway activity was measured with caffeine in the absence of external Na and Ca, or with twitches in the presence of thapsigargin and no external Na. The irreversible nature of thapsigargin meant that it could not be used for the experiments in this chapter. Some preliminary experiments were conducted with caffeine and 0 Na-0 Ca solutions, but it was found that the cells were sensitive to the re-introduction of normal external solution and often did not survive to the end of the protocol.

Nonetheless, from the experiments in this chapter and Chapter 3, there was some evidence that inhibition of NCX by 10 mmol/L Ni may have been adequate. Firstly, examination of the raw current traces when caffeine + Ni was applied generally showed little inward (NCX) current (e.g. see Figure 3.4). Secondly (although more indirectly), the measured systolic and diastolic Ca flux at steady state can be used to test the assumptions regarding the relative contribution of electrogenic and non-electrogenic removal pathways. The role of these pathways was determined from the relative rates of Ca removal with caffeine in the absence and presence of Ni, as discussed in section 4.1.1. The calculated correction factor for non-electrogenic (i.e. slow) pathways was

then applied to the integrated tail current to determine total diastolic Ca flux. The fact that this calculated flux matched closely the measured systolic flux on I_{Ca} (see Table 4.2) implies that the correction factor is valid. Thirdly, one would expect that the percentage contribution of NCX + slow pathways to Ca removal should match the percentage contribution of I_{Ca} to the systolic Ca transient (since relative flux across the sarcolemma in systole should match that in diastole). Mean data for Sham cells suggest that the former is around 41% and the latter around 35%, showing reasonable agreement.

4.4.6.3 Diastolic Ca flux in LVD

In both endocardial and epicardial cells there is a reduction in NCX function in LVD (see Chapter 3). SERCA activity is reduced in LVD epicardial cells (see Figure 4.10), and is a little lower (although not significantly so) in LVD endocardial cells. Overall, the relative contribution of NCX to Ca removal is reduced in LVD (21.5 ± 1.2 % *vs* 28.8 ± 2.0 %; p=0.003) and changes in the other two systems are not significant (for SERCA, 63.5 ± 1.1 % *vs* 58.6 ± 2.7 %; p=0.10; for slow pathways, 15.0 ± 1.2 % *vs* 12.6 ± 1.3 %; p=0.17).

Bers (2000) has reported values for cells from rabbits with combined pressure and volume overload, based on data from Pogwizd *et al.* (1999). As discussed previously, NCX is upregulated in this model, and extrusion by this route becomes more important – indeed it matches the amount removed by the SR (both 49%). This model would appear to be phenotypically different from that described in this thesis, perhaps because of the different mechanism of inducing heart failure.

4.5 Conclusions

The experiments in this chapter have examined Ca handling throughout the cardiac cycle in cells from sham-operated and post-infarction animals. In general, LVD cells display smaller Ca transients, with slower Ca decay in diastole. SR Ca content is significantly lower in LVD cells, and this may be related to reduced SERCA activity, particularly for epicardial cells. Ca entry *via* $I_{Ca,L}$ appears unchanged in the post-infarction myocytes, however, the gain of E-C coupling is significantly reduced. Small endocardial-epicardial differences in SERCA activity are present (significant for Sham cells) and, coupled with the transmural differences in NCX demonstrated in Chapter 3, SR uptake accounts for proportionally more Ca removal in epicardial cells for both animal types.

CHAPTER 5

MANIPULATION OF CALCIUM HANDLING

5.1 Introduction

A large number of methods can be used to alter cellular Ca handling from baseline levels. Simple methods such as changing the stimulation frequency or voltage pulse duration can alter the size of Ca transients and SR Ca content (e.g. Maier *et al.*, 2000; Janczewski *et al.*, 1995). Similarly, changing [Ca] in the superfusate can have dramatic effects on intracellular [Ca] and contraction (e.g. Trafford *et al.*, 2001). Many studies have used blocking agents or inhibitors in an attempt to alter one particular aspect of Ca handling and examine the effect. However, it can prove difficult to restrict the effects of such agents to the one area of interest – often even fairly specific blockers will affect other cellular processes (reviewed by Taylor & Broad, 1998). For example, preliminary experiments for this chapter using the NCX inhibitor 2',4'-dichlorobenzamil showed that, at a concentration of 0.1 mmol/L, it successfully inhibited NCX current, but also reduced peak I_{Ca} current by around 40% and shifted the peak of the I_{Ca} *I-V* curve a few millivolts more positive.

In this chapter, two methods were used to alter E-C coupling and overall Ca handling. Firstly, low concentrations of caffeine were used to alter the sensitivity of the ryanodine receptor to Ca, transiently enhancing SR Ca release. Secondly, Ca handling was examined with an altered holding potential, inhibiting Ca efflux *via* NCX, and resulting in changes in SR Ca content.

5.1.1 Effects of caffeine on Ca handling

The methylxanthine caffeine has been shown to have several effects on different aspects of cardiac myocyte physiology. It has been known for over 20 years that caffeine is a potent enhancer of myofilament Ca sensitivity. It also acts as a

phosphodiesterase (PDE) inhibitor, increasing intracellular cyclic AMP (cAMP), leading to a cascade of effects through increased phosphorylation of a variety of Ca-handling proteins (for reviews, see Bers, 2001, Chapters 2 & 10). The property of caffeine exploited in this chapter is its action at the sarcoplasmic reticulum, aspects of which will now be discussed.

In previous chapters 10 mmol/L caffeine has been used to cause release of Ca from the SR, enabling its quantification. It exerts this effect by increasing the Ca-sensitivity of the RyR, such that the open probability of the receptor is markedly increased (both frequency and duration of opening) for a given $[Ca]_i$ (Rousseau & Meissner, 1989). At lower concentrations of caffeine, this modulatory effect on CICR can be used to give insights into the complex relationship between trigger [Ca], SR Ca release, Ca transient properties and the balance of Ca influx and efflux. Such studies have been performed in detail by Eisner and colleagues (e.g. O'Neill & Eisner, 1990; Trafford *et al.*, 1998; Trafford *et al.*, 2000; reviewed in Eisner *et al.*, 1998).

5.1.1.1 "Autoregulation" of SR Ca release

One consistent finding of Eisner and colleagues has been that maintained alterations in SR Ca release (e.g. by low concentrations of caffeine) have only short-lived effects on the Ca transient. This has been termed "autoregulation", and results from compensatory changes in the SR Ca content, which normalise SR Ca release. For example, when cells are stimulated in the presence of low concentrations of caffeine, initial transients will be increased in size due to enhanced release of Ca from the SR. However, in the absence of changes in SERCA function, this will progressively unload the SR, with net loss of Ca from the cell *via* NCX and other extrusion processes. A

new steady state will be achieved where the combination of a sustained increase in SR fractional release and reduced SR Ca content will return overall SR Ca release to pre-caffeine levels. With no change in sarcolemmal Ca influx and efflux this steady state should be reached at the point where the Ca transients have returned to control levels. Trafford *et al.* measured the Ca fluxes involved in this process and showed that for rat ventricular myocytes in the presence of 0.1 mmol/L caffeine, the SR Ca content had fallen by around 20% at steady state (Trafford *et al.*, 1998).

For this chapter, preliminary experiments were performed with 0.1 mmol/L, 0.25 mmol/L, 0.5 mmol/L and 1 mmol/L caffeine. The two higher concentrations were chosen for further study since they lead to reproducible increases in the initial Ca transients and reductions in the steady-state SR Ca content.

5.1.2 Reversible inhibition of Ca efflux via *NCX*

Given the findings in Chapter 3 of reduced NCX activity in LVD, one aim of the studies in the current chapter was to examine the effects of acute inhibition of NCX function on cellular Ca handling. As discussed above, some available NCX inhibitors have additional actions on the cell, which would complicate analysis of their effects. Instead of pharmacological inhibition, it was decided to make use of the fact that the cells were voltage-clamped to alter Ca extrusion during the diastolic period. Since NCX is electrogenic, the driving force for forward-mode Ca efflux can be reduced by elevating the membrane potential. Thus, a voltage protocol was designed which included a period of stimulation with the holding potential raised by 20 mV. The effects of this intervention could then be elucidated.

5.2 Methods

5.2.1 Solution compositions

Internal and external solutions were once again chosen to allow accurate quantification of Ca fluxes, as outlined in sections 2.5.4 and 3.2.2.1.

5.2.2 Manipulation of SR Ca handling with caffeine

5.2.2.1 Experiment protocol

Cells were loaded with Fura-2, as previously described, and were voltage-clamped with a holding potential of -80 mV. All experiments were performed at 37 °C. The experimental protocol is outlined in Figure 5.1. First, steady-state Ca transients were achieved by stimulating at 0.5 Hz, with a 150 ms step to 0 mV. 10 mmol/L caffeine was then rapidly applied and the baseline SR Ca content determined, as described in section 4.2.2.2. Cells were then stimulated again to re-load the SR, and once this was achieved the superfusate was switched to one containing 0.5 mmol/L caffeine. Cells were stimulated for a further 30 s, and then the SR Ca content was again estimated using 10 mmol/L caffeine. The protocol was repeated using 1 mmol/L caffeine in the superfusate.

5.2.2.2 Data analysis

After conversion of Fura-2 ratio signals to $[Ca]_i$, systolic and diastolic values for Ca transients were determined at several points in the protocol. Steady-state Ca transients were measured before and after the switch to the low concentration of caffeine by averaging the last few transients of each train (at points **a**, **c** and **e** on Figure 5.1). Transients at **a** and **c** are obtained under identical conditions and were combined to determine the mean "pre-caffeine" Ca transient. The first transient after the switch to

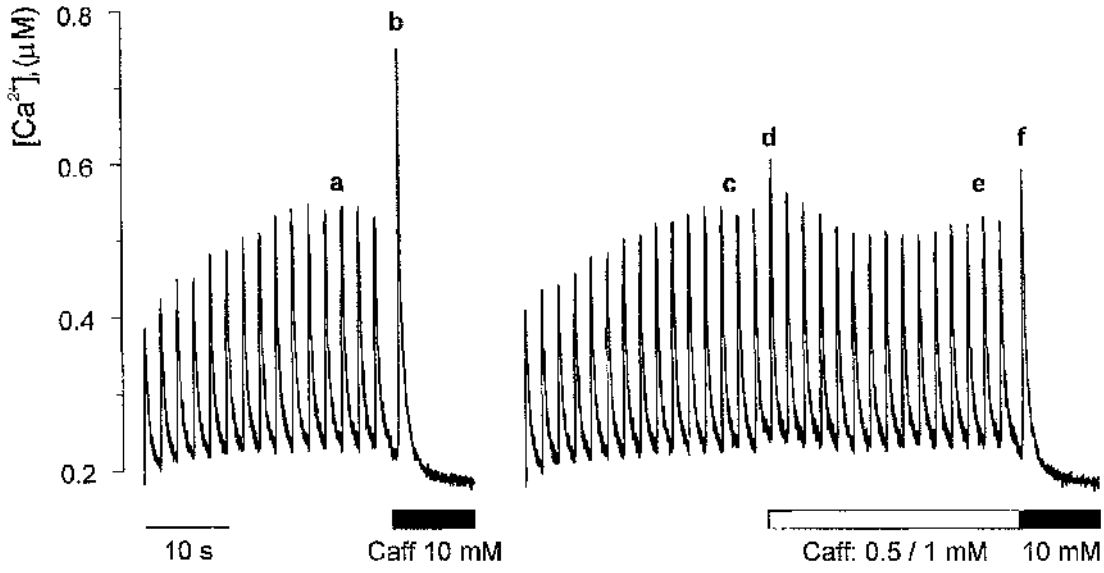

Figure 5.1 Protocol for altering SR Ca release with low concentrations of caffeine. Cells were stimulated at 0.5 Hz to achieve steady-state Ca transients (**a**), then 10 mmol/L caffeine (Caff, **b**) was applied to give an estimate of SR Ca content under baseline conditions. SR content was determined from the integral of the NCX inward current, as outlined in Figures 4.1 & 4.2. Steady-state Ca transients were once more established (**c**), then the perfusion solution was rapidly switched to one containing 0.5 or 1 mmol/L caffeine (open bar). Characteristics of the initial (**d**) and steady-state (**e**) transients were determined. 10 mmol/L caffeine was once more applied (**f**) and the new SR Ca content was measured.

0.5 mmol/L or 1 mmol/L caffeine was also measured (point **d** on Figure 5.1). Thus, data for "initial" (**d**) and "steady-state" (**e**) transients were obtained after the switch to caffeine.

SR Ca content was estimated from the integral of the inward NCX current, as outlined in Figures 4.1 & 4.2. This measure was made before (**b**) and after (**f**) the switch to 0.5

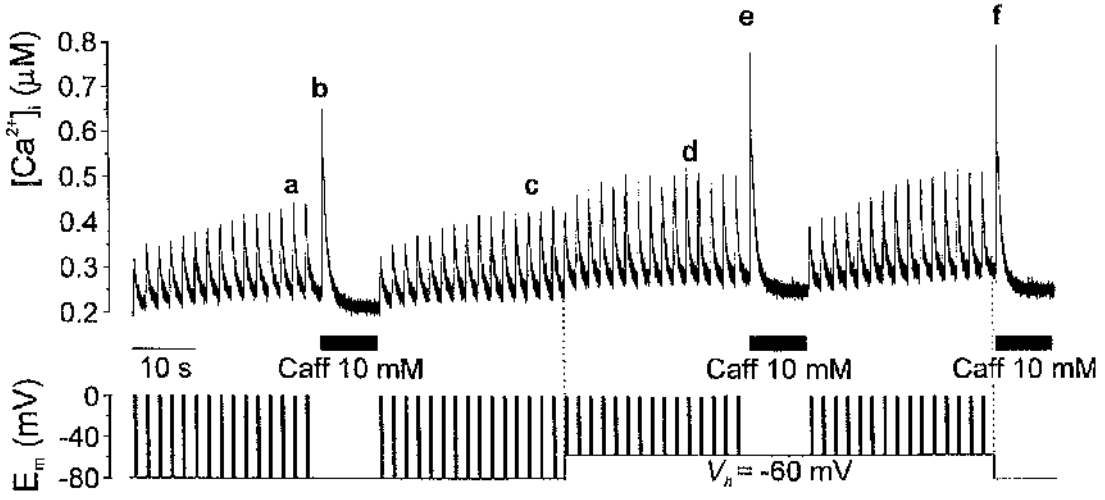

Figure 5.2 NCX inhibition protocol. Cells were initially stimulated at 0.5 Hz from a holding potential (V_h) of -80 mV until steady state was achieved (**a**). 10 mmol/L caffeine (Caff) was then applied (**b**) and SR Ca content estimated as previously described. After a further period of stimulation (**c**), the holding potential was changed to -60 mV and stimulation continued. At steady state (**d**), caffeine was again applied (**e**). The rate constant of Ca decay in the presence of caffeine at -60 mV (**e**) was compared with that at -80 mV (**b**) to give an estimate of the degree of inhibition of NCX function, as described in the text. Finally, cells were stimulated again to load the SR at V_h = -60 mV and the SR Ca content was estimated by applying caffeine at V_h = -80 mV (**f**).

mmol/L or 1 mmol/L caffeine. For each cell, Ca transients and SR content before and after the switch to 0.5 mmol/L or 1 mmol/L caffeine were compared using paired t-tests. Comparisons between separate cell groups were first made by ANOVA, and where a significant F-value was achieved, subsequent *post hoc* two-tailed t-tests were performed (see section 2.8).

5.2.3 Inhibition of NCX

5.2.3.1 Experiment protocol

The protocol for altering NCX function is outlined in Figure 5.2. Baseline characteristics of Ca transients and SR Ca content were determined with a 0.5 Hz train of stimuli (**a**), followed by application of 10 mmol/L caffeine (**b**), as described above. Steady-state Ca transients were once more achieved (**c**), then the holding potential between voltage steps was increased to -60 mV (**d**). This reduces the driving force for Ca extrusion on NCX, as discussed in section 5.1.2. The degree of inhibition of NCX was estimated by examining the Ca decay on application of 10 mmol/L caffeine at a holding potential of -60 mV (**e**), as described below. A further stimulation train was used to load the SR again with Ca (at the higher holding potential), then the SR content was determined by applying caffeine at a holding potential of -80 mV (**f**). The latter caffeine application was performed at -80 mV rather than -60 mV to standardise conditions under which SR Ca content was determined, allowing a direct comparison with the baseline value (since the altered holding potential affects the resting current level and timecourse of Ca extrusion).

5.2.3.2 Data analysis

Characteristics of steady-state Ca transients were determined before (**a** and **c** combined) and after (**d**) the switch in holding potential to -60 mV. Corresponding SR Ca contents were measured (**b** and **f**), as previously described. An estimate of NCX activity was made by examining the Ca decay on application of 10 mmol/L caffeine. The rate constant of Ca decay was determined by fitting a single exponential function to the converted Ca data (see Figure 3.4). The contribution of NCX to this decay was estimated by subtracting the mean rate constant for non-NCX removal mechanisms

previously determined for each cell type (see Figure 3.10). The degree of inhibition of forward-mode NCX activity using the voltage protocol described above was estimated by comparing the corrected rate constant obtained at a holding potential of -60 mV (**e**) with that obtained at -80 mV (**b**).

As with the previous protocol, for each cell paired t-tests were used for statistical analysis of Ca transients and SR Ca content before and after the switch in holding potential to -60 mV. ANOVA and subsequent unpaired two-tailed t-tests were used to compare cells from different groups, as outlined in section 2.8.

5.2.4 Analysis of Ca handling

For each of the protocols outlined above, a similar analysis of Ca handling to that described in section 4.3.6 was performed. As before, buffering characteristics were determined for each individual cell (see section 4.3.4) and these were used to convert free $[Ca]_i$ to total Ca. This allowed $\Delta[Ca]_{Total}$ to be calculated for transients at different stages of the protocols. Systolic Ca entry was either measured directly from the integral of I_{Ca} or calculated from the integral of the tail current, as described in section 4.3.5.1. Using this value, SR Ca release, SR fractional release and E-C coupling gain could be calculated (see section 4.3.6).

5.3 Results

The experiments in this chapter were designed to alter aspects of myocyte Ca handling to gain insights into E-C coupling amongst the cell types. Low concentrations of caffeine were used to increase the open probability of the ryanodine receptor, causing changes in the SR Ca content and altered SR Ca release in systole and diastole. In separate experiments, the membrane potential in diastole was manipulated to alter Ca extrusion, with resulting changes in SR Ca handling.

For the caffeine experiments, data were obtained from 8 Sham animals and 10 LVD animals, and for the NCX inhibition experiments, 4 animals of each type were used.

5.3.1 Effects of low concentrations of caffeine on steady-state SR Ca content

By altering the relationship between $[Ca]_i$ and SR Ca release, low concentrations of caffeine have the effect of unloading the SR. Figure 5.3 shows the absolute and relative effect of 0.5 mmol/L and 1 mmol/L caffeine on steady-state SR Ca content (all figures and tables for experiments with low concentrations of caffeine are grouped at the end of section 5.3.4). For each individual cell, paired *t*-tests show the incremental effects of 0.5 mmol/L and 1 mmol/L caffeine on the SR content, with significance levels generally $p<0.001$. Each caffeine concentration lowered the SR content by similar relative amounts, irrespective of the cell type (see Figure 5.3 B). In general, 0.5 mmol/L and 1 mmol/L caffeine reduced the SR content to around 65% and 45% of baseline levels, respectively. The only statistical difference apparent between cell types was that 1 mmol/L caffeine lowered the SR content in LVD endocardial cells by more than it did for Sham endocardial cells (to 37 ± 4 % of baseline SR content, *vs* 52 ± 3 %, $p=0.02$).

Comparisons of the absolute levels of SR Ca content amongst the different cell types are made in Figure 5.3 A. Baseline Ca content (i.e. in the absence of caffeine in the superfusate) shows the same trend as the results in Chapter 4 (see Figure 4.9), although with fewer cells, the only comparison reaching statistical significance was that between Sham epicardial cells and LVD epicardial cells. On application of 0.5 mmol/L and 1 mmol/L caffeine, smaller steady-state SR Ca contents were obtained for LVD endocardial cells than Sham endocardial cells. The application of caffeine also revealed small differences between LVD endocardial and epicardial cells, with higher SR contents in epicardial cells at each caffeine concentration.

5.3.2 Effects of low concentrations of caffeine on Ca transient characteristics

5.3.2.1 Diastolic & systolic $[Ca]_i$

Table 5.1 summarises the changes in diastolic and systolic $[Ca]_i$ with the switch to 0.5 mmol/L and 1 mmol/L caffeine in the superfusate. For each cell type, values are given for the first Ca transient after the switch to caffeine (point **d** on Figure 5.1) and for the steady-state Ca transient (mean of transients at point **e** on Figure 5.1). In general, the data show that on initially applying caffeine there was a small rise in diastolic $[Ca]_i$, particularly with 1 mmol/L caffeine. This measure was made at the *end* of the first transient, i.e. just before the upstroke of the second transient. The elevated diastolic $[Ca]_i$ at this point in the protocol may be due to the increased release of Ca from the SR, before extrusion processes have had a chance to cause net loss of Ca from the cell. Once steady state was achieved, diastolic $[Ca]_i$ was no different to baseline values (except for Sham epicardial cells with 0.5 mmol/L caffeine, where it was a little lower).

In all cases, except for LVD endocardial cells with 0.5 mmol/L caffeine, the first transient after the switch to caffeine had a significantly higher systolic $[Ca]_i$ than the baseline level. However, overall steady-state values of systolic $[Ca]_i$ were slightly *lower* in the presence of caffeine, reaching statistical significance for Sham epicardial cells at 0.5 mmol/L caffeine, and for Sham endocardial and LVD endocardial cells at 1 mmol/L caffeine.

5.3.2.2 $\Delta[Ca]_{Total}$ immediately after switch to caffeine

The above values for diastolic and systolic free [Ca] were converted to total [Ca] using the buffering properties of each cell, as described in section 4.3.6. This enabled calculation of $\Delta[Ca]_{Total}$ at different stages of the protocol. The results are presented in Figures 5.4 and 5.5 for initial transients and steady-state transients, respectively.

As expected, $\Delta[Ca]_{Total}$ for the first transient after the switch to each concentration of caffeine was higher than baseline values for all cell types (see Figure 5.4, p-values by paired t-tests generally <0.01 or <0.001). In the majority of cases, 1 mmol/L caffeine produced an incremental increase over 0.5 mmol/L caffeine. Interestingly, there appear to be regional differences in the amount that caffeine enhances the size of the transient. As shown in Figure 5.4 B, caffeine increased the relative size of the transient more in epicardial cells than endocardial cells. This reached statistical significance for both concentrations of caffeine in LVD cells (p=0.003 for 0.5 mmol/L caffeine, p=0.02 for 1 mmol/L caffeine), and for 1 mmol/L caffeine in Sham cells (p=0.03).

Caffeine was less effective at increasing $\Delta[Ca]_{Total}$ for LVD endocardial cells than Sham endocardial cells, but it seemed equally effective when epicardial cells were compared (Figure 5.4 B).

Differences in absolute $\Delta[Ca]_{Total}$ amongst the cell types are outlined in Figure 5.4 A. For each cell region, at 0.5 mmol/L and 1 mmol/L caffeine, $\Delta[Ca]_{Total}$ was smaller in LVD cells than Sham cells. This was also true for baseline $\Delta[Ca]_{Total}$ for epicardial cells (see Figure 4.12 for full comparison of baseline Ca handling).

5.3.2.3 Steady-state $\Delta[Ca]_{Total}$

Changes in $\Delta[Ca]_{Total}$ at steady state after the switch to caffeine are presented in Figure 5.5. Panels A and B show that for each cell type $\Delta[Ca]_{Total}$ is lower in the presence of caffeine (statistically significant, except for Sham epicardial cells with 1 mmol/L caffeine). Steady-state transients with low concentrations of caffeine were around 85-95 % of the amplitude of baseline transients. For Sham endocardial cells the effect of caffeine was incremental, with a greater reduction in $\Delta[Ca]_{Total}$ with 1 mmol/L caffeine compared to 0.5 mmol/L caffeine. Reduced Ca transient amplitude in the presence of low concentrations of caffeine was also apparent when free [Ca] was analysed (data not shown).

These consistent findings are at odds with the theory that acute alterations in RyR function will only produce transient changes in Ca transient amplitude (Eisner *et al.*, 1998; Trafford *et al.*, 2000; Eisner *et al.*, 2000). As discussed earlier (section 5.1.1.1), Eisner and colleagues showed that enhanced SR release (through caffeine application)

initially causes larger transients (as seen in this chapter), but this leads to net loss of Ca from the cell, causing unloading of the SR and hence reduced SR Ca release. This autoregulation returns the transients to the same size as before caffeine was applied. The fact that the steady-state transients measured in this chapter are smaller than those at baseline implies one of two main possibilities: that less Ca is entering the cell in systole and/or that SR Ca cycling is altered. The first of these possibilities was examined in a subset of cells, where systolic Ca entry was measured before and after the switch to caffeine (as described in section 4.2.5 and Figure 4.6). This showed no significant difference between systolic Ca entry before (13.7 ± 1.7 μmoles/L cytosol) and after (13.8 ± 1.6 μmoles/L cytosol) the switch to caffeine (n=10 cells; p value by paired t-test = 0.58). This implies that the smaller transients are due to a persisting alteration in SR Ca cycling. This possibility is examined further in the Discussion, section 5.4.1.2.

When different cell types were compared, transients in LVD epicardial cells were smaller than those in Sham epicardial cells at all concentrations of caffeine (Figure 5.5 A). The differences between Sham and LVD endocardial cells did not reach statistical significance.

5.3.3 Effects of low concentrations of caffeine on SR fractional release

SR fractional release of Ca was determined before and after the switch to caffeine, as previously described (see section 4.3.6). Again, results are presented for the 1st transient after the switch (Figure 5.6) and for transients at steady state (Figure 5.7).

For the first transient after the rapid switch to caffeine, it was assumed that the SR Ca content had not altered from the baseline level (i.e. it was the same as that determined at point **b** on Figure 5.1). This assumption is likely to be reasonable since depletion of the SR through increased RyR Ca "leak" would be negligible in the short period (<1 s) prior to the subsequent transient. As expected, by enhancing RyR sensitivity to Ca, the rapid application of a low concentration of caffeine lead to increased fractional release for the first transient after the switch (Figure 5.6). This was true for all cell types and, in general, 1 mmol/L caffeine had an incremental effect over 0.5 mmol/L caffeine.

Figure 5.6 B shows that for endocardial or epicardial cells, the degree of enhancement of fractional release was similar for Sham and LVD cells at each concentration of caffeine. There was a trend towards proportionally greater increases in fractional release for epicardial cells compared to endocardial cells (statistically-significant for 1 mmol/L caffeine for Sham cells, and 0.5 mmol/L caffeine for LVD cells). This is in keeping with the results for $\Delta[Ca]_{Total}$ described in section 5.3.2.2.

At steady state in the presence of low concentrations of caffeine, the SR is depleted of Ca through enhanced release and net loss of Ca from the cell (see Figure 5.3). A new balance of SR uptake and release relative to SR content will be achieved. At very low SR Ca contents other factors, in addition to enhanced RyR activity, may start to play a role in determining the overall Ca release. This could affect the final steady-state fractional release, may affect overall $\Delta[Ca]_{Total}$, and is discussed in more detail in section 5.4.1.2.

Figure 5.7 shows the measured effects of 0.5 mmol/L and 1 mmol/L caffeine on steady-state SR fractional release for each of the cell types. The figure shows that 1 mmol/L caffeine significantly enhanced fractional release for all cell types, more than doubling fractional release for Sham epicardial, LVD endocardial and LVD epicardial cells. The relative increase for Sham endocardial cells was less (see Figure 5.7 B), but was still significant (p=0.008). 0.5 mmol/L caffeine had a smaller effect on fractional release, but almost reached statistical significance for Sham endocardial cells (p=0.064) and LVD endocardial cells (p=0.054).

5.3.4 Effects of low concentrations of caffeine on E-C coupling gain

E-C coupling gain was calculated as in the previous chapter ($(\Delta[Ca]_{Total} - \int I_{Ca}) / \int I_{Ca}$). As expected, for the initial transient after the switch to caffeine, the effects on E-C coupling gain (Figure 5.8) match the effects on fractional release (Figure 5.6), with increased gain in the presence of caffeine. The percentage increase in gain (Figure 5.8 B) at each concentration of caffeine is also similar to that for fractional release (Figure 5.6 B). At baseline and at each concentration of caffeine, gain was higher in Sham endocardial cells than LVD endocardial cells (Figure 5.8 A). This did not quite reach statistical significance for the comparison between Sham epicardial cells and LVD epicardial cells (p=0.09, 0.14 and 0.08, for baseline, 0.5 mmol/L caffeine and 1 mmol/L caffeine, respectively). As for fractional release, there were small differences in the percentage increase in gain achieved in epicardial cells, compared to endocardial cells.

Figure 5.9 shows the results for steady-state transients in the presence of caffeine. Given that there was no significant change in systolic Ca entry (see section 5.3.2.3), if there was full autoregulation of SR Ca release then one would expect E-C coupling

gain to remain the same as it was at baseline (absolute SR Ca release would be maintained by increased fractional release in the face of a smaller SR Ca content). In fact, gain was significantly lower in the presence of caffeine (significantly so for all cell types except Sham epicardial cells at 1 mmol/L caffeine, where p=0.064). In broad terms, the relative changes in gain (Figure 5.9 B) match those for $\Delta[Ca]_{Total}$ (Figure 5.5 B). In a similar manner to the findings for the 1st transient after the switch to caffeine, gain was lower for LVD endocardial cells than Sham endocardial cells (although statistical significance was not reached at 0.5 mmol/L caffeine, p=0.11). The analysis of Ca handling is taken further in section 5.3.9.

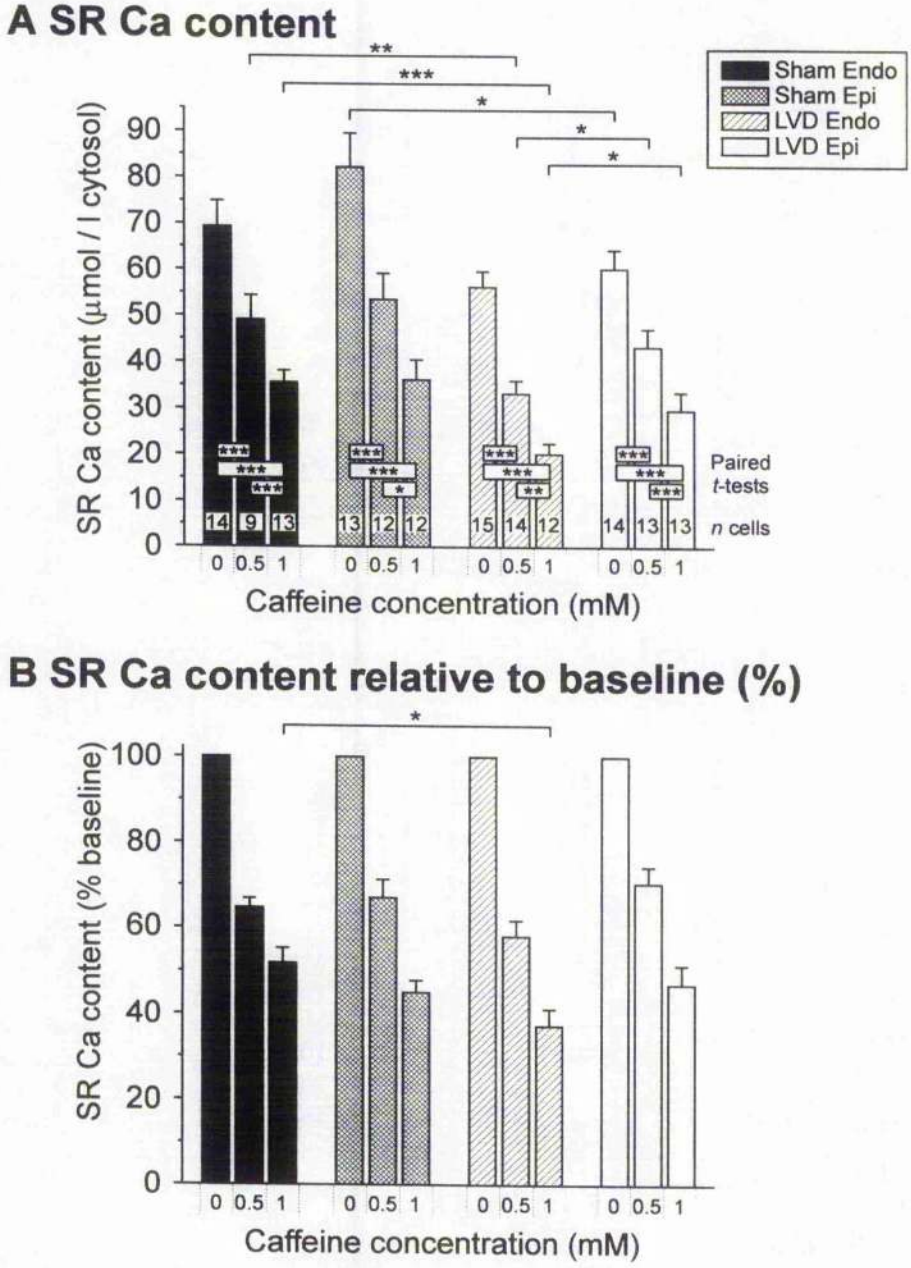

Figure 5.3 Effect of different concentrations of caffeine on SR Ca content. **A:** Absolute values. **B:** Values relative to baseline (in the absence of caffeine in the superfusate). Key and number of cells, *n*, shown on each column in **A** apply to both panels. Comparisons by paired t-tests within cell types are shown across columns, unpaired t-tests, after determining significance by ANOVA, are shown above columns. * $p<0.05$, ** $p<0.01$, *** $p<0.001$.

A Diastolic $[Ca]_i$

Cell type	Baseline	0.5 mmol/L caffeine		1 mmol/L caffeine	
		1st	SS	1st	SS
Sham Endo	260 ± 37	303 ± 48 **	273 ± 42	283 ± 42 *	267 ± 40
Sham Epi	262 ± 37	273 ± 38	250 ± 36 *	279 ± 41 **	253 ± 40
LVD Endo	203 ± 34	214 ± 31	200 ± 28	223 ± 36 **	201 ± 32
LVD Epi	211 ± 25	242 ± 28 *	229 ± 28	232 ± 33	207 ± 25

B Systolic $[Ca]_i$

Cell type	Baseline	0.5 mmol/L caffeine		1 mmol/L caffeine	
		1st	SS	1st	SS
Sham Endo	558 ± 60	689 ± 94 **	535 ± 59	701 ± 88 **	503 ± 53 **
Sham Epi	469 ± 49	526 ± 48 *	420 ± 43 **	593 ± 67 *** †	446 ± 59
LVD Endo	476 ± 58	482 ± 58	415 ± 48	515 ± 65 *** †	411 ± 51 *
LVD Epi	370 ± 41	446 ± 50***	383 ± 43	447 ± 57 **	351 ± 39

Table 5.1 Diastolic (A) and systolic (B) $[Ca]_i$ at baseline and with switching to 0.5 mmol/L and 1 mmol/L caffeine. Values for the first transient on switching to caffeine (1^{st}) and steady-state transients (SS) are given, in nmol/L. Statistically-significant comparisons by paired t-test are indicated: *$p<0.05$, **$p<0.01$, ***$p<0.001$, all *vs* baseline; †$p<0.05$ *vs* 0.5 mmol/L caff, 1^{st} transient. No comparisons amongst cell types were significant. Number of cells for each cell type matches those in Figures 5.4 & 5.5.

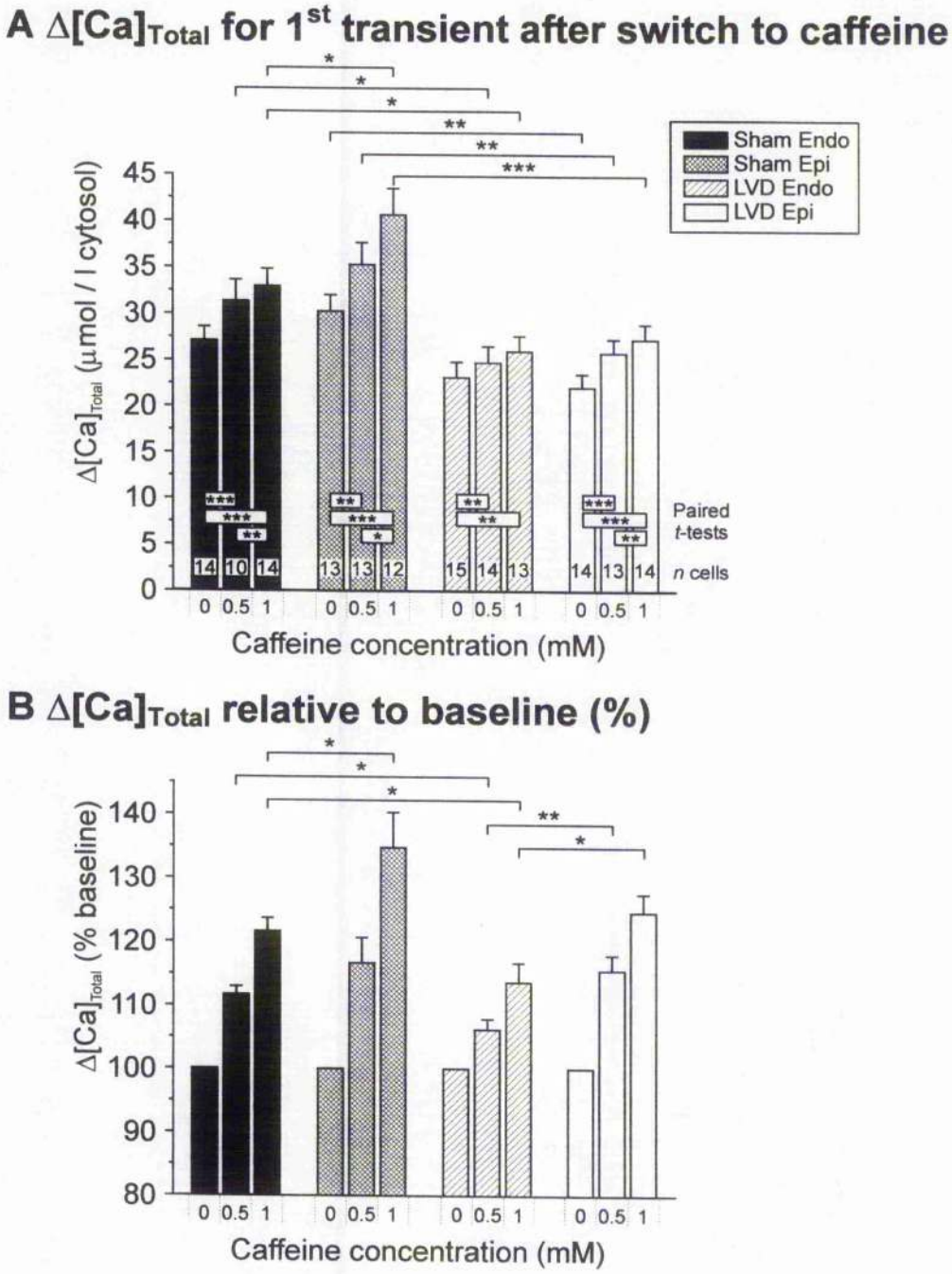

Figure 5.4 $\Delta[Ca]_{Total}$ at baseline and immediately after switching to 0.5 mmol/L and 1 mmol/L caffeine. Full figure legend as for Figure 5.3.

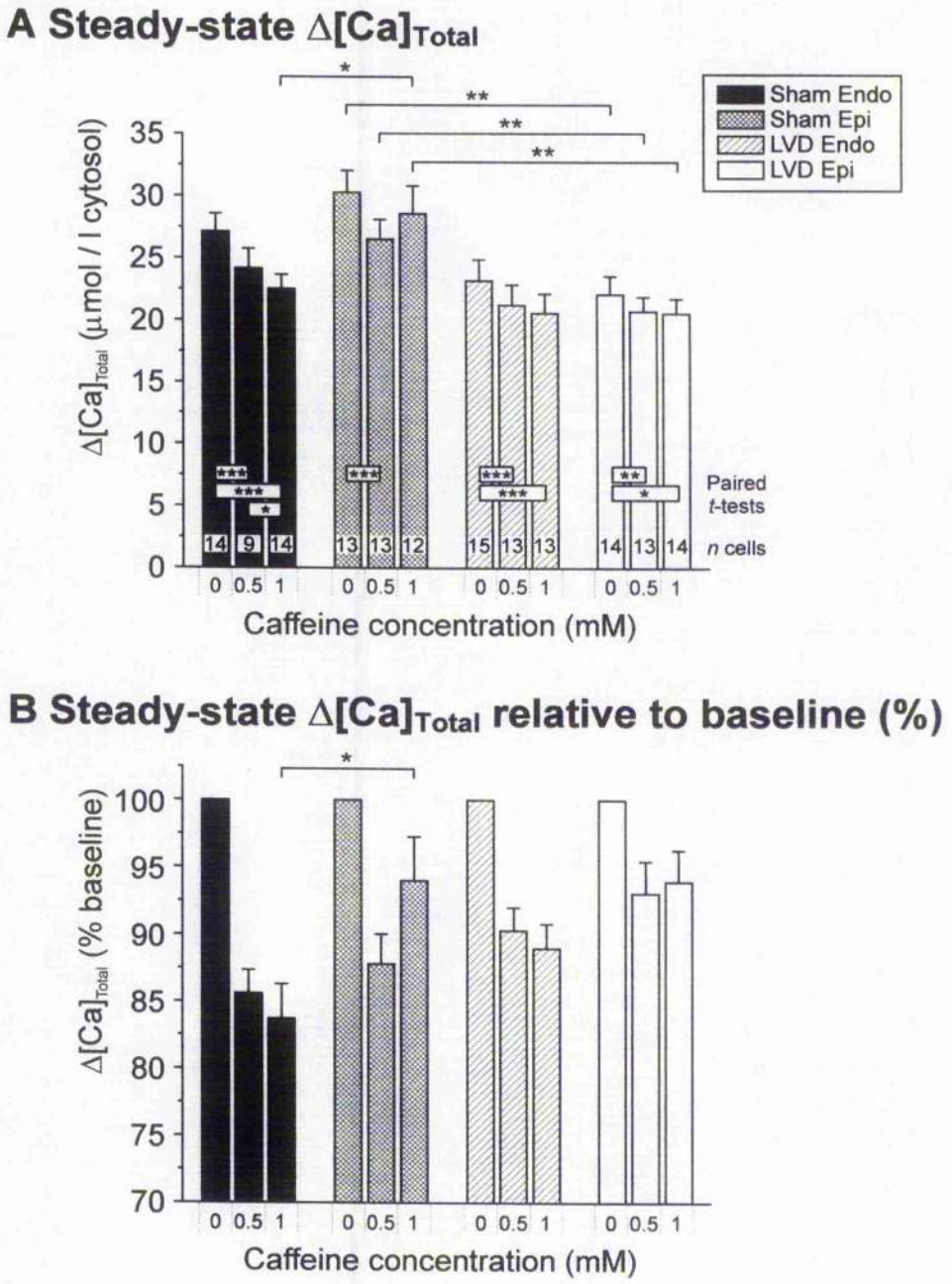

Figure 5.5 $\Delta[Ca]_{Total}$ at baseline and in steady-state after switching to 0.5 mmol/L and 1 mmol/L caffeine. Full figure legend as for Figure 5.3.

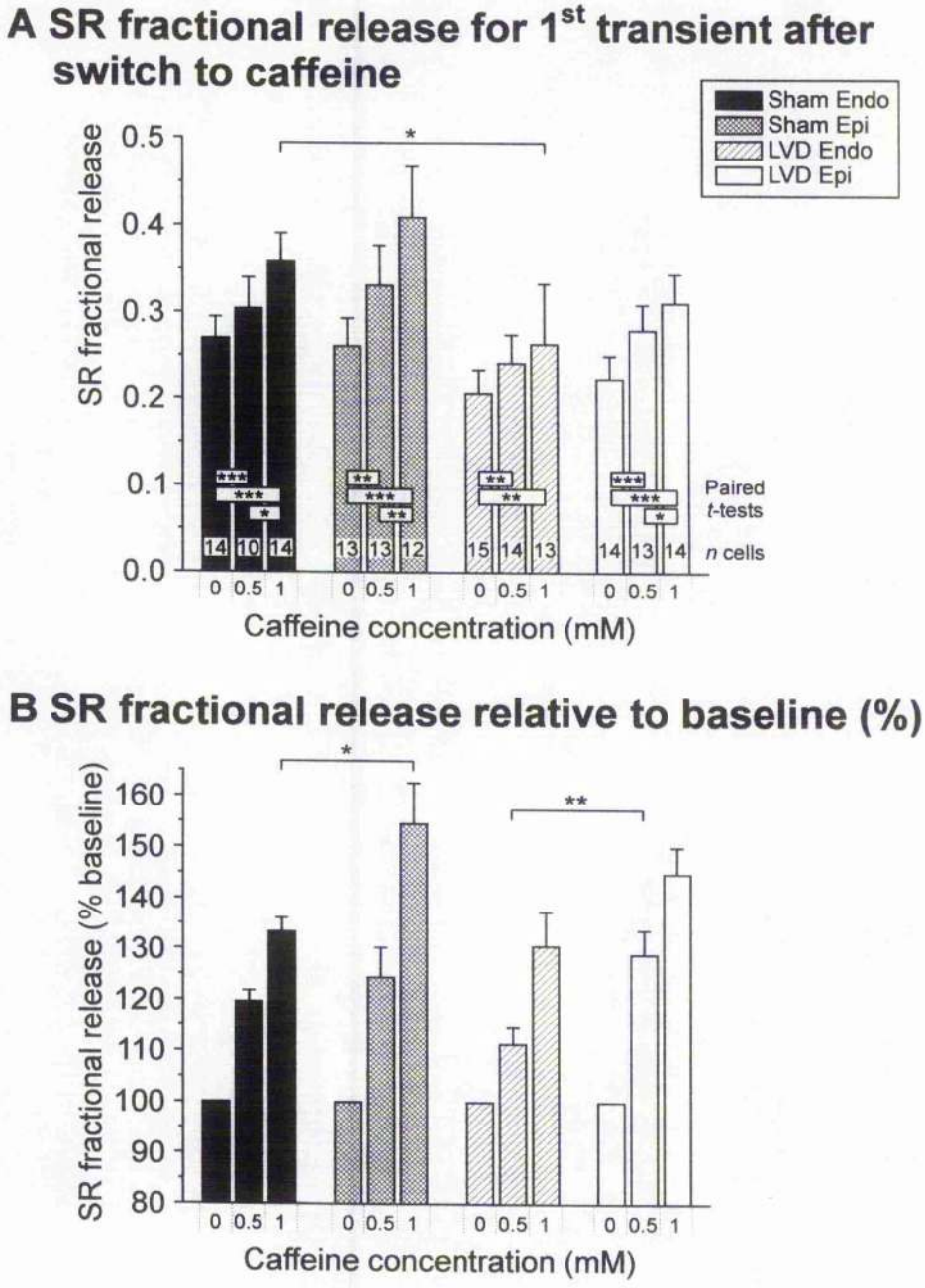

Figure 5.6 SR fractional release at baseline and immediately after switching to 0.5 mmol/L and 1 mmol/L caffeine. Full figure legend as for Figure 5.3.

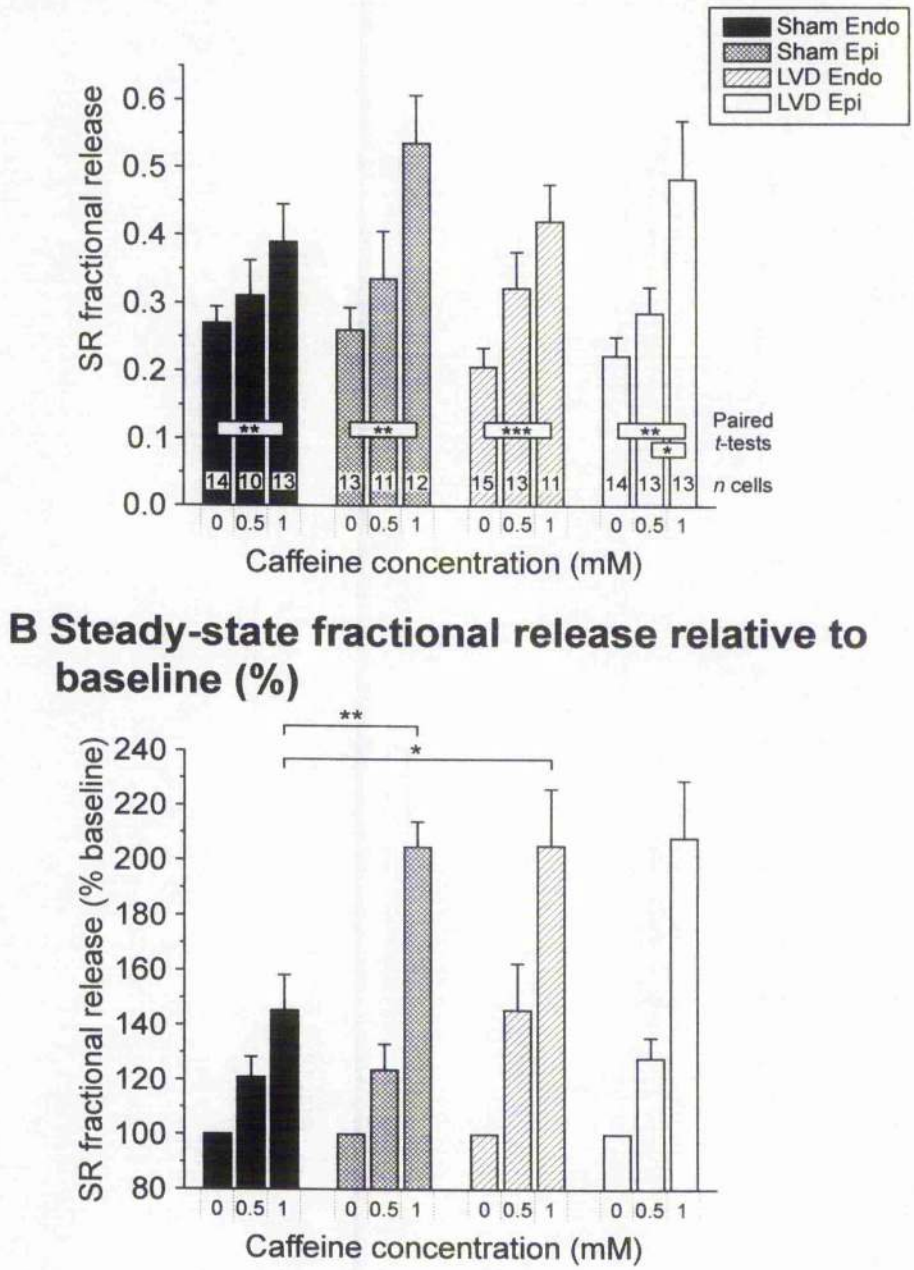

Figure 5.7 SR fractional release at baseline and in steady-state after switching to 0.5 mmol/L and 1 mmol/L caffeine. Full figure legend as for Figure 5.3.

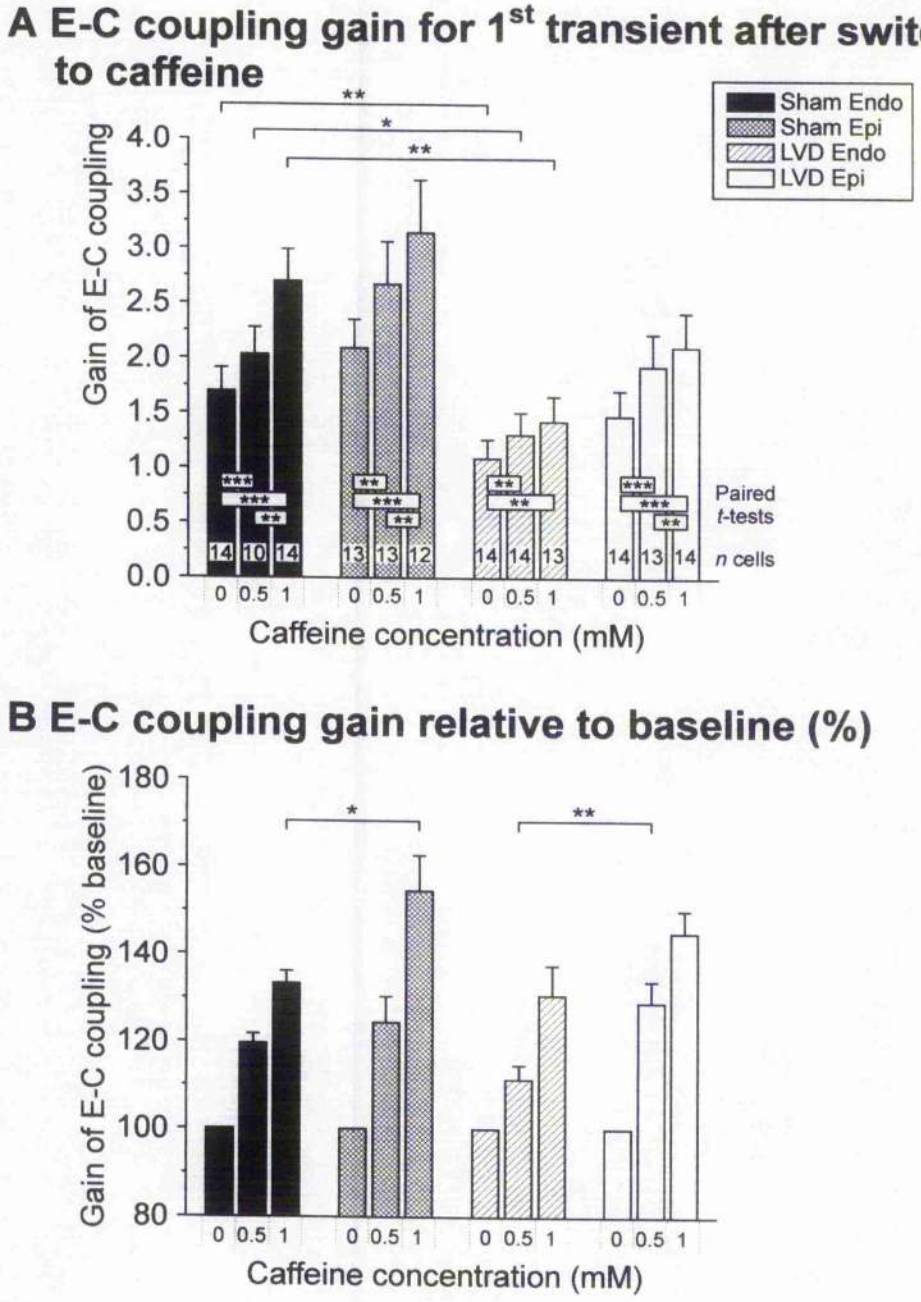

Figure 5.8 E-C coupling gain at baseline and immediately after switching to 0.5 mmol/L and 1 mmol/L caffeine. Full figure legend as for Figure 5.3.

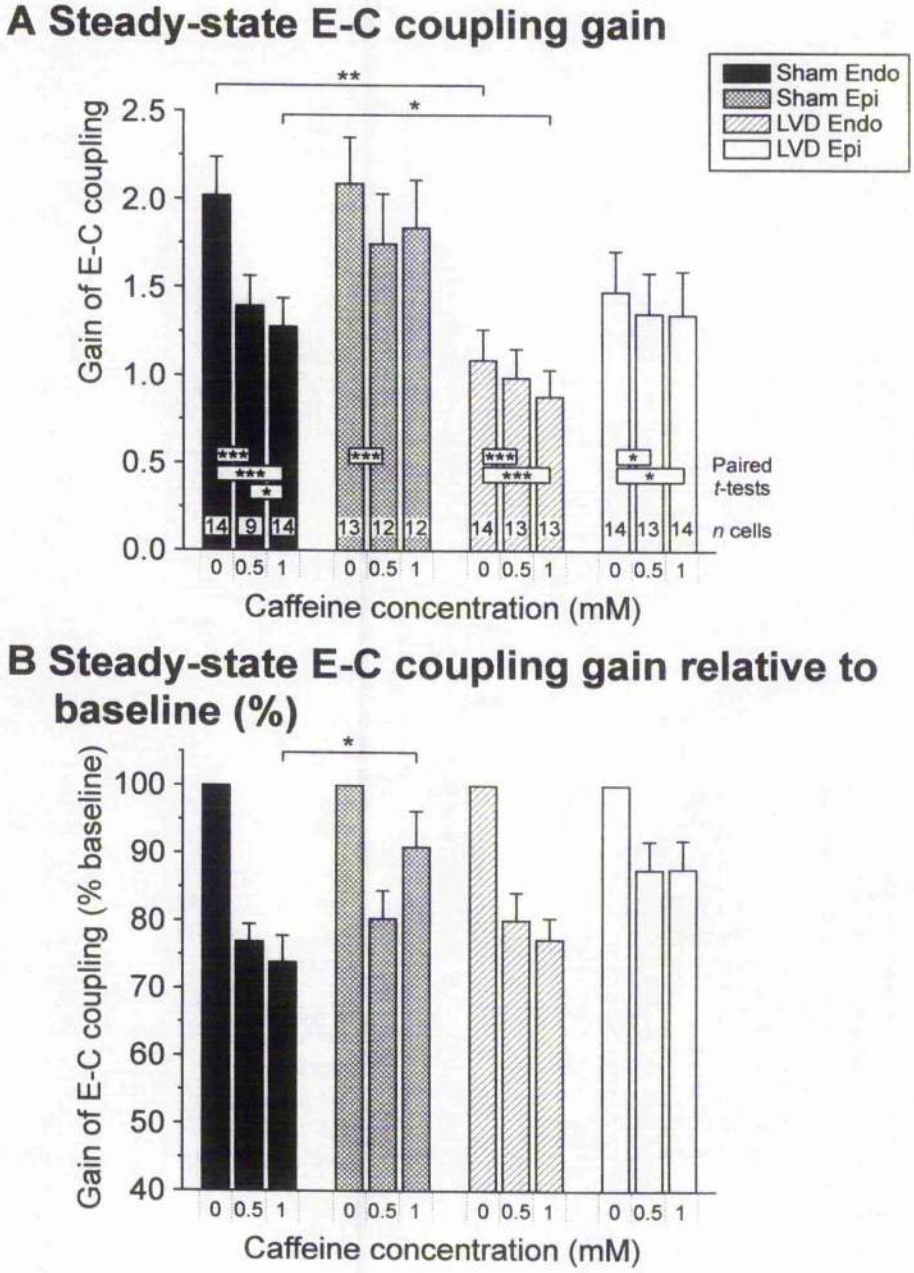

Figure 5.9 E-C coupling gain at baseline and in steady-state after switching to 0.5 mmol/L and 1 mmol/L caffeine. Full figure legend as for Figure 5.3.

5.3.5 Effects of altered resting membrane potential on NCX function and I_{Ca}

An estimate of the effect on NCX activity of raising the resting membrane potential from -80 mV to -60 mV was made as described in section 5.2.3. In brief, the decay of Ca after application of 10 mmol/L caffeine was compared at each of the holding potentials, with corrections made for non-NCX removal mechanisms. Overall, this showed that NCX function was inhibited by 23.9 ± 1.7 % (n=44 cells), with no significant difference amongst the cell types by ANOVA (p=0.25). Ca flux on I_{Ca} was also measured before and after the switch in holding potential. As for the previous chapter, there were no significant differences amongst the cell groups in I_{Ca} flux at baseline. However, changing the holding potential to -60 mV significantly reduced I_{Ca} flux, to 89.1 ± 1.8 % of the flux at -80 mV (n=43 cells, p<0.0001, by paired t-test). This is unlikely to be due to the smaller size of the voltage prepulse to -40 mV, since negligible I_{Ca} is activated below this level. Instead, the reduced I_{Ca} flux is likely to be caused by the elevation in diastolic $[Ca]_i$ (see below). The effects of these alterations in systolic and diastolic Ca handling will now be described.

5.3.6 Effects of altered resting membrane potential on steady-state SR Ca content

By inhibiting removal of Ca from the cell during the diastolic period, a new balance will be achieved between efflux of cytoplasmic Ca and its uptake into the SR. Figure 5.10 shows the effect that this has on SR Ca content (all figures and tables for experiments with altered resting membrane potential are grouped at the end of section 5.3.8). In all cases, SR content is significantly increased, and in each case this is by around the same relative amount (between 24 % and 32 %).

5.3.7 Effects of altered resting membrane potential on Ca transient characteristics

5.3.7.1 Diastolic & systolic $[Ca]_i$

Table 5.2 summarises the data for diastolic and systolic $[Ca]_i$ for each of the cell types. In all cases, there was a significant elevation in diastolic and peak systolic $[Ca]_i$ when the resting membrane potential was raised to -60 mV. The proportional increase in diastolic $[Ca]_i$ was slightly greater than the proportional increase in systolic $[Ca]_i$ (around 14 % *vs* 10 %, respectively; p=0.002, n=44 cells).

5.3.7.2 Steady-state $\Delta[Ca]_{Total}$

Given the above findings, when $[Ca]_i$ was converted to total [Ca], there was little change in $\Delta[Ca]_{Total}$, as shown in Figure 5.11. For Sham endocardial cells, and LVD endocardial cells, there was a small, but significant, fall in $\Delta[Ca]_{Total}$ at the -60 mV holding potential (to around 95% of baseline levels). For epicardial cells, any differences were not significant. As shown in Figure 5.11 B, in Sham animals, this regional disparity in effects on $\Delta[Ca]_{Total}$ lead to a significant difference between the relative change in $\Delta[Ca]_{Total}$ for endocardial and epicardial cells (94.5 ± 1.8 % *vs* 101.4 ± 1.2 %; p=0.003).

5.3.8 Effects of altered resting membrane potential on SR fractional release and E-C coupling gain

In all cases, SR fractional release was lower at a holding potential of -60 mV, compared to -80 mV, as shown in Figure 5.12. For both Sham and LVD animals, the decrease in fractional release was more marked for endocardial cells than epicardial cells (Figure

5.12 B). Overall, at baseline and at -60 mV, fractional release was lower for LVD endocardial cells than for Sham endocardial cells.

The findings for E-C coupling gain are outlined in Figure 5.13. With the reduced trigger Ca due to smaller I_{Ca} flux (see section 5.3.5), to maintain the observed levels of $\Delta[Ca]_{Total}$, E-C coupling gain was a little higher for all cell types. This was statistically significant for Sham endocardial cells ($p=0.02$) and LVD epicardial cells ($p=0.0005$) and almost reached significance for Sham epicardial cells ($p=0.056$). The increase was smaller, and non-significant, for LVD endocardial cells. As for SR fractional release, gain was lower at both holding potentials for LVD endocardial cells compared to Sham endocardial cells.

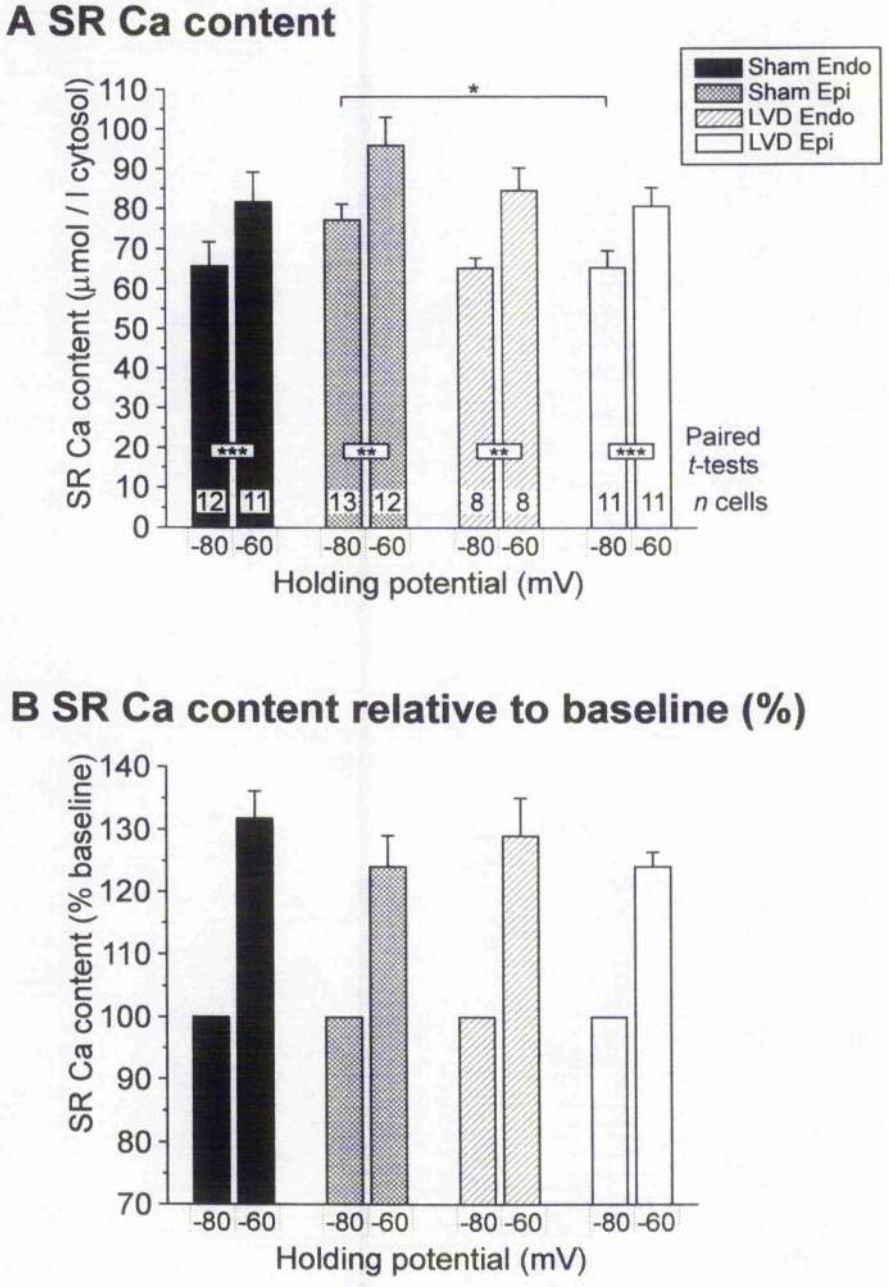

Figure 5.10 Effects of altering resting membrane potential from -80 mV to -60 mV on steady-state SR Ca content. **A:** Absolute values. **B:** Values relative to baseline (in the absence of caffeine in the superfusate). Key and number of cells, *n*, shown on each column in **A** apply to both panels. Comparisons by paired t-tests within cell types are shown across columns, unpaired t-tests, after determining significance by ANOVA, are shown above columns. * $p<0.05$, ** $p<0.01$, *** $p<0.001$.

Cell type	Diastolic $[Ca]_i$		Systolic $[Ca]_i$	
	-80	-60	-80	-60
Sham Endo (*n*=12)	340 ± 50	394 ± 54 ***	660 ± 63	730 ± 72 ***
Sham Epi (*n*=13)	330 ± 46	372 ± 53 ***	657 ± 63	734 ± 75 ***
LVD Endo (*n*=8)	315 ± 44	345 ± 47 **	596 ± 61	627 ± 64 *
LVD Epi (*n*=11)	244 ± 44	280 ± 48 **	531 ± 51	591 ± 59 ***

Table 5.2 Diastolic and systolic $[Ca]_i$ at resting membrane potentials of -80 and -60 mV. All values in nmol/L. Number of cells (*n*) indicated for each row. For each cell type, statistically-significant comparisons by paired t-test are indicated: *$p<0.05$, **$p<0.01$, ***$p<0.001$, all *vs* baseline values at -80 mV. No comparisons amongst different cell types were significant by ANOVA.

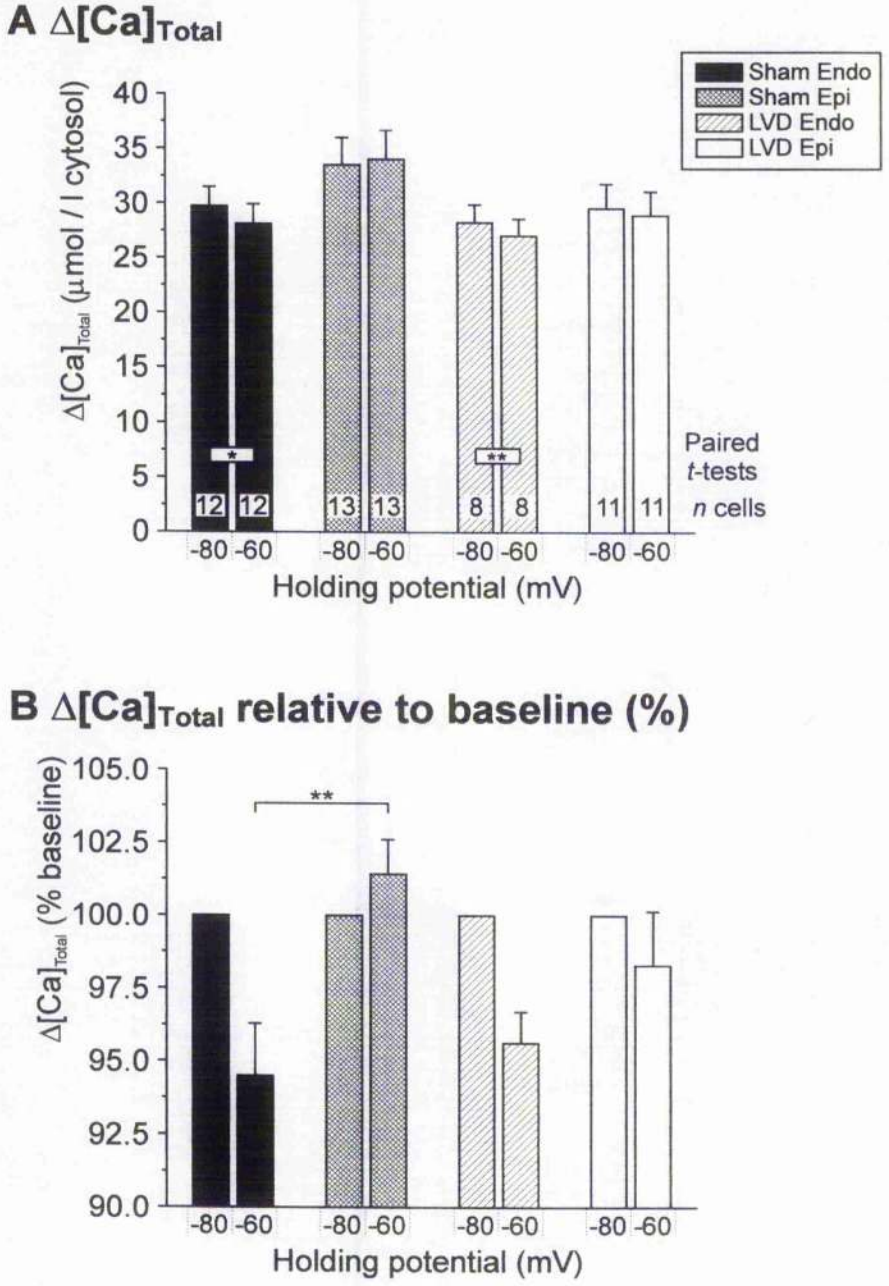

Figure 5.11 Effects of altering resting membrane potential from -80 mV to -60 mV on steady-state $\Delta[Ca]_{Total}$. Full figure legend as for Figure 5.10.

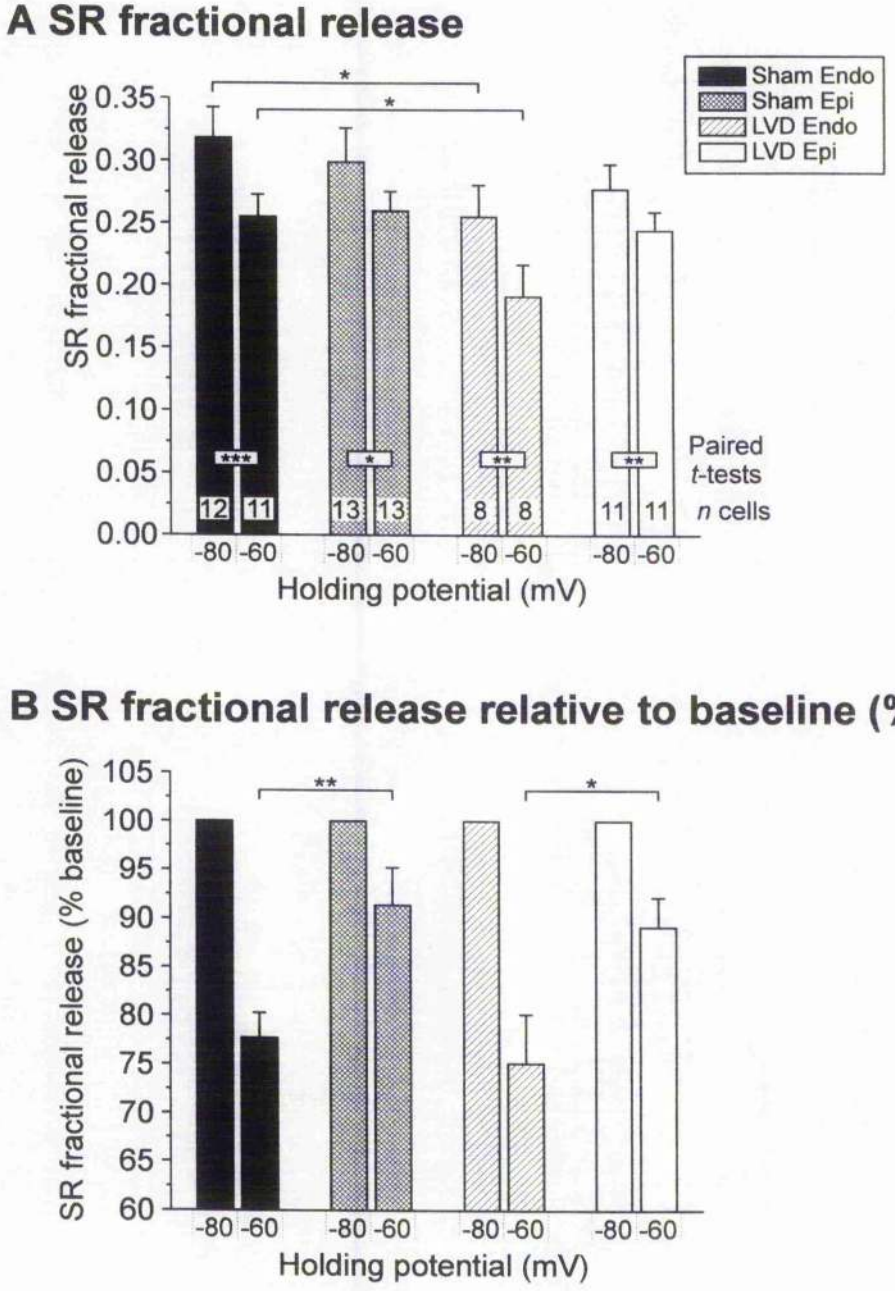

Figure 5.12 Effects of altering resting membrane potential from -80 mV to -60 mV on steady-state SR fractional release. Full figure legend as for Figure 5.10.

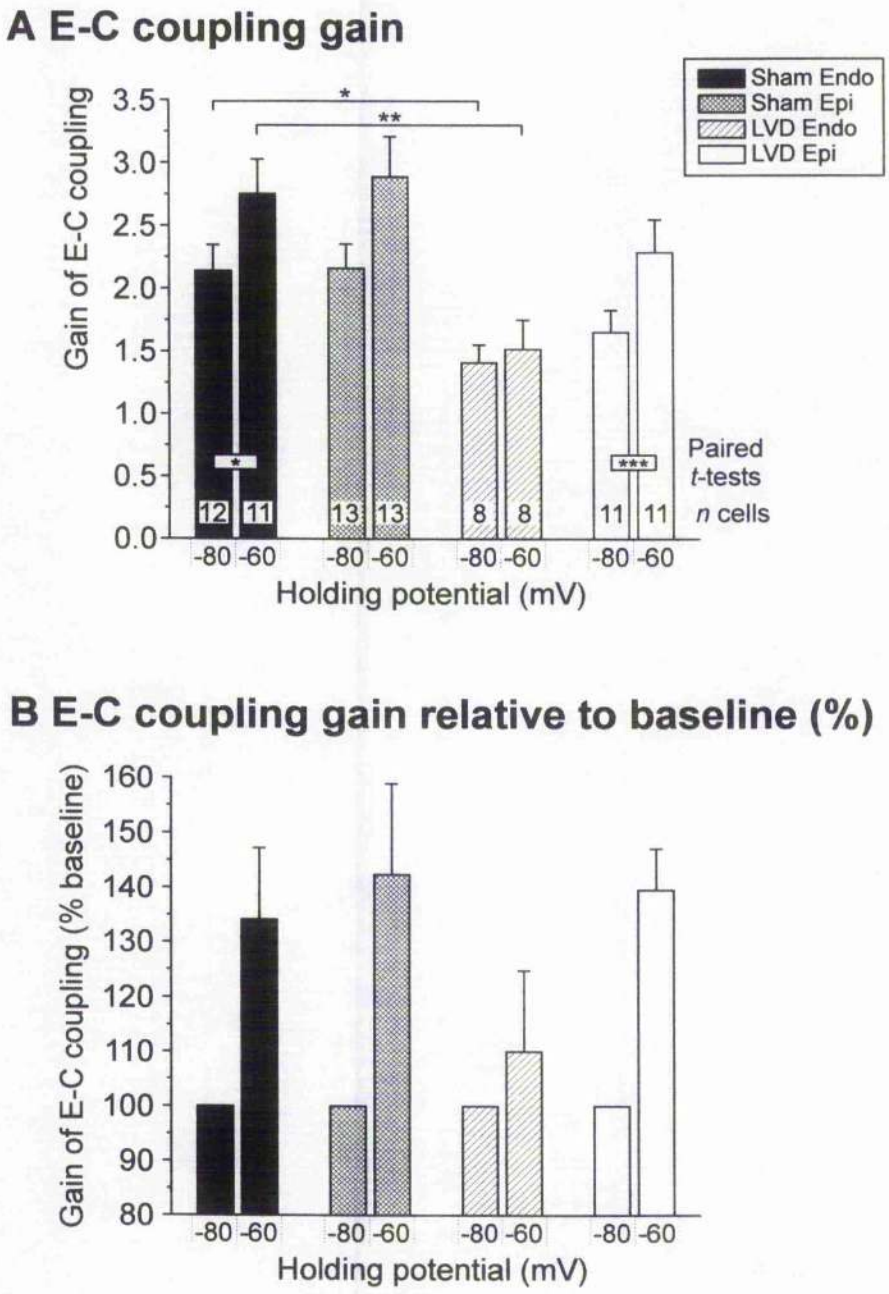

Figure 5.13 Effects of altering resting membrane potential from -80 mV to -60 mV on steady-state E-C coupling gain. Full figure legend as for Figure 5.10.

5.3.9 Characteristics of E-C coupling with manipulation of Ca handling

The overall effects of the above interventions on various aspects of E-C coupling, in relation to the SR Ca content are summarised in Figure 5.14. The four panels of the figure match those of the baseline findings, presented in Figure 4.16, with added datapoints for the steady-state findings in the presence of 0.5 mmol/L and 1 mmol/L caffeine, and with raised resting membrane potential. The number of cells for each datapoint matches those for the corresponding cell type and conditions in the previous figures. Panel A shows the findings for $\Delta[Ca]_{Total}$, and the general fall in Ca transient size in the presence of caffeine is illustrated. Were full autoregulation to take place, for each cell type the datapoints for $\Delta[Ca]_{Total}$ would shift to the left as SR Ca content was reduced, but they would not fall. Panel B displays the results for absolute SR release relative to SR content. Examining the four datapoints at baseline, and those with each intervention, in general the relationship between the cell types is preserved – Sham Epi > Sham Endo > LVD Epi > LVD Endo. Overall, it appears that as SR content falls, absolute SR release also falls. The opposite relationship appears to occur for fractional release, as shown in panel C. This appearance is mainly due to the enhanced fractional release caused by low concentrations of caffeine, in the presence of reduced SR content. In addition, with the increased SR Ca content when the resting membrane potential was elevated (see section 5.3.6), there was a slight fall in fractional release. This may partly be due to the reduced trigger Ca and is discussed further in section 5.4.2. The pattern of findings for E-C coupling gain (panel D), are similar to those for SR Ca release shown in panel B.

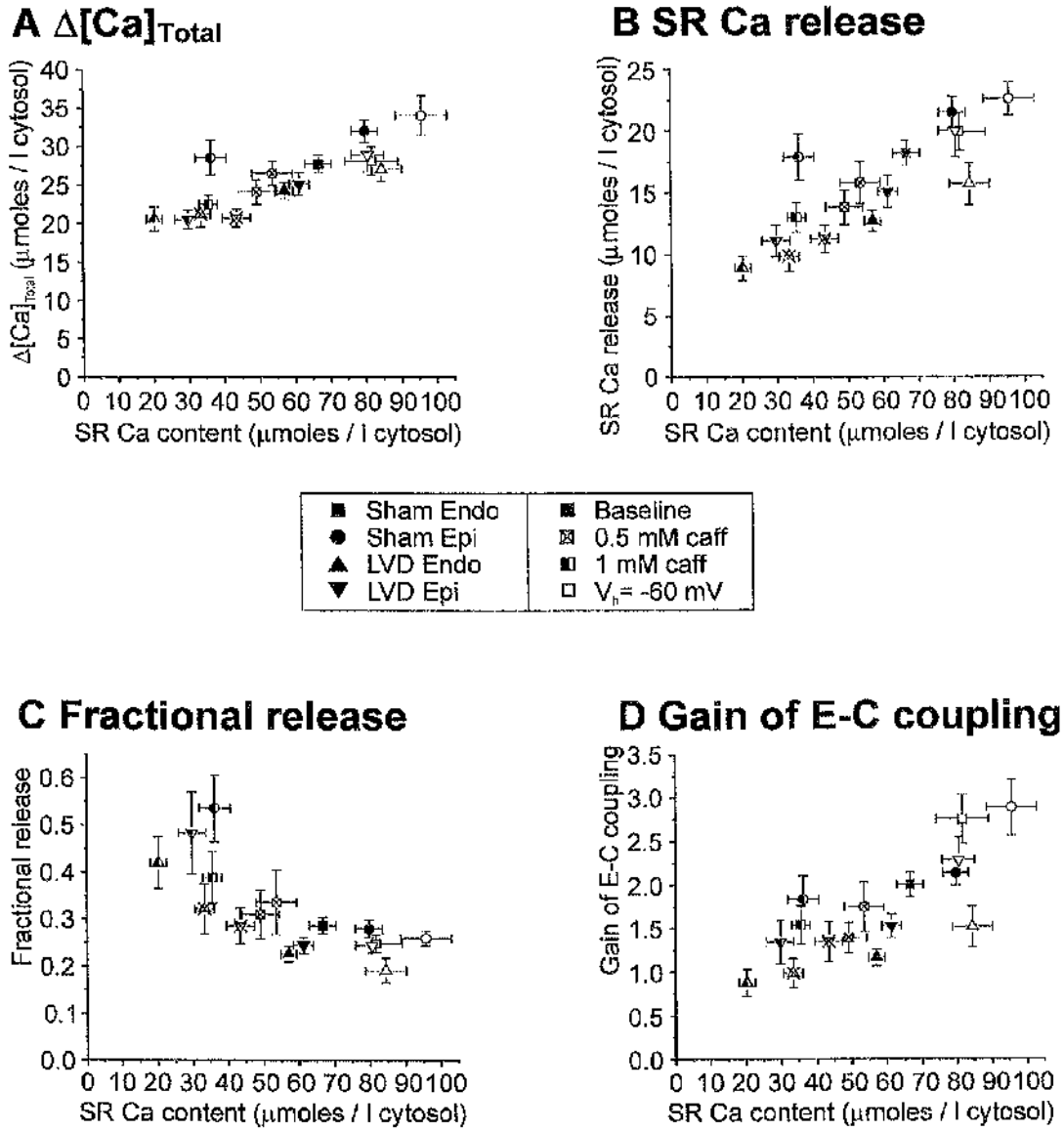

Figure 5.14 Characteristics of E-C coupling in relation to SR Ca content, at baseline and with altered Ca handling. **A:** $\Delta[Ca]_{Total}$. **B:** Absolute SR Ca release. **C:** Fractional SR Ca release. **D:** Gain of E-C coupling. Key refers to all panels – left panel identifies cell types, right panel identifies conditions under which measurement was made – baseline (filled symbols), steady-state 0.5 mmol/L caffeine (crossed symbols), steady-state 1 mmol/L caffeine (half-filled symbols) and with elevated resting membrane potential (open symbols). Each datapoint represents a mean of 8-32 cells ("baseline" values are combined datasets from the previous figures).

5.4 Discussion

Experiments in the previous chapter showed that cells isolated from rabbits with infarct-induced LVD had smaller Ca transients and reduced E-C coupling gain. These findings appeared to be mainly due to reduced SR Ca content (see sections 4.4.4.2 & 4.4.5). The experiments in this chapter were designed to alter aspects of Ca handling, including SR Ca content, and to examine the effects on the Ca transient.

5.4.1 Effects of caffeine on Ca handling

5.4.1.1 Effects on the initial Ca transient

The rapid application of caffeine causes an abrupt increase in RyR sensitivity to Ca, such that the first Ca transient after the switch will be increased in size for the same trigger Ca. This is apparent in Figure 5.4, and the concomitant increases in SR fractional release and E-C coupling gain are demonstrated in Figures 5.6 and 5.8, respectively. As presented in sections 5.3.2.2, 5.3.3 and 5.3.4, the results suggest that caffeine was more effective at increasing initial SR fractional release, E-C coupling gain and resulting $\Delta[Ca]_{Total}$ in epicardial cells than endocardial cells. Other workers in the laboratory have examined regional expression of RyR and found evidence that ryanodine receptor mRNA and protein levels were higher in epicardial cells than endocardial cells (Currie *et al.*, 2003). This was true in both Sham and LVD animals and was also apparent in binding studies using tritiated ryanodine. Although it must be accepted that complex regulation of the RyR occurs, one could speculate that higher RyR density in epicardial cells could make a given concentration of caffeine more effective in enhancing E-C coupling in this region.

Figure 5.4 B also shows that caffeine was less effective at increasing $\Delta[Ca]_{Total}$ for LVD endocardial cells compared to Sham endocardial cells, but that the relative increase in $\Delta[Ca]_{Total}$ for epicardial cells was similar in both Sham and LVD. Again, this fits with findings for RyR expression and labelled ryanodine binding. Currie *et al.* reported that RyR mRNA and protein levels were reduced by ~25% and ~40%, respectively, in LVD endocardial cells compared to Sham endocardial cells, and this was supported by experiments with specific ryanodine binding (Currie *et al.*, 2003). In contrast, there were no significant changes in these parameters for epicardial cells.

As discussed in Chapter 1, there has been much recent debate regarding the importance of RyR density and regulation in the pathogenesis of heart failure (for reviews, see Bers *et al.*, 2003; Marks *et al.*, 2002; Hasenfuss & Pieske, 2002). Studies into the levels of RyR mRNA and protein in heart failure have given disparate results (reviewed in Bers, 2001, Chapter 10). In a rabbit model of heart failure induced by pulmonary artery banding, Matsui *et al.* reported reduced RyR mRNA (Matsui *et al.*, 1995). In our laboratory, Neary *et al.* measured RyR-mediated SR Ca flux in intact, permeabilised rabbit myocytes from the same model of heart failure as that studied in this chapter (Neary *et al.*, 2002). RyR-mediated Ca efflux was reduced by around 50%, and this was coupled with a similar decrease in SERCA-mediated uptake. The cells in this study were not separated into transmural regions, but the findings do suggest that overall there is a reduction in RyR activity in this model of LVD.

5.4.1.2 Effects on steady-state Ca transients

In all but one case (Sham epicardial cells with 1 mmol/L caffeine), the maintained application of low concentrations of caffeine caused reduced steady-state $\Delta[Ca]_{Total}$ compared to levels before caffeine was applied (see Figures 5.5 & 5.14). It was demonstrated that this was not a consequence of reduced Ca entry on I_{Ca} (see section 5.3.2.3). This implies some persisting alteration in SR Ca handling in the presence of caffeine which means that "autoregulation" does not fully occur. A number of possibilities must be considered:

(i) non-linearities in negative feedback system,

(ii) altered SR Ca uptake and/or NCX function,

(iii) marked SR Ca depletion,

(iv) altered diastolic SR leak,

(v) other effects of caffeine in the cell.

To examine the effects of some of these possibilities it is instructive to model the situation which leads to autoregulation. Eisner *et al.* proposed a simple model which includes the main parameters of Ca flux and E-C coupling (Eisner *et al.*, 1998). At the n^{th} stimulus, $\Delta[Ca]_{Total}$ will be determined by Ca entry on I_{Ca} and the fraction, f, of Ca released from the SR. Thus:

$$\Delta[Ca]_{Total} = f * SR_n + I_{Ca} \qquad \textbf{Equation 5.1}$$

Eisner's model included a scaling factor, a, but with the sum expressed as $\Delta[Ca]_{Total}$, and for simplicity, we can assume that a = 1. A proportion, r, of this Ca will be removed from the cell, with the rest taken up into the SR. Thus:

$$Ca_{out} = \Delta[Ca]_{Total} * r \qquad \textbf{Equation 5.2}$$

The resulting amount of Ca in the SR before the next systole will be:

$$SR_{n+1} = SR_n + I_{Ca} - Ca_{out} \qquad \textbf{Equation 5.3}$$

From Equation 5.3 it can be seen that at steady state (i.e. $SR_{n+1} = SR_n$), I_{Ca} must equal Ca_{out} and the cell is in net Ca balance.

Figure 5.15 A simulates how this model will behave when fractional release, f, is doubled from 0.25 to 0.5 (e.g. in the presence of a low concentration of caffeine). With the equations above, the system will autoregulate and steady-state $\Delta[Ca]_{Total}$ at the higher fractional release (point **b** on the figure) is the same as that at baseline (point **a**). This autoregulation will only occur if the amount of Ca removed from the cell relative to that taken up into the SR (r) remains constant (e.g. it is set at 0.33 in Figure 5.15). If this relationship alters then a new steady state will be achieved, with a different resulting $\Delta[Ca]_{Total}$. This is illustrated in Figure 5.15 B, where r was changed to 0.38 during the period where the fractional release was increased. In this case the final $\Delta[Ca]_{Total}$ is around 86% of the baseline level. Given the complex kinetics of Ca removal systems, including differing affinity for Ca and effects of cytoplasmic and SR

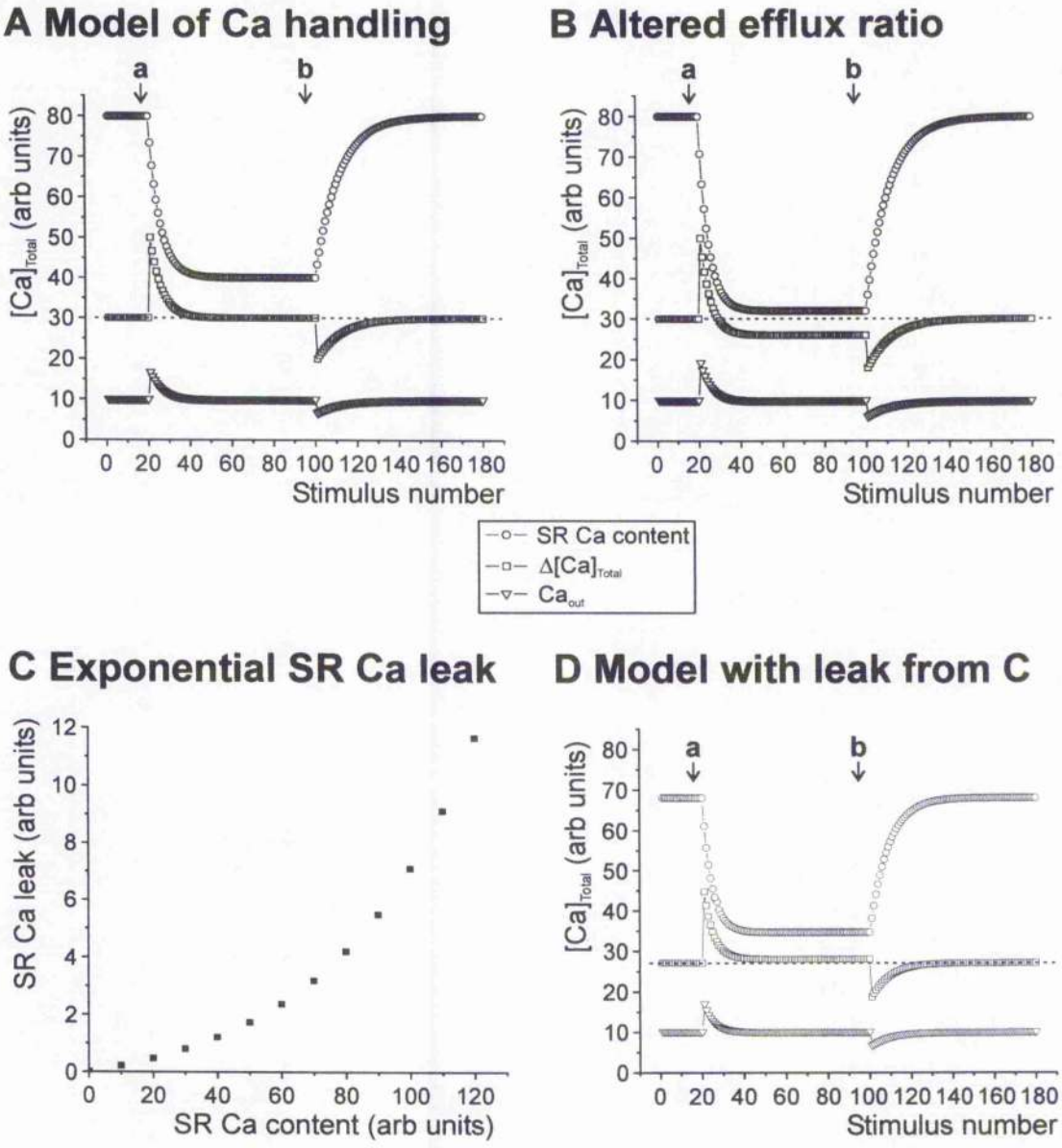

Figure 5.15 Modelling of Ca handling with caffeine application. Full details of model are described in text. **A:** Simple model. Between stimuli 20 and 100, fractional release, *f*, was increased from 0.25 to 0.5. **B:** Model, with altered ratio of Ca efflux to SR uptake during the period where fractional release was increased. **C:** Simulation of SR Ca leak exponentially related to SR Ca content. **D:** Model incorporating exponential SR Ca leak depicted in **C**. Key refers to panels **A**, **B** and **D**.

luminal [Ca], it would not be surprising for non-linearities in r to occur. This may be particularly apparent for species, such as the rabbit, where sarcolemmal transport plays a proportionally greater role in Ca removal (see Chapter 4) than it does in species such as the rat, where around 92% of Ca removal is by SERCA (Bassani *et al.*, 1994).

One would also expect significant deviation from the model in situations where the SR is heavily depleted of Ca – e.g. at higher concentrations of caffeine. With markedly increased fractional release, the SR content may fall to very low levels. The SR Ca content at this point may be insufficient to support the level of Ca release required to maintain $\Delta[Ca]_{Total}$, or, indeed, a threshold level may be passed where SR release fails altogether (see Shannon *et al.*, 2000). Both these circumstances will cause smaller steady-state Ca transients, however, it is unlikely that the SR content reached such levels in the experiments presented in this chapter.

Persisting leak of Ca from the SR during diastole will also complicate the analysis. Given the low stimulation rate (0.5 Hz) relative to the physiological heart rate of the animals (around 3 – 5 Hz), diastolic leak may be particularly important to consider in such experimental studies. If it is assumed that any Ca leaked into the cytoplasm during diastole is removed in the same way as Ca released during systole (i.e. the proportion removed from the cell remains r), then Equation 5.2 becomes:

$$Ca_{out} - \Delta[Ca]_{Total} * r + SR_{leak} * r \qquad \textbf{Equation 5.4}$$

In the simplest situation of a leak linearly proportional to the SR content (i.e. dependent only on the SR-cytoplasm [Ca] gradient):

$$SR_{leak} = a_1 * SR_n \qquad \textbf{Equation 5.5}$$

where a_1 is a constant. In this situation, autoregulation will fail and $\Delta[Ca]_{Total}$ will increase slightly as SR content falls. However, if it is assumed that alterations in SR fractional release have the same effect on SR leak (i.e. if caffeine doubles fractional release, the SR leak also doubles) then:

$$SR_{leak} = a_2 * f * SR_n \qquad \textbf{Equation 5.6}$$

Under these circumstances, autoregulation will once more occur – $\Delta[Ca]_{Total}$ will be smaller than it was in the absence of SR leak, but will remain the same as fractional release is changed.

The relationship between SR Ca content and SR leak, however, is complex. Shannon *et al.* made a quantitative assessment of this relationship in isolated rabbit ventricular myocytes (Shannon *et al.*, 2002). They estimated that resting SR leak was around 12 μmol/L/s, and that this depended heavily on the SR content. As SR Ca content increased, SR leak increased in a non-linear manner, with a much steeper relationship at higher SR loads. They postulated that SR Ca content, as well as providing the driving force (gradient) for leak, also affected the leak process itself through effects on RyR gating. They fitted their data with a modified exponential function, but for the purposes of modelling in this chapter, a simple exponential function can be used for illustrative purposes. Thus:

$$SR_{leak} = a_3 * f * e^{(SR_n - x_0)/t} \qquad \textbf{Equation 5.7}$$

This again includes a dependence on fractional release, f. Values of a_3, x_0 and t were chosen to give an approximation of the relationship reported by Shannon *et al*. Figure 5.15 illustrates this leak-load relationship in panel C, along with the resulting effects when fractional release is doubled, in panel D. In this case, steady-state $\Delta[Ca]_{Total}$ at the higher fractional release is slightly increased compared to baseline levels.

It should also be recognised that the removal of Ca which has leaked from the SR may differ from the removal of bulk cytoplasmic Ca released during systole. If the SR leak is principally *via* RyRs, then it will mainly be into the dyadic cleft. One could postulate that the relative removal of Ca from this space by NCX and SERCA may be different from the situation where Ca is being removed from the bulk cytoplasm. If this is the case then a different value of r would be required for the SR_{leak} in Equation 5.4.

The above analysis has illustrated that if complexities are introduced into the simple model of E-C coupling then autoregulation may not occur. One further consideration is that caffeine may have other effects on the cell, which could alter cellular Ca fluxes. As discussed in section 5.1.1, caffeine is a PDE inhibitor and can change intracellular levels of cAMP. This could alter the phosphorylation of a number of proteins involved in Ca handling, changing their activity. This could feasibly lead to changes in the proportion of Ca removed from the cell (r) compared to that taken back up into the SR, although the overall effects of PDE inhibition on the Ca transient are unpredictable and would need to be addressed by separate experiments.

Finally, it should be remembered that the estimation of $\Delta[Ca]_{Total}$ used in this chapter, and in much of the literature, is based on the amplitude of the Ca transient ($[Ca]_{peak}$ - $[Ca]_{trough}$), which makes some assumptions about Ca release. Since this is an "instantaneous" measure ($[Ca]_{peak}$ is one moment in time) it does not account for the profile of Ca release. One could envisage a situation where the same *total* amount of Ca could be released over a longer time (e.g. see Litwin *et al.*, 2000), giving removal mechanisms a chance to act during the upstroke of the transient. This would result in a lower $[Ca]_{peak}$ and hence a lower estimation of $\Delta[Ca]_{Total}$. Even though the Ca removal mechanisms would not "see" as high a $[Ca]_{peak}$, the same total Ca efflux could be achieved – these efflux mechanisms operate throughout the cardiac cycle and the "average" [Ca] that they act on could be the same. Thus, Ca influx and efflux could balance as before, with a smaller Ca transient amplitude.

5.4.2 Effects of raised resting membrane potential on Ca handling

Figure 5.11 shows that elevating the resting membrane potential from -80 mV to -60 mV had a less dramatic effect on $\Delta[Ca]_{Total}$ than did the application of low concentrations of caffeine. For all cell types, SR Ca content was increased by around 25–30% (Figure 5.10 B). Given the dependence of SR release on SR content demonstrated in Chapter 4, if this were the only change then one would expect that $\Delta[Ca]_{Total}$ would also be increased. Indeed, using the simple model of Ca handling (Equations 5.1 to 5.3), if r is altered to simulate a 25% reduction in Ca efflux (e.g. changed from 0.33 to 0.27), SR content increases by 33% and $\Delta[Ca]_{Total}$ rises by 22% (Figure 5.16 A). However, the results presented in Figure 5.11 show that this was not the case – for epicardial cells from both Sham and LVD animals $\Delta[Ca]_{Total}$ did not alter,

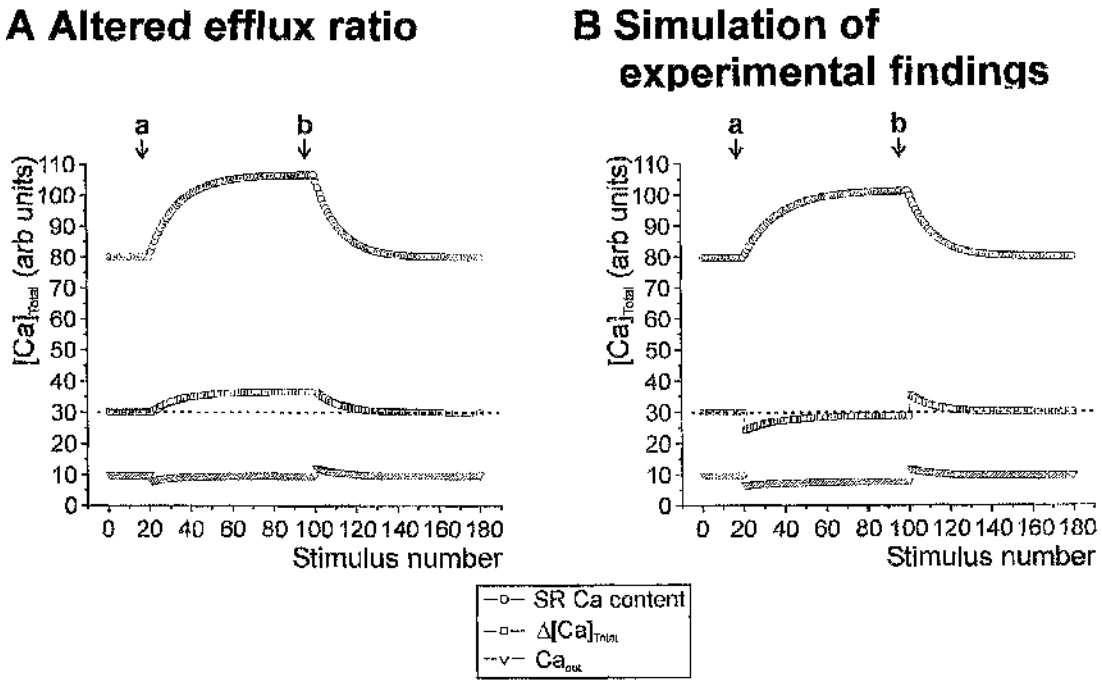

Figure 5.16 Modelling of Ca handling with altered efflux parameters. **A:** Between stimuli 20 and 100, the proportion of Ca removed from the cell, r, was reduced from 0.33 to 0.27. Other parameters were kept constant. **B:** In addition to reducing r, influx on I_{Ca} was reduced from 10 to 8 arbitrary units and fractional release was reduced from 0.25 to 0.21. See text for full explanation. Key refers to both panels.

and for endocardial cells from both animal types it fell by a small, but significant, amount.

For the model to begin to approximate the experimental findings, two other factors must be taken into account. Firstly, as shown in section 5.3.5, there was a significant fall in the trigger Ca, probably due to raised diastolic [Ca]. Secondly, for all cell types, fractional release was slightly reduced at the higher resting membrane potential (see Figure 5.12). At first, this latter point appears at odds with the relationship between fractional release and SR content described in the previous chapter (see Figure 4.16)

and in the literature (Shannon *et al.*, 2000). However, these relationships were determined for a (relatively) constant I_{Ca}. If I_{Ca} is reduced then fractional release for a given SR Ca content will fall, and overall, the relationship between the two will be flatter (see Bassani *et al.*, 1995). Thus, the situation could arise where the fall in I_{Ca} reduces the overall fractional release in spite of an elevated SR Ca content.

The above considerations were included in the model for Figure 5.16 B. The proportion of Ca extruded from the cell, r, was altered as before, and in addition, I_{Ca} was reduced from 10 to 8 arbitrary units and f was reduced from 0.25 to 0.21, based on the mean measured reduction in fractional release. Under these circumstances, steady-state $\Delta[Ca]_{Total}$ is slightly reduced, in keeping with the experimental findings. Similar results were obtained when the model included terms for SR Ca leak (not shown).

Further examination of Ca handling under these circumstances shows that the smaller trigger Ca is more effective at causing release of Ca from the SR (i.e. the gain is increased – see Figure 5.13). This may be a consequence of the elevated SR Ca content increasing the sensitivity of the RyR to cytosolic Ca. As discussed in Chapter 1, such luminal regulation has been demonstrated in RyRs in lipid bilayers (Györke & Györke, 1998) and in intact ventricular myocytes (Lukyanenko *et al.*, 1996; reviewed in Guatimosim *et al.*, 2002). The findings discussed above emphasize the complex relationship between trigger Ca, SR content, E-C coupling gain and $\Delta[Ca]_{Total}$.

5.5 Conclusions

In this chapter, experimental protocols were used to alter Ca handling in cells from each animal type. Low concentrations of caffeine were used to increase SR fractional release, reducing steady-state SR Ca content. In contrast, altering the resting membrane potential to reduce Ca efflux *via* NCX was used to increase SR Ca content. These techniques can give insights into the cellular processes involved in E-C coupling. Results were consistent with transmural differences in RyR function, in keeping with previous work by others in the group. The findings in the presence of low concentrations of caffeine did not fit with a simple model of cellular / SR Ca fluxes and imply that some persisting change in Ca cycling occurs under these conditions. When SR Ca content was increased using a voltage protocol, only small changes (if any) in $\Delta[Ca]_{Total}$ were observed. This appears to be the consequence of reduced Ca entry *via* I_{Ca} with resulting changes in SR Ca release. The broader implications of the findings in this chapter are discussed in Chapter 6.

CHAPTER 6

GENERAL DISCUSSION

6.1 Cellular phenotype in the rabbit infarct model of LVD

Experiments in this thesis have explored the characteristics of Ca handling in cells from the left ventricle of rabbits with infarct-induced LV dysfunction. In general, the findings have shown reduced Ca transient size compared to sham-operated animals, and this was associated with lower SR Ca content, lower SERCA activity (statistically significant for epicardial cells), and reduced gain of E-C coupling, with maintained Ca flux *via* I_{Ca} (Chapter 4). There was also evidence of a reduction in NCX activity of around ⅓, with differences in the allosteric regulation of the exchanger by [Ca] (Chapter 3). A discrepancy between NCX protein levels and activity was also noted, emphasizing the importance of making functional measurements before conclusions are drawn from biochemical results. The critical factor in determining the magnitude of the Ca transient appeared to be the SR Ca content, as discussed in Chapter 4. Although the gain of E-C coupling was reduced, this appeared to be in keeping with the fall in SR Ca content – i.e. the "effectiveness" of E-C coupling was relatively unchanged.

6.1.1 Relationship of cellular findings to arrhythmic risk

One might expect that the findings in LVD of reduced SR Ca content and lower diastolic [Ca] would lead to a reduction in the incidence of arrhythmogenic spontaneous Ca release. This was not directly studied in this thesis, but the increased incidence of sudden death in LVD (see Figure 2.1) suggests that arrhythmias may be *more* likely in the HF animals. Other factors may be important in increasing the arrhythmic risk. Ng *et al.* demonstrated that there were differences in the duration of Ca transients across the epicardial surface in HF (Ng *et al.*, 1998), and it is known that inhomogeneities in repolarisation and/or refractoriness can increase the likelihood of reentrant ventricular arrhythmias (Burton & Cobbe, 2000). The infarct border zone

may also be a site where arrhythmias can arise, and the infarct scar tissue could provide a substrate for reentry. Other factors at a cellular level can be considered. Pogwizd *et al.* showed that in their combined pressure and volume overload rabbit model of HF, cells retained β-adrenergic responsiveness and stimulation by isoprenaline could elevate the SR Ca content and trigger spontaneous Ca release (Pogwizd *et al.*, 2001). Such factors could be important *in vivo*.

An additional consideration for the propensity to arrhythmias is the ease with which a given Ca release can depolarise the membrane. To some extent this depends on the ohmic properties of the membrane, including the "background" currents present at the resting potential. Pogwizd *et al.* found a steeper relationship between injected current and resulting change in membrane potential in HF, consistent with reduced background K currents (Pogwizd *et al.*, 2001). Preliminary experiments were performed in this thesis under current clamp conditions, with small positive and negative 50 ms square-wave current injections and measurement of E_m at the end of each current step. The results are summarised in Figure 6.1, and show that there was no significant difference in resting membrane potential or ΔE_m for a given current injection. Similar findings were obtained when the current injections were made just before each AP in a stimulated train at 0.5 Hz, 1 Hz and 2 Hz (data not shown). Thus the ohmic properties of the membrane do not appear to differ between Sham and LVD cells and a similar ΔE_m would be expected for a given arrhythmogenic current.

6.1.2 Relationship of cellular findings to overall cardiac performance

The findings for Ca handling outlined above would be consistent with what has been found for this model of LVD at the whole-heart level. The reduced Ca transients would

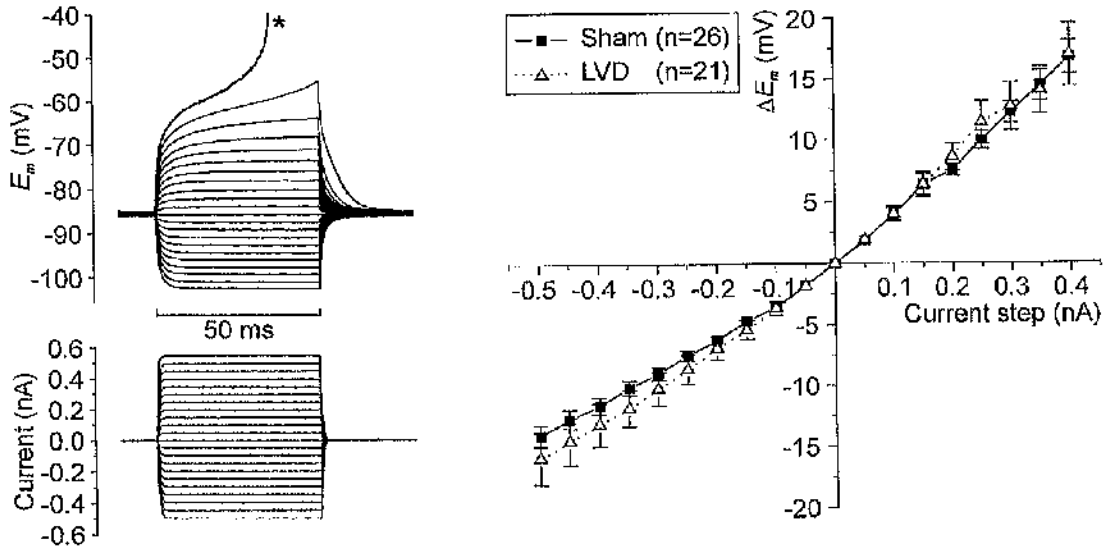

Figure 6.1 Ohmic properties of the cell membrane in Sham and LVD cells. Quiescent cells were studied under current clamp conditions and small 50 ms current injections were performed. **A:** Example of protocol, with family of current injections (**lower panel**) and resulting membrane voltage (**upper panel**). In this case the final current injection of 0.55 nA triggered an action potential (*). Resting membrane potential was no different between Sham and LVD cells (-85.4 ± 0.5 mV vs -85.7 ± 1.1 mV; p=0.8). **B:** Mean data for each cell type, showing ΔE_m for each current step. Sham and LVD cells behaved similarly.

be reflected by impaired contractile performance, as demonstrated on echocardiography (Table 2.1). Reductions in NCX and SERCA function resulted in a significant slowing of the Ca transient decay (see Figure 4.7 B), and it is known that LV relaxation is prolonged in this model in whole-animal studies (Mahaffey *et al.*, 1995). This would contribute to the increased LV end-diastolic pressure that is observed (Pye *et al.*, 1996; Mahaffey *et al.*, 1995). These factors could combine to produce the signs of tissue congestion reflected in the greater liver and lung weights in the LVD animals (see Table 2.1).

6.2 Can manipulation of Ca handling in Sham cells mimic the phenotype of LVD cells?

The experiments in Chapter 5 were designed to examine the outcome of mimicking two of the findings in LVD – reduced NCX function, and reduced SR Ca content. When NCX activity was acutely inhibited (by ~24% – i.e. approaching the observed reduction in NCX seen in LVD animals) using a voltage protocol, this lead to an increase in the SR content, implying that there is an inverse relationship between forward-mode NCX activity and SR Ca content. This differs from the findings in LVD, where NCX function and SR Ca content are *both* reduced compared to Sham animals. This implies that some other factor in LVD is more important in determining the SR Ca content, and the experiments in Chapter 4 suggest that SERCA function may be the critical determinant (see Figure 4.11). Thus, reduced NCX function alone does not bring about changes in Ca handling to mimic those in LVD.

Further experiments in Chapter 5 were designed to alter SR Ca content by increasing the [Ca]-sensitivity of the RyR, using low concentrations of caffeine. This causes unloading of the SR, and 0.5 mmol/L caffeine reduced the SR Ca content of Sham cells to around the same level as the baseline content in LVD cells (see Figure 5.3). This did indeed lead to small, but significant, reductions in steady-state $\Delta[Ca]_{Total}$ (see Figure 5.5). However, given the complex feedback mechanisms and "autoregulation" of SR content and Ca release (see section 5.1.1.1), it is unlikely that increased RyR [Ca]-sensitivity is the underlying defect in LVD. As discussed in section 5.4.1.1, there is some evidence that RyR-mediated Ca flux is *reduced* in LVD for a given [Ca].

Given the findings in this thesis and the literature, it is clear that alterations in several different cellular processes conspire to produce the phenotype observed in LVD. This includes changes in the expression of critical Ca handling proteins, and differences in their regulation. Structural changes in the cell, for example altered T-tubule structure, also play a role (see section 3.4.4). At a tissue level, fibrosis and remodelling will affect contractile performance, and the overall haemodynamic state will also be affected by altered neurohumoral regulation of the kidneys and vasculature.

6.2.1 Possible further experiments

To confirm some of the above assertions, it would be enlightening to carry out experiments where SERCA function was directly affected in cells from sham-operated animals – for example through partial inhibition by an appropriate concentration of thapsigargin or cyclopiazonic acid. This should reduce the SR Ca content and the resulting effects on Ca handling could be determined. It would also be possible to design experiments to look in more detail at SR Ca leak in intact myocytes, for example using the technique of Shannon *et al.*, as outlined in section 4.4.3 (Shannon *et al.*, 2003b).

Given the complex changes observed in LVD, computer modelling could be used to suggest the outcome when multiple parameters are altered together. Programs such as LabHEART (D. Bers & J. Puglisi, Dept of Physiology, Loyola University, Chicago), model the properties of several ion channels and transporters along with cellular buffering processes and SR function. Simulations could give insight into the relative importance of different factors in determining the action potential shape and properties of the Ca transient.

6.3 Can contractile function in LVD be "rescued"? Potential therapeutic targets

6.3.1 SERCA function and SR Ca content

One important aspect of investigating the cellular changes in LVD is to determine whether particular processes could be targeted in an attempt to restore function and prevent adverse complications. From the point of view of systolic contractile performance and diastolic relaxation, it would be beneficial to increase SR content and enhance removal of Ca from the cytoplasm. An increase in SERCA activity could achieve this dual objective, and this has been attempted by a number of groups. In general, this has been accomplished by either overexpressing SERCA protein or decreasing the inhibitory influence of phospholamban (reviewed by Prestle *et al.*, 2003; del Monte & Hajjar, 2003; Scoote *et al.*, 2003). Schmidt *et al.* used adenoviral transfection of SERCA2a to restore contractile function in senescent rat hearts (Schmidt *et al.*, 2000), and the same technique has been shown to increase SR Ca uptake and accelerate diastolic Ca removal in rats (Meyer & Dillmann, 1998) and rabbits (Davia *et al.*, 2001). Transfected animals have demonstrated improved survival following induction of HF (see del Monte & Hajjar, 2003). Transgenic mice overexpressing SERCA2a display enhanced contraction and relaxation (Meyer & Dillmann, 1998), and show preserved contractile function in the face of LVH induced by pressure overload, compared to similarly-treated wild-type mice (Ito *et al.*, 2001). Knock-out of PLB has also been shown to increase SR Ca transport and reverse some of the abnormalities seen in LVH induced by calsequestrin overexpression (Sato *et al.*, 2001). Thus, targeting of abnormal SR Ca uptake has shown promising results in animal studies. Similar improvements in contractile function have been shown for failing human cells *in vitro* (reviewed by del Monte & Hajjar, 2003), and some

pharmacological compounds exist which can enhance SR Ca uptake (see Prestle *et al.*, 2003), but the application of such principles to patients with HF remains a distant prospect.

Experiments in Chapter 5 increased SR Ca content in LVD cells by raising the membrane potential during diastole, causing inhibition of NCX. However, this did not lead to larger Ca transients (see Figure 5.11), probably because of other effects of the elevated membrane potential on the cell. As discussed in section 5.4.2, reduced Ca flux *via* I_{Ca} was observed, which seemed to be a consequence of raised diastolic [Ca] (Table 5.2). This emphasizes the fact that altering one aspect of Ca handling can lead to compensatory changes in other cellular processes, reversing some of the anticipated beneficial effects.

6.3.2 RyR function and SR Ca leak

The central role of the RyR in systolic Ca release and diastolic Ca leak has lead to interest in targeting its function in HF. One therapeutic possibility which has been considered is to stabilise the RyR cluster, through a similar mechanism to FKBP12.6. This could improve cooperative gating, leading to better synchronisation of Ca release in systole, and could also reduce Ca leak in diastole (discussed in Prestle *et al.*, 2003). However, the role of the RyR in HF remains under debate (see sections 1.4.1.4 & 5.4.1.1) and isolated changes in RyR function may not lead to lasting effects on the Ca transient (for reviews, see Eisner *et al.*, 1998; Eisner & Trafford, 2002). Also, RyR-specific pharmacological compounds with the necessary properties have not yet been isolated (see Prestle *et al.*, 2003). Thus, there are practical and theoretical reasons why targeting the RyR may not be fruitful.

6.3.3 NCX

In Chapter 3, it was shown that NCX activity was reduced by around ⅓ in this model of HF, and this may be detrimental to Ca removal from the cytoplasm. It was also demonstrated that adenoviral transfection of NCX lead to a measurable increase in I_{NCX} in single cardiac myocytes (Figure 3.9). The consequences of this NCX upregulation on Ca handling would require further investigation. There has been some interest in targeting NCX in HF, however, a number of issues make modulation of NCX function less attractive as a therapeutic option. Firstly, NCX expression / activity does not change in a consistent direction in HF (see sections 1.4.1.6 & 3.4.5.3) and this variability is also seen from patient to patient (Hasenfuss *et al.*, 1999). Secondly, the ubiquitous nature of NCX means that changing its activity could have widespread side-effects on other tissues. Thirdly, some changes in NCX may be compensatory, for example increased NCX in some models of HF may offset reduced SERCA function and improve diastolic relaxation (e.g. see Pogwizd *et al.*, 1999). Inhibition of NCX in these circumstances could impair relaxation and increase diastolic [Ca]. Also, if reverse-mode NCX is important in contributing to SR Ca loading in HF (see Litwin & Bridge, 1997), then NCX inhibition could also impair systolic Ca handling.

One indirect way of affecting Ca efflux is through the use of cardiac glycosides such as digoxin. By inhibiting the sarcolemmal Na-K exchanger, digoxin leads to increased $[Na]_i$ and this will shift E_{NCX} and reduce Ca efflux. A large multicentre trial of digoxin in patients with heart failure showed that it reduced hospitalisations due to HF, but did not improve mortality (The Digitalis Investigation Group, 1997).

6.3.4 Potential problems with targeting Ca handling in heart failure

One danger of targeting the SR Ca content in HF is the theoretical risk of cellular Ca overload and triggered arrhythmias caused by spontaneous Ca release (see section 1.3.3.1). The threshold level of SR [Ca] where spontaneous release begins to occur may be the same in HF and control cells – in their rabbit model of HF, Pogwizd *et al.* showed that the threshold level was just above 100 μmol/L cytosol in both cases (Pogwizd *et al.*, 2001). Thus, there may be a window within which the SR content could be enhanced without triggering arrhythmias, although this [Ca] range may be relatively narrow.

As mentioned in section 6.1.1, additional factors also need taken into account when assessing arrhythmic risk – for example, the level of resting [Ca] and the β-adrenergic state are both important. Davia *et al.* showed that reduction of diastolic [Ca] by enhanced SERCA function could *reduce* arrhythmogenic Ca release even in the face of an almost doubled SR content (Davia *et al.*, 2001). Thus, targeting of SERCA still has its attractions. The presence of residual β-adrenergic responsiveness (Pogwizd *et al.*, 2001) suggests that one of the beneficial effects of β-blockade in HF may be to limit catecholamine-induced Ca overload.

Finally, significant endocardial-epicardial differences in Ca handling were demonstrated in this thesis (Chapters 3 & 4), particularly for Sham cells, and others have shown regional differences across the epicardial surface in HF (Ng *et al.*, 1998). If any intervention affected cells in one part of the heart more than another then it would risk amplifying such inhomogeneities, increasing the risk of ventricular arrhythmias.

6.4 Conclusions

The cellular response to left ventricular dysfunction is complex and depends on several factors including the species studied, the means of producing LVD, the timing of investigations and the region of the heart analysed. The work presented in this thesis has furthered the understanding of Ca handling in a rabbit model of heart failure, 8 weeks after myocardial infarction. It is hoped that studies such as this will give insights into the underlying mechanisms of heart failure, and suggest potential future directions for the treatment of this prevalent, debilitating and often fatal condition.

REFERENCE LIST

Antos, C. L., Frey, N., Marx, S. O., Reiken, S., Gaburjakova, M., Richardson, J. A., Marks, A. R., & Olson, E. N. (2001). Dilated cardiomyopathy and sudden death resulting from constitutive activation of protein kinase A. *Circulation Research* **89**, 997.

Antzelevitch, C., Sicouri, S., Litovsky, S. H., Lukas, A., Krishnan, S. C., Di Diego, J. M., Gintant, G. A., & Liu, D.-W. (1991). Heterogeneity within the ventricular wall - electrophysiology and pharmacology of epicardial, endocardial and M cells. *Circulation Research* **69**, 1427-1449.

Arnolda, L., McGrath, B., Cocks, M., Sumithran, E., & Johnston, C. (1985). Adriamycin cardiomyopathy in the rabbit: an animal model of low output cardiac failure with activation of vasoconstrictor mechanisms. *Cardiovascular Research* **19**, 378-382.

Axelsen, P. H. & Bassingthwaighte, J. B. (1988). A constraint on possible stoichiometries of myocardial sodium-calcium exchange. *Basic Research in Cardiology* **83**, 314-326.

Axelsen, P. H. & Bridge, J. H. B. (1985). Electrochemical ion gradients and the Na/Ca exchange stoichiometry. Measurements of these gradients are thermodynamically consistent with a stoichiometric coefficient ≥ 3. *Journal of General Physiology* **85**, 471-478.

Baartscheer, A., Schumacher, C. A., Belterman, C. N. W., Coronel, R., & Fiolet, J. W. T. (2003). SR calcium handling and calcium after-transients in a rabbit model of heart failure. *Cardiovascular Research* **58**, 99-108.

Baker, P. F. & Blaustein, M. P. (1968). Sodium-dependent uptake of calcium by crab nerve. *Biochimica et Biophysica Acta* **150**, 167-170.

Baker, P. F., Blaustein, M. P., Hodgkin, A. L., & Steinhardt, R. A. (1967). The effect of sodium concentration on calcium movements in giant axons of *Loligo forbesi*. *Journal of Physiology* **192**, 43P-44P.

Baker, P. F., Blaustein, M. P., Hodgkin, A. L., & Steinhardt, R. A. (1969). The influence of calcium on sodium efflux in squid axons. *Journal of Physiology* **200**, 431-458.

Balke, C. W. & Shorofsky, S. R. (1998). Alterations in calcium handling in cardiac hypertrophy and heart failure. *Cardiovascular Research* **37**, 290-299.

Barth, E., Stämler, G., Speiser, B., & Schaper, J. (1992). Ultrastructural quantitation of mitochondria and myofilaments in cardiac muscle from 10 different animal species, including man. *Journal of Molecular & Cellular Cardiology* **24**, 669-681.

Bassani, J. W. M., Bassani, R. A., & Bers, D. M. (1994). Relaxation in rabbit and rat cardiac cells: species-dependent differences in cellular mechanisms. *Journal of Physiology* **476**, 279-293.

Bassani, J. W. M., Yuan, W., & Bers, D. M. (1995). Fractional SR Ca release is regulated by trigger Ca and SR Ca content in cardiac myocytes. *American Journal of Physiology* **268**, C1313-C1329.

Bassani, R. A., Bassani, J. W. M., & Bers, D. M. (1992). Mitochondrial and sarcolemmal Ca^{2+} transport reduce $[Ca^{2+}]_i$ during caffeine contractures in rabbit cardiac myocytes. *Journal of Physiology* **453**, 591-608.

Berlin, J. R., Bassani, J. W. M., & Bers, D. M. (1994). Intrinsic cytosolic calcium buffering properties of single rat cardiac myocytes. *Biophysical Journal* **67**, 1775-1787.

Bers, D. M. (2000). Calcium fluxes involved in control of cardiac myocyte contraction. *Circulation Research* **87**, 275-281.

Bers, D. M. (2001). *Excitation-contraction coupling and cardiac contractile force*, Second ed. Kluwer Academic Publishers.

Bers, D. M. (2002). Cardiac excitation-contraction coupling. *Nature* **415**, 198-205.

Bers, D. M. & Bridge, J. H. B. (1989). Relaxation of rabbit ventricular muscle by Na-Ca exchange and sarcoplasmic reticulum calcium pump. *Circulation Research* **65**, 334-342.

Bers, D. M., Eisner, D. A., & Valdivia, H. H. (2003). Sarcoplasmic reticulum Ca^{2+} and heart failure: roles of diastolic leak and Ca^{2+} transport. *Circulation Research* **93**, 487-490.

Bers, D. M. & Ellis, D. (1982). Intracellular calcium and sodium activity in sheep heart Purkinje fibres. Effect of changes of external sodium and intracellular pH. *Pflugers Archiv-European Journal of Physiology* **393**, 171-178.

Bers, D. M. & Stiffel, V. M. (1993). Ratio of ryanodine to dihydropyridine receptors in cardiac and skeletal muscle and implications for E-C coupling. *American Journal of Physiology* **264**, C1587-C1593.

Blaustein, M. P. & Hodgkin, A. L. (1969). The effect of cyanide on the efflux of calcium from squid axons. *Journal of Physiology* **200**, 497-527.

Blaustein, M. P. & Lederer, W. J. (1999). Sodium/calcium exchange: its physiological implications. *Physiological Reviews* **79**, 763-854.

Boateng, S. Y., Naqvi, R. U., Koban, M. U., Yacoub, M. H., MacLeod, K. T., & Boheler, K. R. (2001). Low-dose ramipril treatment improves relaxation and calcium cycling after established cardiac hypertrophy. *American Journal of Physiology* **280**, H1029-H1038.

Brette, F. & Orchard, C. H. (2003). T-tubule function in mammalian cardiac myocytes. *Circulation Research* **92**, 1182-1192.

Bridge, J. H. B., Smolley, J. R., & Spitzer, K. W. (1990). The relationship between charge movements associated with I_{Ca} and I_{Na-Ca} in cardiac myocytes. *Science* **241**, 376-378.

Briggs, A. H. & Melvin, S. (1961). Ion movement in isolated rabbit aortic strips. *American Journal of Physiology* **201**, 365-368.

Bryant, S. M., Shipsey, S. J., & Hart, G. (1997). Regional differences in electrical and mechanical properties of myocytes from guinea-pig hearts with mild left ventricular hypertrophy. *Cardiovascular Research* **35**, 315-323.

Burton, F. L. & Cobbe, S. M. (2000). Ventricular fibrillation threshold and local dispersion of refractoriness in isolated rabbit hearts with left ventricular dysfunction. *Basic Research in Cardiology* **95**, 359-367.

Cannell, M. B., Grantham, C. J., Main, M. J., & Evans, A. M. (1996). The roles of the sodium and calcium current in triggering calcium release from the sarcoplasmic reticulum. *Annals of the New York Academy of Sciences* **779**, 443-450.

Capogrossi, M. C., Houser, S. R., Bahinski, A., & Lakatta, E. G. (1987). Synchronous occurrence of spontaneous localized calcium release from the sarcoplasmic reticulum generates action potentials in rat cardiac ventricular myocytes at normal resting membrane potential. *Circulation Research* **61**, 498-503.

Carr, A. N., Schmidt, A. G., Suzuki, Y., del Monte, F., Sato, Y., Lanner, C., Breeden, K., Jing, S., Allen, P. B., Greengard, P., Yatani, A., Hoit, B. D., Grupp, I. L., Hajjar, R. J., DePaoli-Roach, A. A., & Kranias, E. G. (2002). Type 1 phosphatase - a negative regulator of cardiac function. *Molecular and Cellular Biology* **22**, 4124-4135.

Chamunorwa, J. P. & O'Neill, S. C. (1995). Regional differences in rest decay and recoveries of contraction and the calcium transient in rabbit ventricular muscle. *Pflugers Archiv-European Journal of Physiology* **430**, 195-204.

Chen, F., Mottino, G., Klitzner, T. S., Philipson, K. D., & Frank, J. S. (1995). Distribution of the Na^+/Ca^{2+} exchange protein in developing rabbit myocytes. *American Journal of Physiology* **268**, C1126-C1132.

Cheng, H., Lederer, M. R., Lederer, W. J., & Cannell, M. B. (1996). Calcium sparks and $[Ca^{2+}]_i$ waves in cardiac myocytes. *AJP - Cell Physiology* **270**, C148-C159.

Cheng, H., Lederer, W. J., & Cannell, M. B. (1993). Calcium sparks: elementary events underlying excitation-contraction coupling in heart muscle. *Science* **262**, 740-744.

Ching, L. L., Williams, A. J., & Sitsapesan, R. (2001). Evidence for Ca^{2+} activation and inactivation sites on the luminal side of the cardiac ryanodine receptor complex. *Circulation Research* **87**, 201-206.

Choi, H. S. & Eisner, D. A. (1999a). The effects of inhibition of the sarcolemmal Ca-ATPase on systolic calcium fluxes and intracellular calcium concentration in rat ventricular myocytes. *Pflugers Archiv-European Journal of Physiology* **437**, 966-971.

Choi, H. S. & Eisner, D. A. (1999b). The role of sarcolemmal Ca^{2+}-ATPase in the regulation of resting calcium concentration in rat ventricular myocytes. *Journal of Physiology* **515**, 109-118.

Chung, M. K., Pogwizd, S. M., Miller, D. P., & Cain, M. E. (1997). Three-dimensional mapping of the initiation of nonsustained ventricular tachycardia in the human heart. *Circulation* **95**, 2517-2527.

Cleland, J. G. F., Gemmell, I., Khand, A., & Boddy, A. (1999). Is the prognosis of heart failure improving? *European Journal of Heart Failure* **1**, 229-241.

Clusin, W. T. (1983). Caffeine induces a transient inward current in cultured cardiac cells. *Nature* **301**, 248-250.

Clusin, W. T., Buchbinder, M., & Harrison, D. C. (1983a). Calcium overload, "injury" current, and early ischaemic cardiac arrhythmias - a direct connection. *Lancet* **1**, 272-274.

Clusin, W. T., Fischmeister, R., & DeHaan, R. L. (1983b). Caffeine-induced current in embryonic heart cells: time course and voltage-dependence. *American Journal of Physiology* **245**, H528-H532.

Colyer, J. & Wang, J. H. (1991). Dependence of cardiac sarcoplasmic reticulum calcium pump activity on the phosphorylation status of phospholamban. *Journal of Biological Chemistry* **266**, 17486-17493.

Convery, M. K. & Hancox, J. C. (1999). Comparison of Na^+-Ca^{2+} exchange current elicited from isolated rabbit ventricular myocytes by voltage ramp and step protocols. *Pflugers Archiv-European Journal of Physiology* **437**, 944-954.

Cook, S. J., Chamunorwa, J. P., Lancaster, M. K., & O'Neill, S. C. (1997). Regional differences in the regulation of intracellular sodium and in action potential configuration in rabbit left ventricle. *Pflugers Archiv-European Journal of Physiology* **433**, 515-522.

Coraboeuf, E., Gautier, P., & Guiraudou, P. (1981). Potential and tension changes induced by sodium removal in dog Purkinje fibres: role of an electrogenic sodium-calcium exchange. *Journal of Physiology* **311**, 605-622.

Cordeiro, J. M., Bridge, J. H. B., & Spitzer, K. W. (2001). Early and delayed afterdepolarizations in rabbit heart Purkinje cells viewed by confocal microscopy. *Cell Calcium* **29**, 289-297.

Cosmos, E. E. & Harris, E. J. (1961). In vitro studies of the gain and exchange of calcium in frog skeletal muscle. *Journal of General Physiology* **44**, 1121-1130.

Cranefield, P. F. (1975). *The conduction of the cardiac impulse: the slow response and cardiac arrhythmias* Futura Press, Mt. Kisco.

Crespo, L. M., Grantham, C. J., & Cannell, M. B. (1990). Kinetics, stoichiometry and role of the Na-Ca exchange mechanism in isolated cardiac myocytes. *Nature* **345**, 618-621.

Currie, S., Sayeed, R. A., & Smith, G. L. (2003). Selective down-regulation of subendocardial ryanodine receptors in a rabbit model of left ventricular dysfunction. *Journal of Physiology* **552P**, C36.

Currie, S. & Smith, G. L. (1999). Enhanced phosphorylation of phospholamban and downregulation of sarco / endoplasmic reticulum Ca^{2+} ATPase type 2 (SERCA 2) in cardiac sarcoplasmic reticulum from rabbits with heart failure. *Cardiovascular Research* **41**, 135-146.

Davia, K., Bernobich, E., Ranu, H. K., del Monte, F., Terracciano, C. M. N., MacLeod, K. T., Adamson, D. L., Chaudhri, B., Hajjar, R. J., & Harding, S. E. (2001). SERCA2a overexpression decreases the incidence of aftercontractions in adult rabbit ventricular myocytes. *Journal of Molecular And Cellular Cardiology* **33**, 1005-1015.

Davies, C. H., Davia, K., Bennett, J. G., Pepper, J. R., Poole-Wilson, P. A., & Harding, S. E. (1995). Reduced contraction and altered frequency response of isolated ventricular myocytes from patients with heart failure. *Circulation* **92**, 2540-2549.

del Monte, F. & Hajjar, R. J. (2003). Targeting calcium cycling proteins in heart failure through gene transfer. *Journal of Physiology* **546**, 49-61.

Delbridge, L. M. W., Bassani, J. W. M., & Bers, D. M. (1996). Steady-state twitch Ca^{2+} fluxes and cytosolic Ca^{2+} buffering in rabbit ventricular myocytes. *American Journal of Physiology* **270**, C192-C199.

Dixon, I. M., Hata, T., & Dhalla, N. S. (1992). Sarcolemmal calcium transport in congestive heart failure due to myocardial infarction in rats. *American Journal of Physiology* **262**, H1387-H1394.

Diaz, M. E., Cook, S. J., Chamunorwa, J. P., Trafford, A. W., Lancaster, M. K., O'Neill, S. C., & Eisner, D. A. (1996). Variability of spontaneous Ca^{2+} release between different rat ventricular myocytes is correlated with Na^{+}-Ca^{2+} exchange and $[Na+]_i$. *Circulation Research* **78**, 857-862.

Diaz, M. E., Graham, H. K., & Trafford, A. W. (2004). Enhanced sarcolemmal Ca^{2+} efflux reduces sarcoplasmic reticulum Ca^{2+} and systolic Ca^{2+} in cardiac hypertrophy. *Cardiovascular Research* **62**, 538-547.

Edgell, R. M., De Souza, A. I., & MacLeod, K. T. (2000). Relative importance of SR load and cytoplasmic calcium concentration in the genesis of aftercontractions in cardiac myocytes. *Cardiovascular Research* **47**, 769-777.

Ehara, T., Matsuoka, S., & Noma, A. (1989). Measurement of reversal potential of Na^{+}-Ca^{2+} exchange current in single guinea-pig ventricular cells. *Journal of Physiology* **410**, 227-249.

Eisner, D. A., Choi, H. S., Diaz, M. E., O'Neill, S. C., & Trafford, A. W. (2000). Integrative analysis of calcium cycling in cardiac muscle. *Circulation Research* **87**, 1087-1094.

Eisner, D. A. & Lederer, W. J. (1985). Na-ca exchange: stoichiometry and electrogenicity. *American Journal of Physiology* **248**, C189-C202.

Eisner, D. A. & Trafford, A. W. (2002). Heart failure and the ryanodine receptor: does Occam's razor rule? *Circulation Research* **91**, 979-981.

Eisner, D. A., Trafford, A. W., Diaz, M. E., Overend, C. L., & O'Neill, S. C. (1998). The control of Ca release from the cardiac sarcoplasmic reticulum, regulation versus autoregulation. *Cardiovascular Research* **38**, 589-604.

Eng, J., Lynch, R. M., & Balaban, R. S. (1989). Nicotinamide adenine dinucleotide fluorescence spectroscopy and imaging of isolated cardiac myocytes. *Biophysical Journal* **55**, 621-630.

Evans, A. M. & Cannell, M. B. (1997). The role of L-type Ca^{2+} current and Na^{+} current-stimulated Na/Ca exchange in triggering SR calcium release in guinea-pig cardiac ventricular myocytes. *Cardiovascular Research* **35**, 294-302.

Fan, J. S. & Palade, P. (1999). One calcium ion may suffice to open the tetrameric cardiac ryanodine receptor in rat ventricular myocytes. *The Journal of Physiology* **516**, 769-780.

Fang, Y., Condrescu, M., & Reeves, J. P. (1998). Regulation of the Na^{+}/Ca^{2+} exchange activity by cytosolic Ca in transfected Chinese hamster ovary cells. *American Journal of Physiology* **275**, C50-C55.

Figuerdo, V. M., Brandes, R., Weiner, M. W., Massie, B. M., & Camacho, S. A. (1993). Endocardial versus epicardial differences of intracellular free calcium under normal and ischemic conditions in perfused rat hearts. *Circulation Research* **72**, 1082-1090.

Fill, M. & Copello, J. A. (2002). Ryanodine receptor calcium release channels. *Physiological Reviews* **82**, 893-922.

Flesch, M., Schwinger, R. H. G., Schiffer, F., Frank, K., Sudkamp, M., Kuhn-Regnier, F., Arnold, G., & Bohm, M. (1996). Evidence for functional relevance of an enhanced expression of the Na^{+}-Ca^{2+} exchanger in failing human myocardium. *Circulation* **94**, 992-1002.

Frank, J. S., Mottino, G., Reid, D., Molday, R. S., & Philipson, K. D. (1992). Distribution of the Na^+-Ca^{2+} exchange protein in mammalian cardiac myocytes: an immunofluorescence and immunocolloidal gold-labelling study. *Journal of Cell Biology* **117**, 337-345.

Frank, K. F., Bölck, B., Erdmann, E., & Schwinger, R. H. G. (2003). Sarcoplasmic reticulum Ca^{2+}-ATPase modulates cardiac contraction and relaxation. *Cardiovascular Research* **57**, 20-27.

Fujioka, Y., Komeda, M., & Matsuoka, S. (2000). Stoichiometry of Na^+-Ca^{2-} exchange in inside-out patches excised from guinea-pig ventricular myocytes. *Journal of Physiology* **523**, 339-351.

Glitsch, H. G., Reuter, H., & Scholz, H. (1970). The effect of the internal sodium concentration on calcium fluxes in isolated guinea-pig auricles. *Journal of Physiology* **209**, 25-43.

Goodford, P. J. (1967). The calcium content of the smooth muscle of the guinea-pig taenia coli. *Journal of Physiology* **192**, 145-157.

Gómez, A. M., Guatimosim, S., Dilly, K. W., Vassort, G., & Lederer, W. J. (2001). Heart failure after myocardial infarction - altered excitation-contraction coupling. *Circulation* **104**, 688-693.

Grantham, C. J. & Cannell, M. B. (1996). Ca^{2+} influx during the cardiac action potential in guinea pig ventricular myocytes. *Circulation Research* **79** , 194-200.

Grynkiewicz, G., Poenie, M., & Tsien, R. Y. (1985). A new generation of Ca indicators with greatly improved fluorescence properties. *Journal of Biological Chemistry* **260**, 3440-3450.

Guatimosim, S., Dilly, K. W., Santana, L. F., Jafri, M. S., Sobie, E. A., & Lederer, W. J. (2002). Local Ca^{2+} signalling and EC coupling in heart: Ca^{2+} sparks and the regulation of the $[Ca^{2+}]_i$ transient. *Journal of Molecular And Cellular Cardiology* **34**, 941-950.

Györke, I. & Györke, S. (1998). Regulation of the cardiac ryanodine receptor channel by luminal Ca^{2+} involves luminal Ca^{2+} sensing sites. *Biophysical Journal* **75**, 2801-2810.

Hasenfuss, G. (1998). Alterations of calcium-regulatory proteins in heart failure. *Cardiovascular Research* **37**, 279-289.

Hasenfuss, G. & Pieske, B. (2002). Calcium cycling in congestive heart failure. *Journal of Molecular & Cellular Cardiology* **34**, 951-969.

Hasenfuss, G., Schillinger, W., Lehnart, S. E., Preuss, M., Peiske, B., Maier, L. S., Prestle, J., Minami, K., & Just, H. (1999). Relationship between Na^{+}-Ca^{2+}-exchanger protein levels and diastolic function of failing human myocardium. *Circulation* **99**, 641-648.

He, J. Q., Conklin, M. W., Foell, J. D., Wolff, M. R., Haworth, R. A., Coronado, R., & Kamp, T. J. (2001). Reduction in density of transverse tubules and L-type Ca2+ channels in canine tachycardia-induced heart failure. *Cardiovascular Research* **49**, 298-307.

Heerdt, P. M., Holmes, J. W., Cai, B., Barbone, A., Madigan, J. D., Reiken, S., Lee, D. L., Oz, M. C., Marks, A. R., & Burkhoff, D. (2000). Chronic unloading by left ventricular assist device reverses contractile dysfunction and alters gene expression in end-stage heart failure. *Circulation* **102**, 2713-2719.

Hilgemann,D.W., Collins,A., Cash,D.P. (1991). Cardiac Na^{+}-Ca^{2+} exchange system in giant membrane patches. *Annals of the New York Academy of Sciences* **639**, 127-139.

Hilgemann, D. W., Collins, A., & Matsuoka, S. (1992). Steady state and dynamic properties of cardiac sodium-calcium exchange: secondary modulation by cytoplasmic calcium and ATP. *Journal of General Physiology* **100**, 933-961.

Hobai, I. A. & O'Rourke, B. (2000). Enhanced Ca^{2+}-activated Na^{+}-Ca^{2+} exchange activity in canine pacing-induced heart failure. *Circulation Research* **87**, 690-698.

Hobai, I. A. & O'Rourke, B. (2001). Decreased sarcoplasmic reticulum calcium content is responsible for defective excitation-contraction coupling in canine heart failure. *Circulation* **103**, 1577-1584.

Houser, S. R. & Margulies, K. B. (2003). Is depressed myocyte contractility centrally involved in heart failure? *Circulation Research* **92**, 350-358.

Houser, S. R., Piacentino III, V., & Weisser, J. (2000). Abnormalities of calcium cycling in the hypertrophied and failing heart. *Journal of Molecular & Cellular Cardiology* **32**, 1595-1607.

Igarashi-Saito, K., Tsutsui, H., Takahashi, M., Kinugawa, S., Egashira, K., & Takeshita, A. (1999). Endocardial versus epicardial differences of sarcoplasmic reticulum Ca^{2+}-ATPase gene expression in the canine failing myocardium. *Basic Research in Cardiology* **94**, 267-273.

Ishide, N., Urayama, T., Inoue, K.-I., Komaru, T., & Takishima, T. (1990). Propagation and collision characteristics of calcium waves in rat myocytes. *American Journal of Physiology* **259**, H940-H950.

Ito, K., Yan, X., Feng, X., Manning, W. J., Dillmann, W. H., & Lorell, B. H. (2001). Transgenic expression of sarcoplasmic reticulum Ca^{2+} ATPase modifies the transition from hypertrophy to early heart failure. *Circulation Research* **89**, 422-429.

Iwamoto, T., Pan, Y., Wakabayashi, S., Imagawa, T., Yamanaka, H. I., & Shigekawa, M. (1996). Phosphorylation-dependent regulation of cardiac Na^{+}/Ca^{2+} exchanger via protein kinase C. *Journal of Biological Chemistry* **271**, 13609-13615.

Janczewski, A. M., Spurgeon, H. A., Stern, M. D., & Lakatta, E. G. (1995). Effects of sarcoplasmic reticulum Ca^{2+} load on the gain function of Ca^{2+} release by Ca^{2+} current in cardiac cells. *American Journal of Physiology* **268**, H916-H920.

January, C. T. & Fozzard, H. A. (1988). Delayed afterdepolarizations in heart muscle: mechanisms and relevance. *Pharmacological Reviews* **40**, 219-227.

Janvier, N. C. & Boyett, M. R. (1996). The role of Na-Ca exchange current in the cardiac action potential. *Cardiovascular Research* **32**, 69-84.

Janvier, N. C., Harrison, S. M., & Boyett, M. R. (1997a). The role of inward Na^{+}-Ca^{2+} exchange current in the ferret ventricular action potential. *Journal of Physiology* **498**, 611-625.

Janvier, N. C., McMorn, S. O., Harrison, S. M., Taggart, P., & Boyett, M. R. (1997b). The role of Na^{+}-Ca^{2-} exchange current in electrical restitution in ferret ventricular cells. *Journal of Physiology* **504**, 301-314.

Jiang, M. T., Lokuta, A. J., Farrell, E. F., Wolff, M. R., Haworth, R. A., & Valdivia, H. H. (2002). Abnormal Ca^{2+} release, but normal ryanodine receptors, in canine and human heart failure. *Circulation Research* **91**, 1015-1022.

Kass, R. S., Tsien, R. W., & Weingart, R. (1978). Ionic basis of the transient inward current induced by strophanthidinin cardiac Purkinje fibres. *Journal of Physiology* **281**, 209-226.

Kieval, R. S., Bloch, R. J., Lindenmayer, G. E., Ambesi, A., & Lederer, W. J. (1992). Immunofluorescence localization of the Na-Ca exchanger in heart cells. *American Journal of Physiology* **263**, C545-C550.

Kim, I., Koh, G. Y., & Lee, C. O. (1998). Identification of alternatively spliced Na^+-Ca^{2+} exchanger isoforms expressed in the heart. *Comparative Biochemistry and Physiology Part B: Biochemistry and Molecular Biology* **119**, 157-161.

Kimura, J., Miyamae, S., & Noma, A. (1987). Identification of sodium-calcium exchange current in single ventricular cells of guinea-pig. *Journal of Physiology* **384**, 199-222.

Kimura, J., Noma, A., & Irisawa, H. (1986). Na-Ca exchange current in mammalian heart cells. *Nature* **319**, 596-597.

Koban, M. U., Moorman, A. F. M., Holtz, J., Yacoub, M. H., & Boheler, K. R. (1998). Expressional analysis of the cardiac Na-Ca exchanger in rat development and senescence. *Cardiovascular Research* **37**, 405-423.

Kofuji, P., Hadley, R. W., Kieval, R. S., Lederer, W. J., & Schulze, D. H. (1992). Expression of the Na-Ca exchanger in diverse tissues: a study using the cloned human cardiac Na-Ca exchanger. *American Journal of Physiology* **263**, C1241-C1249.

Komuro, I., Wenninger, K. E., Philipson, K. D., & Izumo, S. (1992). Molecular cloning and characterization of the human cardiac Na^+ /Ca^{2+} exchanger cDNA. *Procedings of the National Academy of Sciencev of the United States of America* **89**, 4769-4773.

Kostin, S., Scholz, D., Shimada, T., Maeno, Y., Mollnau, H., Hein, S., & Schaper, J. (1998). The internal and external protein scaffold of the T-tubular system in cardiomyocytes. *Cell and Tissue Research* **294**, 449-460.

Kubo, H., Margulies, K. B., Piacentino III, V., Gaughan, J. P., & Houser, S. R. (2001). Patients with end-stage congestive heart failure treated with β-adrenergic receptor antagonists have improved ventricular myocyte calcium regulatory protein abundance. *Circulation* **104**, 1012-1018.

Laurita, K. R., Katra, R., Wible, B., Wan, X., & Koo, M. H. (2003). Transmural heterogeneity of calcium handling in canine. *Circulation Research* **92**, 668-675.

Leblanc, N. & Hume, J. R. (1990). Sodium current-induced release of calcium from cardiac sarcoplasmic reticulum. *Science* **241**, 372-376.

Lederer, W. J., Niggli, E., & Hadley, R. W. (1990). Sodium-calcium exchange in excitable cells: fuzzy space. *Science* **241**, 283.

Levi, A. J., Spitzer, K. W., Kohmoto, O., & Bridge, J. H. B. (1994). Depolarization-induced Ca entry via Na-Ca exchange triggers SR release in guinea pig cardiac myocytes. *American Journal of Physiology* **266**, H1422-H1433.

Levitsky, D. O., Benevolensky, D. S., Levchenko, T. S., Smirnov, V. N., & Chazov, E. I. (1981). Calcium-binding rate and capacity of cardiac sarcoplasmic reticulum. *Journal of Molecular And Cellular Cardiology* **13**, 785-796.

Levitsky, D. O., Nicoll, D. A., & Philipson, K. D. (1994). Identification of the high affinity Ca-binding domain of the cardiac Na^{+}-Ca^{2+} exchanger. *Journal of Biological Chemistry* **269**, 22847-22852.

Lindner, M., Erdmann, E., & Beuckelmann, D. J. (1998). Calcium content of the sarcoplasmic reticulum in isolated ventricular myocytes from patients with terminal heart failure. *Journal of Molecular And Cellular Cardiology* **30**, 743-749.

Lipp, P. & Niggli, E. (1994). Sodium current-induced calcium signals in isolated guinea-pig ventricular myocytes. *Journal of Physiology* **474**, 439-446.

Litwin, S. E. & Bridge, J. H. B. (1997). Enhanced Na^{+}-Ca^{2+} exchange in the infarcted heart. *Circulation Research* **81**, 1083-1093.

Litwin, S. E., Li, J., & Bridge, J. H. B. (1998). Na-Ca exchange and the trigger for sarcoplasmic reticulum Ca release: studies in adult rabbit ventricular myocytes. *Biophysical Journal* **75**, 359-371.

Litwin, S. E., Zhang, D., & Bridge, J. H. B. (2000). Dyssynchronous Ca^{2+} sparks in myocytes from infarcted hearts. *Circulation Research* **87**, 1040-1047.

Lukyanenko, V., Györke, I., & Györke, S. (1996). Regulation of calcium release by calcium inside the sarcoplasmic reticulum in ventricular myocytes. *Pflugers Archiv-European Journal of Physiology* **432**, 1047-1054.

Luo, C. H. & Rudy, Y. (1994). A dynamic model of the cardiac ventricular action potential: I. Simulations of ionic currents and concentration changes. *Circulation Research* **74**, 1071-1096.

Lüttgau, H. C. & Niedergerke, R. (1958). The antagonism between Ca and Na ions on the frog's heart. *Journal of Physiology* **143**, 486-505.

MacLennan, D. H., Rice, W. J., & Green, N. M. (1997). The mechanism of Ca^{2+} transport by sarco(endo)plasmic reticulum Ca^{2+}-ATPases. *Journal of Biological Chemistry* **272**, 28815-28818.

Mahaffey, K. W., Raya, T. E., Pennock, G. D., Morkin, E., & Goldman, S. (1995). Left ventricular performance and remodelling in rabbits after myocardial infarction. *Circulation* **91**, 794-801.

Maier, L. S., Bers, D. M., & Pieske, B. (2000). Differences in Ca^{2+}-handling and sarcoplasmic reticulum Ca^{2+}-content in isolated rat and rabbit myocardium. *Journal of Molecular & Cellular Cardiology* **32**, 2249-2258.

Maier, L. S. & Bers, D. M. (2002). Calcium, calmodulin, and calcium-calmodulin kinase II: heartbeat to heartbeat and beyond. *Journal of Molecular And Cellular Cardiology* **34**, 919-939.

Makino, N., Hata, T., Sugano, M., Dixon, I. M. C., & Yang, W. (1996). Regression of hypertrophy after myocardial infarction is produced by the chronic blockade of angiotensin type 1 receptor in rats. *J Mol Cell Cardiol* **28**, 507-517.

Marbán, E., Robinson, S. W., & Weir, W. G. (1986). Mechanisms of arrhythmogenic delayed and early afterdepolarizations in ferret ventricular muscle. *Journal of Clinical Investigation* **78**, 1185-1192.

Marks, A. R., Reiken, S., & Marx, S. O. (2002). Progression of heart failure: is protein kinase A hyperphosphorylation of the ryanodine receptor a contributing factor? *Circulation* **105**, 272-275.

Martin, D. L. & DeLuca, H. F. (1969). Influence of sodium on calcium transport by the rat small intestine. *American Journal of Physiology* **216**, 1351-1359.

Marx, S. O., Gaburjakova, J., Gaburjakova, M., Henrikson, C., Ondrias, K., & Marks, A. R. (2001). Coupled gating between cardiac calcium release channels (ryanodine receptors). *Circulation Research* **88**, 1158.

Marx, S. O., Reiken, S., Hisamatsu, Y., Jayaraman, T., Burkhoff, D., Rosemblit, N., & Marks, A. R. (2000). PKA phosphorylation dissociates FKBP12.6 from the calcium release channel (ryanodine receptor): defective regulation in failing hearts. *Cell* **101**, 365-376.

Matsui, H., MacLennan, D. H., Alpert, N. R., & Periasamy, M. (1995). Sarcoplasmic reticulum gene expression in pressure overload-induced cardiac hypertrophy in rabbit. *American Journal of Physiology* **268**, C252-C258.

Matsuoka, S., Nicoll, D. A., Hryshko, L. V., Levitsky, D. O., Weiss, J. N., & Philipson, K. D. (1995). Regulation of the cardiac Na^{+}-Ca^{2-} exchanger by Ca: mutational analysis of the Ca binding domain. *Journal of General Physiology* **105**, 403-420.

Maxwell, M. P., Hearse, D. J., & Yellon, D. M. (1987). Species variation in the coronary collateral circulation during regional myocardial ischaemia: a critical determinant of the rate of evolution and extent of myocardial infarction. *Cardiovascular Research* **21**, 737-746.

McCall, E., Ginsburg, K. S., Bassani, R. A., Shannon, T. R., Qi, M., Samarel, A. M., & Bers, D. M. (1998). Ca flux, contractility and excitation-contraction coupling in hypertrophic rat ventricular myocytes. *American Journal of Physiology* **274**, H1348-H1360.

McDonald, R. L., Colyer, J., & Harrison, S. M. (2000). Quantitative analysis of Na^{+}-Ca^{2+} exchanger expression in guinea-pig heart. *European Journal of Biochemistry* **267**, 5142-5148.

McIntosh, M. A., Cobbe, S. M., Kane, K. A., & Rankin, A. C. (1998). Action potential prolongation and potassium currents in left-ventricular myocytes isolated from hypertrophied rabbit hearts. *J Mol Cell Cardiol* **30**, 43-53.

McIntosh, M. A., Cobbe, S. M., & Smith, G. L. (2000). Heterogeneous changes in action potential and intracellular Ca^{2+} in left ventricular myocyte sub-types from rabbits with heart failure. *Cardiovascular Research* **45**, 397-409.

McMurray, J. J. & Stewart, S. (2000). Epidemiology, aetiology, and prognosis of heart failure. *Heart* **83**, 596-602.

Mechmann, S. & Pott, L. (1986). Identification of Na-Ca exchange current in single cardiac myocytes. *Nature* **319**, 597-599.

Meyer, M. & Dillmann, W. H. (1998). Sarcoplasmic reticulum Ca^{2+}-ATPase overexpression by adenovirus mediated gene transfer and in transgenic mice. *Cardiovascular Research* **37**, 360-366.

Mészáros, J., Khananshvili, D., & Hart, G. (2001). Mechanisms underlying delayed afterdepolarizations in hypertrophied left ventricular myocytes of rats. *American Journal of Physiology* **281**, H903-H914.

Milnes, J. T. & MacLeod, K. T. (2001). Reduced ryanodine receptor to dihydropyridine receptor ratio may underlie slowed contraction in a rabbit model of left ventricular cardiac hypertrophy. *Journal of Molecular & Cellular Cardiology* **33**, 473-485.

Min, J.-Y., Sullivan, M. F., Yan, X., Feng, X., Chu, V., Wang, J.-F., Amende, I., Morgan, J. P., Philipson, K. D., & Hampton, T. G. (2002). Overexpression of Na^{+}/Ca^{2+} exchanger gene attenuates postinfarction myocardial dysfunction. *American Journal of Physiology* **283**, H2466-H2471.

Ming, Z., Aronson, R., & Nordin, C. (1994). Mechanism of current-induced early afterdepolarizations in guinea pig ventricular myocytes. *American Journal of Physiology* **267**, H1419-H1428.

Mittmann, C., Eschenhagen, T., & Scholz, H. (1998). Cellular and molecular aspects of contractile dysfunction in heart failure. *Cardiovascular Research* **39**, 267-275.

Miura, M., Ishide, N., Oda, H., Sakurai, M., Shinozaki, T., & Takishima, T. (1993). Spatial features of calcium transients during early and delayed afterdepolarizations. *American Journal of Physiology* **265**, H439-H444.

Miura, Y. & Kimura, J. (1989). Sodium-calcium exchange current: dependence on internal Ca and Na and competitive binding of external Na and Ca. *Journal of General Physiology* **93**, 1129-1145.

Movsesian, M. A. & Schwinger, R. H. G. (1998). Calcium sequestration by the sarcoplasmic reticulum in heart failure. *Cardiovascular Research* **37**, 352-359.

Muders, F., Friedrich, E., Luchner, A., Pfeifer, M., Ickenstein, G., Hamelbeck, B., Riegger, G. A., & Elsner, D. (1999). Hemodynamic changes and neurohumoral regulation during development of

congestive heart failure in a model of epinephrine-induced cardiomyopathy in conscious rabbits. *Journal of Cardiac Failure* **5**, 109-116.

Muller-Ehmsen, J., McDonough, A. A., Farley, R. A., & Schwinger, R. H. G. (2002). Sodium pump isoform expression in heart failure: implication for treatment. *Basic Research in Cardiology* **97 Suppl 1**, I25-I30.

Mullins, L. J. (1979). The generation of electric currents in cardiac fibers by Na/Ca exchange. *American Journal of Physiology* **236**, C103-C110.

Naqvi, R. U., Tweedie, D., & MacLeod, K. T. (2001). Evidence for the action potential mediating the changes to contraction observed in cardiac hypertrophy in the rabbit. *International Journal of Cardiology* **77**, 189-206.

Näbauer, M., Beuckelmann, D. J., Überfuhr, P., & Steinbeck, G. (1996). Regional differences in current density and rate-dependent properties of the transient inward current in subepicardial and subendocardial myocytes of human left ventricle. *Circulation* **93**, 168-177.

Neary, P., Duncan, A. M., Cobbe, S. M., & Smith, G. L. (2002). Assessment of sarcoplasmic reticulum Ca^{2+} flux pathways in cardiomyocytes from rabbits with infarct-induced left-ventricular dysfunction. *Pflugers Archiv-European Journal of Physiology* **444**, 360-371.

Negretti, N., O'Neill, S. C., & Eisner, D. A. (1993). The relative contributions of different intracellular and sarcolemmal systems to relaxation in rat ventricular myocytes. *Cardiovascular Research* **27**, 1826-1830.

Negretti, N., Varro, A., & Eisner, D. A. (1995). Estimate of net calcium fluxes and sarcoplasmic-reticulum calcium content during systole in rat ventricular myocytes. *Journal of Physiology* **486**, 581-591.

Ng, G. A., Cobbe, S. M., & Smith, G. L. (1998). Non-uniform prolongation of intracellular Ca^{2+} transients recorded from the epicardial surface of isolated hearts from rabbits with heart failure. *Cardiovascular Research* **37**, 489-502.

Nicoll, D. A., Longoni, S., & Philipson, K. D. (1990). Molecular cloning and functional expression of the cardiac sarcolemmal Na^{+}-Ca^{2+} exchanger. *Science* **250**, 562-565.

Nicoll, D. A., Ottolia, M., Lu, L., Lu, Y., & Philipson, K. D. (1999). A new topological model of the cardiac sarcolemmal Na^{+}-Ca^{2+} exchanger. *Journal of Biological Chemistry* **274**, 910-917.

Niedergerke, R. (1963). Movements of Ca in frog heart ventricles at rest and during contractures. *Journal of Physiology* **167**, 515-550.

Noble, D., Noble, S. J., Bett, G. C. L., Earm, Y. E., Ho, W. K., & So, I. K. (1991). The role of sodium-calcium exchange during the cardiac action potential. *Annals of the New York Academy of Sciences* **639**, 334-353.

O'Neill, S. C. & Eisner, D. A. (1990). A mechanism for the effects of caffeine on Ca^{2+} release during diastole and systole in isolated rat ventricular myocytes. *Journal of Physiology* **430**, 519-536.

O'Rourke, B., Kass, D. A., Tomaselli, G. F., Kääb, S., Tunin, R. S., & Marbán, E. (1999). Mechanisms of altered excitation-contraction coupling in canine tachycardia-induced heart failure, I: experimental studies. *Circulation Research* **84**, 562-570.

Paganelli, F., Mougenot, R., & Maixenti, J. M. (2001). Defective activity and isoform of the Na,K-ATPase in the dilated cardiomyopathic hamster. *Cellular & Molecular Biology* **47** , 255-260.

Perchenet, L., Hinde, A. K., Patel, K. C. R., Hancox, J. C., & Levi, A. J. (2000). Stimulation of Na/Ca exchange by the β-adrenergic/protein kinase A pathway in guinea-pig ventricular myocytes at 37°C. *Pflugers Archiv-European Journal of Physiology* **439**, 822-828.

Periasamy, M. & Huke, S. (2001). SERCA pump level is a critical determinant of Ca^{2+} homeostasis and cardiac contractility. *Journal of Molecular & Cellular Cardiology* **33**, 1053-1063.

Philipson, K. D. & Nicoll, D. A. (2000). Sodium-calcium exchange: a molecular perspective. *Annual Review of Physiology* **62**, 111-133.

Phillips, R. M., Narayan, P., Gómez, A. M., Dilly, K., Jones, L. R., Lederer, W. J., & Altschuld, R. A. (1998). Sarcoplasmic reticulum in heart failure: central player or bystander? *Cardiovascular Research* **37**, 346-351.

Piacentino III, V., Dipla, K., Gaughan, J. P., & Houser, S. R. (2000). Voltage-dependent Ca^{2+} release from the SR of feline ventricular myocytes is explained by Ca^{2+}-induced Ca^{2+} release. *Journal of Physiology* **523**, 533-548.

Piacentino III, V., Weber, C. R., Chen, X., Weisser-Thomas, J., Margulies, K. B., Bers, D. M., & Houser, S. R. (2003). Cellular basis of abnormal calcium transients of failing human ventricular myocytes. *Circulation Research* **92**, 651-658.

Pieske, B., Maier, L. S., Bers, D. M., & Hasenfuss, G. (1999). Ca^{2+} handling and sarcoplasmic reticulum Ca^{2+} content in isolated failing and nonfailing human myocardium. *Circulation Research* **85**, 38-46.

Piot, C., Lemaire, S., Albat, B., Seguin, J., Nargeot, J., & Richard, S. (1996). High frequency-induced upregulation of human cardiac calcium currents. *Circulation* **93**, 120-128.

Piper, C., Bilger, J., Henrichs, E. M., Schultheiss, H. P., Horskotte, D., & Doerner, A. (2000). Is myocardial Na^{+}/Ca^{2+} exchanger transcription a marker for different stages of myocardial dysfunction? Quantitative polymerase chain reaction of the messenger RNA in endomyocardial biopsies of patients with heart failure. *Journal of the American College of Cardiology* **36**, 233-241.

Pitts, B. J. (1979). Stoichiometry of sodium-calcium exchange in cardiac sarcolemmal vesicles. Coupling to the sodium pump. *Journal of Biological Chemistry* **254**, 6232-6235.

Pogwizd, S. M. (1994). Focal mechanisms underlying ventricular tachycardia during prolonged ischaemic cardiomyopathy. *Circulation* **90**, 1441-1458.

Pogwizd, S. M. (1995). Nonreentrant mechanisms underlying spontaneous ventricular arrhythmias in a model of nonischaemic heart failure in rabbits. *Circulation* **92**, 1034-1048.

Pogwizd, S. M. (2000). Increased Na^{+}-Ca^{2+} exchanger in the failing heart. *Circulation Research* **87**, 641-643.

Pogwizd, S. M., McKenzie, J. P., & Cain, M. E. (1998). Mechanisms underlying spontaneous and induced ventricular arrhythmias in patients with idiopathic dilated cardiomyopathy. *Circulation* **98**, 2404-2414.

Pogwizd, S. M., Qi, M., Yuan, W., Samarel, A. M., & Bers, D. M. (1999). Upregulation of Na^{+}/Ca^{2+} exchanger expression and function in an arrhythmogenic rabbit model of heart failure. *Circulation Research* **85**, 1009-1019.

Pogwizd, S. M., Schlotthauer, K., Li, L., Yuan, W., & Bers, D. M. (2001). Arrhythmogenesis and contractile dysfunction in heart failure: roles of sodium-calcium exchange, inward rectifier potassium current, and residual β-adrenergic responsiveness. *Circulation Research* **88**, 1159-1167.

Prestle, J., Dieterich, S., Preuss, M., Bieligk, U., & Hasenfuss, G. (1999). Heterogeneous transmural gene expression of calcium-handling proteins and natriuretic peptides in the failing human heart. *Cardiovascular Research* **43**, 323-331.

Prestle, J., Janssen, P. M. L., Janssen, A. P., Zeitz, O., Lehnart, S. E., Bruce, L., Smith, G. L., & Hasenfuss, G. (2001). Overexpression of FK506-binding protein FKBP12.6 in cardiomyocytes reduces ryanodine receptor-mediated Ca^{2+} leak from the sarcoplasmic reticulum and increases contractility. *Circulation Research* **88**, 188-194.

Prestle, J., Quinn, F. R., & Smith, G. L. (2003). Ca^{2+}-handling proteins and heart failure: novel molecular targets? *Current Medicinal Chemistry* **10**, 1241-1253.

Pu, J., Robinson, R. B., & Boyden, P. A. (2000). Abnormalities in Ca_i handling in myocytes that survive in the infarcted heart are not just due to alterations in repolarization. *Journal of Molecular & Cellular Cardiology* **32**, 1509-1523.

Puglisi, J. L., Bassani, R. A., Bassani, J. W. M., Amin, J. N., & Bers, D. M. (1996). Temperature and relative contributions of Ca transport systems in cardiac myocyte relaxation. *American Journal of Physiology* **270**, H1772-H1778.

Pye, M. P., Black, M., & Cobbe, S. M. (1996). Comparison of *in vivo* and *in vitro* haemodynamic function in experimental heart failure: use of echocardiography. *Cardiovascular Research* **31**, 873-881.

Pye, M. P. & Cobbe, S. M. (1996). Arrhythmogenesis in experimental models of heart failure: the role of increased load. *Cardiovascular Research* **32**, 248-257.

Quednau, B. D., Nicoll, D. A., & Philipson, K. D. (1997). Tissue specificity and alternative splicing of the Na^+/Ca^{2+} exchanger isoforms NCX1, NCX2, and NCX3 in rat. *AJP - Cell Physiology* **272**, C1250.

Quinn, F. R., Currie, S., Duncan, A. M., Miller, S., Sayeed, R. A., Cobbe, S. M., & Smith, G. L. (2003). Myocardial infarction causes increased expression but decreased activity of the myocardial Na^+-Ca^{2+} exchanger in the rabbit. *Journal of Physiology* **553**, 229-242.

Rapundalo, S. T. (1998). Cardiac protein phosphorylation: functional and pathophysiological correlates. *Cardiovascular Research* **38**, 559-588.

Reeves, J. P. & Condrescu, M. (2003). Allosteric activation of sodium-calcium exchange activity by calcium: persistence at low calcium concentrations. *Journal of General Physiology* **122**, 621-639.

Reeves, J. P. & Hale, C. C. (1984). The stoichiometry of the cardiac sodium-calcium exchange system. *Journal of Biological Chemistry* **259**, 7733-7739.

Reinecke, H., Studer, R., Vetter, R., Holtz, J., & Drexler, H. (1996). Cardiac Na^+/Ca^{2+} exchange activity in patients with end-stage heart failure. *Cardiovascular Research* **31**, 48-54.

Reuter, H. & Seitz, N. (1968). The dependence of calcium efflux from cardiac muscle on temperature and external ion composition. *Journal of Physiology* **195**, 451-470.

Richard, S., Leclercq, F., Lemaire, S., Piot, C., & Nargeot, J. (1998). Ca^{2+} currents in compensated hypertrophy and heart failure. *Cardiovascular Research* 37, 300-311.

Rousseau, E. & Meissner, G. (1989). Single cardiac sarcoplasmic reticulum Ca^{2+}-release channel: activation by caffeine. *American Journal of Physiology* **256**, H328-H333.

Ruknudin, A., He, S., Lederer, W. J., & Schulze, D. H. (2000). Functional differences between cardiac and renal isoforms of the rat Na^+-Ca^{2+} exchanger NCX1 expressed in *Xenopus* oocytes. *Journal of Physiology* **529**, 599-610.

Sato, Y., Kiriazis, H., Yatani, A., Schmidt, A. G., Hahn, H., Ferguson, D. G., Sako, H., Mitarai, S., Honda, R., Mesnard-Rouiller, L., Frank, K. F., Beyermann, B., Wu, G., Fujimori, K., Dorn, G. W., II, & Kranias, E. G. (2001). Rescue of contractile parameters and myocyte hypertrophy in calsequestrin overexpressing myocardium by phospholamban ablation. *Journal of Biological Chemistry* **276**, 9392-9399.

Satoh, H., Delbridge, L. M., Blatter, L. A., & Bers, D. M. (1996). Surface:volume relationships in cardiac myocytes studied with confocal microscopy and membrane capacitance measurements: species-dependence and developmental effects. *Biophysical Journal* **70**, 1494-1504.

Schillinger, W., Schneider, H., Minami, K., Ferrari, R., & Hasenfuss, G. (2002). Importance of sympathetic activation for the expression of Na^{+}-Ca^{2+} exchanger in end-stage failing human myocardium. *European Heart Journal* **23**, 1118-1124.

Schlotthauer, K. & Bers, D. M. (2000). Sarcoplasmic reticulum Ca^{2+} release causes myocyte depolarization: underlying mechanism and threshold for triggered action potentials. *Circulation Research* **87**, 774-780.

Schmidt, U., del Monte, F., Miyamoto, M. I., Matsui, T., Gwathmey, J. K., Rosenzweig, A., & Hajjar, R. J. (2000). Restoration of diastolic funciton in senescent rat hearts through adenoviral gene transfer of sarcoplasmic reticulum Ca^{2+}-ATPase. *Circulation* **101**, 790-796.

Schram, G., Pourrier, M., Melnyk, P., & Nattel, S. (2002). Differential distribution of cardiac ion channel expression as a basis for regional specialization in electrical function. *Circulation Research* **90**, 939-950.

Schwinger, R. H. G., Wang, J., Frank, K., Muller-Ehmsen, J., Brixius, K., McDonough, A. A., & Erdmann, E. (1999). Reduced sodium pump α1, α3, and β1-isoform protein levels and Na^{+},K^{+}-ATPase activity but unchanged Na^{+}-Ca^{2+} exchanger protein levels in human heart failure. *Circulation* **99**, 2105-2112.

Scoote, M., Poole-Wilson, P. A., & Williams, A. J. (2003). The therapeutic potential of new insights into myocardial excitation-contraction coupling. *Heart* **89**, 371-376.

Segel, I. H. (1993). *Enzyme kinetics. Behavior and analysis of rapid equilibrium and steady-state enzyme systems*, pp. 957. John Wiley & sons, Inc., New York.

Seidler, T., Miller, S. L. W., Loughrey, C. M., Kania, A., Burow, A., Kettlewell, S., Teucher, N., Wagner, S., Kögler, H., Meyers, M. B., Hasenfuss, G., & Smith, G. L. (2003). Effects of adenovirus-mediated sorcin overexpression on excitation-contraction coupling in isolated rabbit cardiomyocytes. *Circulation Research* **93**, 132-139.

Sethi, R., Dhalla, K. S., Ganguly, P. K., Ferrari, R., & Dhalla, N. S. (1999). Beneficial effects of propionyl L-carnitine on sarcolemmal changes in congestive heart failure due to myocardial infarction. *Cardiovascular Research* **42**, 607-615.

Shah, H. R., Vaynblat, M., Ramdev, G., Cunningham, J. N. J., & Chiavarelli, M. (1997). Experimental cardiomyopathy as a model of chronic heart failure. *Journal of Investigative Surgery* **10**, 387-396.

Sham, J. S. K., Cleeman, L., & Morad, M. (1992). Gating of the cardiac Ca^{2+} release channel: the role of Na^{+} current and Na^{+}-Ca^{2+} exchange. *Science* **255**, 850-853.

Shannon, T. R., Ginsburg, K. S., & Bers, D. M. (2000). Potentiation of fractional sarcoplasmic reticulum calcium release by total and free intra-sarcoplasmic reticulum calcium concentration. *Biophysical Journal* **78**, 334-343.

Shannon, T. R., Ginsburg, K. S., & Bers, D. M. (2002). Quantitative assessment of the SR Ca^{2+} leak-load relationship. *Circulation Research* **91**, 594-600.

Shannon, T. R., Guo, T., & Bers, D. M. (2003a). Ca^{2+} scraps: local depletions of free [Ca^{2+}] in cardiac sarcoplasmic reticulum during contractions leave substantial Ca^{2+} reserve. *Circulation Research* **93**, 40-45.

Shannon, T. R., Pogwizd, S. M., & Bers, D. M. (2003b). Elevated sarcoplasmic reticulum Ca^{2+} leak in intact ventricular myocytes from rabbits in heart failure. *Circulation Research* **93**, 592-594.

Sheu, S. S. & Fozzard, H. A. (1985). Transmembrane Na^{+} and Ca^{2+} electrochemical gradients in cardiac muscle and their relationship to force development. *Journal of General Physiology* **80**, 325-351.

Shigekawa, M. & Iwamoto, T. (2001). Cardiac Na^{+}-Ca^{2+} exchange. Molecular and pharmacological aspects. *Circulation Research* **88**, 864-876.

Sipido, K. R., Maes, M., & van de Werf, F. (1997). Low efficiency of Ca^{2+} entry through the Na^{+}-Ca^{2+} exchanger as a trigger for Ca^{2+} release from the sarcoplasmic reticulum. *Circulation Research* **81**, 1034-1044.

Sipido, K. R., Volders, P. G. A., de Groot, S. H. M., Verdonck, F., van de Werf, F., Wellens, H. J. J., & Vos, M. A. (2000). Enhanced Ca^{2+} release and Na/Ca exchange activity in hypertrophied canine ventricular myocytes. *Circulation* **102**, 2137-2144.

Sipido, K. R. & Callewaert, G. (1995). How to measure intracellular [Ca^{2+}] in single cardiac cells with Fura-2 or Indo-1. *Cardiovascular Research* **29** , 717-726.

Sipido, K. R., Volders, P. G. A., Vos, M. A., & Verdonck, F. (2002). Altered Na/Ca exchange activity in cardiac hypertrophy and heart failure: a new target for therapy? *Cardiovascular Research* **53**, 782-805.

Sitsapesan, R. & Williams, A. J. (1994). Regulation of the gating of the sheep cardiac sarcoplasmic reticulum Ca^{2+}-release channel by luminal Ca^{2+}. *Journal of Membrane Biology* **137**, 215-226.

Sjaastad, I., Wasserstrom, J. A., & Sejersted, O. M. (2003). Heart failure - a challenge to our current concepts of excitation-contraction coupling. *Journal of Physiology* **546**, 33-47.

Sobie, E. A., Dilly, K. W., dos Santos Cruz, J., Lederer, W. J., & Jafri, M. S. (2002). Termination of cardiac Ca^{2+} sparks: an investigative mathematical model of calcium-induced calcium release. *Biophysical Journal* **83**, 59-78.

Spragg, D. D., Leclercq, C., Loghmani, M., Faris, O. P., Tunin, R. S., DiSilestre, D., McVeigh, E. R., Tomaselli, G. F., & Kass, D. A. (2003). Regional alterations in protein expression in the dyssynchronous failing heart. *Circulation* **108**, 929-932.

Stern, M. D. (1992). Theory of excitation-contraction coupling in cardiac muscle. *Biophysical Journal* **63**, 497-517.

Stewart, S., MacIntyre, K., Hole, D. J., Capewell, S., & McMurray, J. J. (2001). More "malignant" than cancer? Five year survival following a first admission for heart failure. *European Journal of Heart Failure* **3**, 315-322.

Studer, R., Reinecke, H., Bilger, J., Eschenhagen, T., Bohm, M., Hasenfuss, G., Just, H., Holtz, J., & Drexler, H. (1994). Gene expression of the cardiac Na^{+}-Ca^{2+} exchanger in end-stage human heart failure. *Circulation Research* **75**, 443-453.

Su, Z., Bridge, J. H. B., Philipson, K. D., Spitzer, K. W., & Barry, W. H. (1999). Quantitation of Na/Ca exchanger function in single ventricular myocytes. *Journal of Molecular & Cellular Cardiology* **31**, 1125-1135.

Szabo, B., Kovacs, T., & Lazzara, R. (1995). Role of calcium loading in early afterdepolarizations generated by Cs^{+} in canine and guinea pig Purkinje fibers. *Journal of Cardiovascular Electrophysiology* **6**, 796-812.

Takahashi, N., Nakada, S., Takeishi, Y., & Tomoike, H. (2000). Alterations in the inotropic responses to forskolin and Ca^{2+} and reduced gene expressions of Ca^{2+}-signalling proteins induced by chronic volume overload in rabbits. *Japanese Circulation Journal* **64**, 861-867.

Task force for the diagnosis and treatment of chronic heart failure (2001). Guidelines for the diagnosis and treatment of chronic heart failure. *European Heart Journal* **22**, 1527-1560.

Taylor, C. W. & Broad, L. M. (1998). Pharmacological analysis of intracellular Ca^{2+} signalling: problems and pitfalls. *Trends in Pharmacological Sciences* **19**, 370-375.

Terracciano, C. M. N., Harding, S. E., Adamson, D., Koban, M. U., Tansley, P., Birks, E. J., Barton, P. J. R., & Yacoub, M. H. (2003). Changes in sarcolemmal Ca entry and sarcoplasmic reticulum Ca content in ventricular myocytes from patients with end-stage heart failure following myocardial recovery after combined pharmacological and ventricular assist device therapy . *European Heart Journal* **24**, 1329-1339.

The Digitalis Investigation Group (1997). The effect of digoxin on mortality and morbidity in patients with heart failure. *New England Journal of Medicine* **336**, 525-533.

Trafford, A. W., Díaz, M. E., & Eisner, D. A. (1998). Stimulation of Ca-induced Ca release only transiently increases the systolic Ca transient: measurements of Ca fluxes and s.r. Ca. *Cardiovascular Research* **37**, 710-717.

Trafford, A. W., Díaz, M. E., & Eisner, D. A. (1999). A novel, rapid and reversible method to measure Ca buffering and time-course of total sarcoplasmic reticulum Ca content in cardiac ventricular myocytes. *Pflugers Archiv-European Journal of Physiology* **437**, 501-503.

Trafford, A. W., Díaz, M. E., & Eisner, D. A. (2001). Coordinated control of cell Ca^{2+} loading and triggered release from the sarcoplasmic reticulum underlis the rapid inotropic response to increased L-type Ca^{2+} current. *Circulation Research* **88**, 195-201.

Trafford, A. W., Díaz, M. E., O'Neill, S. C., & Eisner, D. A. (1995). Comparison of subsarcolemmal and bulk calcium-concentration during spontaneous calcium-release in rat ventricular myocytes. *Journal of Physiology-London* **488**, 577-586.

Trafford, A. W., Díaz, M. E., Sibbring, G. C., & Eisner, D. A. (2000). Modulation of CICR has no maintained effect on systolic Ca^{2+}: simultaneous measurements of sarcoplasmic reticulum and sarcolemmal Ca^{2+} fluxes in rat ventricular myocytes. *Journal of Physiology* **522**, 259-270.

Tripathy, A. & Meissner, G. (1996). Sarcoplasmic reticulum lumenal Ca^{2+} has access to cytosolic activation and inactivation sites of skeletal muscle Ca^{2+} release channel. *Biophysical Journal* **70**, 2600-2615.

Underwood, R. D., Sra, J., & Akhtar, M. (1997). Evaluation and treatment strategies in patients at high risk of sudden death post myocardial infarction. *Clinical Cardiology* **20**, 753-758.

Varro, A., Negretti, N., Hester, S. B., & Eisner, D. A. (1993). An estimate of the calcium content of the sarcoplasmic-reticulum in rat ventricular myocytes. *Pflugers Archiv-European Journal of Physiology* **423**, 158-160.

Verkerk, A. O., Veldkamp, M. W., Bouman, L. N., & van Ginneken, A. C. G. (2000). Calcium-activated Cl^- current contributes to delayed afterdepolarizations in single Purkinje and ventricular myocytes. *Circulation* **101**, 2639-2644.

Volders, P. G. A., Vos, M. A., Szabo, B., Sipido, K. R., de Groot, S. H. M., Gorgels, A. P. M., Wellens, H. J. J., & Lazzara, R. (2000). Progress in the understanding of cardiac early afterdepolarizations and torsade de pointes: time to revise current concepts. *Cardiovascular Research* **46**, 376-392.

Wakabayashi, S. & Goshima, K. (1981). Kinetic studies on sodium-dependent calcium uptake by myocardial cells and neuroblastoma cells in culture. *Biochimica et Biophysica Acta* **642**, 158-172.

Wang, S.-Q., Song, L.-S., Lakatta, E. G., & Cheng, H. (2001a). Ca^{2+} signalling between single L-type Ca^{2+} channels and ryanodine receptors in heart cells. *Nature* **410**, 592-596.

Wang, Z., Nolan, B., Kutschke, W., & Hill, J. A. (2001b). Na^{+}-Ca^{2+} exchanger remodelling in pressure overload cardiac hypertrophy. *Journal of Biological Chemistry* **276**, 17706-17711.

Wasserstrom, J. A., Holt, E., Sjaastad, I., Lunde, P. K., Ødegaard, A., & Sejersted, O. M. (2000). Altered E-C coupling in rat ventricular myocytes from failing hearts 6 wk after MI. *American Journal of Physiology* **279**, H798-H807.

Wasserstrom, J. A. & Vites, A.-M. (1996). The role of Na^{+}-Ca^{2+} exchange in activation of excitation-contraction coupling in rat ventricular myocytes. *Journal of Physiology* **493**, 529-542.

Weber, C. R., Ginsburg, K. S., Philipson, K. D., Shannon, T. R., & Bers, D. M. (2001). Allosteric regulation of Na/Ca exchange current by cytosolic Ca in intact cardiac myocytes. *Journal of General Physiology* **117**, 119-131.

Weber, C. R., Piacentino III, V., Ginsburg, K. S., Houser, S. R., & Bers, D. M. (2002). Na^{+}-Ca^{2+} exchange current and submembrane $[Ca^{2+}]$ during the cardiac action potential. *Circulation Research* **90**, 182-189.

Weber, C. R., Piacentino III, V., Houser, S. R., & Bers, D. M. (2003). Dynamic regulation of sodium/calcium exchange function in human heart failure. *Circulation* **108**, 2224-2229.

Wehrens, X. H., Lehnart, S. E., Reiken, S. R., & Marks, A. R. (2004). Ca^{2+}/calmodulin-dependent protein kinase II phosphorylation regulates the cardiac ryanodine receptor. *Circulation Research* **94**, e61-e70.

Weir, W. G. & Balke, C. W. (1999). Ca^{2+} release mechanisms, Ca^{2+} sparks, and local control of excitation-contraction coupling in normal heart muscle. *Circulation Research* **85**, 770-776.

Wickenden, A. D., Kaprielian, R., Kassiri, Z., Tsoporis, J. N., Tsushima, R., Fishman, G. I., & Backx, P. H. (1998). The role of action potential prolongation and altered intracellular calcium handling in the pathogenesis of heart failure. *Cardiovascular Research* **37**, 312-323.

Wilbrandt, W. & Koller, H. (1948). Die Calciumwirkung am Froschherzen als Funktion des Ionengleichgewichts zwischen Zellmembran und Umgebung. *Helv Physiol Pharmacol Acta* **6**, 208-221.

Yang, Z., Pascarel, C., Steele, D. S., Komukai, K., Brette, F., & Orchard, C. H. (2002). Na^{+}-Ca^{2+} exchange activity is localized in the t-tubules of rat ventricular myocytes. *Circulation Research* **91**, 315-322.

Yao, A., Su, Z., Nonaka, A., Zubair, I., Spitzer, K. W., Bridge, J. H. B., Muelheims, G., Ross, J. J., & Barry, W. H. (1998). Abnormal myocyte Ca^{2+} homeostasis in rabbits with pacing-induced heart failure. *American Journal of Physiology* **274**, H1441-H1448.

Yasui, K. & Kimura, J. (1990). Is potassium co-transported by the cardiac Na-Ca exchange? *Pflugers Archiv-European Journal of Physiology* **415**, 513-515.

Yokoyama, H., Gunasegaram, S., Harding, S. E., & Avkiran, M. (2000). Sarcolemmal Na^+/H^+ exchanger activity and expression in human ventricular myocardium. *Journal of the American College of Cardiology* **36**, 534-540.

Yoshiyama, M., Takeuchi, K., Hanatani, A., Kim, S., Omura, T., Toda, I., Teragaki, M., Akioka, K., Iwao, H., & Yoshikawa, J. (1997). Differences in expression of sarcoplasmic reticulum Ca^{2+}-ATPase and Na^+-Ca^{2+} exchanger genes between adjacent and remote noninfarcted myocardium after myocardial infarction. *Journal of Molecular And Cellular Cardiology* **29**, 255-264.

Zhang, X.-Q., Musch, T. I., Zelis, R., & Cheung, J. Y. (1999). Effects of impaired Ca^{2+} homeostasis on contraction in postinfarction myocytes. *Journal of Applied Physiology* **86**, 943-950.

Zhang, X.-Q., Ng, Y.-C., Musch, T. I., Moore, R. L., Zelis, R., & Cheung, J. Y. (1998). Sprint training attenuates myocyte hypertrophy and improves Ca^{2+} homeostasis in postinfarction myocytes. *Journal of Applied Physiology* **84**, 544-552.

Zhang, X.-Q., Tillotson, D. L., Moore, R. L., Zelis, R., & Cheung, J. Y. (1996). Na^+/Ca^{2+} exchange currents and SR Ca^{2+} contents in postinfarction myocytes. *American Journal of Physiology* **271**, C1800-C1807.

Zile, M. R. & Brutsaert, D. L. (2002). New concepts in diastolic dysfunction and diastolic heart failure: Part I: diagnosis, prognosis, and measurements of diastolic function. *Circulation* **105**, 1387-1393.

Zygmunt, A. C., Goodrow, R. J., & Antzelevitch, C. (2000). I_{NaCa} contributes to electrical heterogeneity within the canine ventricle. *American Journal of Physiology* **278**, H1671-H1678.

Zygmunt, A. C., Goodrow, R. J., & Weigel, C. M. (1998). I_{NaCa} and $I_{Cl(Ca)}$ contribute to isoproterenol-induced delayed afterdepolarizations in midmyocardial cells. *American Journal of Physiology* **275**, H1979-H1992.